Luís Manuel Panchorrinha Fernandes

Characterization of large area avalanche photodiodes for detection of X-rays, vacuum ultraviolet and visible light

This Thesis is submitted to the Faculty of Sciences and Technology in the University of Coimbra for the degree of Doctor of Philosophy in Physics

University of Coimbra

2005

Gratefulness

To Prof. Doctor Joaquim Marques Ferreira dos Santos for the exemplary orientation of the works carried through during the last years, for helpful comments and suggestions, essential for the conclusion of this thesis, and for the attention and support that he has always offered to me.

To Doctor José António Matias Lopes for the constant interest, support and patience in the execution of its co-orientation role, for the special treatment he always revealed and for important suggestions concerning the thesis.

To all the laboratory colleagues for the excellent working environment, solidarity and friendship always present. In particular, to Prof. Doctor Carlos Alberto Nabais Conde and Doctor João Veloso for their contribution and support.

To the colleagues I had the pleasure to work with at the PSI (Switzerland) for their availability and enthusiasm transmitting new knowledge, as well as for the group scientific spirit that they have transmitted to me.

To Ana for the dedication and patience with the complex problems of secretariat, to Carlos and Mr. António Marques for their promptitude in the execution of some mechanic components of the experimental system, and to Mr. João Carlos for his aid and tenacity in the laboratory tasks.

To my colleagues and professors in the Physics Department for the share and transmission of knowledge. In particular, to Fernanda, Susete and Filipa for their interest and affection.

To all my friends for their affection and exceptional leisure moments spent with me, for their important presence in the good and bad moments. In particular, to André for his constant support throughout the thesis writing.

This work was financed by the Science and Technology Foundation (Portugal), through a PhD grant with the reference SFRH/BD/5426/2001.

Characterization of large area avalanche photodiodes for detection of X-rays, vacuum ultraviolet and visible light

Luis Manuel Panchorrinha Fernandes

Physics Department - FCTUC

Summary

In this work, original studies of the properties of large area avalanche photodiodes (LAAPD), used as X-ray detectors as well as photosensors for vacuum ultraviolet (VUV) and visible light, are presented.

The operational characteristics of four LAAPDs manufactured by *Advanced Photonix Inc.* (API) were investigated at room temperature for detection of X-rays. The energy resolution for 5.9 keV X-rays, obtained in the four investigated photodiodes, is found in the 10-18% range for the optimum gain of each LAAPD due to the dark current differences between the several used LAAPDs. The dark current contributes to the electronic noise, affecting the energy resolution and the minimum detectable energy. Photodiodes with lower dark current can detect minimum energies of about 1 keV. Despite the LAAPD limited area, previous characteristics together with its simplicity, compact structure, absence of radiation window and high counting rate capability (up to about 10^5/s) turn it out to be useful in varied applications, mainly in low energy X-ray detection. LAAPDs with lower dark current are able to achieve better performance than proportional counters.

The non-uniformity of the silicon resistivity originates gain variations due to the local absorption of X-rays, degrading the energy resolution. The non-uniformity effect was investigated and gain relative variations of 2-3% (standard deviation) were measured. Further than this effect, the peaks in the energy spectra present some asymmetry due to a low-energy tail. This background results from X-ray absorptions in different regions of the LAAPD, generating pulses with different amplitudes. The application of digital discrimination techniques, based on pulse risetime, allows a

significant background reduction, improving the energy resolution and leading to better discrimination between low-amplitude signals and noise.

LAAPDs have been used as VUV-light photosensors in gas proportional scintillation counters, where they present advantages compared to photomultiplier tubes. The LAAPD characterization in light detection requires the use of X-rays as a reference to determine the energy deposited in the silicon. However, for higher gains, space charge effects resulting from X-ray local absorptions originate a non-linearity between the gains obtained for X-rays and light pulses. The gain ratio between 5.9 keV X-rays and VUV light was determined. For a gain of 200, 10 and 6% variations were observed for VUV light produced in argon (~128 nm) and xenon (~173 nm), respectively. The non-linearity was also investigated for visible light and a variation significantly lower was observed (less than 1% for a gain of 200).

The LAAPD gain and dark current dependence with temperature was investigated. The gain was determined for X-rays, VUV light and visible light, being observed relative variations with temperature of about -5% per ºC for the highest gains. The obtained values are significantly higher than the ones stated in the literature (-3% per ºC). The strong reduction of the dark current when the LAAPD is cooled originates significant improvements on the energy resolution and minimum detectable energy. The excess noise factor, another contribution to the energy resolution, was also determined, having been obtained values of 1.8 and 2.3 for gains of 50 and 300, independently on temperature. The results show that the energy resolution variation with temperature is not related to the excess noise factor, but is mainly related to the dark current.

LAAPDs have been used as 1.9 keV X-ray detectors in the muonic hydrogen Lamb shift experiment. The LAAPD was selected because its response in X-ray detection practically does not vary with the presence of magnetic fields of intensity up to 5 T, required for the experiment. Moreover, its compact structure and fast time response constitute additional advantages in comparison with the tested gaseous detectors. The disadvantage of the LAAPD is associated to its limited area. This was partially eliminated using two series of LAAPDs. The several parts of the experimental system are described and the results of the experiment are presented.

Acronyms

APD	Avalanche photodiode
API	*Advanced Photonix Inc.*
GPSC	Gas proportional scintillation counter
FET	Field effect transistor
GIAN	*Atomic and Nuclear Instrumentation Group*
HPGe	High purity Germanium
JFET	Junction field effect transistor
LAAPD	Large area avalanche photodiode
LED	Light emitting diode
LYSO	Lutetium Yttrium Orthosilicate
MEC	Muon extraction channel
PMT	Photomultiplier tube
PSI	*Paul Scherrer Institute*
RAL	*Rutherford Appleton Laboratory*
RMD	*Radiation Monitoring Devices Inc.*
VUV	Vacuum ultraviolet
YAG	Yttrium Aluminium Garnet

Contents

Introduction

Avalanche photodiodes have been used as radiation detectors in an increasing number of applications. This is mainly due to its simple operation and sensitivity to different radiation types, being able to detect light in the whole visible spectrum, from the infrared to the vacuum ultraviolet region, and also low and average energy X-rays (up to about 25 keV).

The main objective of this thesis is to evaluate the use of large area avalanche photodiodes (LAAPD), manufactured by API[*], as detectors for X-rays and vacuum ultraviolet (VUV) light, where their compact structure and wide dynamic range are advantages. The potentialities and limitations of avalanche photodiodes are evaluated and compared to other X-ray detectors. The application of LAAPDs to X-ray spectrometry is evaluated and their performance in the detection of low energy fluorescence X-rays is investigated. In addition, the application of LAAPDs to the muonic hydrogen Lamb shift experiment, where they are used as 1.9 keV X-ray detectors operating under a 5 T magnetic field, is investigated.

The high quantum efficiency of avalanche photodiodes in a wide spectral range makes it possible to use LAAPDs as photosensors. In particular, the appearance of photodiodes sensitive to the scintillation light produced in rare gases has provided their incorporation in gas proportional scintillation counters (GPSC) as a VUV-light photosensors. A study of a LAAPD as VUV photosensor, integrated in a GPSC, was performed in previous works [Lopes *et al.* 2000, Lopes *et al.* 2001, Monteiro *et al.* 2001]. The study is here complemented by the investigation of the effect of temperature on the LAAPD gain and

[*] Advanced Photonix, Inc., 1240 Avenida Acaso, Camarillo, CA 93012, USA.
Internet: http://www.advancedphotonix.com

performance, the effect of strong magnetic fields in its response to VUV light detection and the non-linearity between X-ray and VUV-light gains.

The behaviour of LAAPDs under intense magnetic fields was investigated during the tests performed in order to evaluate their application to the muonic hydrogen Lamb shift experiment. The LAAPD was used as a photosensor integrated in a GPSC as well as an X-ray detector, both being tested as alternatives for application to the experiment. The LAAPD response to VUV-light and X-ray detection was investigated for magnetic fields up to 5 T.

The strong dependence of the LAAPD gain on temperature leads to the necessity of temperature control during the measurements. The knowledge of the gain variation with temperature is important because it provides corrections in cases where a precise temperature control is not possible. Additionally to the gain, temperature also affects the dark current and consequently the LAAPD performance. The effect of the temperature on the LAAPD gain and performance is evaluated for X-ray and light (VUV and visible) detection.

The present thesis is subdivided in four chapters:

In Chapter 1, a theoretical analysis of avalanche photodiodes is made. The operation principle is described and the main operational parameters are evaluated. The potentialities of avalanche photodiodes used as photosensors or X-ray detectors are evaluated and compared to other detectors. Finally, an analysis of the energy resolution contributions is made, leading to a prediction of the LAAPD operational parameters.

In Chapter 2, the study of large area avalanche photodiodes as X-ray detectors is presented, including its operational characteristics and the effect of dark current on the LAAPD performance, the spatial non-uniformity, the counting rate capability and space charge effects. The application of LAAPDs to X-ray spectroscopy is evaluated by obtaining fluorescence spectra and evaluating the energy linearity and resolution. The application of digital signal processing techniques, based on risetime discrimination, to

X-ray induced LAAPD pulses is studied in order to improve the LAAPD performance. The LAAPD non-linear response to X-rays is presented by comparison with its response to VUV light.

Chapter 3 describes the effect of the temperature on the LAAPD operational characteristics for detection of X-rays, VUV and visible light. The non-linearity between the LAAPD response to X-ray and visible light detection is studied as a function of temperature. The excess noise factor is experimentally determined for different temperatures and the effect of the temperature on the energy resolution is evaluated by the analysis of different contributions, in particular the electronic noise. The advantages of the LAAPD cooling for X-ray spectrometry applications are mentioned, being evaluated the effect of the temperature on the obtained energy spectra and on the minimum detectable energy.

Chapter 4 describes the application of avalanche photodiodes to the muonic hydrogen Lamb shift experiment. The principle of the experiment and the different parts of the experimental system are described. Some tests had been performed in order to select the 1.9 keV X-ray detector more suitable to the experiment. The results of these tests are described and a comparison with other tested detectors is established. The LAAPD behaviour under intense magnetic fields is analyzed for light and X-ray detection. The LAAPD capability to detect X-rays from muonic atoms is evaluated and several discrimination techniques for background reduction in the energy spectra are analyzed. Finally, the results of two phases of the experiment, carried through in 2002 and 2003, are discussed.

The works described in this thesis were carried out in the Atomic and Nuclear Instrumentation Group (GIAN) of the Physics Department of the University of Coimbra (Portugal) and in the Paul Scherrer Institute (Switzerland).

The studies described in this thesis gave origin to the following publications:

Publications in International Magazines with Evaluation

1. "Application of large area avalanche photodiodes to energy dispersive X-ray fluorescence analysis", L.M.P. Fernandes, J.A.M. Lopes, J.M.F. dos Santos, C.A.N. Conde, *X-Ray Spectrometry,* vol. 30 (2001) 164-169.

2. "Non-linear behaviour of large-area avalanche photodiodes", L.M.P. Fernandes, J.A.M. Lopes, C.M.B. Hunter, J.M.F. dos Santos, R.E. Morgado, *Nuclear Instruments and Methods in Physics Research A,* vol. 478 (2002) 395-399.

3. "Digital rise-time discrimination of large-area avalanche photodiode signals in X-ray detection", L.M.P. Fernandes, P.C.P.S. Simões, J.M.F. dos Santos, R.E. Morgado, *IEEE Transactions on Nuclear Science,* vol. 49 (2002) 1699-1703.

4. "Behaviour of large-area avalanche photodiodes under intense magnetic fields for VUV, visible and X-ray photon detection", L.M.P. Fernandes, A. Antognini, M. Boucher, C.A.N. Conde, O. Huot, P.E. Knowles, F. Kottmann, L. Ludhova, F. Mulhauser, R. Pohl, J.M.F. dos Santos, L.A. Schaller, D. Taqqu, J.F.C.A. Veloso, *Nuclear Instruments and Methods in Physics Research A,* vol. 498 (2003) 362-368.

5. "Large-area APDs for low-energy X-ray detection in intense magnetic fields", M. Boucher, O. Huot, P.E. Knowles, L. Ludhova, F. Mulhauser, L.A. Schaller, C.A.N. Conde, J.M.F. dos Santos, L.M.P. Fernandes, J.F.C.A. Veloso, F. Kottmann, A. Antognini, R. Pohl, D. Taqqu, *Nuclear Instruments and Methods in Physics Research A,* vol. 505 (2003) 136-139.

6. "Application of large-area avalanche photodiodes to X-ray spectrometry of muonic atoms", L.M.P. Fernandes, A. Antognini, M. Boucher, C.A.N. Conde, O. Huot, P.E. Knowles, F. Kottmann, L. Ludhova, F. Mulhauser, R. Pohl, J.M.F. dos Santos, L.A. Schaller, D. Taqqu, J.F.C.A. Veloso, *Spectrochimica Acta B,* vol. 58 (2003) 2255-2260.

7. "VUV detection in large-area avalanche photodiodes as function of temperature", J.A.M. Lopes, L.M.P. Fernandes, J.M.F. dos Santos, R.E. Morgado, C.A.N. Conde, *Nuclear Instruments and Methods in Physics Research A,* vol. 504 (2003) 331-334.

8. "X-ray spectrometry with Peltier-cooled large-area avalanche photodiodes", L.M.P. Fernandes, J.A.M. Lopes, J.M.F. dos Santos, C.A.N. Conde, *Nuclear Instruments and Methods in Physics Research B,* vol. 213 (2004) 267-271.

9. "LAAPD low temperature performance in X-ray and visible-light detection", L.M.P. Fernandes, J.A.M. Lopes, J.M.F. dos Santos, P.E. Knowles, L. Ludhova, F. Mulhauser, F. Kottmann, R. Pohl, D. Taqqu, *IEEE Transactions on Nuclear Science*, vol. 51 (2004) 1575-1580.

10. "Excess noise factor in large area avalanche photodiodes for different temperatures", L.M.P. Fernandes, J.A.M. Lopes, J.M.F. dos Santos, *Nuclear Instruments and Methods in Physics Research A,* vol. 531 (2004) 566-568.

11. "Planar LAAPDs: temperature dependence, performance and application in low energy X-ray spectroscopy", L. Ludhova, F.D. Amaro, A. Antognini, J.M.R. Cardoso, C.A.N. Conde, A. Dax, S. Dhawan, L.M.P. Fernandes, O. Huot, P.E. Knowles, F. Kottmann, J.A.M. Lopes, C.M.B. Monteiro, F. Mulhauser, R. Pohl, J.M.F. dos Santos, L.A. Schaller, D. Taqqu, J.F.C.A. Veloso, *Nuclear Instruments and Methods in Physics Research A,* vol. 540 (2005) 169-179.

Publications in the Proceedings of International Conferences

1. "Application of a large area avalanche photodiode in energy dispersive X-ray fluorescence analysis", L.M.P. Fernandes, J.A.M. Lopes, J.M.F. dos Santos, C.A.N. Conde, *Proceedings of the European Conference on Energy Dispersive X-ray Spectrometry (2000).*

2. "Non-linear behaviour of large-area avalanche photodiodes", L.M.P. Fernandes, J.A.M. Lopes, C.M.B. Monteiro, J.M.F. dos Santos, R.E. Morgado, *Proceedings of the 9th Vienna Conference on Instrumentation (2002).*

3. "Digital processing of large-area avalanche photodiode signals for X-ray spectrometry applications", L.M.P. Fernandes, P.C.P.S. Simões, J.M.F. dos Santos, R.E. Morgado, *2001 IEEE Conference Record (2002),* in CD-ROM.

4. "LAAPD low temperature performance in X-ray and visible-light detection", L.M.P. Fernandes, J.A.M. Lopes, J.M.F. dos Santos, P.E. Knowles, L. Ludhova, F. Mulhauser, F. Kottmann, R. Pohl, D. Taqqu, *2003 IEEE Conference Record (2004),* in CD-ROM.

Chapter 1

Avalanche photodiodes

In many applications, for example spectrometers, remote sensors and medical imaging, a photodetector capable of quantitative response to low light levels is necessary. For a long time, only photomultiplier tubes (PMT) and conventional photodiodes provided quantitative detection for the whole visible light spectrum. However, both photosensor types present some disadvantages, as it will be shown next. In reply, large area avalanche photodiodes (LAAPD) have been developed in order to keep some advantages of both photosensors, attenuating their limitations.

Figure 1.1 illustrates the working principle of the PMT and a conventional photodiode, the PIN (positive-intrinsic-negative) diode, a device made of a silicon semiconductor with a large depletion region, a neutrally doped intrinsic zone between two semiconductor regions with p and n-type doping, composed of impurities acceptor and donor of electrons, respectively. The concentration of impurities in the diode intrinsic region is very low.

The PMT operation takes place in vacuum. The photon enters the tube through a window and is absorbed in a photocathode, producing an electron. This photoelectron is accelerated towards a dynode (an electrode with a positive electric potential relatively to the photocathode). The electron energy is high enough to produce in average more than one secondary electron by collision with the dynode. This process is repeated through a number of dynodes, originating a gain in the final electrode (the anode) that can reach about 10^6. In the PIN diode, the photon absorption in the depletion region creates a number of electron-hole pairs that depends on the diode quantum efficiency and on the incident radiation energy. A low intensity electric field in the photodiode leads to the migration of the produced charge carriers (electrons and holes) in opposite directions

towards two external electrodes. The amplitude of this signal is proportional to the flux of incident photons.

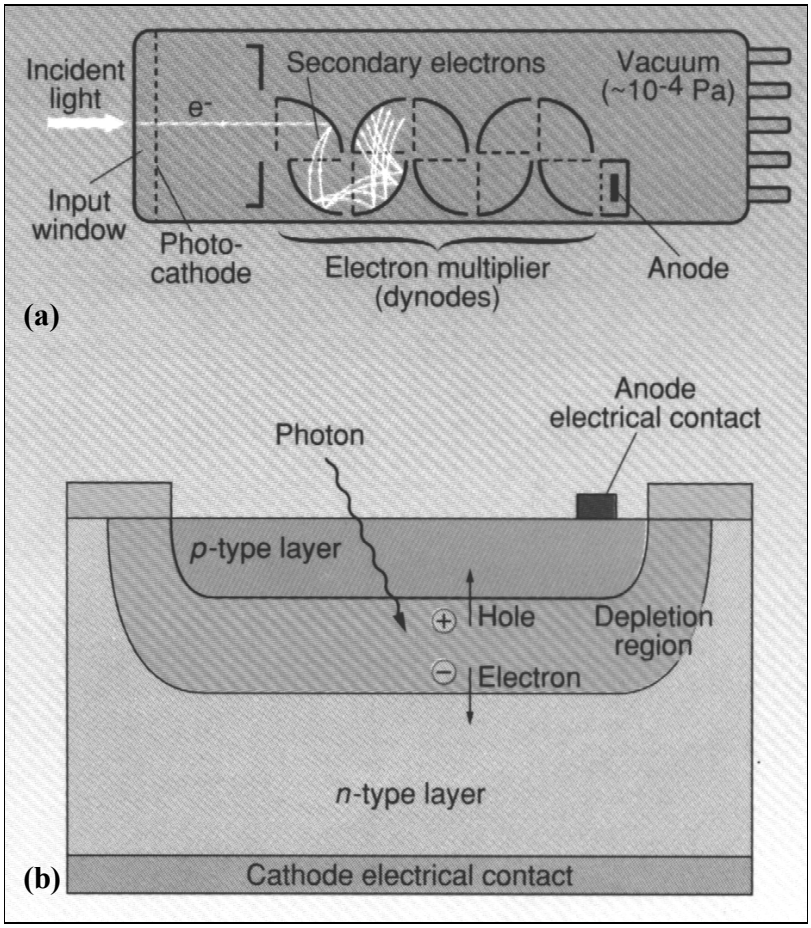

Figure 1.1 – Working principle of the PMT (a) and the PIN diode (b). In the PMT, electrons are accelerated between the dynodes inside a vacuum tube and the gain is obtained by electron impact in the successive dynodes. In the PIN diode, the incident photons are converted into charge carriers (electrons and holes) [Koren et al. 1998].

The PIN photodiode is a monolithic and compact device, in general much smaller than the PMT. Although not having internal gain, the PIN diode constitutes a low cost detector for applications with high light levels. The PMT is the preferable detector for applications with very low light levels due to its high gain, providing single photon detection. The electronic noise level in the photodiode is typically three orders of magnitude higher than the one in the PMT [Koren *et al.* 1998], restraining the detector capability at low light levels.

The avalanche photodiode (APD) combines the benefits of both photosensors presented in Figure 1.1 since it is a silicon photodiode with internal gain, although considerably lower than the one that can be obtained with the PMT, reaching less than 10^3. The gain is obtained applying a high reverse bias voltage to the photodiode, which establishes an intense electric field inside the APD, accelerating the electrons. The collision of these electrons with silicon atoms produce secondary electrons and the electronic avalanche then produced constitutes the APD gain.

The noise associated to a photodiode results from two different contributions. The first one is produced in the input stage of the preamplifier and increases with the capacitance of the detector, leading to high noise levels for photodiode areas higher than 1 cm^2. The second one is mainly attributed to the fluctuations in the photodiode dark current and also tends to increase with the photodiode size, what makes it difficult to use PIN diodes with more than 1 cm^2 area. The APD internal gain constitutes an advantage relatively to conventional photodiodes. For this reason, the photodiode-preamplifier system is about 10 to 100 times more sensitive to light detection in the case of the APD for gains around the optimum one [Koren *et al.* 1998].

In this chapter, the structure and working principle of avalanche photodiodes are described and their operational parameters are discussed. The advantages of LAAPDs for VUV-light detection are analyzed in comparison with PMTs and its applicability to X-ray detection is investigated. The LAAPD response is discussed as a function of the operational parameters. Finally, a theoretical analysis of the several contributions to the energy resolution is made, mainly the noise sources. Based on theoretical models, a prediction of the APD functional parameters is obtained. The optimum gain and the energy resolution dependence on gain are estimated.

1.1. Avalanche photodiodes: basic principles

Although simple in theory, a photodiode design capable to sustain the high voltage required to produce gain presents several problems. Such a high voltage can generate huge leakage currents through the APD surface and volume. On the other hand, the volumetric dark current is dependent on the number of defects in the silicon substrate.

For many years, avalanche photodiodes with small dimensions (less than 1 cm^2 area) and gains of about 50 had been used in applications limited to its reduced area. The first generation of large area avalanche photodiodes was demonstrated in research laboratories in the end of the 1980 decade [Koren *et al.* 1998]. The mass production of practical prototypes was achieved by *Advanced Photonix Inc.* (API) in the beginning of the 1990 decade, constituting the second generation of LAAPDs.

Several techniques had been introduced in order to eliminate some problems in the APD manufacture. For example, when a reverse bias voltage is applied to the photodiode, the maximum electric field is reached around the p-n junction and at higher voltages the field would be strong enough to induce rupture of the junction edges. This problem was avoided by using a bevelled edge geometry. This procedure reduces the electric field strength in the junction edges, avoiding their rupture. The developed techniques provided the production of prototypes with diameters up to 15 mm, with gains of a few hundreds and rupture voltages higher than 2 kV [Koren *et al.* 1998].

The analysis of the typical failure mechanisms on the prototypes production and the development of new manufacture processes lead to the appearance of a third generation of LAAPDs with better performance and longer lifetime. A specific goal was to reduce the number of defects and local non-homogeneities in the several silicon layers, pointed out as the main causes of failure in the LAAPD performance. Another innovation was the inclusion of lower resistivity silicon, leading to obtain similar gains at voltages of about 1 kV lower. These and other factors provided the repetitive production of LAAPDs with long lifetimes (more than 100 thousand hours) and active areas with 5 to 20 mm diameter.

The API technology was compared to the one developed by other manufacturers [Moszynski *et al.* 2001], showing that API LAAPDs present higher quantum efficiency, higher gains and lower noise levels. On the basis of this technology is the development of silicon crystals with n-type doping obtained by neutron transmutation, with more uniform resistivity, what provides larger avalanche regions with more moderate electric fields and therefore lower dark current.

The resistivity uniformity around the p-n junction is very important for the gain achievement in the LAAPD, preventing the occurrence of local avalanches that could originate discharges in the photodiode. According to API, only crystals with resistivity variations lower than 5% are used in the fabrication of LAAPDs.

1.1.1. Operating principle of the APD

Figure 1.2 represents the structure of a bevelled edge LAAPD, illustrating its working principle. Light photons, X-rays or charged particles incident in the photodiode p-zone are converted into electron-hole pairs. The primary electrons cross the depletion region, being accelerated by the electric field. The electric field, generated by an applied positive voltage to the photodiode cathode, is high around the p-n junction. In this zone, electrons obtain enough energy to ionize silicon atoms, producing new electron-hole pairs. The generation of secondary electrons by successive collisions of the primary electrons is similar to the electron multiplication process in a proportional counter. The produced secondary electrons are also accelerated by the field, originating an avalanche process. The electric signal is multiplied by a factor that defines the LAAPD gain.

Figure 1.3 represents schematically a LAAPD section, showing the different regions and the electric field profile inside the photodiode. When a voltage is applied to the LAAPD only a small part of the p-zone remains undepleted, the drift region (A). The electric field is very weak in this region, but in the depletion region (B) it increases with depth, reaching a maximum near the p-n junction. The electron avalanche is formed in the region where the electric field reaches the highest values ($E > E_0$ in Figure 1.3), the multiplication region (C). For API LAAPDs, the drift region is 5-10 μm thick, while the

multiplication region thickness is 10-20 μm [Gullikson *et al.* 1995]. The depletion region thickness is about 170 μm for intermediate bias voltage values (1600 to 1800 V) [Moszynski *et al.* 2001].

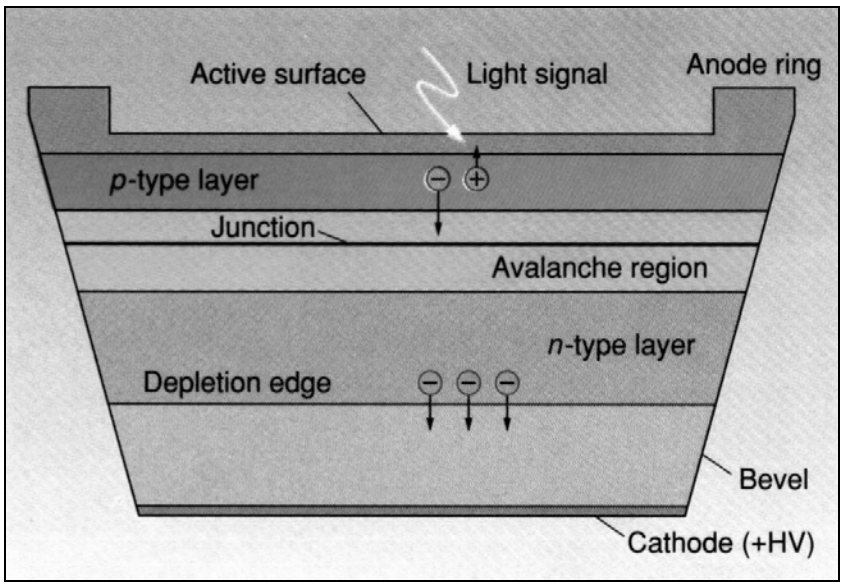

Figure 1.2 – Working principle of a bevelled edge avalanche photodiode. Electrons produced by the incident radiation are accelerated under the influence of a strong electric field in the APD, ionizing the silicon atoms and originating an electron avalanche [Koren *et al.* 1998].

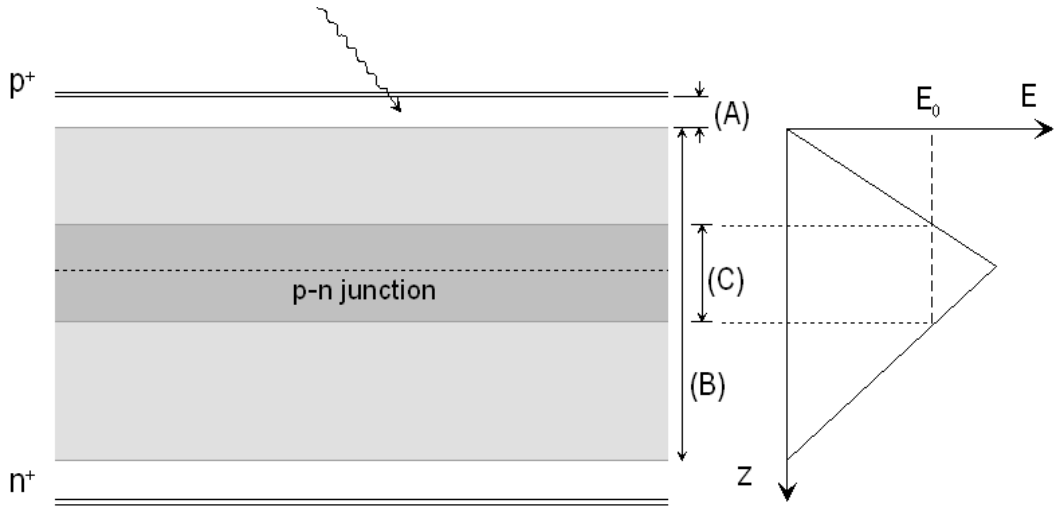

Figure 1.3 – Schematic of a LAAPD section and electric field profile (E) inside the photodiode. The drift, depletion and multiplication regions are represented by (A), (B) and (C), respectively.

The timing properties of avalanche photodiodes can be quite good for keV X-rays. For the ideal case, the limiting factor corresponds to the variation of the electron drift time with the interaction point of the incident photon in the photodiode. These variations lead to a typical variability of about 1 ns in the avalanche trigger time [Knoll 2000]. In addition, the noise superimposed to the signal leads to a timing uncertainty that often dominates the achievable time resolution. Typically, a time resolution of a few ns can be obtained [Knoll 2000]. Due to the superior signal to noise ratio generated by the gain, shorter time constants can be used for processing APD signals in comparison with conventional photodiodes, leading to higher counting rates and better time resolution.

1.1.2. The p-n junction

The depletion region presents some very attractive properties as a medium for radiation detection. The electric field inside that region induces the migration of the electrons towards the n-type material, at the same time that holes drift towards the p-type region. Thus, the concentration of electrons and holes in the depletion region is largely suppressed. Only the stationary charges (donor and acceptor impurities) remain in the region. As these charges do not contribute to the conductivity, the depletion region presents much higher resistivity than n and p-type materials. Electron-hole pairs created by radiation absorption in the depletion region move away from this region by the electric field, and this current constitutes the electric signal.

Even in the absence of ionizing radiation, photodiodes present some conductivity as the thermal generation of mobile charges induces a steady-state leakage current. The concentration of these charges is very low in the depletion region because the collection time of the produced charges (a few ns) is several orders of magnitude shorter than the time necessary to establish the thermal equilibrium [Knoll 2000]. As a result, the number of mobile charges produced by an ionizing particle is easily detected above the number of thermally generated charges. Subsequently, the reversely polarized p-n junction constitutes an attractive radiation detector since the charges produced inside the depletion region can be fast and efficiently collected.

In a non-polarized junction, the contact potential spontaneously created across the junction, of about 1V [Knoll 2000], is insufficient to produce an electric field strong enough to generate a fast flow of charge carriers. Therefore, charges can be quickly lost by recombination or captured by the material impurities, originating an incomplete charge collection. The noise performance of a non-polarized junction, connected to a preamplifier input stage, is limited by the small thickness of the depletion region and by the junction high capacitance [Knoll 2000].

When a junction is reversely polarized (the p-side voltage is negative relatively to the n-side voltage), the potential difference between both sides of the junction is strengthened by the applied voltage. In these circumstances, the minority carriers (holes in the n-side and electrons in the p-side) are attracted towards the junction and, as their concentration is relatively low, the reverse current across the diode is very low. As a result, the p-n junction acts as a rectifying element, causing a relatively free current flow in a direction and inhibiting the flow in the opposite direction.

For reduced bias voltages, electron recombination or capture by impurities may take place, originating an incomplete collection of the produced charges. The fraction of non-collected charges decreases as the electric field increases since the time available for recombination is reduced. For voltages high enough, charge collection becomes complete and the amplitude of pulses produced by radiation interactions in the APD increases exponentially with the voltage once charge multiplication arises. After the multiplication process, electrons continue to drift towards the cathode, while holes are attracted in the opposite direction. For electric fields high enough, holes can also undergo multiplication. This process also produces free electrons, contributing to the photodiode gain. In these conditions, the gain exponential dependence on the applied voltage does not take place anymore.

The thickness of the depletion zone varies with the reverse bias voltage. For this reason, the detector capacitance also varies with the voltage, so its operation stability requires the use of charge-sensitive preamplifiers to convert the collected charge (electrons resulting from the avalanche) into a voltage signal. A quantitative analysis of the properties of a reverse-polarized junction can be reviewed in [Knoll 2000].

1.1.3. Dark current

When a voltage is applied to a photodiode in order to polarize reversely its p-n junction, a low-intensity current, typically about a fraction of μA, is observed. The current might be originated in the detector volume or surface.

The volumetric dark current (generated inside the semiconductor volume) can be attributed to two different mechanisms. Due to the electric field direction in the depletion region, majority carriers created in the p and n-regions are repelled by the junction towards the depletion region edges. However, minority carriers are attracted to the junction, being conducted through it. These charges are continuously generated in both sides of the junction, being able to freely spread out and originating a stationary current approximately proportional to the junction area. For most of the cases, the contribution of minority carriers to the dark current is not significant. The second source of volumetric dark current is the thermal generation of electron-hole pairs in the depletion region, which increases with the volume of that region and decreases with the cooling. For silicon diodes, the thermal generation current is sufficiently low (less than 1 nA) to provide their use at room temperature.

The superficial dark current is generated in the p-n junction edges due to high voltage gradients nearby. The produced dark current may undergo large variations, depending on factors like the type of detector packaging, humidity and any surface contamination with fingerprints, oil or condensed vapours.

The dark current monitoring is an important procedure that can also notice the appearance of an abnormal behaviour in the detector operation. Any abrupt change or increase of dark current may point out a variation of the detector performance, being able to degrade the energy resolution. It is also useful to monitor the dark current when voltage is applied to the photodiode. The dark current usually increases with bias voltage. However, an unexpected increasing may correspond to detector breakdown. In this case, the voltage must be reduced to a lower value in order to prevent the photodiode destruction. At last, the dark current long-time behaviour often indicates the radiation damage degree of the detector when used in extreme conditions.

Dark current affects the APD performance, being a determining factor of the obtained energy resolution. Dark current fluctuations constitute a noise source, as it was stated before for PIN photodiodes. In section 1.3 a more detailed analysis of the energy resolution contributions in avalanche photodiodes will be made.

Beyond its effect on the energy resolution, dark current involves another practical influence on the photodiode operation. The bias voltage is applied in series with a high resistance for power supply protection. This way, the real value of the applied voltage is lower than the supplied value. The difference between these values is equal to the product of the dark current by the series resistance. If the dark current is high enough, the voltage drop across the resistance may lead to a considerably reduction of the photodiode applied voltage. That loss can be corrected by increasing the voltage in the power supply.

As stated before, the noise depends directly on the dark current, which increases considerably with temperature [Lopes *et al.* 2003, Fernandes *et al.* 2004A]. As a result, electronic noise levels can be reduced by cooling the APD. In Chapter 3, the effect of the dark current variation with temperature will be evaluated in VUV-light, visible-light and X-ray detection by analysing the LAAPD response at different temperatures.

1.2. Potentialities and response of LAAPDs

Avalanche photodiodes present attractive properties in the detection of low amplitude signals due to their fast time response. The high electric field assures that the transit time of the electrons across the multiplication region is very short, generating pulses with short risetimes (a few tens of ns) and time resolutions of about 1 ns [Knoll 2000]. This combination of properties permits the use of APDs with a good signal-to-noise ratio. Part of this sensitivity results from the use of very short time constants, which reduce the noise level.

The LAAPD provides the detection of low intensity light pulses, covering the spectrum regions from the ultraviolet, passing through the visible, to the infrared. It can also detect charged particles and X-rays, which makes it competitive in various applications. The most common employ of LAAPDs is as optical photosensors associated with scintillators for X-ray and γ-ray detection in calorimetry and high energy physics applications [Pansart 1997, Karar *et al.* 1999], nuclear physics [Farrell *et al.* 1997] and medical instrumentation for PET (positron emission tomography) [Chen *et al.* 1999]. Recently, they have been applied as vacuum ultraviolet (VUV) light photosensors in gas proportional scintillation counters [Lopes *et al.* 2001, Monteiro *et al.* 2001] and as X-ray detectors for spectrometry [Fernandes *et al.* 2001].

In VUV light detection, photon absorption takes place in the first silicon layers due to the reduced absorption length of those photons, of about 5 nm [Barnard *et al.* 1993]. In visible light detection, the photon absorption takes place deeper but even before the multiplication region. In these cases, the LAAPD response does not significantly vary from event to event. In opposite, X-rays can interact in different regions of the LAAPD, producing pulses with different energy and time responses, as it will be seen afterwards. Moreover, in VUV and visible-light detection the effect of non-uniformity is not significant considering that radiation is distributed over the whole LAAPD area, while in X-ray detection the LAAPD response depends on each photon interaction point.

1.2.1. Light detection

The employ of LAAPDs as optical photosensors has emerged as compensation for the disadvantages of the traditional photomultiplier tubes. The most obvious advantage of the LAAPD is its monolithic compact structure, commonly useful in applications where the space is critical and the detector is subjected to crashes or vibrations. Opposite to the LAAPD, a typical PMT is a relatively voluminous and mechanically fragile glass tube with considerably higher power consumption. Figure 1.4 shows a photograph of a typical PMT and a 16 mm diameter LAAPD. The physical differences between both photosensors are obvious.

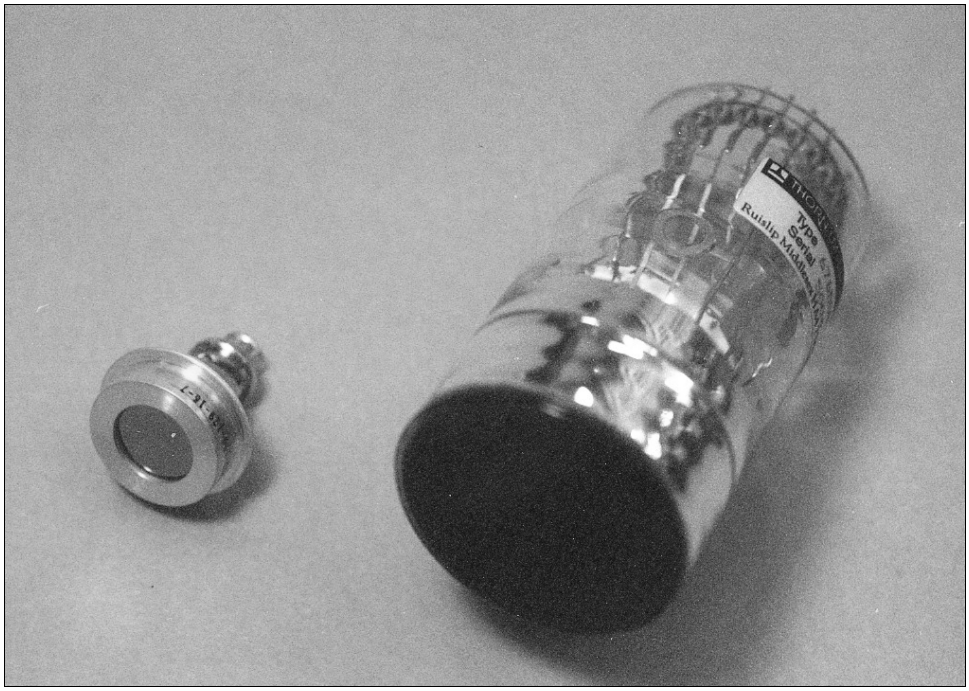

Figure 1.4 – Photograph of a 16 mm diameter LAAPD manufactured by API (to the left) and a 51 mm diameter traditional PMT (to the right) [Lopes 2002].

An additional advantage of solid state technology is the wider dynamic range. The linear response of a typical PMT is limited to a range of about 4 orders of magnitude, while the LAAPD makes possible a linear response in a range of about 6 orders of magnitude [Koren *et al.* 1998].

Another advantage of the LAAPD is the quantum efficiency, which corresponds, in practice, to the number of electron-hole pairs created in silicon per incident photon. In a typical PMT, only 10 to 25% incident photons (with 300 to 500 nm wavelengths) are converted into photoelectrons in the photocathode. Figure 1.5 presents the quantum efficiency as a function of the incident light wavelength for PMTs with different photocathodes and several LAAPDs from API. Depending on the wavelength range intended to detect, several photodiode types can be used, with maximum efficiencies in the ultraviolet, blue or red zone. For each presented LAAPD, the quantum efficiency reaches significantly higher values (up to about 90%) and broadens throughout a wider spectral range compared to the traditional photocathodes of PMTs. This extensive

spectral response is particularly important in the case of scintillators with emission spectra which present a significant yield at higher wavelengths.

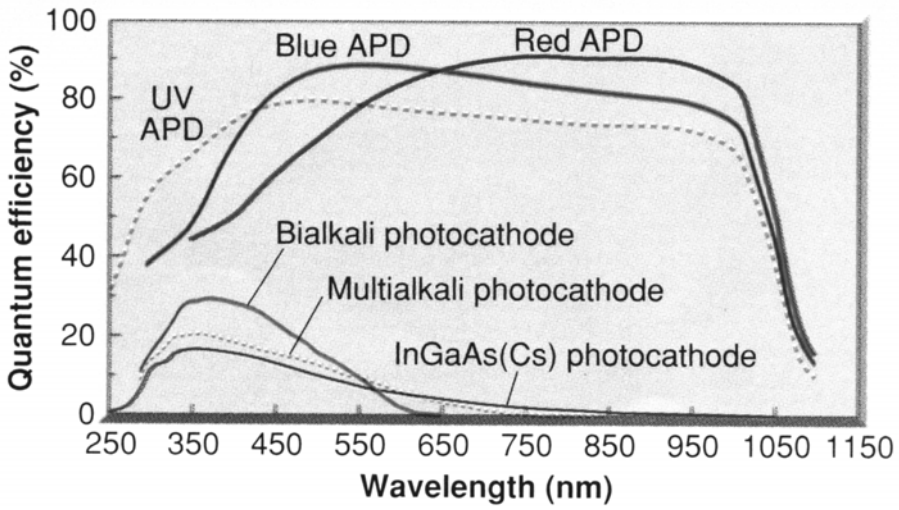

Figure 1.5 – Quantum efficiency of three typical PMTs, with different photocathodes, and three APDs from *Advanced Photonix Inc.* [Koren *et al.* 1998].

The necessity to find substitutes for traditional PMTs in VUV-light detection in gas proportional scintillation counters (GPSC) lead to the development (by API) of a series of LAAPDs (*Deep-UV windowless series*) particularly sensitive in the VUV spectral region. The high quantum efficiency in that region results from a demanding quality control in the entrance layer of the photodiode and in the interface between that layer and the silicon crystal. Figure 1.6 presents the quantum efficiency variation with wavelength for the VUV light sensitive series of LAAPDs. In that region, the quantum efficiency is high, reaching more than 100% for a wavelength range. The maximum value reaches 120% at 160 nm.

The quantum efficiency is determined by two factors: the fraction of photons incident in the APD which enter the silicon (transmission) and the number of electron-hole pairs produced per absorbed photon (intrinsic quantum efficiency). If there are no internal losses in the photodiode, quantum efficiency can be defined as the product of those two factors. The transmission depends on the silicon refractive index and on the refractive index and thickness of the anti-reflecting layer.

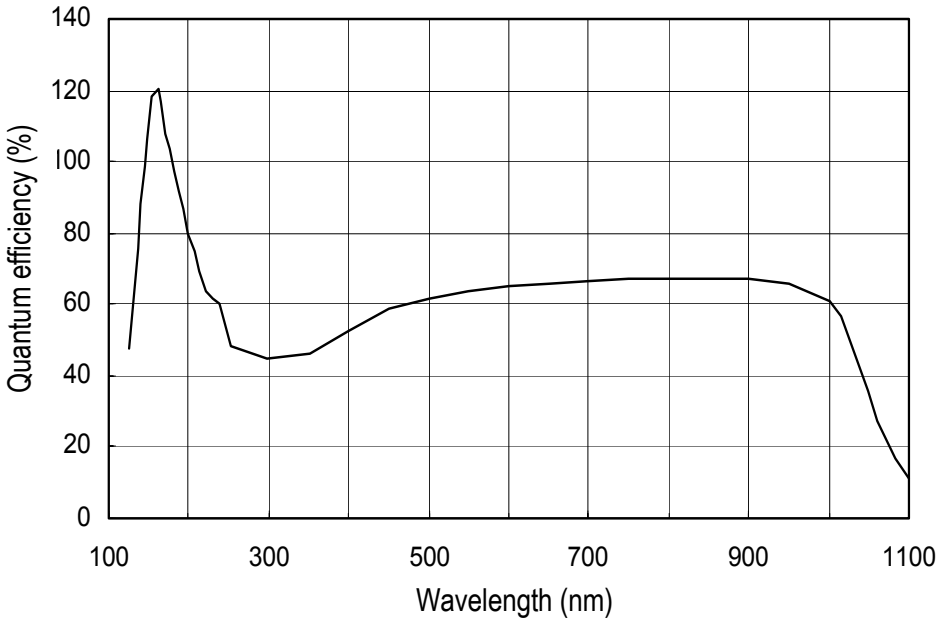

Figure 1.6 – Quantum efficiency as a function of wavelength for the VUV light sensitive series of LAAPDs from *Advanced Photonix Inc.* [Zhou *et al.* 1999].

In the VUV region, the transmission reaches the maximum value of 0.5 at 160 nm. In this zone, the photon energy is high enough to generate more than one electron-hole pair, meaning that the intrinsic quantum efficiency is higher than 1. Its value at 160 nm is 2.5 [Zhou *et al.* 1999], justifying the maximum quantum efficiency of 120%. The intrinsic quantum efficiency increases continuously below 160 nm. However, the anti-reflecting layer becomes gradually gloomier, what explains the fast drop of the efficiency at wavelengths below 160 nm.

The LAAPD presents other less obvious advantages in comparison to the PMT, which can be critical in some applications. One of them is related to the radiation window between the photocathode and the exterior. For a PMT, the window is essential since it is a part of the vacuum enclosure. The hermetic structure of the LAAPD prevents any air entrance, turning out optional the window. The absence of window provides the connection of the photodiode directly to a scintillator, what is particularly useful in the case of gaseous scintillators under high pressure.

On the other hand, both photosensors benefit from cooling. In the PMT, the temperature reduction lowers the photocathode thermal emission, decreasing the dark current.

Cooling the LAAPD also reduces the dark current due to the lower number of thermally generated charge carriers. Furthermore, the cooling increases the gain for a given bias voltage. This happens because at lower temperatures the mean free path of the photoelectrons is higher and the electrons get more energy from the electric field, increasing the conversion efficiency [API 1999]. The temperature drop also reduces the rupture voltage (about 2V per ºC for API photodiodes) [Koren *et al.* 1998].

In addition to the larger detection area, the PMT presents a great advantage compared to the LAAPD, its high internal gain (up to 10^6), which leads to the detection of single photons. For this reason, the PMT is the only detector used for photon counting and in very low light level applications at room temperature. This presents only about 10% of the applications [Koren *et al.* 1998]. For most of the applications there is no need of such high gains and quantum efficiency is more important than gain in determining the total performance. In these cases, the LAAPD is more advantageous, preserving the input signal more than the PMT.

1.2.2. X-ray detection

Having been developed as visible-light photosensors, soon the use of APDs to directly detect X-rays was recognized [Webb *et al.* 1976, Farrell *et al.* 1991, Baron *et al.* 1994, Ochi *et al.* 1996, Moszynski *et al.* 2002A].

X-rays incident in the LAAPD are absorbed in silicon with an average absorption length that varies with the X-ray energy according to Figure 1.7. The majority of X-rays absorbed originate a fast electron whose energy is approximately equal to the incident photon energy. This electron is stopped in successive collisions, originating an electron-hole pair per each 3.62 eV of energy deposited in silicon [Knoll 2000]. Each event corresponding to an absorbed X-ray can be considered as a local deposition of E_x/ε electron-hole pairs, where E_x is the incident X-ray energy (in eV) and ε the average energy required to generate an electron-hole pair.

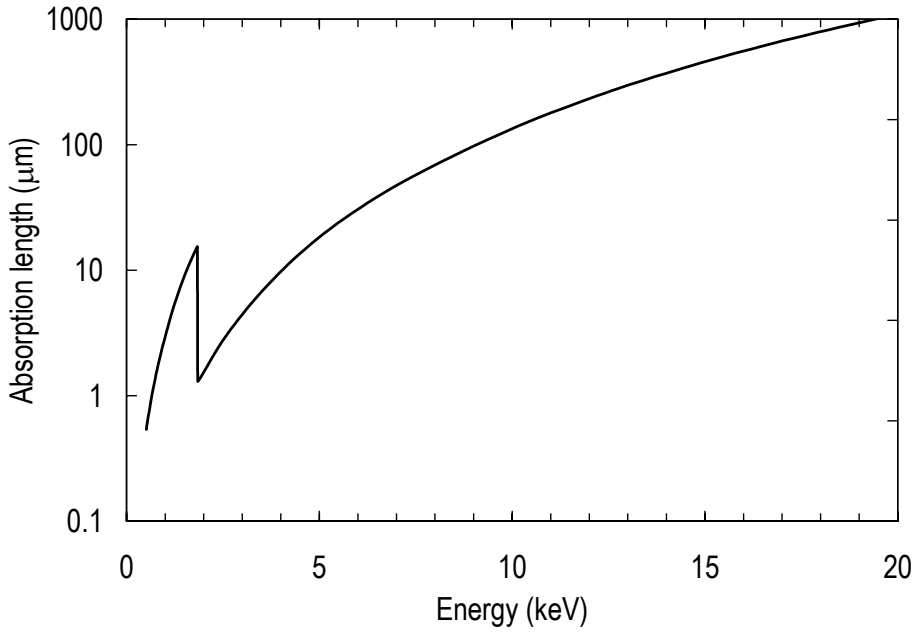

Figure 1.7 – Average absorption length for X-rays in silicon, as a function of the X-ray energy. The K-edge energy is 1.83 keV. The presented values were derived from the linear attenuation coefficients (http://physics.nist.gov/PhysRefData/FFast/html/form.html).

The absorption length in silicon is about 30 μm for 6 keV X-rays, increasing rapidly with the energy and reaching about 70, 130 and 450 μm for X-ray energies of 8, 10 and 15 keV, respectively. The high probability of an X-ray interaction taking place at different depths in the multiplication region leads to partial amplification pulses, affecting the LAAPD energy linearity. This effect is more significant at high gains and will be studied in Chapter 2.

The X-ray absorption length dependence on energy also affects the LAAPD detection efficiency, which is defined by the ratio between the number of pulses obtained in the LAAPD output and the number of photons incident in the photodiode surface. The efficiency decreases rapidly for X-ray energies above 6 keV, presenting values of about 45, 25, 8 and 4% for energies of 8, 10, 15 and 20 keV, respectively, for API photodiodes [Farrell *et al.* 1991, Baron *et al.* 1994]. The corresponding silicon active thickness for those photodiodes is about 50 μm [Baron *et al.* 1994]. The active thickness extends from the photodiode surface to the multiplication region edge in the n-type side. The minimum detection limit at low energies is imposed by the electronic noise.

The LAAPD response in the detection of X-rays absorbed in the silicon active thickness depends on the position where the absorption takes place. The active zone can be divided in three different regions, with different responses to the absorbed X-rays:

(i) the drift region;

(ii) the part of the depletion region where the electric field is not enough to provide electron multiplication;

(iii) the multiplication zone.

To understand the differences on the LAAPD response to X-rays absorbed in each one of the regions (i), (ii) and (iii), Figure 1.8 shows the doping profile (a), the electric field intensity (b) and the electron ionization coefficient (c) inside the LAAPD. The doping profile is the difference between acceptor and donor concentrations. The ionization coefficient is defined as the inverse of the average distance required for an electron to originate an electron-hole pair.

The frontal part of the p-zone presents a residual electric field of about 50 V/cm [API 1999] due to the high acceptor concentration in this region, as Figure 1.8 (a) illustrates. According to Figure 1.8 (b), the maximum value of the electric field is achieved close to the junction, reaching about 1.8×10^5 V/cm [API 1991], a value high enough to cause ionization by electron impact. The distribution of the electron ionization coefficient, shown in Figure 1.8 (c), is a measure of the gain experimented by an electron bypassing the LAAPD volume. In silicon, the ionization coefficient of holes is much lower than for electrons. The ratio between those coefficients is about 0.002 [API 1991]. Thus, the amplification of holes can be neglected as first approximation.

X-rays absorbed in the region (i) produce electrons that drift slowly towards the depletion region edge due to the weak electric field. Once in the depletion zone, the field increases and the electrons are quickly conducted to the multiplication region, where they are amplified. The resulting pulses present longer time response due to the time that electrons need to cross the region (i). In this region, electrons can also be captured for long times, from tens to thousands of ns [Baron *et al.* 1994], leading to an

amplitude reduction of the current pulse that drifts towards the strong electric field zone and originating lower amplitude pulses at the LAAPD output.

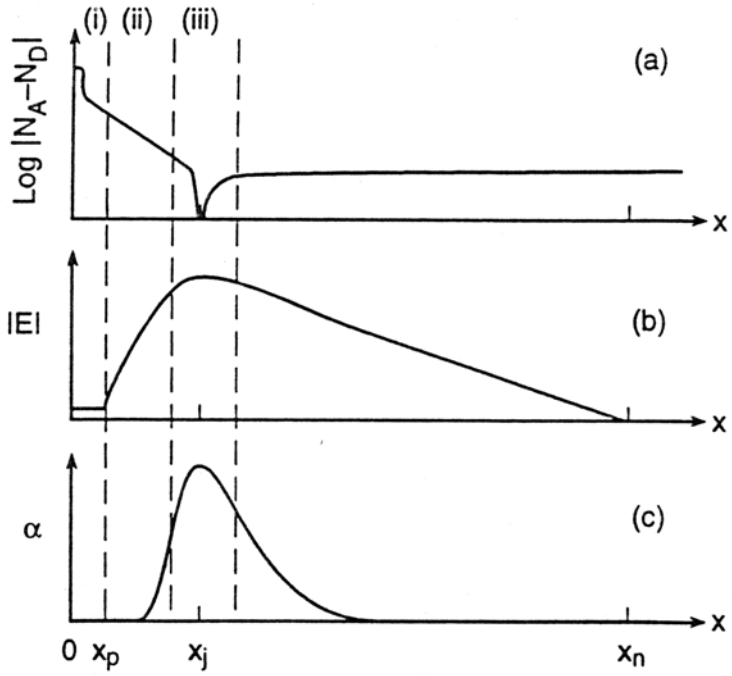

Figure 1.8 – Doping profile (a), electric field intensity (b) and electron ionization coefficient (c) as a function of depth in silicon, for API LAAPDs. The vertical lines divide the different regions of the silicon active thickness, the x_p and x_n abscissas represent the depletion zone edges and x_j corresponds to the p-n junction position [Baron *et al.* 1994].

X-rays absorbed in the region (ii) originate fully amplified pulses with faster time response comparatively to the pulses produced by X-ray interactions in the region (i). Electrons are rapidly carried to the high electric field region, undergoing an average amplification equal to the photodiode gain. The local absorption of X-rays originates events with different gains depending on the interaction point in the photodiode due to the non-uniformity of the silicon crystal. The relative standard deviation associated to the gain variation at different positions in the LAAPD is about 2% [Fernandes *et al.* 2001]. On the other hand, even for a fixed average gain, there is a statistical variation associated to the avalanche multiplication process.

X-rays absorbed in the multiplication region (iii) produce electrons that will be partially amplified, originating pulses with lower amplitude than the pulses created by X-ray

absorptions in the region (ii). The amplitude of these pulses may vary continuously down to zero.

In the same measurement, X-rays with the same energy can be absorbed in any of the regions (i), (ii) or (iii). The amplitude distribution of the resulting pulses deviates from a Gaussian curve due to the presence of a tail in the lower energy side. The tail is associated to the lower amplitude pulses produced in regions (i) and (iii).

The LAAPD time response also depends on the region where X-rays are absorbed. For X-rays absorbed in the region (i), the time response of the resulting pulses is longer than the one of fully amplified pulses produced by X-ray interactions in the region (i), while X-rays absorbed in the multiplication region originate faster pulses. Since these differences should be observable in the pulse risetime distributions, the discrimination of the anomalous pulses in order to improve the detector performance is possible. The application of digital discrimination techniques, based on pulse risetime, to LAAPDs will be investigated in Chapter 2.

1.3. Energy resolution in avalanche photodiodes

The fluctuations associated to radiation detection in avalanche photodiodes is originated by several factors. Generally, energy resolution contributions are:

1) statistical fluctuations associated to the number of electron-hole pairs produced in silicon and to the avalanche process (ΔE_S);

1) the gain non-uniformity within the APD detection volume (ΔE_U);

2) the detector noise, associated to the dark current, and the electronic system noise, mainly related to the preamplifier (ΔE_N).

The broadening (ΔE) in the energy distribution corresponding to APD pulses results from the quadratic addition of those three contributions:

$$\Delta E^2 = \Delta E_S{}^2 + \Delta E_U{}^2 + \Delta E_N{}^2 \qquad \text{(Eq. 1.1)}$$

The relative contribution of the mentioned factors depends on the type of detected radiation. There is a clear difference between light detection and direct detection of ionizing particles, such as X-rays. In particular, the non-uniformity contribution is different in both cases, being negligible in light detection if the whole APD area contributes to the electric signal amplification. In this case, there are no significant differences from pulse to pulse and the final pulse results from the average response to the entire number of photons interacting in silicon. In X-ray detection, each pulse is locally produced and the final distribution is affected by the local variation of the gain.

1.3.1. Intrinsic resolution

The intrinsic resolution is a characteristic inherent to the APD and corresponds to the energy resolution without the electronic noise contribution (Equation 1.1).

The intrinsic resolution is mainly attributed to statistical fluctuations associated to the number of electron-hole pairs produced by the incident radiation and to the avalanche process associated to each primary electron. The error propagation formula determines the output signal variance associated to the statistical limitation, in number of primary electrons, as [Knoll 2000]:

$$\sigma_S{}^2 = \sigma_n{}^2 + N\ \sigma_A{}^2 / G^2 \qquad \text{(Eq. 1.2)}$$

where N is the number of primary electrons, $\sigma_n{}^2$ its variance, G the APD gain and $\sigma_A{}^2$ the variance of the avalanche gain.

In the analysis of the signal statistical uncertainty, it is common to use the excess noise factor (F), defined as:

$$F = 1 + \sigma_A{}^2 / G^2 \qquad \text{(Eq. 1.3)}$$

As a result of electronic avalanche fluctuations, F is higher than 1 and varies with the gain. One cause of those fluctuations is the discrete nature of the multiplication process, where an electron (or hole) with high speed causes an ionization and the subsequent production of an electron-hole pair, leading to statistical fluctuations of the gain.

In silicon, the ionization probability by holes is much lower than the one induced by electrons, as it was stated before. However, the ionization induced by holes becomes significant for high gains. If a hole resulting from a primary avalanche originates an ion pair, a new electronic avalanche begins. If the hole-induced ionization occurs next to the entrance of the multiplication zone, the resulting avalanche undergoes a gain almost as high as the one of a primary avalanche. This positive feedback mechanism explains the fast increase of the gain with bias voltage, causing rupture at a critical value of the voltage. The positive feedback is an intrinsically noisy process and, near the rupture voltage, F increases linearly with the gain [API 1991].

The excess noise factor variation with gain depends on the ionization coefficients of electrons and holes, and will be derived from the McIntyre model in the next section.

The variance of the APD output signal, associated to the statistical limitation, can be described as a function of F:

$$\sigma_S^{\,2} = \sigma_n^{\,2} + N\ (F-1) \qquad \text{(Eq. 1.4)}$$

The first term of Equation 1.4 symbolize the statistical error associated to fluctuations in the number of primary electrons and the second one is related to avalanche gain fluctuations.

For light pulse detection, the variance in the number of primary electrons (N) is described by Poisson statistics:

$$\sigma_n^{\,2}(\text{light}) = N \qquad \text{(Eq. 1.5)}$$

Combining Equations 1.4 and 1.5, the statistical error associated to light detection, in number of primary electrons, is given by:

$$\sigma_S{}^2(\text{light}) = N\ F \qquad \text{(Eq. 1.6)}$$

The intrinsic resolution of avalanche photodiodes in light detection is basically determined by the statistical contribution:

$$R_{\text{int}}(\text{light}) = 2.36\,\frac{\sigma_S}{N} = 2.36\,\sqrt{\frac{F}{N}} \qquad \text{(Eq. 1.7)}$$

For X-ray detection, the peak broadening process is more complex than the one described for light pulses. The statistical fluctuations associated to the primary electrons are now attenuated by the Fano factor *f*, which describes the relative variance in the process of creation of primary electrons in comparison to a purely Gaussian process [Santos 1994]. In silicon, the *f* value is about 0.12 for keV X-rays [Perotti *et al.* 1999]. Thus, the variance in the number of primary electrons takes the form:

$$\sigma_n{}^2(\text{X rays}) = N\,f \qquad \text{(Eq. 1.8)}$$

The statistical contribution to the energy resolution is now:

$$\sigma_S{}^2(\text{X rays}) = N\,(F + f - 1) \qquad \text{(Eq. 1.9)}$$

The energy resolution for X-rays can be seriously degraded due to the gain non-uniformity in the detection volume [Moszynski *et al.* 2002A]. This happens because each pulse results from an X-ray locally absorbed, experiencing a gain that varies with the X-ray interaction point. The gain local variation is mainly attributed to the non-homogeneity of the silicon resistivity.

Being σ_U / G the relative standard deviation associated to the non-uniformity of the APD gain, the intrinsic resolution for X-rays can be described by:

$$R_{\text{int}}(\text{X rays}) = 2.36\,\sqrt{\frac{F + f - 1}{N} + \left(\frac{\sigma_U}{G}\right)^2} \qquad \text{(Eq. 1.10)}$$

The number of primary electrons produced by X-rays with energy E interacting in the LAAPD is $N = E/\varepsilon$, where ε is the average energy required to produce an electron-hole pair (3.62 eV in silicon). For light detection, the light pulse equivalent energy can be determined comparing the amplitude of the corresponding LAAPD signal with the one produced by X-rays, as it will be shown in Chapter 3.

Equations 1.7 and 1.10 make possible a comparison between the intrinsic resolution for light pulses and X-rays. The variation of the intrinsic resolution with energy can be estimated for typical values of the indicated parameters. Figure 1.9 represents the intrinsic resolution as a function of energy, considering a non-uniformity $\sigma_U / G = 2\%$ and $F = 2$. The figure also shows the statistical contribution for X-rays, which was obtained excluding the non-uniformity effect in the intrinsic resolution. The statistical contribution is slightly lower for X-rays since the variance in the number of primary electrons is smaller.

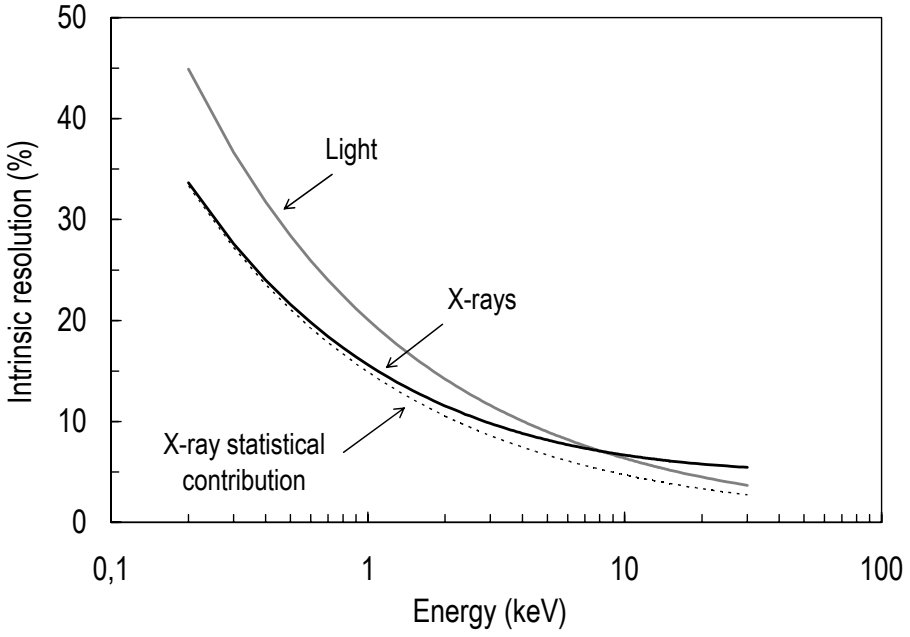

Figure 1.9 – Intrinsic resolution of the APD as a function of the energy, for light and X-rays, considering a non-uniformity σ_U/G = 2% and F = 2. The dotted curve corresponds to the statistical contribution for X-rays.

For low energy X-rays, the intrinsic resolution is mainly determined by the statistical contribution, while for higher energies it is strongly affected by the non-uniformity. For this reason, in the case of Figure 1.9, the intrinsic resolution is higher for X-rays with energies above 8 keV than for light pulses with the same deposited energy.

The non-uniformity of avalanche photodiodes depends on the manufacture process, varying from prototype to prototype. For the detection of high energy X-rays, a good LAAPD uniformity is important. The relative standard deviation used in Figure 1.9 describes a LAAPD with good uniformity, being 2% a typical value for API photodiodes. In the worst case, corresponding to 5% non-uniformity, the intrinsic resolution for X-rays is obviously higher. In that case, the X-ray intrinsic resolution would be higher than the one corresponding to light pulses for energies above 1.3 keV.

Due to the intrinsic energy resolution dependence on the excess noise factor F, the knowledge of the variation of F with gain, which will be derived in the next section, provides a theoretical prediction of the APD operational parameters, such as the energy resolution and the optimum gain.

1.3.2. Noise analysis in avalanche photodiodes

The contribution of the electronic noise to the energy resolution results from two different sources: the detector dark current and the associated electronic system.

Dark current is constituted of two different components. One of them (I_{DS}) is not dependent on gain and corresponds to the superficial current and to a small fraction of the volumetric current resulting from the thermal generation of electron-hole pairs in the n-region. The other component (I_{DV}) is amplified by the APD gain and corresponds to the volumetric current resulting from the generation of electron-hole pairs in the p-region. The total current at the APD output can be described as:

$$I = I_{DS} + G\, I_{DV} + G\, I_0 \qquad \text{(Eq. 1.11)}$$

where G is the APD gain and I_0 is the non-amplified signal current, corresponding to electron-hole pairs produced by the absorbed radiation.

A detailed noise analysis in avalanche photodiodes, in terms of noise spectral density, was discussed by McIntyre [McIntyre 1966]. The noise current density can be described in terms of the dark current and the amplifier components:

$$\phi = \frac{\mathrm{d}\,\overline{i_N^{\,2}}}{\mathrm{d}f} = \phi_D + \phi_A \qquad \text{(Eq. 1.12)}$$

The dark current contribution can be represented by [Webb *et al.* 1976]:

$$\phi_D = 2q\,(I_{DS} + I_{DV}\,G^2\,F) \qquad \text{(Eq. 1.13)}$$

where q is the electron charge and F is the excess noise factor.

The parameters G and F for signal amplification and dark current amplification are not exactly equal since the spatial distribution of the thermally generated electron-hole pairs is not equal to the distribution of pairs created by the incident radiation [Pansart 1997]. However, if the majority of the signal and the noise amplified component result from electrons generated in the drift region [API 1991], the values of G and F are supposed to be approximately equal for both signal and dark current amplification.

The noise associated to the electronic system is mainly determined by the FET (field effect transistor) at the preamplifier input. The major noise source is related to fluctuations in the FET channel current. As this current is essentially due to majority carriers, that contribution is similar to thermal noise and can be represented by a noise equivalent resistance (R_{eq}) in the preamplifier input. The corresponding noise current density can be represented by [Nicholson 1974]:

$$\phi_A = 4\,k_B T / R_{eq} \qquad \text{(Eq. 1.14)}$$

where k_B is the Boltzmann constant (1.38×10^{-23} J/K) and T is the temperature (in K).

The noise equivalent resistance for a junction FET (JFET), commonly used in charge sensitive preamplifiers for semiconductors, is given by:

$$R_{eq} = \frac{2}{3\, g_m} \qquad \text{(Eq. 1.15)}$$

where g_m is the FET mutual conductance.

Fluctuations in the channel current also lead to a floating current through the FET capacitance C_{gs} (gate-source capacitance). As this capacitance is usually small (a few pF in a JFET), the contribution of that current to the noise is neglected [Nicholson 1974].

The FET input current also contributes to the noise. However, that current is of the order of 10^{-12} A in a JFET and its corresponding contribution to noise can be ignored if compared for example to the detector dark current contribution.

Beyond the described noise sources, the FET presents a low-frequency component (excess noise). For a JFET this contribution is not significant and will not be considered in the electronic noise analysis.

An additional preamplifier noise source results from the resistor applied in series with the detector bias voltage. That resistance is generally high, typically 100 MΩ, and its contribution to noise may also be neglected.

The relevant contribution for the preamplifier noise is the one described by Equation 1.14. Thus, the total noise current density (Equation 1.12) can be approximated by:

$$\phi = \frac{4\, k_B T}{R_{eq}} + 2\, q \left(I_{DS} + I_{DV}\, G^2\, F \right) \qquad \text{(Eq. 1.16)}$$

Being C_T the total effective capacitance in the preamplifier input (including the detector and the FET input capacitances) and considering that the preamplifier is connected to a linear amplifier with equal differentiation and integration constants, the noise voltage (RMS value) is given by [Webb *et al.* 1976]:

$$V_N^{\,2} = \frac{k_B T R_{eq}}{2\tau} + \frac{\tau q}{4 C_T^{\,2}} (I_{DS} + I_{DV} G^2 F) \qquad \text{(Eq. 1.17)}$$

where τ is the value of the shaping constants in the linear amplifier.

Considering that the detector time response is fast in relation to the shaping time constants in the linear amplifier, the signal voltage can be written as:

$$V_S = \frac{Q}{e C_T} = \frac{E q G}{e \varepsilon C_T} \qquad \text{(Eq. 1.18)}$$

where Q is the deposited charge, $e \cong 2{,}718$ is the number of Nepper and E is the energy corresponding to the absorbed radiation.

The electronic noise contribution to the peak broadening (in units of energy) is:

$$\Delta E_N = 2.36 \frac{V_N}{V_S} E \qquad \text{(Eq. 1.19)}$$

Substituting V_N and V_S as defined by Equations 1.17 and 1.18 [Webb *et al.* 1976]:

$$\Delta E_N^{\,2} = \left(2.36 \frac{e\varepsilon}{qG} \right)^2 \left[\frac{k_B T R_{eq}}{2\tau} C_T^{\,2} + \frac{\tau q}{4} (I_{DS} + I_{DV} G^2 F) \right] \qquad \text{(Eq. 1.20)}$$

The first term in Equation 1.20 describes the noise of the electronic system associated to the detector (input capacitance and noise equivalent resistance of the preamplifier), while the second one corresponds to the dark current contribution. Both of the terms depend on the shaping time constants used in the linear amplifier. The noise contribution also depends on the gain and on the excess noise factor. The dependence between F and G can be derived from the McIntyre model.

Excess noise factor

The McIntyre model describes an avalanche photodiode extending from x = 0 (the n^+ electrode) to x = L (the p^+ surface). Photoelectrons are injected next to the p-zone

surface, being accelerated towards the n^+ electrode, where they are collected. Near the p-n junction, the electric field is high and ionization may take place. Consequently, electron-hole pairs are created, originating an avalanche. Being $\alpha(x)$ and $\beta(x)$ the ionization probabilities per unit of length for electrons and holes, respectively, an electron-hole pair produced at the interaction point x undergoes a gain [McIntyre 1972]:

$$G(x) = \frac{\exp\left(-\int_x^L [\alpha(x) - \beta(x)]\, dx\right)}{1 - \int_0^L \alpha(x)\, \exp\left(-\int_x^L [\alpha(x') - \beta(x')]\, dx'\right) dx} \qquad \text{(Eq. 1.21)}$$

For electrons injected at x = L, their corresponding gain is G(L). In these conditions, the excess noise factor is given by [API 1991]:

$$F = 2 - G + \frac{2}{G} \int_0^L \alpha(x) G^2(x)\, dx \qquad \text{(Eq. 1.22)}$$

Thus, expressions defined by Equations 1.21 and 1.22 are equivalent to:

$$G = \frac{1 - k_1}{\exp[-\delta(1 - k_0)] - k_1} \qquad \text{(Eq. 1.23)}$$

$$F = G\, \frac{k_2 - k_1^{\,2}}{1 - k_2} + 2\,(1 - k_1) - \frac{(1 - k_1)^2}{G(1 - k_2)} \qquad \text{(Eq. 1.24)}$$

where the specified coefficients are:

$$\begin{aligned} \delta &= \int_0^L \alpha(x)\, dx \\ k_0 &= \int_0^L \beta(x)\, dx \Big/ \int_0^L \alpha(x)\, dx \\ k_1 &= \int_0^L \beta(x) G(x)\, dx \Big/ \int_0^L \alpha(x) G(x)\, dx \\ k_2 &= \int_0^L \beta(x) G^2(x)\, dx \Big/ \int_0^L \alpha(x) G^2(x)\, dx \end{aligned} \qquad \text{(Eq. 1.25)}$$

The parameter δ is the ionization coefficient for electrons. Factors k_0, k_1 and k_2 are different measures of the ratio between the ionization coefficients for holes and electrons.

In a low noise APD, the k factors are very small compared to 1 and more or less equal. Thus, equation 1.24 takes a simpler approximated form:

$$F \cong G\, k_{ef} + \left(2 - \frac{1}{G}\right)\left(1 - k_{ef}\right) \qquad \text{(Eq. 1.26)}$$

where $k_{ef} = (k_2 - k_1^{\,2})/(1 - k_2)$ is the effective ratio between the ionization coefficients.

For high gains, the variation of the k factors with voltage is very low. Since $k_{ef} << 1$, for lower gains (not below a few tens) $F \approx 2 - 1/G$, meaning that F practically does not vary with k_{ef}. Thus, considering k_{ef} constant is a good approximation. For API photodiodes, the k_{ef} value is about 0.0015 [API 1991]. The dependence of F on gain was estimated for k_{ef} = 0.0015, as Figure 1.10 shows. For the useful gain range, F increases linearly with the gain, as represents the linear fit at gains above 30.

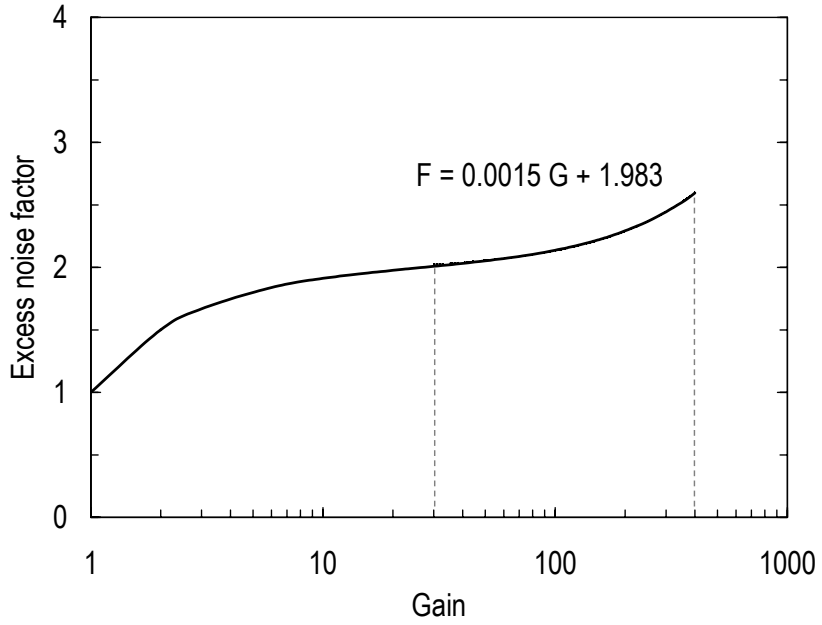

Figure 1.10 – Excess noise factor as a function of gain according to Equation 1.26, considering k_{ef} = 0.0015. The variation of F with G is linear between the vertical lines (for gains above 30).

The results obtained for API avalanche photodiodes are in accordance with Figure 1.10 [API 1991, Moszynski *et al.* 2002A]. The excess noise factor has been experimentally determined as a function of gain for different temperatures. The results obtained will be presented in Chapter 3.

1.3.3. Prediction of the APD operational parameters

The correlation between the excess noise factor and the gain makes possible to predict the noise contribution to the energy resolution. However, the estimation depends on the APD dark current, which depends extremely on each individual photodiode. Using typical values of the parameters, Equation 1.20 can be used to obtain an estimate of the noise contribution to the energy resolution.

Typical values of the dark current in API avalanche photodiodes, with 16 mm diameter, are I_{DS} = 100 nA and I_{DV} = 0.3 nA, at room temperature (294 K), while the typical capacitance of those photodiodes in the useful gain range is about 130 pF [API 1999]. Considering the use of a charge sensitive preamplifier, with a JFET mutual conductance of 20 mS and an input capacitance of 1 pF, in Equation 1.20 we find $R_{eq} \cong 33\ \Omega$ and $C_T \cong 130\ \text{pF}$. Figure 1.11 represents an estimate of the noise contribution (in keV), defined by Equation 1.20, for different shaping time constants.

While the gain increases, the noise contribution initially decreases, reaching a minimum value, and then increases. For reduced gains, the noise is mainly determined by the preamplifier, decreasing as the time constants increase. For higher gains, the dark current contribution dominates and the noise increases with the shaping time constants, as Figure 1.11 shows. The gain corresponding to the minimum value of the noise contribution depends on the time constants, being about 80 for 1μs and 240 for 100 ns. The use of lower time constants benefits the detector performance against noise but may cut the pulse risetime, leading to partial signal loss.

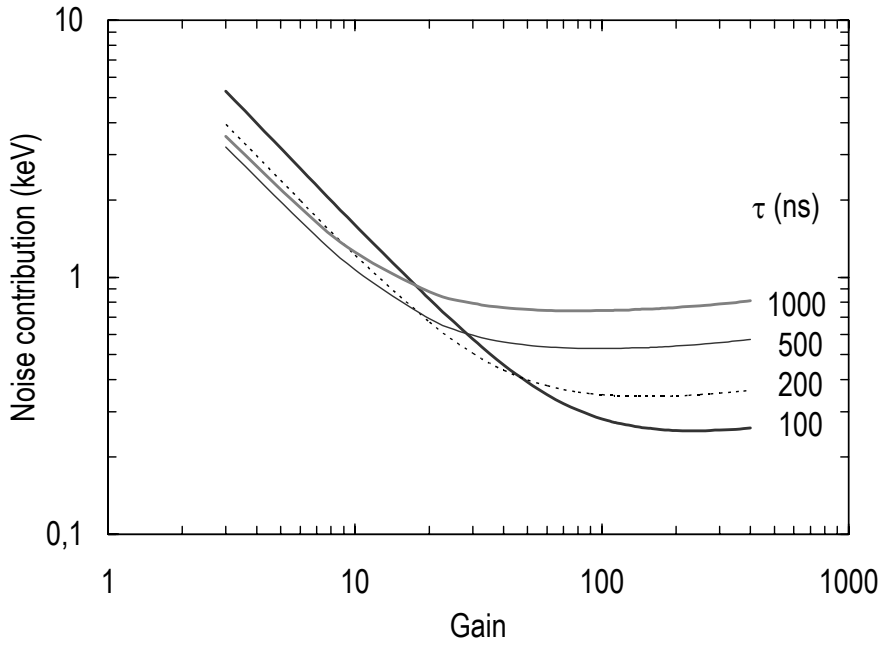

Figure 1.11 – Estimate of the electronic noise contribution (Equation 1.20) as a function of gain, for different shaping time constants. The results of Figure 1.10 and typical values of the APD and preamplifier parameters have been used.

The choice of the optimum gain must take into account not only the noise contribution but also the total energy resolution behaviour as a function of gain. As shown before, the intrinsic resolution varies with the type of detected radiation and depends on the excess noise factor and on the incident radiation energy.

In X-ray detection, the APD intrinsic resolution is described by Equation 1.10 and its variation with gain depends on the relationship between F and G. Considering a 2% non-uniformity, results of Figure 1.10 provide the estimate of the intrinsic resolution as a function of gain, for different energies, using Equation 1.10. The total energy resolution was then derived for different energies combining the estimated intrinsic resolution and the noise contribution (Figure 1.11). Figure 1.12 represents the energy resolution as a function of gain for shaping time constants of 200 ns. The figure shows that the optimum gain, corresponding to the minimum value of the energy resolution, decreases slightly as the energy increases, being about 120, 100 and 80 for X-ray energies of 3, 6 and 12 keV, respectively.

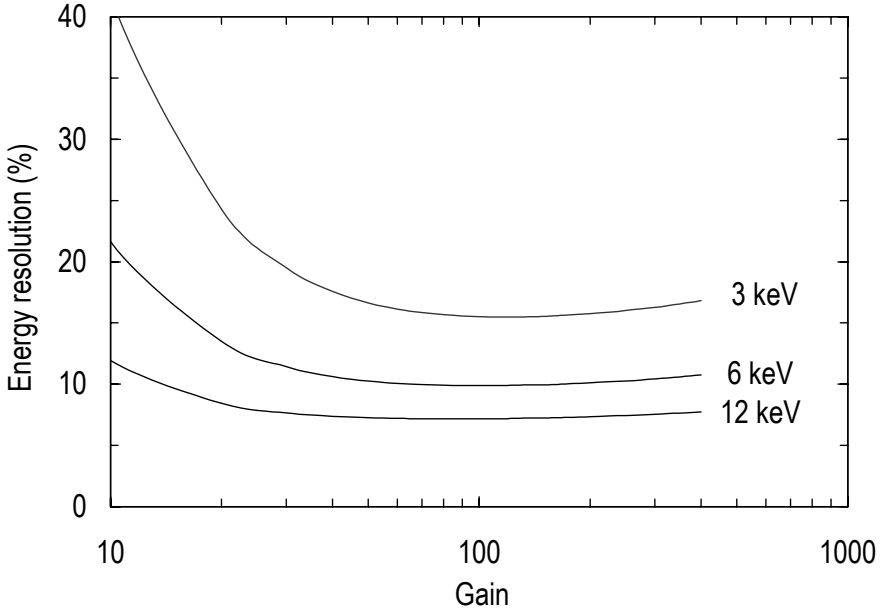

Figure 1.12 – Estimate of the energy resolution as a function of gain for X-rays with energies of 3, 6 and 12 keV, considering 2% non-uniformity and 200 ns shaping time constants.

The non-uniformity depends on each individual photodiode and the same happens with the dark current, which varies considerably from prototype to prototype, leading to differences on the intrinsic resolution and noise contribution for different photodiodes. Since these parameters are inherent to the fabrication process of each photodiode, the energy resolution may vary significantly between different photodiodes, as it will be seen later.

The choice of the best value for differentiation and integration constants depends on the type of radiation proposed to detect due to the differences in the duration of the corresponding pulses. For example, the signal resulting from an X-ray interaction in the photodiode is shorter than a light pulse signal since the last one depends on the time-width of the incident light pulse, while the X-ray signal results from a single photon interaction. Thus, the analysis of the electronic noise contribution is valid for light pulses if their time-width is small in comparison to the shaping time constants.

The APD optimum gain depends on factors like the nature and energy of the incident radiation, shaping time constants, dark current and input capacitance. The optimum gain can be derived taking into account that it corresponds to the local minimum of the curve

representing the energy resolution as a function of gain, *R(G)*. The minimum takes place at $\partial R / \partial G = 0$. The derivation is simpler using the square of the energy resolution:

$$R^2 = R_{\text{int}}{}^2 + \left(2.36\frac{e\varepsilon}{qEG}\right)^2\left[\frac{k_B\,T\,R_{eq}}{2\tau}C_T{}^2 + \frac{\tau q}{4}(I_{DS} + I_{DV}\,G^2\,F)\right] \qquad \text{(Eq. 1.27)}$$

The first term of the previous equation corresponds to the intrinsic resolution while the second one is the electronic noise contribution expressed by Equation 1.20. The intrinsic energy resolution depends on the nature of the incident radiation, being defined by Equations 1.10 and 1.13 for light pulses and X-rays, respectively. Considering that the gain non-uniformity is constant for each LAAPD, in Equations 1.10 and 1.13 only *F* depends on gain. Like so, the derivative of the first term in Equation 1.27 is equal for light pulses and X-rays:

$$\frac{dR_{\text{int}}{}^2}{dG} = (2.36)^2\,\frac{\varepsilon}{E}\frac{dF}{dG} \qquad \text{(Eq. 1.28)}$$

Substituting this result in the derivative of Equation 1.27, the optimum gain is the solution of the equation $dR^2/dG = 0$. This equation can be simplified leading to:

$$\frac{dF}{dG} = \left(\frac{e}{qE}\right)^2\left[\frac{k_B\,T\,R_{eq}}{\tau\,G^3}C_T{}^2 + \frac{\tau q}{4}\left(\frac{2\,I_{DS}}{G^3} - I_{DV}\frac{dF}{dG}\right)\right] \qquad \text{(Eq. 1.29)}$$

In the LAAPD useful gain region, the dependence between *F* and *G* must be linear, as Figure 1.10 illustrates. In this case $dF/dG \approx k_{ef}$ and Equation 1.29 is equivalent to:

$$\left(E + \frac{e^2\varepsilon\,\tau}{4\,q}I_{DV}\right)k_{ef}\,G^3 = \frac{e^2\varepsilon}{q^2}\left(\frac{k_B\,T\,R_{eq}}{\tau}C_T{}^2 + \frac{\tau q}{2}I_{DS}\right) \qquad \text{(Eq. 1. 30)}$$

The solution of this equation corresponds to the optimum gain, given by:

$$G_{\text{opt}}{}^3 = \frac{2}{k_{ef}}\left(I_{DS} + 2\,\frac{k_B\,T}{q}\,\frac{R_{eq}C_T{}^2}{\tau^2}\right)\Bigg/\left(I_{DV} + \frac{4\,q}{e^2\tau}\,\frac{E}{\varepsilon}\right) \qquad \text{(Eq. 1.31)}$$

Equation 1.31 proves that the optimum gain depends on factors inherent to the APD, as k_{ef} and the dark current components, depending also on the preamplifier characteristics and on the shaping time constants used in the linear amplifier. Equation 1.31 shows that the optimum gain decreases slightly with the energy deposited in the APD by the incident radiation.

The optimum gain can be estimated using typical values of the parameters in the Equation 1.31. Considering a LAAPD with $k_{ef} = 0.0015$ and dark current components of I_{DS} = 100 nA and I_{DV} = 0.3 nA, connected to a preamplifier with R_{eq} = 33 Ω and $C_T = 130$ pF in its input, the optimum gain for 6 keV is about 100 for 200 ns time constants, presenting higher values at lower constants (about 130 for 100 ns). In the next chapter these estimates will be compared to the experimental results.

CHAPTER 2

Large area avalanche photodiodes for X-ray detection at room temperature

The major limitation on the application of large area avalanche photodiodes (LAAPDs) is related to the spatial non-uniformity of the silicon resistivity, what leads to local gain variations. However, the development of LAAPDs with better spatial uniformity, providing higher gains for lower biasing voltages, has contributed to the widening of the range of LAAPD applications (API, RMD[*]).

LAAPDs have been mainly used as photosensors connected to scintillators for detection of X-rays and γ-rays, in substitution of photomultiplier tubes [Moszynski *et al.* 2002A]. The viability of using LAAPDs to directly detect X-rays was already demonstrated [Webb *et al.* 1976, Farrell *et al.* 1991, Gullikson *et al.* 1995]. The useful thickness of the LAAPD for X-ray detection is about a few tens of μm, limiting the photodiode efficiency, which decreases quickly for X-rays with energies above 5 keV [Farrell *et al.* 1991], as it was shown in the previous chapter. The techniques for low energy X-ray detection with LAAPDs had been mainly developed to study the properties of charge carriers produced in the photodiode, using X-rays as a reference for light measurements. Nevertheless, the use of LAAPDs as X-ray detectors in the 0.5 to 20 keV range was early suggested [Farrell *et al.* 1991, Gullikson *et al.* 1995, Ochi *et al.* 1996].

In this chapter, the performance of large area avalanche photodiodes manufactured by *Advanced Photonix, Inc.* (API) is investigated for application to X-ray spectrometry at

---

[*] Radiation Monitoring Devices Inc., 44 Hunt Street, Watertown, MA 02472, USA.
Internet: http://www.rmdinc.com

room temperature. The operational characteristics of the investigated LAAPDs are presented, including the obtained gain, the effect of dark current on the energy resolution and minimum detection limit, the spatial non-uniformity, space charge effects and counting rate capability. The energy linearity and resolution are studied as functions of the energy of the fluorescence X-rays emitted by several samples, and energy spectra of multi-elementary samples are registered. The application of digital discrimination techniques to LAAPD pulses is evaluated. The discrimination is based on pulse risetime and its effect is evaluated measuring the energy resolution, the peak-to-background ratio and the peak distortion in the amplitude spectra. Finally, the non-linearity of the LAAPD gain is evaluated in X-ray and light detection. The gain nonlinear behaviour was already investigated for visible light detection with LAAPDs [Pansart 1997, Moszynski *et al.* 2002A], being now extended to the vacuum ultraviolet (VUV) region. The effect of non-linearity is assessed comparing the amplitude of the pulses produced in the LAAPD by X-rays directly absorbed and by VUV scintillation light produced in a GPSC.

2.1. Operational characteristics of LAAPDs for application to X-ray spectrometry

The four investigated avalanche photodiodes belong to the *windowless UV-enhanced* series, manufactured by API, presenting 10 or 16 mm diameters. The operational characteristics of those LAAPDs have been studied, being presented in the paper: "Application of large area avalanche photodiodes to energy dispersive X-ray fluorescence analysis", published in *X-Ray Spectrometry*, vol. 30 (2001), pages 164-169 [Fernandes *et al.* 2001] and attached at the end of this chapter (page 61).

Figure 2.1 represents a typical amplitude spectrum of the LAAPD pulses produced by 5.9 keV X-rays. The distribution includes a peak with shape approximately Gaussian and a background in the low-energy side. This tail is mostly attributed to the absorption of X-rays in the multiplication region of the LAAPD, leading to partial signal

amplification. Moreover, X-rays absorbed in the drift region, where the electric field is very weak, originate a partial loss of charge carriers, which can be lost through the LAAPD surface or captured for long periods of time, as described in the previous chapter. Both of the described event types originate lower amplitude pulses. The amplitude of the pulses produced by X-ray absorptions in the multiplication region should vary between zero and the amplitude of fully amplified pulses, leading to the characteristic background between the noise distribution and the peak.

The noise distribution limits the minimum detectable energy, defined as the energy corresponding to the amplitude at which the noise tail raises above the background level in the amplitude distribution (Figure 2.1).

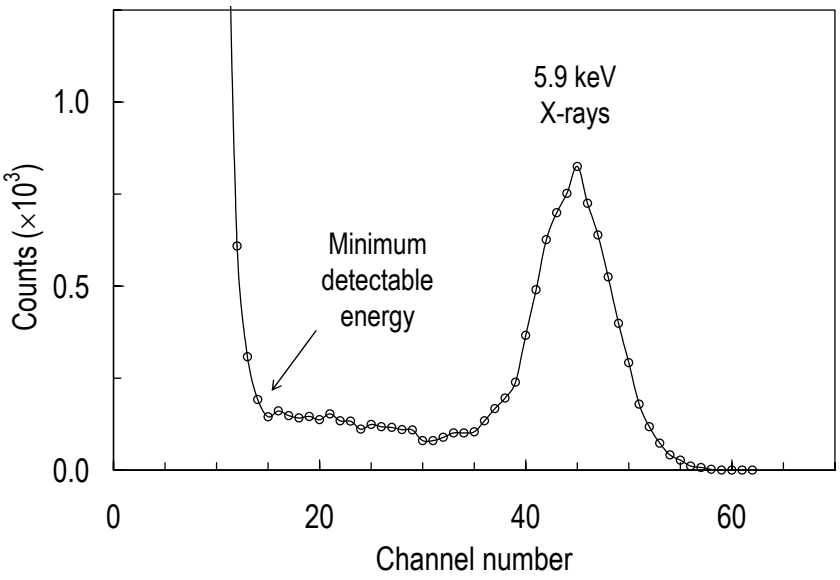

Figure 2.1 – Typical amplitude spectrum of the LAAPD pulses produced by 5.9 keV X-rays emitted by a ^{55}Fe radioactive source (Mn K_α line). The Mn K_β line (6.4 keV X-rays) was efficiently reduced by means of a chromium filter.

The shaping time constants in the linear amplifier have been determined in order to optimize the LAAPD performance for X-ray detection, using a LAAPD (serial number 129-17-05) polarized with 1830 V. The amplifier has been tuned for a fixed gain of 5×64 and the shaping constants have been varied while keeping equal values for the differentiation and integration constants.

Table 2.1 shows the energy resolution for 5.9 keV X-rays and the minimum detectable energy for different shaping time constants. For constants longer than 200 ns, the degradation of the energy resolution is clear and a significant increase of the minimum detectable energy is observed. Since the error in the energy resolution measurements is ± 0.1%, the optimum value for the shaping constants is found to be in the interval 50-200 ns. However, the use of shorter constants (less than 100 ns) originates partial signal loss, cutting the risetime of the pulses at the preamplifier output. The choice of shaping time constants between 100 and 200 ns seems reasonable and is in agreement with the theoretical prediction made in the previous chapter, where the use of lower constants was found to improve the detector performance against noise.

Table 2.1 – Energy resolution for 5.9 keV X-rays and minimum detectable energy for different shaping time constants used in the linear amplifier.

Shaping time constant (ns)	50	100	200	500	1000
Energy resolution (%)	12.6	12.7	13.2	14.6	16.7
Minimum detectable energy (keV)	0.90	0.89	0.96	1.18	1.52

The effect of using different values for the integration and differentiation constants was studied by keeping fixed the differentiation constant (200 ns) and varying the integration constant. The minimum values of the energy resolution and minimum detectable energy were obtained for integration constants between 50 and 200 ns, increasing significantly above 200 ns.

The energy resolution and the minimum detectable energy are slightly higher for 200 ns shaping time constants compared to shorter constants. In order to prevent partial signal loss by using shorter time constants, the choice of 200 ns shaping constants is more appropriate.

2.1.1. Gain and dark current

The amplitude of the signal produced by a 5.9 keV X-ray collimated beam (with 1 mm diameter) was determined as a function of the bias voltage for the different investigated photodiodes. Shaping time constants of 200 ns were used in the linear amplifier. The gain was normalized to the one specified by the manufacturer for low gains, where non-linearity effects are neglected.

Figure 2.2 represents the gain and dark current as specified by the manufacturer (API) and the gain measured for 5.9 keV X-rays as function of the bias voltage, for the LAAPD with serial number 129-02-27. Measurements were carried out at a temperature of 20 ºC. As the figure shows, the gain dependence with bias voltage is approximately exponential. However, for higher gains the contribution of holes to avalanche becomes significant and that dependence turns out to be supra-exponential. In this region, the difference between the gain measured for 5.9 keV X-rays and the one specified by API is significant. The gain determination by the manufacturer was carried out with visible light, what confirms the non-linearity between X-ray and visible-light gains.

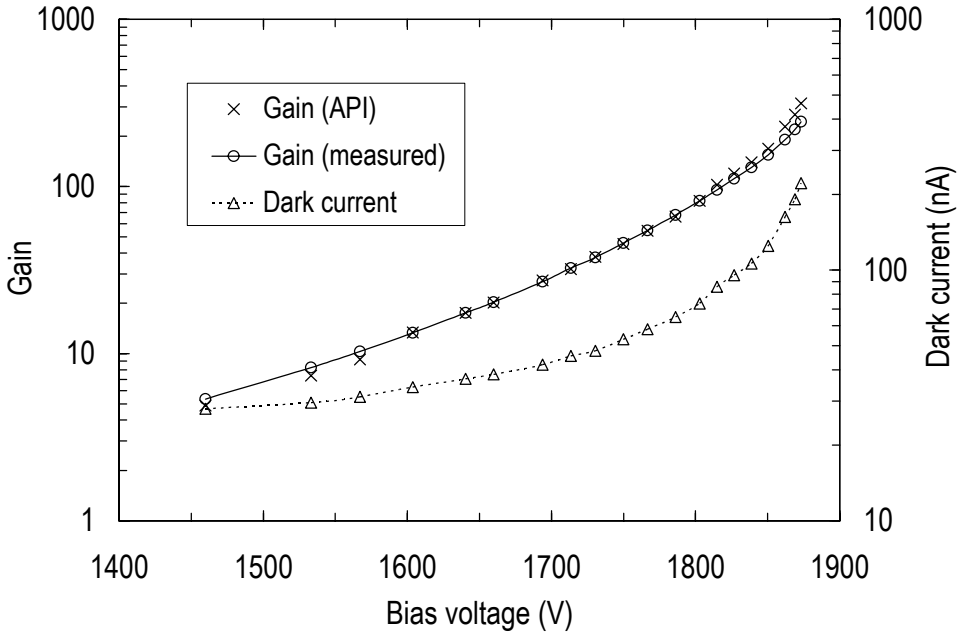

Figure 2.2 – Gain and dark current for an API LAAPD, according to the manufacturer, and gain measured for 5.9 keV X-rays as functions of the bias voltage, at room temperature (20 ºC).

The dark current contributes to the electronic noise, disturbing the detector performance. To evaluate the effect of dark current, the energy resolution for 5.9 keV X-rays and the minimum detection limit were determined as functions of the applied bias voltage. Results are presented in [Fernandes *et al.* 2001]. The optimum gain was found to be about 50-70 for all investigated photodiodes, resulting from a compromise between gain and dark current. Below the optimum gain the energy resolution reduction with gain is associated to the increase of the signal-to-noise ratio. For higher gains, the increase of dark current with bias voltage is more pronounced and the electronic noise increases more than the gain, leading to a degradation of the energy resolution and the minimum detection limit.

The obtained energy resolution can be compared to the values estimated from the theoretical analysis made in the previous chapter. The theoretical estimate requires the knowledge of some parameters of the LAAPD and the associated electronic system.

The intrinsic resolution for X-rays, defined by Equation 1.10, depends on the energy, the excess noise factor F and the gain non-uniformity. As the used X-ray beam is collimated, one assumes that the energy resolution is not significantly affected by the gain non-uniformity. The dependence of F on the gain is assumed to be described by Equation 1.26 considering $k_{ef} = 0.0015$.

The electronic noise contribution (Equation 1.20) depends on the dark current, the excess noise factor, the total capacitance and equivalent noise resistance in the preamplifier input, and on the amplifier shaping time constants as well. The dark current components can be determined through a linear fit ($I_D = I_{DS} + G\, I_{DV}$) when dark current in represented as a function of gain. The typical capacitance of API avalanche photodiodes is 65 or 130 pF for LAAPDs with 10 or 16 mm diameter [API 1999]. The FET input capacitance in the preamplifier (*Canberra* 2004) is 1 pF[*], negligible when compared to the LAAPD capacitance. Thus, the total capacitance in the preamplifier

[*] B-17369 *Schematic Preamplifier Model 2004*, Canberra Industries, Inc.

input is practically determined by the detector. Since the preamplifier JFET* presents a mutual conductance of 20 mS, the equivalent noise resistance in the preamplifier input is $R_{eq} \cong 33\ \Omega$. In the previous conditions, the energy resolution can be estimated as a function of gain for 5.9 keV X-rays, considering shaping time constants of 200 ns.

Figure 2.3 represents the energy resolution, measured for 5.9 keV X-rays with the LAAPD with serial number 121-02-27, and the estimated value assuming 2% non-uniformity, as a function of gain. The dark current specified by the manufacturer is also represented. The linear fit to the dark current values (doted line) determines the components I_{DS} = 24.2 nA and I_{DV} = 0.64 nA. The fit is not valid for the highest gains.

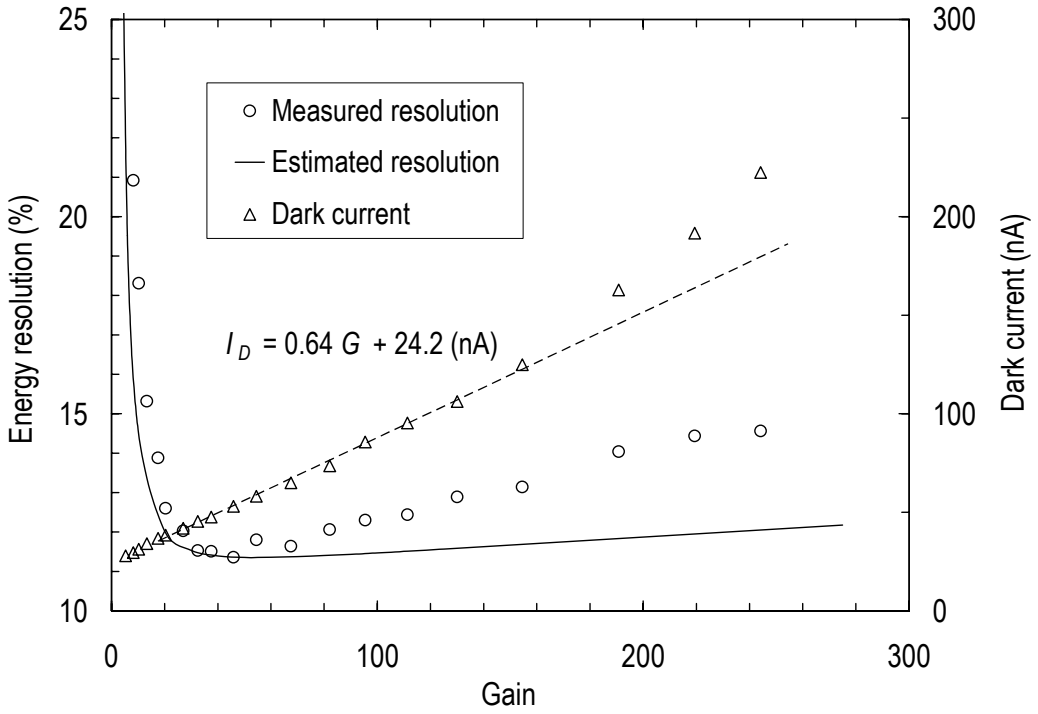

Figure 2.3 – Energy resolution for 5.9 keV X-rays (experimental values and theoretical estimate) and dark current specified by the manufacturer as functions of gain. The linear fit to the dark current values determines the components I_{DS} and I_{DV}.

* 2N5434 *N-Channel JFET Switch*, Calogic Corporation.

Figure 2.3 evidences some differences between the estimated and experimental values of the energy resolution. However, for gains around the optimum (about 50), the differences are very small. Thus, the energy resolution estimate, considering 2% non-uniformity, is reasonably adjusted to the set of experimental measurements. Although the X-ray beam is collimated (with 1 mm diameter), X-rays interact locally in the LAAPD and are able to be absorbed at different depths, experiencing partially the effect of non-uniformity.

Above the optimum gain, the measured energy resolution is higher than the estimated one and this difference increases with gain. In this region, the resolution is mainly affected by the dark current. In Figure 2.3, the linear fit to the dark current values do not include the points corresponding to the highest gains. Moreover, the presented values have not been experimentally measured, being able to originate significant differences. In the used experimental system, the dark current measurement was not possible since the available power supplies were not able to measure current values below 1 μA. Beyond the dark current dependence, for high gains the energy resolution is also affected by the excess noise factor, which was not measured, also contributing to the differences between experimental and theoretical values. In Chapter 3, the excess noise factor will be reported for different temperatures, what together with dark current measurements will provide a more effective comparison between the theoretical model and the experimental results.

The estimated value for the optimum gain is about 80 for the present LAAPD, independently on the assumed non-uniformity. Despite the difference between this theoretical value and the experimental one, around the optimum gain the energy resolution variation is very small. The measured energy resolution varies between 11.4 and 12.0% for gains between 30 and 80, while the estimated resolution reaches a variation of only 0.1% for gains between 50 and 120. In this case, the choice of the optimum gain is not critical since the LAAPD performance practically does not vary in a reasonable range of gains.

The energy resolution and the minimum detectable energy were determined as functions of the bias voltage for the several investigated photodiodes. The best energy resolution

for 5.9 keV X-rays varies significantly between the different LAAPDs, from 10.3% to 17.9%. The corresponding minimum detectable energy varies from 0.9 to 2.2 keV. These differences are mainly determined by the dark current. Higher dark current corresponds to higher noise levels associated to the LAAPD, affecting the achievable minimum detectable energy and energy resolution.

2.1.2. Spatial non-uniformity

The non-uniformity of the silicon resistivity induces local variations of the gain, affecting the achieved energy resolution. This effect has been investigated for different API photodiodes and the obtained results are described in [Fernandes *et al.* 2001], attached at the end of this chapter.

The non-uniformity was investigated for two different LAAPDs and the relative standard deviation obtained was found to be 3 and 2%, respectively. The effect of non-uniformity is perceptible through the energy resolution variation for different collimation conditions, which can be assessed by comparing the energy resolution obtained for a collimated beam (1 mm diameter) and for the total irradiation of the LAAPD area. The energy resolution increased from 11.8 to 14.9% when beam collimation was removed in the first case (σ_U/G = 3%). In the second case (σ_U/G = 2%), the energy resolution absolute variation is lower than 1% (from 17.9 to 18.8%).

The LAAPD spatial non-uniformity originates gain variations, being able to influence the optimum gain. The LAAPD gain was measured as a function of the bias voltage for X-ray beams with different diameters. Table 2.2 presents the optimum gain and the corresponding LAAPD performance characteristics for the detection of 5.9 keV X-rays. The optimum gain decreases from 52 to 38 as the X-ray beam diameter increases from 1 to 16 mm. However, for collimation diameters larger than 10 mm, the variation of the energy resolution for gains between 38 and 52 is lower than the experimental errors (± 0.2%), leading to the conclusion that the choice of the optimum gain is not critical since the energy resolution variation is very small in the optimum gain vicinities. Table 2.2

also shows that the energy resolution varies with the collimation diameter, increasing from 17.1 to 18.8% as the beam diameter increases from 1 to 16 mm.

Table 2.2 – Optimum gain and corresponding operational characteristics for 5.9 keV X-rays detected in the LAAPD, for X-ray beams with different collimation diameters.

Collimation diameter (mm)	Optimum gain	Minimum detectable energy (keV)	Energy resolution (%)
1	52	2.0	17.1 ± 0.2
5	52	1.9	17.7 ± 0.2
10	44	1.8	18.3 ± 0.2
14	38	1.7	18.7 ± 0.2
16	38	1.8	18.8 ± 0.2

2.1.3. Counting rate capability and space charge effects

The counting rate capability and space charge effects were studied, as described in [Fernandes *et al.* 2001]. The results show that LAAPDs are able to work at counting rates as high as 10^4/s without significant degradation of the relative amplitude and energy resolution. This counting rate capability is even better for shorter shaping time constants due to the shorter pulse duration. Decreasing the shaping constants from 200 to 100 ns provides the detection of counting rates up to 2×10^4/s without significant performance degradation.

The non-linear response of LAAPDs for X-rays with different energies, described in [Fernandes *et al.* 2001] for 5.9 and 22.1 keV X-rays, was also investigated for X-rays with higher energy using a ^{241}Am radioactive source emitting 59.6 keV X-rays. The source also emits X-rays with lower energies, 13.9 and 17.6 keV, corresponding to the

Np fluorescence lines L_α and L_β. The ratio of the pulse amplitudes of 59.6 and 17.6 keV X-ray signals was determined as a function of gain, as presented in Figure 2.4.

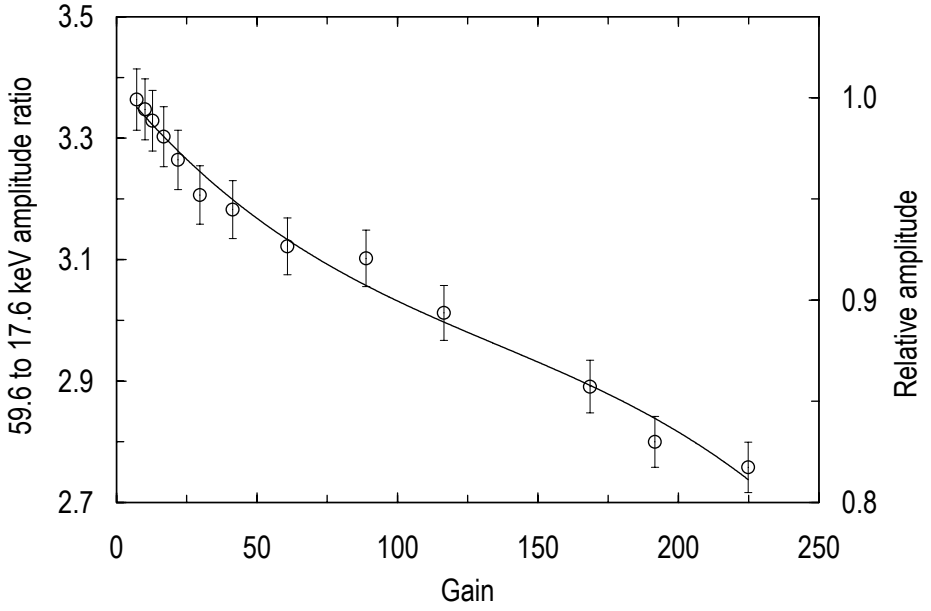

Figure 2.4 – Ratio of the pulse amplitudes for 59.6 and 17.6 keV X-rays emitted by a ^{241}Am radioactive source as a function of gain.

The pulse amplitude ratio between 59.6 and 17.6 keV X-rays presents a variation with gain more significant that the one obtained for 22.1 and 5.9 keV X-rays, mainly at low gains, where the variation seems more pronounced. The variation of the amplitude ratio between both signals resulting from the ^{241}Am source is about 6, 10 and 17% for gains of 50, 100 and 200, respectively, being considerably higher than verified for the preceding case.

The previous results show that the non-linearity between X-rays with different energies can be significant, especially for higher energies. This happens because X-rays of higher energy deposits more energy in silicon, leading to larger avalanches and larger current densities in the photodiode. In Chapter 3, the non-linearity between X-rays with different energies will be investigated as a function of temperature.

The non-linearity of avalanche photodiodes, resulting from space charge effects, is also noticeable in light detection for comparison with X-ray detection. In light measurements

X-rays are frequently used as a reference to determine the energy equivalent to light pulses. This determination is valid as long as space charge effects are negligible. Thus, the use of high energy X-rays or high gains is not recommended since the non-linearity effect can be significant. It is common to use X-rays with energy of about 6 keV and gains up to about 100.

In light detection, photons are generally absorbed before reaching the multiplication region since they present a shorter absorption length in comparison to X-rays. This difference originates different gains for light pulses and X-rays. The ratio between these gains quantifies the LAAPD non-linearity. In section 2.3, the non-linearity effects will be studied relative to the use of X-rays as a reference in VUV light detection comparing the amplitude of the signals produced in the LAAPD by X-rays and VUV scintillation light produced in a GPSC.

2.1.4. Application of LAAPDs to X-ray spectrometry

The application of avalanche photodiodes to X-ray spectrometry was investigated by detecting the fluorescence X-rays resulting from several samples irradiated by ^{55}Fe and ^{109}Cd radioactive sources. Good energy linearity was observed in the energy range from 1.7 to 25 keV for the LAAPD optimum gain [Fernandes *et al.* 2001]. The variation of the energy resolution with the X-ray energy E was also determined. A linear dependence on $E^{-1/2}$ was not demonstrated, especially for higher energies, due to peak distortion. At these energies, a higher fraction of photons interact in the multiplication region, leading to more events partially amplified and pulses with lower amplitude.

Comparatively to typical proportional counters, LAAPDs may achieve better energy resolution, especially at lower energies if the dark current is low enough in order to originate lower noise levels. The X-ray energy distributions obtained with LAAPDs are similar to those obtained with proportional counters [Fernandes *et al.* 2001]. The choice of a LAAPD with low dark current is desirable for X-ray spectrometry applications, providing better performance than a proportional counter.

2.2. Application of pulse risetime discrimination techniques to LAAPDs

The application of digital discrimination techniques to LAAPDs was investigated. The method, based on pulse risetime discrimination, and the obtained results are described in the paper: "Digital risetime discrimination of large-area avalanche photodiode signals in X-ray detection", published in *IEEE Trans. Nucl. Sci.*, vol. 49 (2002), pages 1699-1703 [Fernandes *et al.* 2002B], attached at the end of this chapter (page 67).

The effect of pulse risetime discrimination was studied for 5.9 keV X-rays, operating the LAAPD at the optimum gain. Several energy distributions, corresponding to pulses within different risetime windows, were considered. The effect of the discrimination originates an improvement on the energy resolution and peak-to-background ratio for the obtained partial distributions. It was also shown that the centroid position (for 5.9 keV X-rays) increases slightly with the risetime due to the ballistic deficit.

The ballistic deficit measures the signal amplitude loss due to incomplete signal integration. This happens because, during the creation of the voltage signal in the detector, some charge is lost through the polarization resistance in series with the detector. Thus, the ballistic deficit depends on the shape and duration of the current pulses produced in the detector. In a detector, the charge collection time determines the risetime of the resulting signal. In a LAAPD, X-rays interact at different depths in the silicon, originating pulses with different shapes and risetimes.

The effect of ballistic deficit variation on the signal amplitude can be somewhat corrected normalizing the centroids in the partial distributions obtained for different risetime intervals. For pulses with risetime in the 128-160 ns range, the centroid of each partial distribution (corresponding to time windows of 8 ns width) was normalized to the average value for the distribution resulting from the addition of those distributions. Table 2.3 presents the peak characteristics of the 5.9 keV X-ray signal for three different distributions: the total distribution and two partial distributions for pulses with

risetimes between 128 and 160 ns (corresponding to about 90% of the pulses in the total distribution), obtained before and after the ballistic deficit correction.

Table 2.3 – Peak characteristics of 5.9 keV X-ray signals for the total pulse distribution and two partial distributions obtained before and after the ballistic deficit correction.

Time window	Centroid	Resolution	Peak/Background	Ballistic deficit
TOTAL	379.1	16.5 %	23.4	Not corrected
128-160 ns	378.6	16.1 %	26.5	Not corrected
128-160 ns	378.8	15.1 %	26.3	Corrected

As Table 2.3 shows, the ballistic deficit correction leads to a significant improvement of the energy resolution (from 16.1 to 15.1%) for pulse risetimes between 128 and 160 ns. The peak-to-background ratio practically is not affected by the correction.

The application of pulse risetime discrimination techniques was also investigated for the LAAPD with 10 mm diameter. Since this LAAPD presents lower dark current than the one described in [Fernandes *et al.* 2002B], it provides lower noise levels and consequently better performance in X-ray detection. Therefore, the discrimination effectiveness is smaller for this LAAPD. In Table 2.4 the characteristics of the 5.9 keV X-ray peak are presented for the total distribution and partial pulse distributions for risetimes between 136 and 152 ns.

For both discrimination intervals considered in Table 2.4, the improvement on the energy resolution is not significant. The peak-to-background ratio variation is more pronounced since the background in the amplitude distributions does not depend on the noise but on X-ray interactions inside the LAAPD.

Table 2.4 – Characteristics of the 5.9 keV X-ray peak, obtain in the 10 mm diameter LAAPD, for the total distribution and two partial distributions with different risetime windows.

Time window	Centroid	Resolution	Peak/Background	Relative area
TOTAL	343.3	11.0 %	26.0	100 %
136-144 ns	340.6	10.4 %	31.7	39 %
144-152 ns	345.9	10.6 %	39.4	39 %

In order to verify if the pulse risetime depends on gain, the 10 mm diameter LAAPD was operated with gains of 45, 95 and 190. Figure 2.5 represents the corresponding risetime distributions of pulses produced by 5.9 keV X-ray interactions in the LAAPD. The figure shows small variations of the risetime distributions with gain. However, the average pulse risetime tends to decrease slightly with the gain.

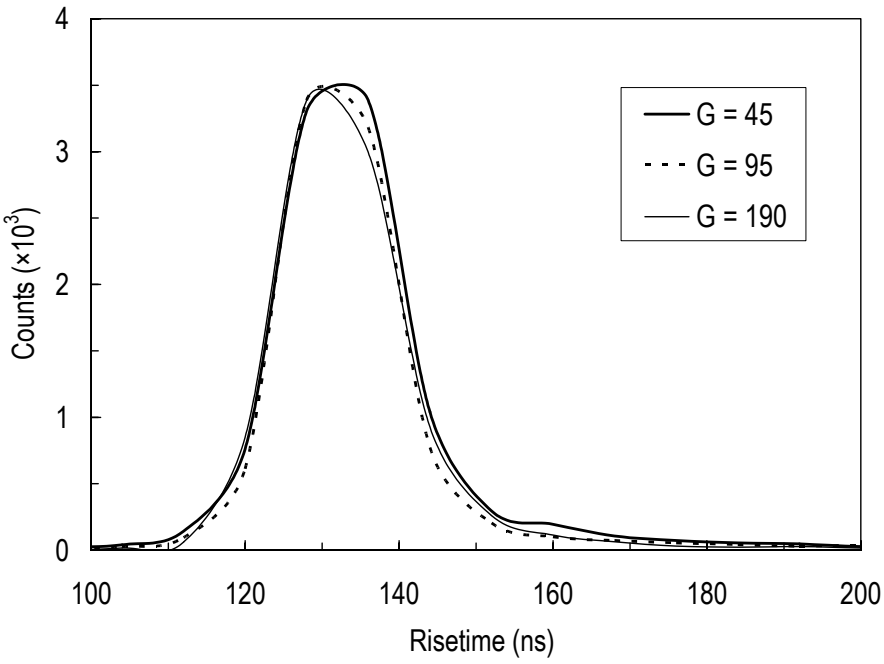

Figure 2.5 – Risetime distributions of pulses produced by 5.9 keV X-rays interacting in the 10 mm diameter LAAPD, for different gains.

The effect of risetime discrimination in the pulses produced by 5.9 keV X-rays was measured for the different gains. Table 2.5 shows the variation of the energy resolution and peak-to-background ratio before and after the discrimination for pulses with risetimes between 128 and 144 ns, using different gains in the photodiode. The fraction of pulses with risetimes in the 128-144 ns range is indicated by the relative area of the corresponding peak.

Table 2.5 – Variation of the energy resolution and peak-to-background ratio for 5.9 keV X-ray pulses, from the total distribution to the one with risetimes between 128 and 144 ns, for different LAAPD gains.

Gain	Energy resolution	Peak/Background	Relative area
45	12.3 → 11.9 %	38 → 55	84 %
95	13.5 → 13.2 %	27 → 34	89 %
190	17.7 → 17.2 %	27 → 32	79 %

Table 2.5 shows that the discrimination of pulses with risetime between 128 and 144 ns does not result in a significant improvement on the energy resolution for the used gains. However, the increase of the peak-to-background ratio is more significant for a gain of 45. Thus, the use of gains close to the optimum value also improves the pulse risetime discrimination when compared to higher gains.

The risetime of LAAPD pulses was measured for different X-ray energies, obtained by fluorescence of some elementary samples. No significant dependence of the risetime distribution on the energy was observed. However, the average value of the distribution tends to decrease as the energy increases. For higher energies, X-rays tend to be absorbed more deeply in the silicon and charges produced in the LAAPD cover a smaller distance until being collected. As a result, the collection time of those charges is shorter, the same happening with the risetime of the resulting pulses.

The effect of risetime discrimination was evaluated in the LAAPD response to low energy fluorescence X-rays emitted by sulphur and silicon samples irradiated by a ^{55}Fe source. Since lower energy X-ray signals are closer to the noise level, the effect of the discrimination is greater. The main advantage of the risetime discrimination is the significant improvement of the peak-to-background ratio. The electronic noise can be efficiently discriminated since the corresponding pulses present longer risetimes than the X-ray pulses. However, if the threshold in the digitizer board is set below the noise level, the data-acquisition throughput is reduced due to the additional time needed for the analysis of noise pulses.

Further than the risetime discrimination, other techniques of background reduction can be used in order to improve peak discrimination in the amplitude spectra. In particular, other techniques will be discussed in Chapter 4, such as the X-ray discrimination by coincidence with electrons resulting from muon decay.

2.3. Non-linearity of the LAAPD response to X-rays compared to VUV-light detection

For long times, the photomultiplier tube was considered the preferred photosensor to convert into a charge signal the scintillation light produced inside a scintillator or a gas proportional scintillation counter. The incorporation of a silicon photodiode in the GPSC volume in order to detect the VUV light there produced was tested, providing a system more compact, robust and simple to operate comparatively to the GPSC with PMT [Lopes *et al.* 2000A].

In general, the detection of the scintillation light of rare gases in a GPSC requires special windows to separate the photosensor from the GPSC volume. The use of these windows limits the photosensor applications since a significant part of scintillation photons is absorbed by the window and the greater distance between the photosensor and the window leads to a reduction on the solid angle. As a result, the number of

collected photons decreases. The need for a window becomes particularly disadvantageous in high pressure (a few atm) applications. The LAAPD does not need a window, being able to be integrated in the gaseous volume of a GPSC [Lopes *et al.* 2000B]. The advantages of the LAAPD in comparison to the PMT had already been discussed in Chapter 1. The development of LAAPDs with a very thin entrance layer, transparent to VUV radiation, has provided high quantum efficiencies for VUV light, reaching about 115% at 170 nm [Canfield *et al.* 1998]. More recently, a series of LAAPDs with quantum efficiencies close to those values were produced by API (the *windowless UV-enhanced series*). Being robust, compact and not requiring a radiation window, the VUV-sensitive LAAPD can be integrated in a GPSC in direct contact with the gas, leading to a more efficient conversion of the scintillation light into charge carriers. Such a LAAPD was tested as photosensor in a GPSC containing xenon [Lopes *et al.* 2001] and argon [Monteiro *et al.* 2001].

The characterization of avalanche photodiodes used as photosensors requires the determination of the number of electron-hole pairs produced by the scintillation light per unit of absorbed energy, providing a quantitative analysis of the number of photons emitted by the luminous source, the noise sources contributing to the energy resolution and the quantum efficiency of the LAAPD. The number of electron-hole pairs can be determined by comparing the amplitude of the signal produced in the photodiode by direct absorption of X-rays and the signal produced by light. The comparison is valid assuming linearity between the initial number of electron-hole pairs and the amplitude of the resulting pulse throughout the range of gains. However, the non-linearity reported at high current densities and attributed to space charge effects originates reduced localised electric fields and heating in the avalanche region [Allier *et al.* 1998].

The non-linear response of a LAAPD manufactured by API for detection of VUV light with wavelength about 128 and 173 nm, produced by 5.9 keV X-rays absorbed in a GPSC containing argon and xenon, respectively, was investigated. The results are presented in the paper: “Non-linear behaviour of large-area avalanche photodiodes”, published in *Nucl. Instr. Meth. A,* vol. 478 (2002), pages 395-399 [Fernandes *et al.* 2002A], attached at the end of this chapter (page 73).

X-rays incident in the GPSC window are mostly absorbed in the gas, originating scintillation light, which is collected by the LAAPD. However, a fraction of X-rays is transmitted through the gas, being directly detected in the photodiode. Since the X-ray transmission through xenon is much lower than the one for argon, the GPSC containing xenon was made without drift region. The LAAPD non-linearity can be evaluated by the simultaneous detection of both signals produced in the LAAPD, in each case.

Figure 2.6 represents the ratio of the pulse amplitudes corresponding to 5.9 keV X-rays and VUV scintillation light produced inside the gas volume (argon and xenon) of a GPSC instrumented with a LAAPD, as a function of the light gain. The deviation from linearity increases with gain. The variation of the relative amplitude is approximately linear, reaching 7 and 10% for xenon and argon, respectively, for gains of about 200. These values are considerably higher than the ones reported for visible light (3% for maximum gains) [Moszynski *et al.* 2002A].

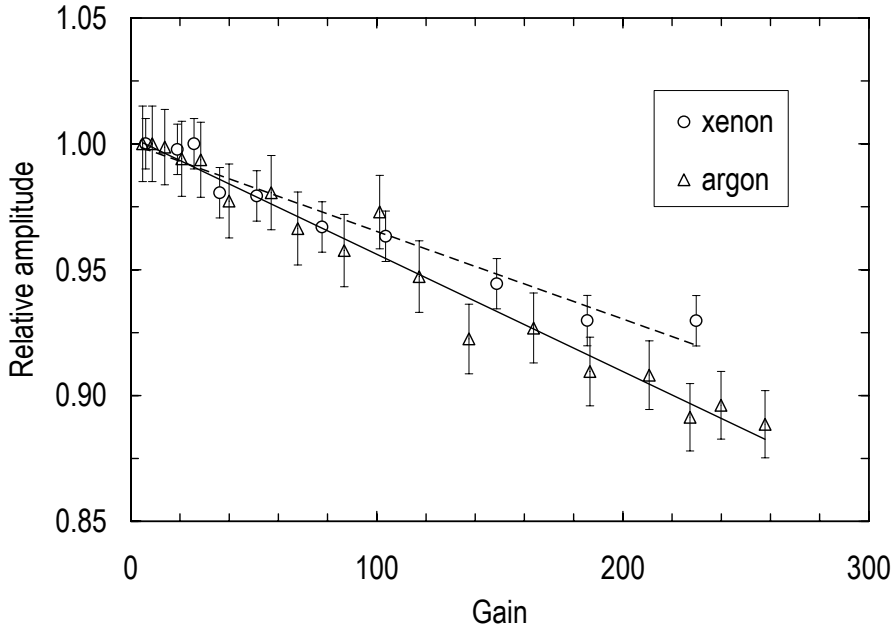

Figure 2.6 – Amplitude ratio between the pulses produced in the LAAPD by 5.9 keV X-rays and VUV scintillation light of argon (~128 nm) and xenon (~173 nm) as a function of gain.

The non-linearity study was also extended to higher energy X-rays, more precisely 22.1 keV X-rays emitted by a ^{109}Cd radioactive source. The variation of the amplitude ratio

between X-ray signals and VUV-light pulses was found to be significantly higher than it was measured for 5.9 keV X-rays, reaching about 13% for a gain of 200. This confirms the LAAPD non-linearity for X-rays with different energies, already stated before and attributed to space charge effects. In addition, the X-ray absorption length increases rapidly for energies above 2 keV, reaching more than 1 mm for 22.1 keV. As a result, the number of interactions in the multiplication zone increases and the pulse amplitude distribution becomes more asymmetrical in the low-energy zone, leading to a reduction of the average amplitude of the obtained signals.

The present study confirms the non-linear behaviour of avalanche photodiodes manufactured by API in VUV-light detection. The results suggest a dependence of the non-linearity on the light wavelength. The non-linearity is more significant for argon scintillation (~128 nm) comparatively to xenon scintillation (~173 nm) and visible light (~600 nm). These results lead to the conclusion that non-linearity cannot be exclusively attributed to space charge effects resulting from the local absorption of X-rays at high gains, being related to the average absorption length of each type of light in silicon.

For both types of light, VUV and visible, photons are absorbed in the drift zone of the LAAPD, where the electric field is very weak and the effect of capture of the produced charges is more significant. Since the absorption is much more superficial for VUV light (~5 nm), the capture effect is greater in this case, but decreases with gain due to the increase of the electric field. Therefore, the VUV-light gain increases slightly relatively to the visible-light gain, whose photons interact more deeply in the LAAPD. Subsequently, the ratio between X-ray and light gains is higher for VUV light.

An accurate determination of the number of charge carriers produced in the LAAPD by VUV scintillation light may be compromised by the stated non-linearity effect. However, for the LAAPD optimum gain, the effect is very small and X-rays (with energy of about 6 keV) can be used as a reference to determine the number of charges produced by the scintillation light.

X-RAY SPECTROMETRY
X-Ray Spectrom. 2001; **30**: 164–169

Application of large-area avalanche photodiodes to energy-dispersive x-ray fluorescence analysis†

L. M. P. Fernandes, J. A. M. Lopes, J. M. F. dos Santos* and C. A. N. Conde

Physics Department, University of Coimbra, P-3004-516 Coimbra, Portugal

Received 27 October 2000; Accepted 15 January 2001

The performance of several large-area avalanche photodiodes (LAAPDs) for application to x-ray spectrometry at room temperature was investigated. Optimum detector performance was obtained for gains of about 50–70. Good energy linearity of the LAAPDs' response to x-rays was observed up to energies of about 25 keV. For this energy range the space charge effects are negligible for gains below 100–150. The energy resolutions obtained with LAAPDs can be better than those obtained with proportional counters. Our results indicate that the energy resolution of an LAAPD is better than that of a proportional counter only when the LAAPD maximum dark current is <300 nA. For this case, minimum detectable x-ray energies of about 1 keV are possible. Spatial non-uniformity is responsible for an absolute increase of 1–2% in energy resolution at 6 keV when illumination of the LAAPD is broadened from 1 mm diameter to full area. Counting rates up to 5×10^4 counts s^{-1} are possible without significant degradation of detector performance.

INTRODUCTION

Avalanche photodiodes (APDs) are compact, monolithic devices made of a silicon p–n junction where the internal electric field can reach values high enough to allow electron multiplication by impact ionization.[1–3] When a high voltage is applied to the APD, only a small region of the p layer, at the front of the diode, remains undepleted—the drift region (Fig. 1). The electric field in this region is low but, in the depleted region, increases with depth, reaching a maximum around the p–n junction. An incident photon absorbed in the drift region or in the p-depleted layer produces electron–hole pairs. The resulting electrons are accelerated towards the n^+ contact and undergo avalanche multiplication owing to the high electric field around the junction. Charge gains of a few hundred are typical and increase exponentially with applied voltage, resulting in a significant improvement of the signal-to-noise ratio. Detailed operation principles of this device have been discussed in the literature.[1–3]

Non-uniformity has been a major drawback in the manufacture of large-area APDs and has limited their applications. Recently, large-area avalanche photodiodes (LAAPDs) have been developed with improved spatial uniformity, delivering higher gains at lower bias voltages[3] (Advanced Photonix, Camarillo, CA, USA; Radiation Monitoring Devices, Watertown, MA, USA). Windowless LAAPDs with extended sensitivity to UV and soft x-ray regions are also commercially available.

Interest in applications of LAAPDs has been increasing over the last several years. They are used mostly as optical photodetectors coupled to scintillators for x- and γ-ray detection in substitution of photomultipliers[3–5] (M. Moszynski, M. Kapusta, J. Zalipska, M. Balcerzyk, D. Wolski, M. Szawlowski and W. Klamra, presented at the 1999 IEEE Nuclear Science Symposium, 24–30 October, Seattle, WA, USA; M. Kapusta, M. Moszynski, M. Balcerzyk, K. Lesniewski, and M. Szawlowski, presented at the 1999 IEEE Nuclear Science Symposium, 24–30 October, Seattle, WA, USA). The feasibility of using LAAPDs as x-ray detectors has been demonstrated[2] (M. Moszynski, M. Szawlowski, M. Kapusta, M. Balcerzyk and D. Wolski, presented at the 1999 IEEE Nuclear Science Symposium, 24–30 October, Seattle, WA, USA). Since the useful thickness for x-ray detection is only a few tens of micrometers, the LAAPD detection efficiency decreases rapidly for energies above 5 keV, being about 45, 25, 8 and 4% for 8, 10, 15 and 20 keV, respectively.[1,6] Although their use as x-ray detectors in the 0.5–20 keV range has been suggested[6–8] (M. Moszynski, M. Szawlowski, M. Kapusta, M. Balcerzyk and D. Wolski, presented at the 1999 IEEE Nuclear Science Symposium, 24–30 October, Seattle, WA, USA), low-energy x-ray detection techniques with APDs were mainly developed to measure charge-carrier properties of the device, using x-rays as a reference for light measurements[3,6,8,9] (M. Moszynski, M. Szawlowski, M. Kapusta, M. Balcerzyk and D. Wolski, presented at the 1999 IEEE Nuclear Science Symposium, 24–30 October, Seattle, WA, USA).

In this work, the performance of LAAPDs, working at room temperature, for energy-dispersive x-ray fluorescence analysis is presented. Energy linearity, energy resolution and count-rate capability were studied as a function of x-ray energy. The effects of detector dark current and gain on the minimum detectable x-ray energy and on the detector energy

*Correspondence to: J. M. F. dos Santos, Physics Department, University of Coimbra, P-3004-516 Coimbra, Portugal.
†Presented at the European Conference on EDXRS, Krakow, Poland, 18–23 June 2000.
Contract/grant sponsor: CERN; Contract/grant number: CERN/P/FIS/15200/99.

DOI: 10.1002/xrs.481

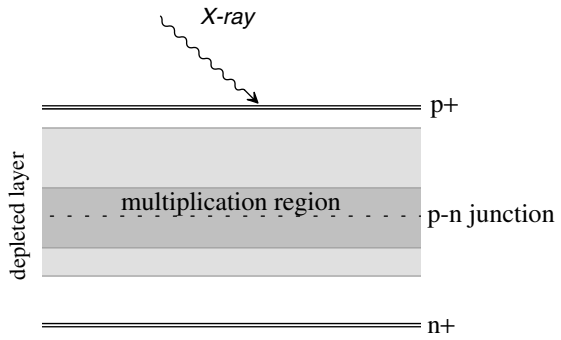

Figure 1. Schematic diagram of typical avalanche photodiode section.

resolution are discussed. Space charge effects for high gains and high-energy x-rays were investigated.

EXPERIMENTAL

Several LAAPDs were investigated. All diodes were of the windowless, UV-enhanced type, produced recently by Advanced Photonix. Three of them are of 16 mm diameter and one of 10 mm diameter. Table 1 lists the main characteristics for each diode according to its data sheet.

The LAAPD was operated in a light-tight box to shield it from ambient light. The LAAPD signals were fed through a low-noise charge preamplifier (Canberra 2004, with a sensitivity of 45 mV MeV^{-1}) to a spectroscopy amplifier (HP5582A, with a gain of 32–256) and sorted in a 1024-channel multi-channel analyser (Nucleus PCA II). For pulse-amplitude and energy-resolution measurements, the x-ray pulse-height distributions were fitted to a Gaussian function superimposed on a linear background, from which the centroid and the full width at half-maximum were determined.

OPERATIONAL CHARACTERISTICS

The detector characteristics were evaluated with 5.9 keV Mn Kα x-rays from a ^{55}Fe source. The 6.4 keV Mn Kβ x-rays were removed by absorption in a chromium filter. These characteristics included determinations of the optimum LAAPD operating voltage and gain, energy resolution, dark current effect, spatial uniformity, lowest detectable x-ray energy and count rate capability. The incident x-ray flux was limited to few thousand photons per second except for the count-rate behaviour study. Optimum shaping time

Table 1. LAAPD parameters just before breakdown, from the data sheets

LAAPD No.	Diameter (mm)	Voltage (V)	Gain	Dark current (nA)
1	16	1840	317	201
2	16	1851	312	336
3	16	1849	303	499
4	10	1873	314	222

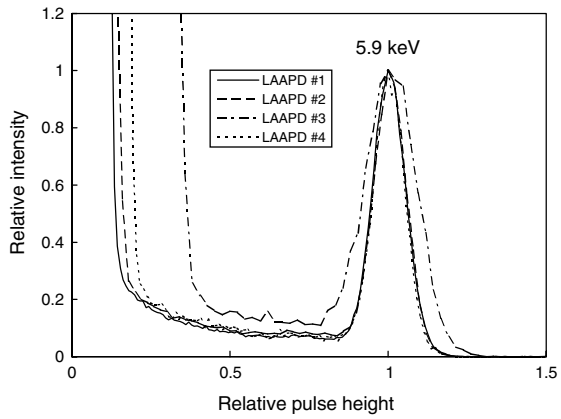

Figure 2. Typical pulse-height distributions for the LAAPDs used in this work for 5.9 keV x-rays, illustrating the low-energy-noise-tail limit.

constants used in the amplifier were found to be about 0.1–0.2 μs.

Figure 2 shows a typical pulse-height distribution for the 5.9 keV x-rays for the different photodiodes. The peak departs from a Gaussian shape, presenting a tail towards the low-energy region. This tail results from x-ray interactions deep within the photodiode multiplication region (Fig. 1), generating pulses that are only partially amplified, resulting in reduced pulse amplitudes.[1] Similarly, x-ray interactions that occur in the weak electric field of the undepleted p-region may result in primary electrons being lost to the front p^+ contact or to traps, again leading to smaller amplitude pulses.[1] The electronic noise tail in the low-energy limit depends on the photodiode dark current and sets a limit to the lowest detectable x-ray energy.

LAAPD gain

Figure 3 depicts the detector gain, energy resolution and low-energy noise tail limit as a function of LAAPD 4 bias voltage, for 5.9 keV x-rays. The relative pulse amplitude was normalized to the value obtained at 1400 V, corresponding to a gain of 3.5 according to the manufacturer. The variation

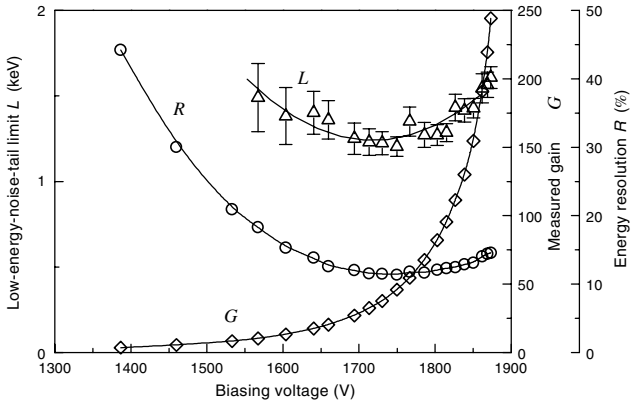

Figure 3. LAAPD 4 relative pulse amplitude, energy resolution and low-energy noise tail limit as a function of reverse bias voltage, for 5.9 keV x-rays. Relative pulse amplitude and energy resolution experimental uncertainties fall within the symbol size.

XRS

Table 2. Optimum performance characteristics for the LAAPDs in this work, for 5.9 keV x-rays

LAAPD No.	Measured gain	Low-energy noise tail limit (keV)	Energy resolution (1 mm collimation) (%)	Energy resolution (full area) (%)
1	72	0.9	10.3	12.3
2	53	1.1	11.8	14.9
3	52	2.2	17.9	18.8
4	46	1.2	11.4	12.3

of detector gain is in good agreement with the exponential gain of the LAAPD specified by the manufacturer. However, the best detector energy resolution is achieved for gains of only 50–70 and degrades with gain at higher values. At these gains, the low-energy noise tail limit has already stabilized around its minimum and increases slightly at higher gains. Table 2 presents the best energy resolutions, low-energy noise tail limit and gains obtained for the different LAAPDs for both 1 mm diameter and full-area x-ray beam illumination.

Dark current effects

Figure 2 and Tables 1 and 2 illustrate the effect of the dark current on LAAPD performance. Higher dark currents result in reduced performance for both detector energy resolution and lowest detectable x-ray energy. The degradation in detector energy resolution with detector bias voltage, for gains above ~50–70, as shown in Fig. 3, is mainly due to the greater increase in dark current.[10] The optimum operating gain depends on the individual LAAPD, and a compromise between gain and dark current has to be obtained for each one.

We note that all the 16 mm diameter LAAPDs used in this work are within the manufacturer's specifications for a maximum dark current of 600 nA at a gain of 200. Still, photodiode performance can be significantly different.

Spatial uniformity

Non-uniform material resistivity of the LAAPD results in gain fluctuations due to localized electric field variations. Thus, the LAAPD response can vary with the x-ray incidence point on the LAAPD surface. Spatial uniformity was studied using a 0.5 mm collimated x-ray beam positioned at 17 equally distributed points over the area of the photodiode: one point at its center and eight points at radial distances of 3 and 6.5 mm for the 16 mm diameter LAAPDs.

The distributions of the gains of LAAPDs 2 and 3, normalized to the average value, are given in Table 3. A ±4% variation of the x-ray pulse amplitude due to non-uniformities was observed. For LAAPD 2, only 50% of the amplitudes are within ±1.5% of the average. The same trend was noted for the different LAAPDs and the results do not suggest any correlation between dark current and non-uniformity. On the other hand, detector non-uniformity increases with increasing gain. This effect is related to the photodiode bias voltage increase, which results in larger local differences of the electric field within the depletion region, leading to larger differences on the avalanche multiplication gain.

Table 3. Distributions of pulse amplitudes normalized to the average value for a 0.5 mm collimated 5.9 keV x-ray beam, measured at 17 points, equally distributed over the photodiode area: one point at its center and 8 points at radial distances of 3 and 6.5 mm for both LAAPD 2 and LAAPD 3

	Normalised amplitude								
LAAPD No.	0.96	0.97	0.98	0.99	1.00	1.01	1.02	1.03	1.04
2	1	1	3	6	1	2	1	2	0
3	1	1	0	6	4	2	1	0	2

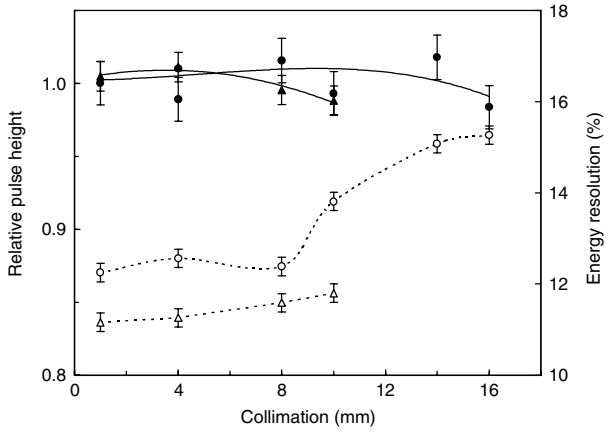

Figure 4. Energy resolution (●, LAAPD 2; ▲, LAAPD 4) and relative amplitude (○, LAAPD 2; △, LAAPD 4) as a function of the x-ray collimation for 5.9 keV x-rays.

As a consequence of the LAAPD non-uniformity, energy resolution degrades with the collimating diameter at the front of the device. In Fig. 4, the detector energy resolution is presented as a function of the x-ray collimation for LAAPDs 2 and 4. A small degradation of the energy resolution is observed, reflecting the small spatial non-uniformity of the diodes.

Count rate capability

The detector pulse amplitude and energy resolution as a function of count rate was investigated for collimated 5.9 keV x-ray beams, 8 mm in diameter, for LAAPD 4. Figure 5 presents the results obtained for LAAPD 4. Count rates of about 4×10^4 counts s^{-1} are possible without significant degradation of LAAPD performance. At this count rate, a reduction of 3% in the pulse amplitude and a degradation from 12% to 13% in the energy resolution were measured. This behaviour results from the short pulse duration (a few

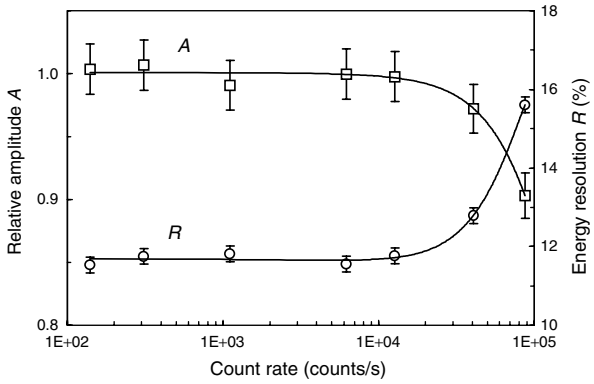

Figure 5. LAAPD 4 relative pulse amplitude and energy resolution as a function of count rate for 8 mm diameter collimated 5.9 keV x-rays.

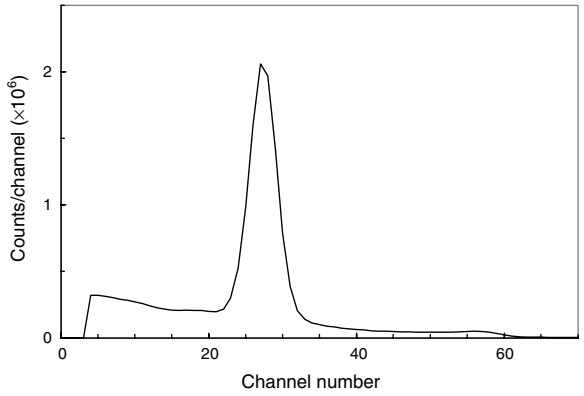

Figure 6. Typical pulse-height distribution for 8×10^4 counts s^{-1} count rate, for 8 mm diameter collimated 5.9 keV x-rays.

hundred nanoseconds), making it possible to count at rates as high as 10^5 counts s^{-1} without significant degradation of the pulse-height distributions. Figure 6 presents the measured pulse-height distribution of x-rays from a ^{55}Fe source for a count rate of 8×10^4 counts s^{-1} and a shaping time of 0.1 μs. No distortions of the peak shape are observed except for the small tail due to pulse pile-up. The same trend was observed for LAAPD 2.

Space charge effects

Space charge effects can be caused by high signal current densities produced by either high-energy x-rays and/or high gains, resulting in a decrease in the electric field and local heating in the avalanche region (M. Moszynski, M. Szawlowski, M. Kapusta, M. Balcerzyk and D. Wolski, presented at the 1999 IEEE Nuclear Science Symposium, 24–30 October, Seattle, WA, USA). These result in a non-linear response of the LAAPD.

We investigated the detector linearity by comparing the LAAPD pulse amplitudes for 5.9 and 22.1 keV x-rays as a function of gain. The results obtained are depicted in Fig. 7. The 22.1-to-5.9 keV pulse amplitude ratio decreases with increasing gain. However, this effect is negligible for gains below 100, and is only noticeable for gains above 150. A decrease of <1% is found for gains up to 100, whereas for

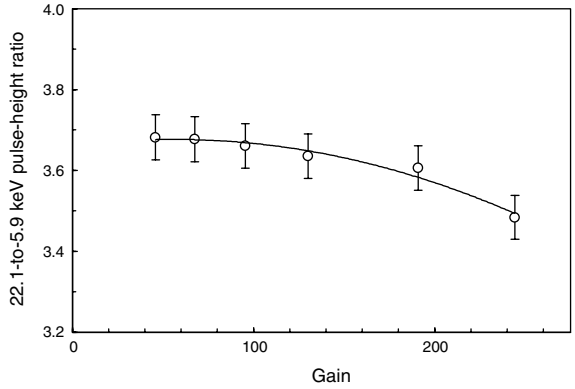

Figure 7. 22.1/5.9 keV x-ray pulse amplitude ratio as a function of LAAPD 4 gain.

gains of about 200 and 250 this decrease is about 3 and 6%, respectively.

Temperature dependence

LAAPD gain and dark current depend significantly on temperature.[8,10] Dark current can be reduced by about one order of magnitude and the minimum detectable energy can be reduced by a factor of two when the LAAPD temperature is reduced from room-temperature to 0 °C.[8] LAAPDs with built-in Peltier cooling devices for controlled-temperature operation are commercially available (Advanced Photonix). During our experiments, room temperature was stabilized at 20 ± 0.3 °C, and gain fluctuations of <1% were observed.

X-RAY SPECTROMETRY APPLICATIONS

Energy linearity and resolution

The energy linearity and energy resolutions of the LAAPDs were determined in the 2–25 keV x-ray energy range using the fluorescent radiation induced in single-element samples (Si, S, Cl, Ca, Ti, Cr, Mn, Fe, Ni, Zn, As, Se, Rb, Nb and Cd) and using direct irradiation of the detector with ^{55}Fe and ^{109}Cd x-ray sources. The measurement geometries are depicted to scale in Fig. 8 for direct irradiation (a) and for fluorescence measurements (b). To delimit the incident x-ray beam, 1 and 5 mm lead collimators were used for (a) and (b), respectively.

LAAPD 4 was used for this study and was operated in the optimum gain region with total count rates of the order of 10^3–10^4 counts s^{-1}. The centroids and relative full width at half-maximum values of the pulse-height distributions are plotted in Fig. 9 as a function of x-ray energy. Good energy linearity is observed throughout the energy range.

The detector energy resolution does not demonstrate a linear dependence on $E^{-1/2}$ but decreases slowly in the high-energy range limit. This behaviour can be attributed to peak distortion due to an increasing number of x-ray interactions in the multiplication region. Fig. 10 plots the LAAPD energy resolution as a function of $E^{-1/2}$. For comparison, a typical energy resolution (14% at 6 keV) of a proportional counter is also depicted. For x-ray energies below 4 keV, the LAAPD energy resolution is worse than the PC. Also, in the high-energy limit above 17 keV, the energy resolution tends to be higher than the PC.

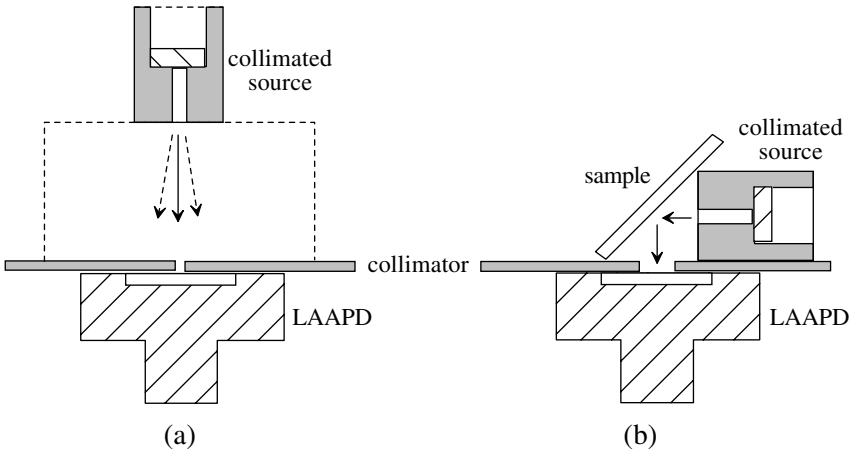

Figure 8. Set-up used for the measurements: (a) direct x-ray source irradiation; (b) fluorescence x-rays.

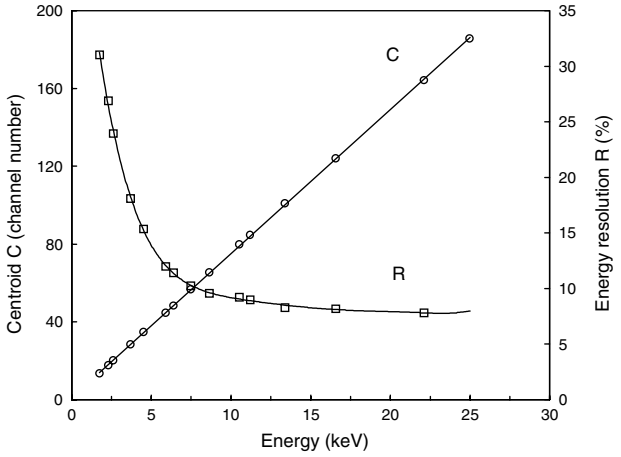

Figure 9. Peak centroid and energy resolution as a function of x-ray energy for LAAPD 4. The experimental uncertainties fall within the symbol size.

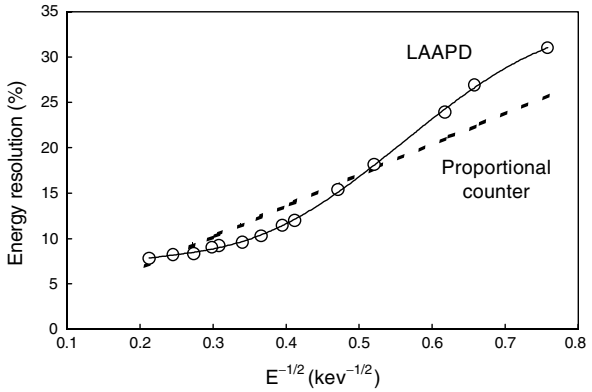

Figure 10. LAAPD energy resolution as a function of $E^{-1/2}$. The dashed line is the typical energy resolution of a proportional counter (PC) with an energy resolution of 14% at 6 keV. The experimental uncertainties fall within the symbol size.

A typical x-ray spectrum obtained for the ^{109}Cd source is presented in Fig. 11 for an applied reverse bias voltage of 1750 V in the LAAPD at a count rate of 500 counts s^{-1} for a period of 500 s.

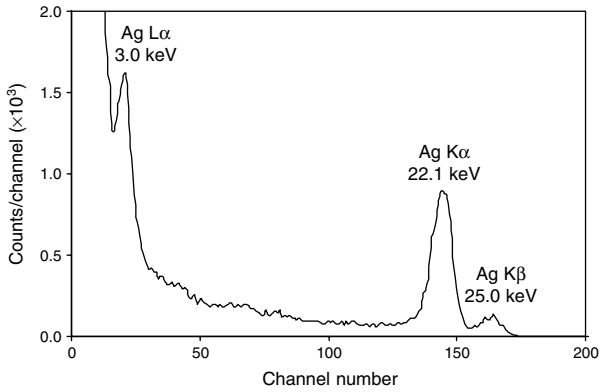

Figure 11. Typical x-ray spectrum obtained for the ^{109}Cd source.

Multi-element target samples

Using the same geometry, x-ray fluorescence spectra were measured for thick samples of gypsum ($CaSO_4$), non-homogeneous pyrite/chalcopyrite and SAES ST707 getter (70% Zr, 5.4% Fe and 24.6% V), excited with a ^{109}Cd x-ray source. The resulting pulse-height distributions are depicted in Fig. 12(a), (b) and (c), respectively. Spectral features include the elemental K-lines, the source backscattered radiation and the Pb L-lines from the source shielding and collimator [Fig. 12(b) and (c)]. The spectra are similar to those achieved with a conventional proportional counter, except for the soft x-ray region, where the windowless LAAPD detector can have an advantage if the device dark current is low enough to allow the detection of the x-ray pulses above the low-energy noise tail.

DISCUSSION

The performance characteristics of the room-temperature response of several LAAPDs to x-rays have been investigated. The results obtained demonstrate the applicability of LAAPDs to x-ray spectrometry in the 2–25 keV range. The optimum detector operating gain, the influence of the dark current on the detector performance, the uniformity of the spatial response and the count rate capability were evaluated. Energy resolution and linearity and also space charge effects were determined for x-rays in the range 2–25 keV.

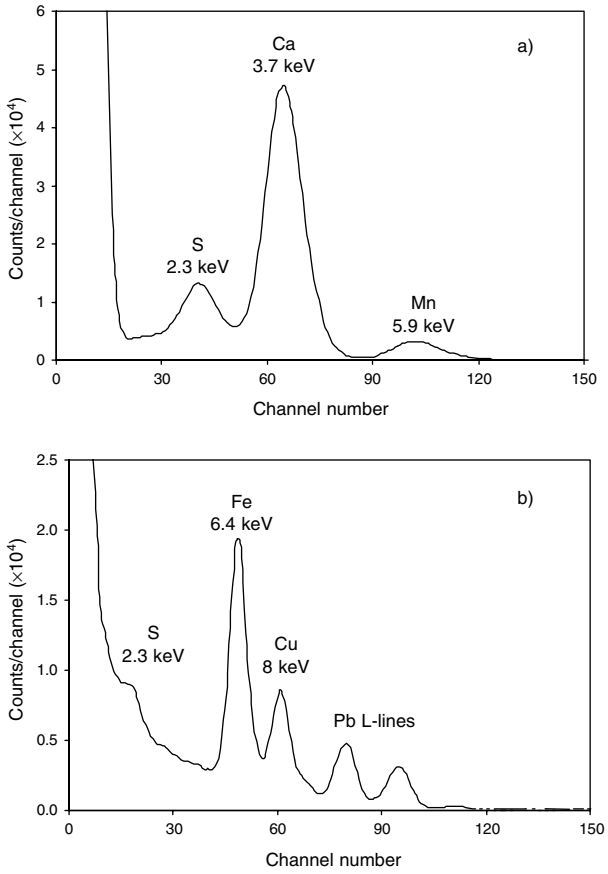

Figure 12. X-ray fluorescence spectra obtained with a ^{109}Cd x-ray source for thick samples of (a) gypsum ($CaSO_4$); (b) non-homogeneous pyrite/chalcopyrite; (c) SAES ST707 getter (70% Zr, 5.4% Fe and 24.6% V).

Compared with proportional counters, the LAAPD is more compact and may provide improved energy resolutions for x-ray energies from a few up to about 20 keV. However, both energy resolution and minimum detectable x-ray energy depend on the LAAPD dark current, and LAAPDs within the manufacturer's specifications may present significantly different performances. For x-ray spectrometric applications, LAAPDs with low dark currents are desirable in order to obtain better energy resolutions than proportional counters.

The LAAPD cost, limited area, limited detection efficiency for medium- and high-energy x-rays, and

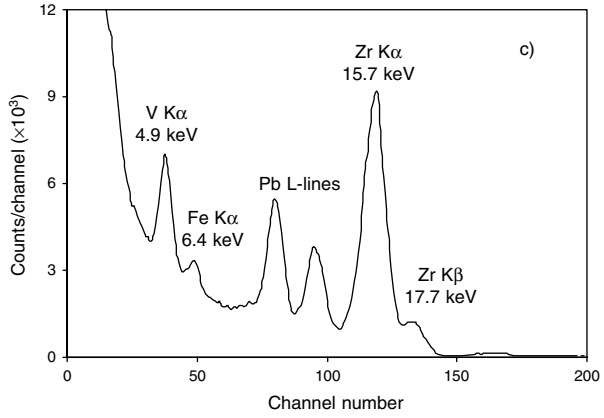

Figure 12. (*continued*).

sensitivity to light and temperature are drawbacks compared with proportional counters. However, its windowless feature may be crucial for the detection of soft x-rays. Additionally, its superior count-rate capability may be crucial for applications at high count rates.

Acknowledgements

The work was carried out in the Atomic and Nuclear Instrumentation Group of the Instrumentation Centre (Unit 217/94) of Departamento de Física, Universidade de Coimbra. Support is acknowledged from project CERN/P/FIS/15200/99.Thanks are due to R. E. Morgado, Los Alamos National Laboratory (LANL), Los Alamos, NM, USA, for revision of the manuscript.

REFERENCES

1. Baron AQR, Ruby SL. *Nucl. Instrum. Methods A* 1994; **343**: 517.
2. Gullikson EM, Gramsch E, Szawlowski M. *Appl. Opti.* 1995; **34**: 4662.
3. Pansart JP. *Nucl. Instrum. Methods A* 1997; **387**: 186.
4. Farrell R, Olschner F, Frederick E, McConchie L, Vanderpuye K, Squillante MR, Entine G. *Nucl. Instrum. Methods A* 1990; **288**: 137.
5. Lopes JAM, dos Santos JMF, Conde CAN. *Nucl. Instrum. Methods A* 2000; **454**: 421.
6. Farrel R, Vanderpuye K, Entine G, Squillante MR. *IEEE Trans. Nucl. Sci.* 1991; **38**: 144.
7. Webb PP, McIntyre RJ. *IEEE Trans. Nucl. Sci.* 1976; **23**: 138.
8. Ochi A, Nishi Y, Tanimori T, *Nucl. Instrum. Methods A* 1996; **378**: 267.
9. Allier CP, Valk H, Bom VR, Hollander RW, van Eijk CWE. *IEEE Trans. Nucl. Sci.* 1998; **45**: 576.
10. LAAPD Application Notes. Advanced Photonix, Camarillo, CA, 1999.

Digital Rise-Time Discrimination of Large-Area Avalanche Photodiode Signals in X-Ray Detection

L. M. P. Fernandes, P. C. P. S. Simões, J. M. F. dos Santos, and R. E. Morgado

***Abstract*—The response of a large-area avalanche photodiode to X-rays was investigated by applying pulse-shape discrimination techniques based on rise time. The method employed analog preshaping with time constants of 200 ns followed by digital signal processing in a commercial 125-MHz digitizer. Pulse rise-time discrimination was applied to improve detector energy resolution, background level, and peak distortion. Electronic noise pulses can be efficiently removed at the expense of data-acquisition throughput.**

***Index Terms*—Avalanche photodiode, pulse-discrimination efficiency, rise-time discrimination, X-ray detection.**

I. Introduction

INTEREST in the use of avalanche photodiodes (APDs) has increased recently with the appearance of commercially available large-area APDs that deliver higher charge gains at lower bias voltages, with improved spatial uniformity. Windowless large-area APDs with extended sensitivity in the ultraviolet and soft X-ray regions are also commercially available.

Large-area APDs are used mainly as optical photosensors coupled to scintillators for X- and γ-ray detection, as a replacement for photomultiplier tubes [1]–[4]. Applications include instrumentation of the large electromagnetic calorimeter of the CERN CMS detector for high-energy physics [1], [5], [6] and the photosensor readout of crystals and plastic scintillators for γ-ray spectrometry in nuclear physics [7], [8] and for positron emission tomography instrumentation in medicine [9], [10]. Although their use as X-ray spectrometers in the 0.5–20 keV range has been suggested [11]–[13], low-energy X-ray detection techniques with APDs were mainly developed to measure charge-carrier properties of the device, using X-rays as a reference for light measurements [1], [13], [14].

The application of large-area APDs (LAAPDs) to energy-dispersive X-ray fluorescence (EDXRF) analysis has been investigated, and energy resolutions similar to those of proportional counters have been achieved [15]. Additionally, the use of LAAPDs in an experiment to measure the Lamb shift of the $2S$–$2P$ atomic states in muonic hydrogen (μp) is being considered [16]. The experiment, to be carried out at the Paul Scherrer Institute (PSI), Switzerland, in collaboration with nine institutions, consists in obtaining long-lived μp atoms in the $2S$-metastable state by stopping a low-energy μ^- beam in a small volume of low-pressure hydrogen in a 5-T magnetic field. A pulsed beam from a tunable laser induces the $2S$–$2P$ transition in μp, and the 1.9-keV X-ray photons resulting from the $2P$–$1S$ deexcitation will be detected. Measuring the coincidences between the laser pulse and the 1.9-keV X-rays as a function of the laser wavelength, the Lamb shift can be determined. Low counting rates are expected, and the 1.9-keV X-ray background will be reduced by gating its coincidence with the signal resulting from the high-energy electron produced in the subsequent muon decay.

However, improvements on the performance of LAAPDs for X-ray detection, mainly in the low-energy range, are needed. One way to improve this performance may be through the application of pulse discrimination techniques. Fully developed X-ray pulses can be effectively distinguished from noise, distorted X-ray pulses, and pulses resulting from charged-particle interactions.

Digital signal-processing techniques and, in particular, digital rise-time discrimination have been proved to be a simple but effective method to improve detector performance through peak enhancement and background suppression [17]–[20]. In this paper, we investigate the application of digital signal-processing techniques to LAAPDs to improve their response to X-rays by means of pulse rise-time discrimination.

II. Rationale

APDs are compact monolithic devices made of a silicon p–n junction where the internal electric field can reach high enough intensities to produce electron multiplication by impact ionization [1], [21], [22]. When high voltage is applied to the APD, only a small region of the p-layer in the front part of the diode remains undepleted—(I) the drift region, Fig. 1. The electric field in this region is low, but in (II), the depleted region, it increases with depth, reaching a maximum near the p–n junction. An incident photon absorbed in either the drift region or the p-depleted layer produces electron–hole pairs. The resulting electrons are accelerated toward the n^+-contact, undergoing avalanche multiplication in the high electric field near the junction. Charge gains of a few hundred are typical and vary exponentially with applied voltage.

Manuscript received November 23, 2001; revised April 5, 2002. This work was supported by Project FIS/13140/98-13140. The work of R. E. Morgado was supported by the Gulbenkian Foundation and the Foundation for Luso-American Development (FLAD).

L. M. P. Fernandes, P. C. P. S. Simões, and J. M. F. dos Santos are with the Physics Department, University of Coimbra, P-3004-516 Coimbra, Portugal (e-mail: jmf@gian.fis.uc.pt).

R. E. Morgado is with Los Alamos National Laboratory, Los Alamos, NM 87545 USA.

Digital Object Identifier 10.1109/TNS.2002.801518

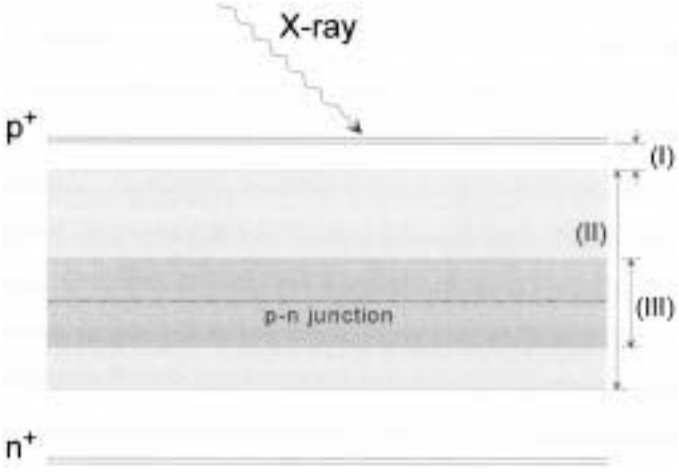

Fig. 1. Schematic diagram of typical avalanche photodiode section: (I) drift region; (II) depleted region; (III) multiplication region.

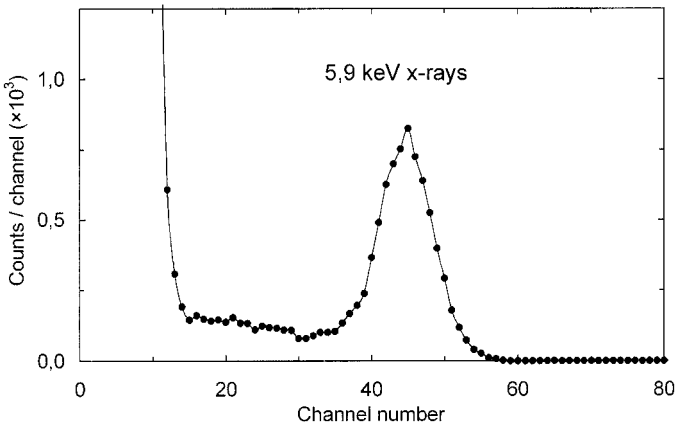

Fig. 2. Typical pulse-height distribution for the LAAPD used in this paper for 5.9-keV X-rays.

For the LAAPD used in this paper,[1] the thickness of the drift region is about 10 μm, while the charge-multiplication region is about 20-μm deep into the depleted region and has a thickness of about 20 μm [21]. Thus, the detection efficiency decreases rapidly for X-ray energies above 5 keV, and a significant number of X-rays interact deep into the multiplication region.

Fig. 2 depicts a pulse-height distribution measured with the LAAPD for 5.9-keV X-rays. The distribution deviates from a Gaussian due to a low-energy tail. This tail results from two possible sources: 1) X-ray absorptions that occur deep in the photodiode, within the avalanche multiplication region (III), undergo only partial amplification, and 2) X-rays that interact in the reduced electric field, in the undepleted p-region, lose primary charge carriers to either the p^+-contact or to traps. Both types of events result in smaller amplitude pulses. For the former type, amplitudes should decrease continuously to zero. The electronic-noise tail in the low-energy region limits the lowest detectable X-ray energy.

X-ray absorption in the undepleted p-region gives rise to pulses with long time-responses because traps may hold electrons for tens to thousands of nanoseconds [21]. The time response for events that occur in the multiplication region is faster than for fully amplified events. These different time responses may result in measurable pulse rise-time differences, allowing for discrimination and rejection of such anomalous pulses and, consequently, for improved detector performance.

III. Experimental Setup

The LAAPD was installed inside a light-tight box to shield it from ambient light. Experimental studies were performed using direct irradiation of the detector with ^{55}Fe X-ray source or X-ray fluorescence from samples positioned in front of the LAAPD in 90° excitation-detection geometry. To delimit the incident X-ray beam, 2- and 10-mm lead collimators were used for each case, respectively.

LAAPD signals were fed through a low-noise charge preamplifier (Canberra 2004, with a sensitivity of 45 mV/MeV) and a spectroscopy amplifier (HP5582A, with gains of 16 to 64) to a digital pulse-height analyzer (DPHA) for further processing. Integration and differentiation shaping-time constants of 200 ns were used in the main amplifier for optimum detector performance [13], [15].

The DPHA was composed of a commercially available digitizer PCI board[2] and the data-processing host computer. The digitizer board has a 12-bit analog-to-digital converter (ADC), and its maximum 125-MHz sampling frequency was used in this work. It has complex triggering capabilities, including data-burst acquisition after or before a certain time interval measured from the instant when the trigger threshold is reached. The input-voltage range is 0–1 V, but only 90% of the ADC full scale is used, as a dc offset is added to the signal prior to digitization. The trigger threshold is set just above the characteristic photodiode electronic noise level for the chosen amplifier gain to avoid dead-time losses analyzing noise pulses.

Pulse-height analysis is performed with a peak-search algorithm, an eighth-order polynomial fitting algorithm, and a modified Newton-tangent method [23]–[25] to determine the peak maximum. If the pulse amplitude is outside of a predefined range, or if more than six iterations are needed for the Newton method to converge, the pulses are rejected. Pulse rise time is defined as the time required for the pulse to increase from 10 to 90% of its maximum amplitude. The different algorithms have been developed for former applications [25] and fine-tuned for this LAAPD X-ray detector—e.g., the eighth-order polynomial fitting and the maximum number of iterations allowed, before convergence is achieved, were chosen for the best pulse discrimination performance and/or for good compromise between pulse discrimination performance and processing time.

The pulse-height and the rise-time distributions are stored simultaneously. The pulse-height distribution is divided into a series of partial distributions on the basis of rise time. The rise-time range of each partial distribution is 8 ns, limited only by the digitizer sampling frequency. For pulse-amplitude, peak-area, and energy-resolution measurements, the pulse-height distributions were fitted to a Gaussian function superimposed on a linear background from which the centroid, the area, and the full-width at half-maximum were determined. The peak-to-background ratio was defined as the Gaussian area

[1]Advanced Photonix, Inc., Camarillo, CA.

[2]PDA12A-1997, Signatec, Corona, CA.

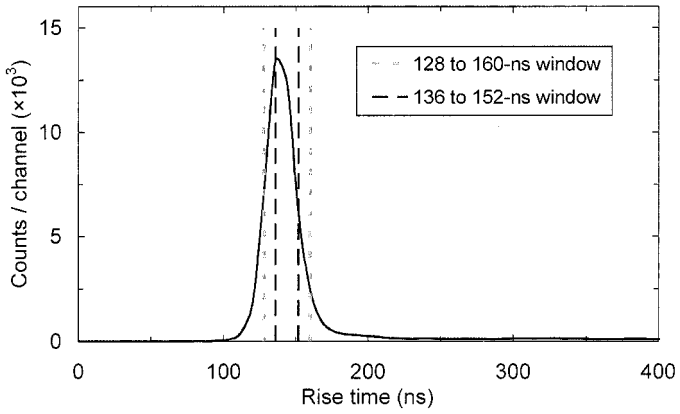

Fig. 3. Pulse rise-time distributions for 5.9-keV X-rays using 200-ns shaping time constants.

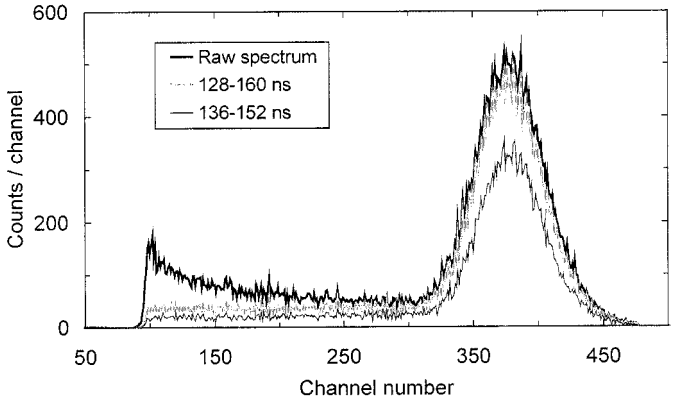

Fig. 4. Pulse-height distributions of different rise-time windows together with the raw spectrum for 5.9-keV X-rays.

divided by the area under the fitted linear background for the peak region.

IV. Experimental Results and Discussion

In Fig. 3, we present the pulse rise-time distributions of the 5.9-keV X-rays detected by a 16-mm-diameter LAAPD for the conditions described above. The dashed lines delimit two time windows of 128–160 and 136–152 ns.

Fig. 4 depicts the pulse-height distributions corresponding to those time windows together with the raw spectrum (total pulse-height distribution without any discrimination). For each partial spectrum, energy resolution and signal-to-background ratio show small improvements from 16.5% and 23 (raw spectrum) to 16.1% and 27 or 15.4% and 29, respectively. However, the relevant feature is the significant reduction of the low-energy tails. This is an important advantage when weaker low-energy lines are superimposed on the tail. For these analyses, rise-time discrimination will result in a significant improvement in the detection sensitivity due to background reduction.

In Fig. 5, we present the raw distribution and three partial pulse-height distributions for time windows outside and inside the 128- to 160-ns rise-time interval. It is observed that a significant number of events with both short and long rise times correspond to events with lower amplitudes than those within the time window. In Table I, the features of the raw spectrum and the relevant partial spectra are characterized according to peak

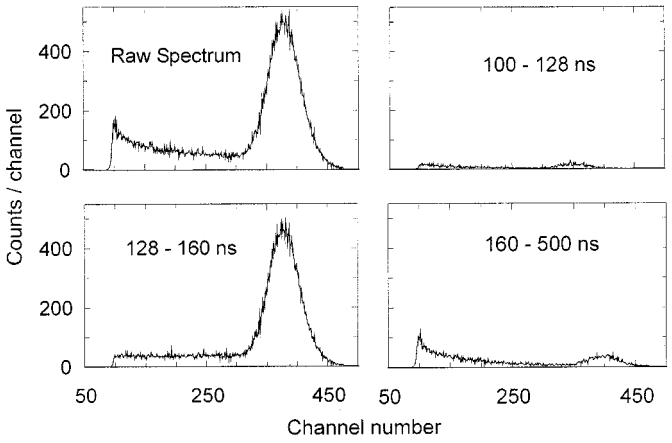

Fig. 5. Raw spectrum and partial spectra for time windows outside and inside the 128- to 160-ns rise-time interval.

TABLE I
Parameters of the Raw Spectrum and the Relevant Partial Spectra Obtained With DPHA for 5.9-keV X-Rays

Rise time window	Centroid	Energy resolution	Peak-to-Background	Relative Area
Total range	379.1	16.5%	23.4	100%
128-136 ns	365.3	15.2%	38.5	16%
136-144 ns	375.6	15.3%	29.1	32%
144-152 ns	383.6	14.9%	31.7	30%
152-160 ns	389.8	14.2%	24.3	12%

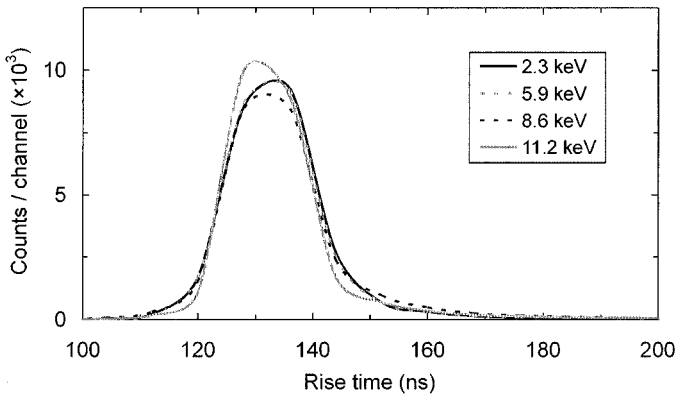

Fig. 6. Pulse rise-time distributions for different X-ray energies using 200-ns shaping time constants.

centroid, energy resolution, peak-to-background ratio, and peak relative area. A slight increase of the peak centroid position of the partial pulse-height distributions with rise time is noticeable due to ballistic deficit. This effect could be corrected after processing the partial spectra, thereby improving the energy resolution and distortions of the final spectrum that result from the sum of several partial spectra. A compromise has to be made between the peak counting efficiency and the pulse-discrimination efficiency. A digital sampling rate higher than 125 MHz would improve the discrimination technique by dividing the partial spectra into narrower rise-time windows.

Fig. 6 depicts several pulse rise-time distributions for different X-ray energies, using the same trigger threshold above

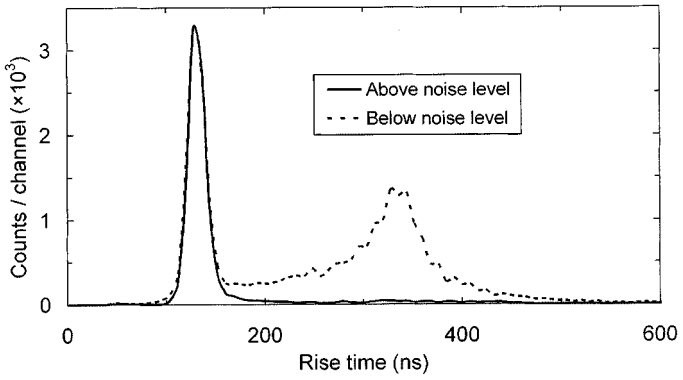

Fig. 7. Pulse rise-time distributions for 5.9-keV X-rays using 200-ns shaping time constants and two different trigger thresholds in the DPHA: just above and below the electronic noise level.

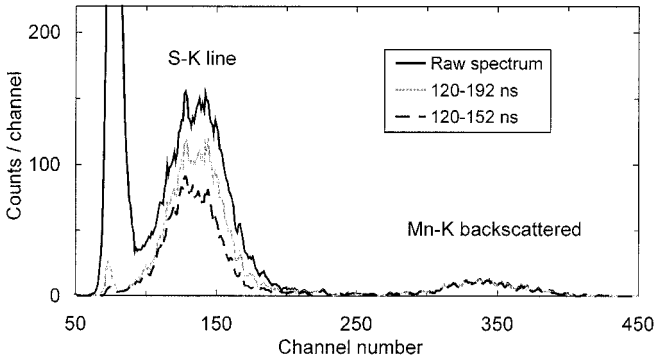

Fig. 8. Pulse-height distributions for the sulphur K-line using 200-ns shaping time constants.

the noise level. The distributions were normalized to the total area. No significant dependence of the rise-time distribution on the X-ray energy is observed.

Pulse rise-time discrimination allows a lowering of the minimum detectable X-ray energy. Fig. 7 depicts two rise-time distributions obtained for 5.9-keV X-rays using different trigger thresholds in the DPHA: just above and below the electric noise level. The figure shows that the electronic noise pulses have longer rise times and, thus, can be efficiently discriminated from the X-ray pulses. However, lowering the trigger threshold in the DPHA results in a reduced data-acquisition throughput due to the time required for analyzing the noise pulses.

We have analyzed the LAAPD response to fluorescence from sulphur and silicon samples excited with a ^{55}Fe X-ray source. In Fig. 8, we present the sulphur total spectrum and two partial spectra obtained for rise-time discrimination windows of 120–192 and 120–152 ns. The energy resolution and the peak-to-background ratio have improved from 32.1% and 8.6 to 31.9% and 53 (81% efficiency) or 30.6% and 51 (57% efficiency), respectively.

The total spectrum and several different partial spectra are depicted in Fig. 9, spanning the full rise-time range. Table II details the features of the total spectrum and the relevant partial spectra for the sulphur K-line. It is observed that ballistic deficit correction could improve the detector energy resolution to values below 29% with an acquisition efficiency of about 90%.

In Fig. 10, the silicon raw spectrum and two partial spectra obtained for rise-time discrimination windows of 120–192 and 120–152 ns are depicted. For the raw spectrum, the noise behavior on the peak region is complex and not well known and, thus, the areas corresponding to the K–Si peak and the respective background cannot be determined with a reasonable precision. The energy resolution and the peak-to-background ratio of the silicon K-line achieve 38% and 4.6 or 36% and 6.1, respectively. The calcium line on the pulse-height distribution is due to the plasticine used to hold the ^{55}Fe source. Table III details the features of the relevant partial spectra for the silicon K-line. Fig. 11 depicts the total spectrum and several relevant partial spectra.

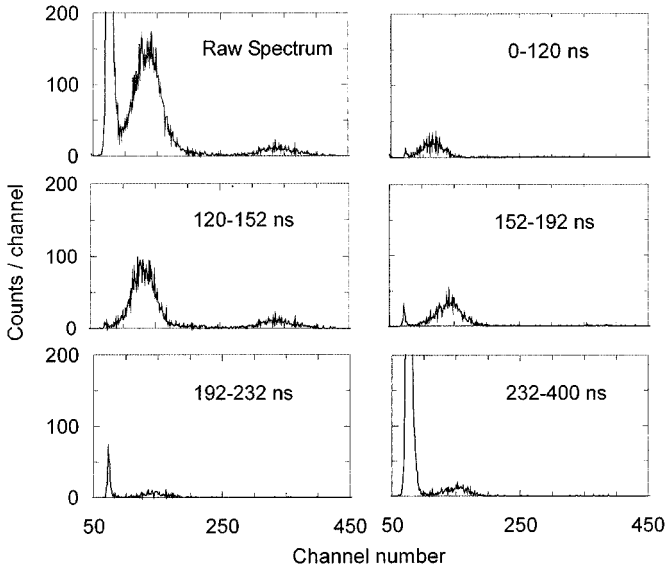

Fig. 9. Raw spectrum and pulse-height distributions of different rise-time windows for sulphur fluorescence.

TABLE II
PARAMETERS OF THE RAW SPECTRUM AND THE RELEVANT PARTIAL SPECTRA OBTAINED WITH DPHA FOR THE SULPHUR K-LINE

Rise time window	Centroid	Energy resolution	Peak-to-Background	Relative Area
Total range	136.4	32.1%	8.5	100%
80-120 ns	115.3	29.1%	24.3	11%
120-136 ns	127.6	28.0%	45.0	27%
136-152 ns	136.0	28.1%	110	29%
152-192 ns	142.1	28.2%	30.5	21%

V. CONCLUSIONS

We have shown that the X-ray response of large-area avalanche photodiodes can be improved by pulse rise-time discrimination. Both measured energy resolution and peak-to-background ratio show some improvements. Low-energy tails are reduced, decreasing the overall background level in the pulse-height distributions. Electronic noise can be efficiently discriminated, but reducing the trigger threshold in the DPHA below the noise level results in longer times for the analysis of noise pulses and reduces the data-acquisition throughput. The discrimination efficiency improves by narrowing the rise-time discrimination windows. However,

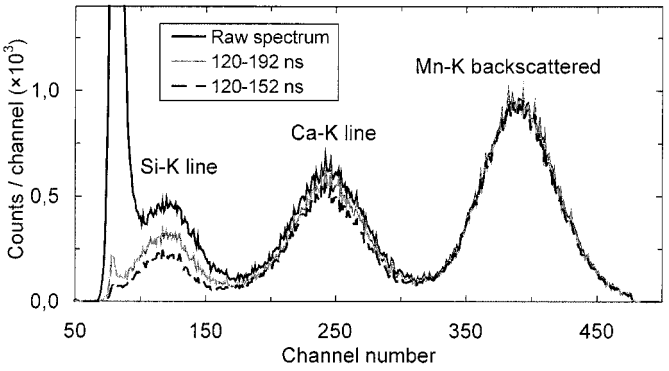

Fig. 10. Pulse-height distributions for the silicon and calcium K-lines using 200-ns shaping time constants.

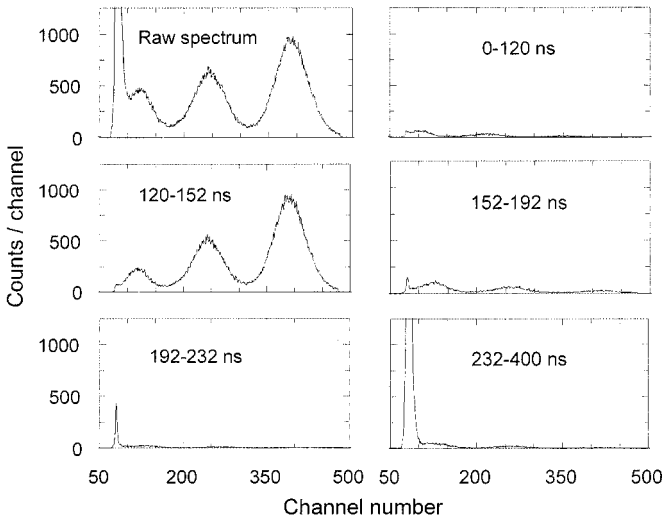

Fig. 11. Raw spectrum and pulse-height distributions of different rise-time windows for silicon fluorescence.

TABLE III
PARAMETERS OF THE RELEVANT PARTIAL SPECTRA OBTAINED WITH DPHA FOR THE SILICON K-LINE

Rise time window	Centroid	Energy resolution	Peak-to-Background	Peak Area
80-120 ns	103.8	29.0%	1.59	1200
120-136 ns	114.0	34.0%	3.93	3650
136-152 ns	121.3	29.6%	3.61	3440
152-192 ns	126.3	33.9%	3.14	3380

a compromise has to be made between the peak counting efficiency and the pulse-discrimination efficiency.

Future work will include the information contained in the midpoint of each pulse for improvement of pulse-discrimination efficiency.

REFERENCES

[1] J. P. Pansart, "Avalanche photodiodes for particle detection," *Nucl. Instrum. Meth.*, vol. A 387, pp. 186–193, 1997.

[2] R. Farrell, F. Olschner, E. Frederick, L. McConchie, K. Vanderpuye, M. R. Squillante, and G. Entine, "Large-area silicon avalanche photodiodes for scintillation detectors," *Nucl. Instrum. Meth.*, vol. A 288, pp. 137–139, 1990.

[3] M. Moszynski, M. Kapusta, J. Zalispka, M. Balcerzyk, D. Wolski, M. Szawlowski, and W. Klamra, "Low energy γ-rays scintillation detection with large area avalanche photodiodes," *IEEE Trans. Nucl. Sci.*, vol. 46, pp. 880–885, 1999.

[4] J. A. M. Lopes, J. M. F. dos Santos, and C. A. N. Conde, "A large area avalanche photodiode as a VUV photosensor readout for gas proportional scintillation counters," *Nucl. Instrum. Meth.*, vol. A 454, pp. 421–425, 2000.

[5] A. Karar, Y. Musienko, and J. C. Vanal, "Characterization of avalanche photodiodes for calorimetric applications," *Nucl. Instrum. Meth.*, vol. A 428, pp. 413–431, 1999.

[6] K. Deiters, Y. Musienko, S. Nicol, B. Patel, D. Renker, S. Reucroft, R. Rusack, T. Sakhelashvili, J. Swain, and P. Vikas, "Properties of the most recent avalanche photodiodes for the CMS electromagnetic calorimeter," *Nucl. Instrum. Meth.*, vol. A 442, pp. 193–197, 2000.

[7] E. Lorentz, S. Natkaniec, D. Renker, and B. Schwartz, "Fast readout of plastic and crystal scintillators by avalanche photodiodes," *Nucl. Instrum. Meth.*, vol. A 344, pp. 64–72, 1994.

[8] R. Farrel, F. Olschner, K. Shah, and M. R. Squillante, "Advances in semiconductor photodetectors for scintillation," *Nucl. Instrum. Meth.*, vol. A 387, pp. 194–198, 1997.

[9] B. Pichler, G. Böning, E. Lorenz, R. Mirzoyan, W. Pimpl, M. Schwaiger, and S. I. Ziegler, "Studies with a prototype high resolution PET scanner based on LSO-APD modules," *IEEE Trans. Nucl. Sci.*, vol. 45, pp. 1298–1302, 1998.

[10] A. Ruru Chen, A. Fremout, S. Tavernier, P. Bruyndonckx, D. Clément, J.-F. Loude, and C. Morel, "Readout of scintillator light with avalanche photodiodes for positron emission tomography," *Nucl. Instrum. Meth.*, vol. A 433, pp. 637–647, 1999.

[11] R. Farrel, K. Vanderpuye, G. Entine, and M. R. Squillante, "High resolution low energy avalanche photodiode x-ray detectors," *IEEE Trans. Nucl. Sci.*, vol. 38, pp. 144–147, 1991.

[12] A. Ochi, Y. Nishi, and T. Tanimori, "Study of a large area avalanche photodiode as a fast photon and soft x-ray detector," *Nucl. Instrum. Meth.*, vol. A 378, pp. 267–274, 1996.

[13] M. Moszynski, M. Szawlowski, M. Kapusta, M. Balcerzyk, and D. Wolski, "Large avalanche photodiodes in x-rays and scintillation detection," *Nucl. Instrum. Meth.*, vol. A 442, pp. 230–237, 2000.

[14] C. P. Allier, H. Valk, V. R. Bom, R. W. Hollander, and C. W. E. van Eijk, "Comparative study of silicon detectors," *IEEE Trans. Nucl. Sci.*, vol. 45, pp. 576–580, 1998.

[15] L. M. P. Fernandes, J. A. M. Lopes, J. M. F. dos Santos, and C. A. N. Conde, "Application of a large area avalanche photodiode in energy dispersive x-ray fluorescence analysis," *X-Ray Spectrom.*, vol. 30, pp. 164–169, 2001.

[16] F. Kottmann, W. Amir, F. Biraben, C. A. N. Conde, S. Dhawan, and T. W. Hänsch *et al.*, "The muonic hydrogen Lamb shift experiment at PSI," Hyperf. Inter., 2002, to be published.

[17] B. Aspacher and A. C. Rester, "Compton continuum suppression by digital pulse shape analysis—Part II," *Nucl. Instrum. Meth.*, vol. A 338, pp. 516–521, 1994.

[18] S. A. Audet, J. J. Friel, T. P. Gagliardi, R. B. Mott, J. I. Patel, and C. G. Waldman, "High resolution energy dispersive spectroscopy with high-purity germanium detectors and digital pulse processing," in *1994 IEEE Conf. Rec.*, vol. 1, 1995, pp. 155–159.

[19] P. C. P. S. Simões, J. F. C. A. Veloso, J. M. F. dos Santos, and C. A. N. Conde, "Application of the digital pulse processing technique to gas proportional scintillation counters," *IEEE Trans. Nucl. Sci.*, vol. 44, pp. 521–526, 1997.

[20] P. C. P. S. Simões, J. M. F. dos Santos, and C. A. N. Conde, "Digital risetime discrimination for peak enhancement in gas proportional scintillation counter x-ray fluorescence analysis," *X-Ray Spectrom.*, vol. 26, pp. 182–188, 1997.

[21] A. Q. R. Baron and S. L. Ruby, "Time resolved detection of x-rays using large area avalanche photodiodes," *Nucl. Instrum. Meth.*, vol. A 343, pp. 517–526, 1994.

[22] E. M. Gullikson, E. Gramsch, and M. Szawlowski, "Large-area avalanche photodiodes for the detection of soft x-rays," *Appl. Opt.*, vol. 34, pp. 4662–4668, 1995.

[23] P. R. Bevington, *Data Reduction and Error Analysis for the Physical Sciences*. New York: McGraw-Hill, 1969, p. 100, 208.

[24] J. B. P. S. Simões, P. C. P. S. Simões, and C. M. B. A. Correia, "Nuclear spectroscopy pulse height analysis based on digital signal processing techniques," *IEEE Trans. Nucl. Sci.*, vol. 42, pp. 700–704, 1995.

[25] P. C. P. S. Simões, J. C. Martins, and C. M. B. A. Correia, "A new digital signal processing technique for applications in nuclear spectroscopy," *IEEE Trans. Nucl. Sci.*, vol. 43, pp. 1804–1809, 1996.

ELSEVIER

Nuclear Instruments and Methods in Physics Research A 478 (2002) 395–399

NUCLEAR INSTRUMENTS & METHODS IN PHYSICS RESEARCH Section A

www.elsevier.com/locate/nima

Non-linear behaviour of large-area avalanche photodiodes

L.M.P. Fernandes[a], J.A.M. Lopes[a], C.M.B. Monteiro[a], J.M.F. dos Santos[a], R.E. Morgado[b,*]

[a] *Physics Department, University of Coimbra, P-3004-516, Coimbra, Portugal*
[b] *Los Alamos National Laboratory, NM 87545, USA*

Abstract

The characterisation of photodiodes used as photosensors requires a determination of the number of electron–hole pairs produced by scintillation light. One method involves comparing signals produced by X-ray absorptions occurring directly in the avalanche photodiode with the light signals. When the light is derived from light-emitting diodes in the 400–600 nm range, significant non-linear behaviour is reported. In the present work, we extend the study of the linear behaviour to large-area avalanche photodiodes, of Advanced Photonix, used as photosensors of the vacuum ultraviolet (VUV) scintillation light produced by argon (128 nm) and xenon (173 nm). We observed greater non-linearities in the avalanche photodiodes for the VUV scintillation light than reported previously for visible light, but considerably less than the non-linearities observed in other commercially available avalanche photodiodes. © 2002 Published by Elsevier Science B.V.

PACS: 29.40.M; 07.85.F; 85.60.D

Keywords: Scintillation detectors; X-ray detectors; Avalanche photodiodes

1. Introduction

Avalanche photodiodes (APDs) have assumed increasingly important instrumentation roles in broad areas of physics where their high quantum efficiency and low noise characteristics compete favourably with photomultiplier tubes. These include large electromagnetic calorimeters for high-energy physics at CERN [1–3], inorganic and plastic scintillator γ-ray spectrometers for nuclear physics [4], and PET scanners [5] for medicine.

These applications have stimulated efforts to characterise the performances of several types of APDs that are now commercially available. An important characterisation is the number of electron–hole pairs produced per unit of absorbed energy, the knowledge of which enables a quantitative analysis of the noise sources contributing to the observed energy resolution. The number of electron–hole pairs is often determined by a comparison of the relative pulse amplitudes produced in the APD by the direct absorption of X-rays with that produced by the scintillation light from a detector. The comparison is valid provided strict linearity between the initial number of

*Corresponding author. Physics Department, University of Coimbra, P-3004-516, Coimbra, Portugal. Tel.: +351-2394-10667; fax: +351-2398-29158.

E-mail address: rmorgado@lanl.gov (R.E. Morgado).

0168-9002/02/$ - see front matter © 2002 Published by Elsevier Science B.V.
PII: S0168-9002(01)01781-8

electron–hole pairs and the resulting pulse amplitude is assumed throughout the range of avalanche multiplication gains.

Non-linearities have been reported, however, at high current densities and attributed to the space-charge effects, reduced localised electric fields, and heating in the avalanche regions [1,3,6,7] of the APD structure. As a result, the efficacy of using X-rays to determine the number of charge carriers produced in light measurements has been compromised to some degree.

The light sources used in these studies were light-emitting diodes in the 400–600 nm range, excluding the deep and vacuum ultraviolet (VUV) regions. With the commercial availability of windowless VUV-sensitive APDs, their instrumentation as photosensors of the scintillation light from noble gases and liquids for PET, X-, and γ-ray spectroscopy is under investigation [8–10].

In this work, we present for the first time, the results of a study to determine the non-linearities in large-area APD[1] responses to the argon and xenon scintillations at ~ 128 and ~ 173 nm, respectively, from gas proportional scintillation counters. We compared the signals due to X-ray interactions occurring directly in the APD with signals from the scintillation light produced by X-ray absorptions in the gas medium of the counter. The non-linearity is determined by comparing the amplitudes as a function of the APD reverse bias voltage.

2. Description

2.1. Argon scintillation measurements

2.1.1. Detector and operation

The argon gas proportional scintillation counter (GPSC) instrumented with a large-area APD is schematically depicted in Fig. 1. Its operational characteristics were described in Ref. [9]. X-rays entering the entrance window are absorbed primarily in the drift region by the photoelectric effect in argon. The cloud of primary electrons drifts toward the scintillation region under the influence of the electric field established between the entrance window and grid G1. The reduced electric field in this region is chosen well below the scintillation and ionisation thresholds in argon.

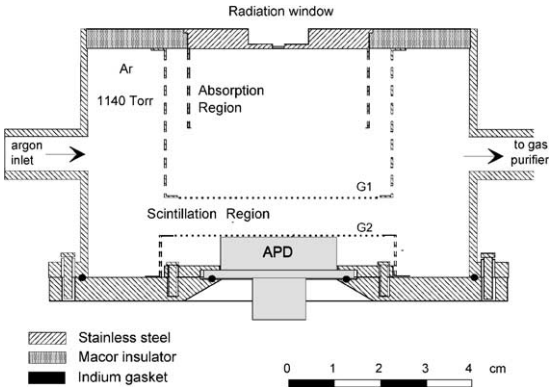

Fig. 1. The schematic of the GPSC with a large-area APD photosensor.

In the scintillation region, the electrons are accelerated in the stronger electric field between G1 and G2, chosen above the scintillation threshold but below the ionisation threshold in argon. Each primary electron produces a number of VUV photons in the scintillation region. Proportionality between the incident X-ray energy, the number of primary electrons, and the number of scintillation photons is maintained throughout the process.

The scintillation photons incident on the sensitive area of the APD produce electron–hole pairs in silicon that are multiplied by the avalanche process. The APD reverse bias voltage determines the multiplication gain in the avalanche process.

Concurrent with the acquisition of the detected signals from the absorption of X-rays in argon, a transmitted fraction of the X-rays are detected directly in the APD. The number of electron–hole pairs produced by direct absorption in the APD is determined from the energy of the X-ray and the w-value in silicon.

The total charge for each multiplication gain is integrated in a $1.5\,\mathrm{V\,pC^{-1}}$ charge-sensitive preamplifier (Canberra 2006), followed by linear amplification (Hewlett Packard 5582A) with a

[1] Advanced Photonix, Inc., 1240 Avenida Acaso, Camarillo, CA 93012, USA.

2-μs shaping time. Pulse height analysis is performed with a 1024 channel multi-channel analyser (Nucleus PCA-II).

The pulse-height distribution is fit with a Gaussian function superimposed on a linear background. The pulse amplitude for each avalanche gain is determined from the centroid of the fitted Gaussian.

2.1.2. Experimental results

The measured pulse-height distribution for the 5.9 keV X-rays from ^{55}Fe with the K_β line filtered by chromium is depicted in Fig. 2. Approximately 10% of the 5.9 keV X-rays are transmitted through the intervening 3.3 cm of argon and 40% of these are absorbed in the depletion region of the APD.

The salient features of the pulse-height distribution include the 5.9 keV X-ray peak from absorptions in the GPSC, the 5.9 keV X-ray peak from direct absorptions in the APD, the escape peaks from the argon K-lines fluorescence, and the system electronic noise.

A direct comparison of the relative amplitudes from the argon scintillation and from the X-ray interaction in the APD can be made for each value of the APD gain.

In Fig. 3, the argon results are plotted as a ratio of the pulse amplitudes from X-ray interactions in the APD and in the GPSC, normalised to the maximum value, as a function of the APD reverse bias voltage. The deviation from linearity is greater than 10% for the APD gains above 200, 4 times larger than what was previously reported for visible light (around 600 nm) [7]. For gains as low as 100, deviations from linearity already exceed 4.5%. Nevertheless, the non-linearity in the Advanced Photonix APD is still smaller than what has been observed with other types of APDs for visible light [7].

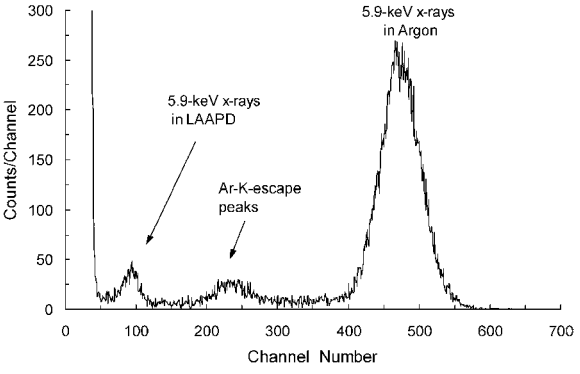

Fig. 2. The pulse-height distribution from an argon GPSC instrumented with a large-area APD for 5.9 keV X-rays. E/p of 0.2 and 5.0 V cm^{-1} Torr^{-1} were used in the drift and scintillation region, respectively; the multiplication gain in the APD was approximately 40.

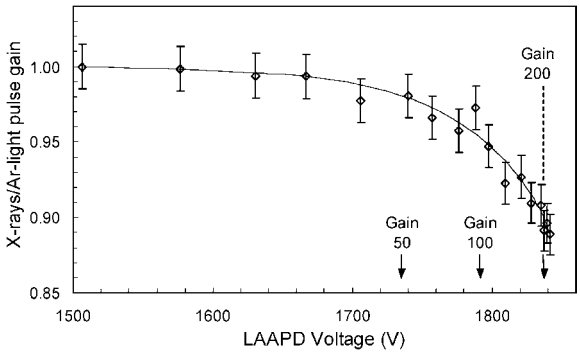

Fig. 3. The ratio of the pulse amplitudes in an argon GPSC instrumented with a large-area APD as a function of the APD reverse bias voltage.

2.2. Xenon scintillation measurements

2.2.1. Detector and operation

The xenon GPSC instrumented with the large-area APD is schematically depicted in Fig. 4. The GPSC is a driftless design with a 1.1 cm deep

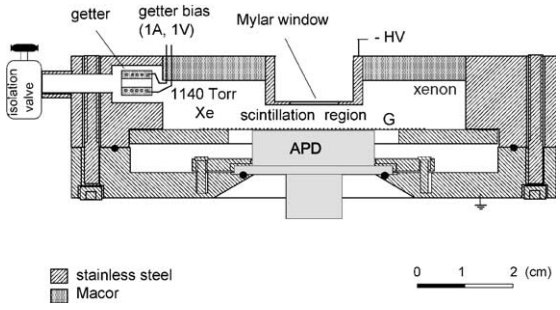

Fig. 4. A xenon driftless GPSC instrumented with a large-area APD.

scintillation region. The APD is positioned just below the electron-collection grid G. The entrance window is maintained at negative potential while grid G and the APD enclosure are maintained at ground potential.

The operation of the xenon driftless GPSC is similar to what has been previously described above with the notable exception that X-rays are now absorbed primarily in the scintillation region. The total number of scintillation photons produced by the primary electron cloud, however, will now depend on how deep into the scintillation region the X-ray-absorption event occurs.

Although the driftless design results in degraded energy resolution for scintillation events, it allows higher transmission of the 5.9 keV X-rays through the xenon and, therefore, more direct X-ray interactions in the APD. The charge collection and processing of the signals generated in xenon and directly in the APD are the same as already described above for argon.

2.2.2. Experimental results

Fig. 5 depicts the pulse-height distribution of 5.9 keV X-rays from chromium-filtered ^{55}Fe measured in the xenon driftless GPSC. Approximately 0.2% of the 5.9 keV X-rays are transmitted through the 1.1 cm of xenon, of which 40% are absorbed in the depletion region of the APD.

The salient features of the pulse-height distribution include the 5.9 keV X-ray full-energy peak from absorptions in the xenon GPSC, the xenon L_α and L_β escape peaks from 5.9 keV X-ray absorptions in the xenon GPSC, the 5.9 keV X-ray peak from absorptions in the APD, the 4.1 and 4.8 keV xenon L_α and L_β fluorescence peaks from absorptions in the APD, and the system electronic noise.

The distribution enabled a comparison between the pulse amplitudes resulting from the xenon scintillation interaction and the X-ray interactions in the APD as a function of the APD gain.

To extend the determination of non-linearity to higher energy X-rays, the pulse-height distributions for the 22.1 keV X-rays from ^{109}Cd were also measured and analysed in the xenon driftless GPSC.

In Fig. 6, we plot the ratio of the pulse amplitudes from the X-ray interactions in the APD and from the GPSC, normalised to the maximum value, as a function of the APD reverse-bias voltage. For 5.9 keV X-rays, the variation is only $\sim$6% for the APD gains of 200 and $\sim$3.5% for gains of about 100. These values, though less than those measured for the argon scintillation, are a factor of 2 larger than for visible light (around 600 nm) [7]. The results for 22.1 keV X-rays demonstrate even greater non-linearity.

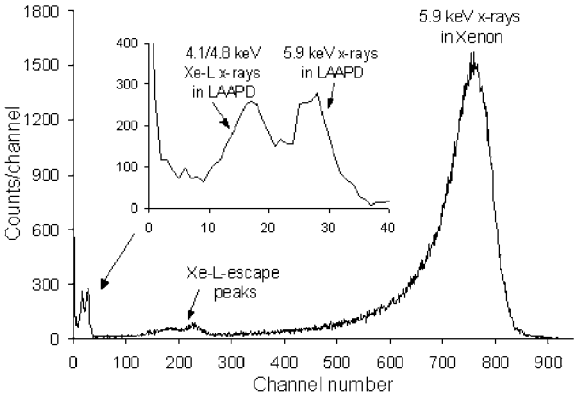

Fig. 5. Pulse-height distribution of 5.9 keV X-rays from xenon driftless GPSC instrumented with a large-area APD. An E/p of 5.5 V cm^{-1} Torr^{-1} was used in the scintillation region; the multiplication gain in the APD was approximately 100.

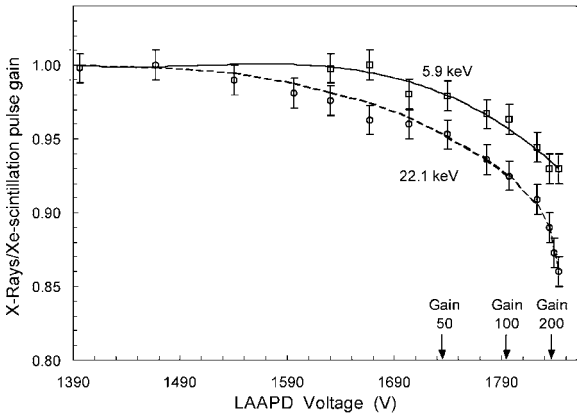

Fig. 6. The ratio of the pulse amplitudes in an xenon driftless GPSC instrumented with a large-area APD as a function of the APD reverse-bias voltage for 5.9 and 22.1 keV X-rays.

3. Analysis and conclusions

We have confirmed the non-linear behaviour of the Advanced Photonix large-area APDs for the VUV scintillations from argon and xenon. The results suggest a dependence of the APD linearity on wavelength as well: the scintillation light from argon (128 nm) demonstrated the largest non-linearity of 10% at a gain of 200, compared to 6% for xenon (173 nm), and 3% for visible light (600 nm) [7].

An accurate determination of the number of charge carriers produced in an APD by the VUV scintillation light may be compromised if strict linearity is assumed with direct X-ray interactions. Nevertheless, the non-linearity reported here for the VUV light in Advanced Photonix large-area APDs is less than what is observed in other types of APDs for visible light [7].

Acknowledgements

This work was carried out in the Atomic and Nuclear Instrumentation Group of the Instrumentation Center (Unit 217/94). R.E. Morgado acknowledges the support of the Calouste Gulbenkian Foundation for his professorship grant. Support is acknowledged from project CERN/P/FIS/15200/99.

References

[1] J.P. Pansart, Nucl. Instr. and Meth. A 387 (1997) 186.
[2] A. Karar, Y. Musienko, J.C. Vanal, Nucl. Instr. and Meth. A 428 (1999) 413.
[3] K. Deiters, et al., Nucl. Instr. and Meth. A 442 (2000) 193.
[4] R. Farrel, et al., Nucl. Instr. and Meth. A 387 (1997) 194.
[5] A. Ruru Chen, et al., Nucl. Instr. and Meth. A 433 (1999) 637.
[6] C.P. Allier, et al., IEEE Trans. Nucl. Sci. NS-45 (1998) 576.
[7] M. Moszynski, et al., Comparative study of avalanche photodiodes with different structures in scintillation detection, Presented at the IEEE Nuclear Science Symposium, Lyon, France, 15–20 October, 2000.
[8] J.A.M. Lopes, J.M.F. dos Santos, R.E. Morgado, C.A.N. Conde, Xenon gas proportional scintillation counter with a UV-sensitive, large area avalanche photodiode, Presented at the IEEE Nuclear Science Symposium, Lyon, France, 15–20 October, 2000; IEEE Trans. Nucl. Sci. 48 (2001), in press.
[9] C.M.B. Monteiro, J.A.M. Lopes, J.M.F. dos Santos, C.A.N. Conde, An argon gas proportional scintillation counter with a UV avalanche photodiode scintillation readout, Presented at the IEEE Nuclear Science Symposium, Lyon, France, 15–20 October, 2000; IEEE Trans Nucl. Sci. 48 (2001), in press.
[10] V.N. Solovov, V. Chepel, A. Hitachi, M.I. Lopes, R. Ferreira Marques, A.J.P.L. Policarpo, Detection of scintillation light of liquid xenon with a LAAPD, Presented at the IEEE Nuclear Science Symposium, Lyon, France, 15–20 October, 2000; IEEE Trans Nucl. Sci. Symp. Conf. Rec., paper #521.

Chapter 3

Effect of temperature in the LAAPD response to X-ray, VUV and visible-light detection

The gain of an avalanche photodiode depends significantly on temperature, what may represent a drawback in many applications. In these cases, temperature control and stabilization during measurements is necessary. One method to stabilize the temperature consists on the use of Peltier devices coupled to photodiodes. In the majority of the cases this procedure is not used and the knowledge of the gain variation with temperature becomes necessary in order to make corrections due to the temperature variation during measurements.

Beyond the gain, also the dark current depends on temperature. As stated in previous chapters, dark current limits the LAAPD performance, influencing for example the obtained energy resolution. Dark current can be reduced about one order of magnitude when temperature varies from the room temperature down to 0 ºC. Then, the noise contribution to the energy resolution decreases and the photodiode performance may improve significantly with the LAAPD cooling.

LAAPDs constitute valid alternatives in the detection of visible light, VUV radiation and X-rays. Up to now, the gain variation with temperature of avalanche photodiodes manufactured by API had been investigated only for visible light. According to the manufacturer, the variation reaches about -3% per ºC for the highest gains [API 1999]. However, some LAAPD characteristics vary with the type of radiation detected, such as the effect of non-linearity [Fernandes *et al.* 2002A] and the behaviour under intense magnetic fields [Fernandes *et al.* 2003A]. Thus, the knowledge of the gain variation with temperature in the detection of the three radiation types is important.

A LAAPD with an integrated Peltier cell, manufactured by API, was incorporated in a GPSC in order to study the LAAPD response to the detection of VUV photons produced in the detector gas volume (xenon) as a function of temperature. The performance of the GPSC thus composed was investigated by [Lopes 2002], being now complemented on the perspective of the LAAPD as a VUV-light detector. The same LAAPD was used to study the response in X-ray detection. The gas was removed from the GPSC, providing direct absorption of X-rays in the LAAPD. However, the system was not able to operate below -5 ºC due to a significant increase of the electronic noise.

In order to characterize the LAAPD performance in a wider temperature range, an alternative cooling system was assembled, providing temperature stabilization from the room temperature down to about -40 ºC. The LAAPD response was studied in that temperature range for X-ray and visible-light detection. In particular, visible-light detection leads to the determination of the excess noise factor, a contribution to the energy resolution. The several contributions were determined as functions of the temperature and compared to the theoretical models described in Chapter 1.

Beyond the LAAPD from API, with a circular area with a 16 mm diameter, another LAAPD, manufactured by RMD, was also investigated. This prototype has a planar structure and a square surface with a 14×14 mm^2 area. Both types of photodiodes have been used in the muonic hydrogen Lamb shift experiment. LAAPDs from API have been used in the first phase of the experiment (2002), having been substituted by planar LAAPDs in the second phase (2003).

In this chapter, the response of LAAPDs is characterized as a function of temperature for X-ray, VUV-light and visible-light detection. The experimental procedures are described and the obtained results are discussed.

3.1. Characterization of the LAAPD with integrated Peltier cell for VUV-light detection

The LAAPD with an integrated Peltier cell, from the *571 cooled head series* of API photodiodes was used as VUV-radiation photosensor in the gas volume of a GPSC containing xenon. The system includes a temperature sensor (thermistor), providing temperature stabilization in the LAAPD within ± 0.1 ºC. The photodiode presents a circular active area with 16 mm diameter and a quantum efficiency of 105% for the VUV radiation produced in xenon (~173 nm) [API 1999]. In the base of the photodiode six metallic pins are located: two for the LAAPD anode and cathode, two for the Peltier cell and two for the thermistor. The thermistor presents a resistance of 7650 Ω (± 12%) at 0 ºC and a negative temperature coefficient. The LAAPD temperature is established by the voltage and current values applied to the Peltier cell. The maximum voltage and current values set in the power supply are 4.3 V and 2 A.

The experimental system description and the obtained results are presented in the paper: "VUV detection in large-area avalanche photodiodes as a function of temperature", published in *Nucl. Instr. Meth. A*, vol. 504 (2003), pages 331-334 [Lopes *et al.* 2003], attached at the end of this chapter (page 105). The results include the LAAPD gain and performance characteristics evaluated for 5.9 keV X-rays absorbed in the GPSC, corresponding to 3.2×10^4 VUV photons detected in the LAAPD. The gain relative variation with temperature was found to be about 2 times higher than the one suggested by the manufacturer for visible light [API 1999]. Due to the significant reduction of the dark current as temperature decreases, the electronic noise level is reduced, improving the minimum number of detectable photons in the LAAPD, which was found to be 0.5×10^3 and 1.3×10^3 VUV photons for temperatures of -5 and 25 ºC, respectively.

Figure 3.1 shows a typical energy spectrum of the pulses produced in the LAAPD, for a temperature of 25 ºC and a bias voltage of 1815 V, corresponding to a gain of 175. The counting rate of the detected pulses is 120/s. The minimum number of detectable photons is determined by normalization of the minimum detectable energy.

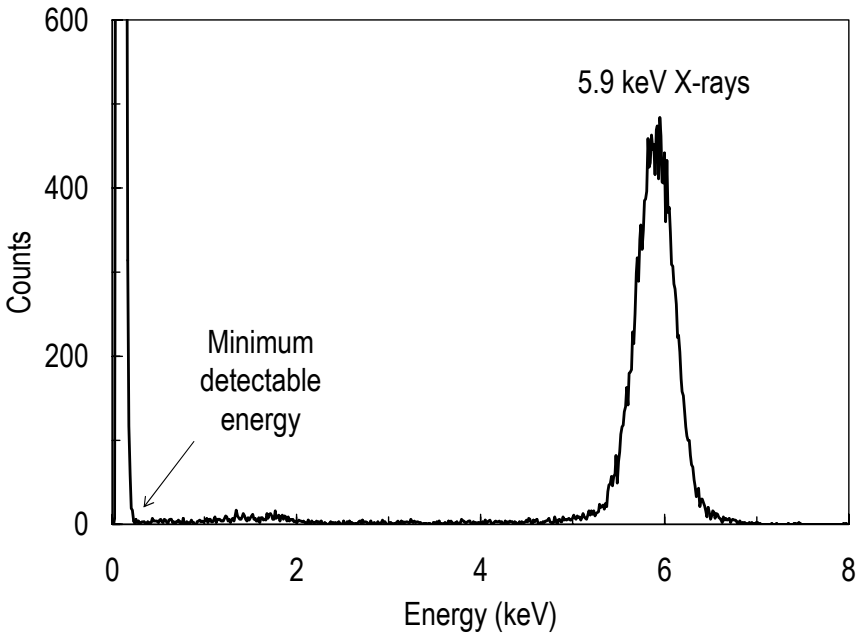

Figure 3.1 – Typical energy spectrum of the pulses produced in the LAAPD by 5.9 keV X-rays absorbed in the GPSC, for a bias voltage of 1815 V and a temperature of 25 ºC. The peak corresponds to 3.2×10^4 VUV photons detected in the LAAPD.

The energy resolution variation with temperature was also investigated. In a GPSC, the statistical fluctuations associated to the light amplification process are negligible in comparison to the fluctuations associated to the creation of the primary electron cloud and to the photon detection and signal amplification in the photosensor.

The fluctuations associated to the creation of primary electrons are well known [Santos 1994] and describe the GPSC intrinsic resolution:

$$R_{\text{int}}(\text{GPSC}) = 2.36\sqrt{\frac{f\,W}{E_x}} \qquad \text{(Eq. 3.1)}$$

where f is the Fano factor, W is the average energy required to ionize a gas atom and E_x is the incident X-ray energy. For a GPSC containing xenon, $f = 0.17$ and $W \cong 22$ eV [Conde 2003]. As follows, Equation 3.1 establishes an intrinsic resolution of 6% for 5.9 keV X-rays interacting in the GPSC.

The statistical fluctuations associated to light detection in the LAAPD have already been analyzed in Chapter 1 (Equation 1.6). The LAAPD intrinsic resolution for light detection (Equation 1.7) depends on the excess noise factor (F) and the number of primary electrons, which is determined by the energy deposited in silicon by the light pulse (E). The LAAPD intrinsic resolution can be written as:

$$R_{\text{int}}\,(\text{LAAPD}) = 2.36\sqrt{\frac{F\varepsilon}{E}} \qquad \text{(Eq. 3.2)}$$

The determination of the energy equivalent to the light pulse (E) requires the comparison of the VUV-light signal with the signal induced by direct X-ray absorptions in the LAAPD. This is not possible in the present experimental system since practically there is no X-ray transmission through the GPSC volume.

The intrinsic resolution variation with gain depends only on the relationship between F and the gain (Figure 1.10), which is assumed linear in the useful gain region. In section 3.3, the value E is determined and the variation of F with the gain is investigated for visible light, making it possible to obtain a better approximation for the LAAPD intrinsic resolution.

Besides the statistical fluctuations associated to the GPSC and the LAAPD, the energy resolution also depends on the electronic noise, which varies with gain according to Equation 1.20. The electronic noise contribution to the energy resolution can be expressed by:

$$R_N = \frac{\Delta E_N}{E} = 2.36\,\frac{e\varepsilon}{q\,E\,G}\sqrt{\frac{k_B\,T\,R_{eq}}{2\tau}\,C_T{}^2 + \frac{\tau\,q}{4}\,(I_{DS} + I_{DV}\,G^2\,F)} \qquad \text{(Eq. 3.3)}$$

The total energy resolution obtained with the GPSC results from the quadratic addition of the three cited contributions:

$$R_{\text{tot}}{}^2 = R_{\text{int}}{}^2\,(\text{GPSC}) + R_{\text{int}}{}^2\,(\text{LAAPD}) + R_N{}^2 \qquad \text{(Eq. 3.4)}$$

The fluctuations associated to VUV-light detection in the LAAPD, including the electronic noise contribution, have been determined excluding the GPSC intrinsic resolution (Equation 3.1) from the total energy resolution (Equation 3.4). For the investigated temperature range, the minimum energy resolution is reached for gains between 100 and 150 [Lopes *et al.* 2003]. The energy resolution degradation for high gains is mainly attributed to the increase of the excess noise factor, which affects the intrinsic resolution (Equation 3.2) and the electronic noise (Equation 3.3). The statistical fluctuations tend to increase with temperature. However, the LAAPD operation at temperatures below 5 ºC does not improve its performance in VUV-light detection, except for higher gains. The system used (LAAPD with a Peltier cell) was designed to operate in the temperature range between 0 and 40 ºC. Therefore, the system does not provide conclusive results for temperatures below 0 ºC.

3.2. Characterization of the LAAPD with integrated Peltier cell for X-ray detection

The effect of temperature on the operation of avalanche photodiodes has particular importance in the detection of X-rays. The dark current reduction for low temperatures leads to an improvement on the minimum detection limit, what presents advantages in X-ray fluorescence applications since lower energy X-rays can be detected. The LAAPD energy resolution at low temperatures may be better compared to proportional counters.

To study the LAAPD response to direct X-ray detection as a function of temperature, the same photodiode investigated for VUV-light detection (*571 cooled head series* from API) was used. The enclosure of the detector previously investigated was used to support the new experimental system, protecting the LAAPD from the ambient light. The gas inside the detector was removed and dry nitrogen, at atmospheric pressure, was put in its place in order to avoid condensation problems for temperatures close to 0 ºC.

The LAAPD gain and performance characteristics were evaluated for 5.9 keV X-rays for different temperatures, being presented in the paper: "X-ray spectrometry with Peltier-cooled large area avalanche photodiodes", published in *Nucl. Instr. Meth. B*, vol. 213 (2004), pages 267-271 [Fernandes *et al.* 2004A], attached at the end of this chapter (page 109). The LAAPD application to X-ray spectrometry is also presented.

The gain variation with the LAAPD bias voltage is presented in Figure 3.2 for different temperatures, showing a significant gain raise as the temperature decreases. The gain was determined by normalization to VUV-light measurements, where the unitary gain was assessed for voltages as low as 500 V. The relative gain variation with temperature was found to be about -4.5% per ºC for the highest gains [Fernandes *et al.* 2004A], being less significant than the one obtained for VUV light.

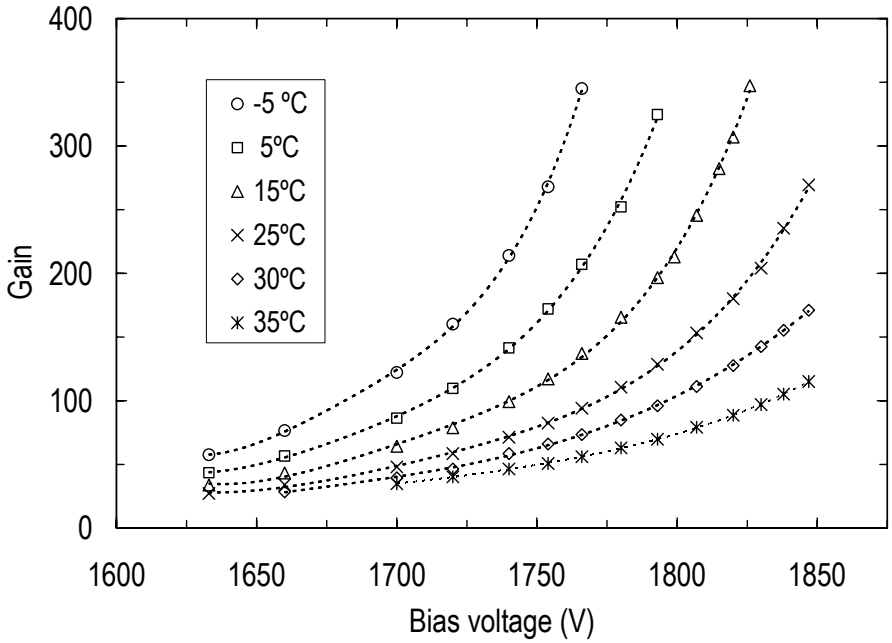

Figure 3.2 – Gain obtained for 5.9 keV X-rays as a function of the LAAPD bias voltage, for different temperatures.

The unitary gain determination using VUV light was possible since the signal-to-noise ratio is significantly higher as a result of the light amplification inside the GPSC. Each 5.9 keV X-ray absorbed in the detector gas generates 3.2×10^4 VUV photons incident in the LAAPD and approximately the same number of primary electrons (the quantum

efficiency is about 100%). The number of primary electrons produced per X-ray with energy E absorbed directly in the LAAPD is $N = E/\varepsilon$, being ε the average energy required to produce an electron-hole pair in silicon. Therefore, each 5.9 keV X-ray directly absorbed in the LAAPD originates approximately 1.6×10^3 primary electrons, about 20 times less than obtained for VUV-light detection.

Figure 3.3 shows typical energy spectra of the pulses produced in the LAAPD by 5.9 keV X-rays, obtained for temperatures of 0 and 25 ºC. The same gain of 130 was used for both temperatures, corresponding to 1793 and 1720 V bias voltages, respectively. The X-ray counting rate in the photodiode is about 10^3/s. By comparing Figures 3.3 and 3.1, it is observed that the signal-to-noise ratio is considerably lower for X-ray detection comparatively to VUV-light detection. Figure 3.3 also confirms the improvement on the LAAPD performance when temperature decreases from 25 to 0 ºC. A dark current reduction from 130 to 22 nA improves the energy resolution from 16.3 to 12.8% and the minimum detectable energy from 1.5 to 1.0 keV.

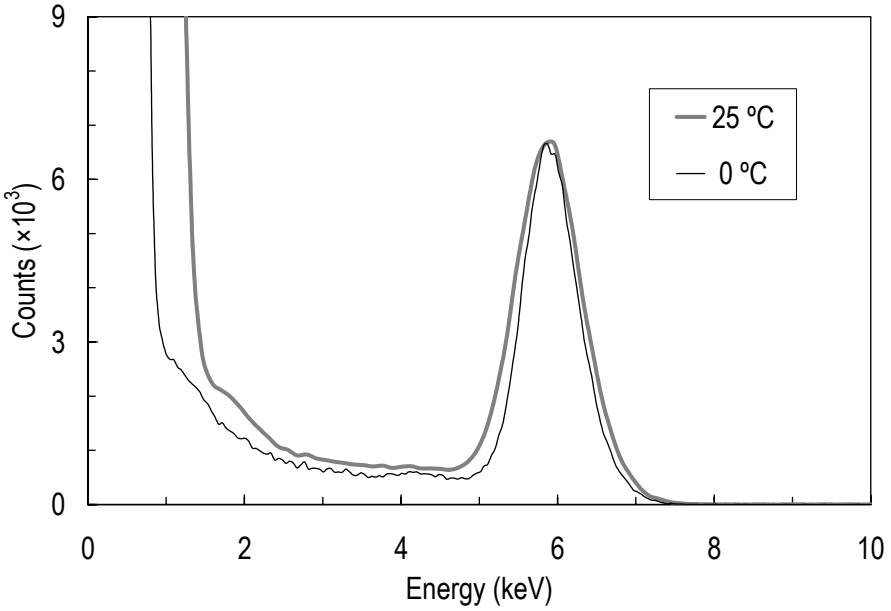

Figure 3.3 – Energy spectra of the pulses produced by 5.9 keV X-rays in the LAAPD, for different temperatures, 0 and 25 ºC. The same gain of 130 was used in the LAAPD.

The effect of dark current on the LAAPD performance for X-ray detection was evaluated by determining the energy resolution and the minimum detectable energy as functions of gain for different temperatures. In general, the temperature reduction improves the energy resolution and the minimum detectable energy as a result of the significant reduction of the dark current (Figure 3.4).

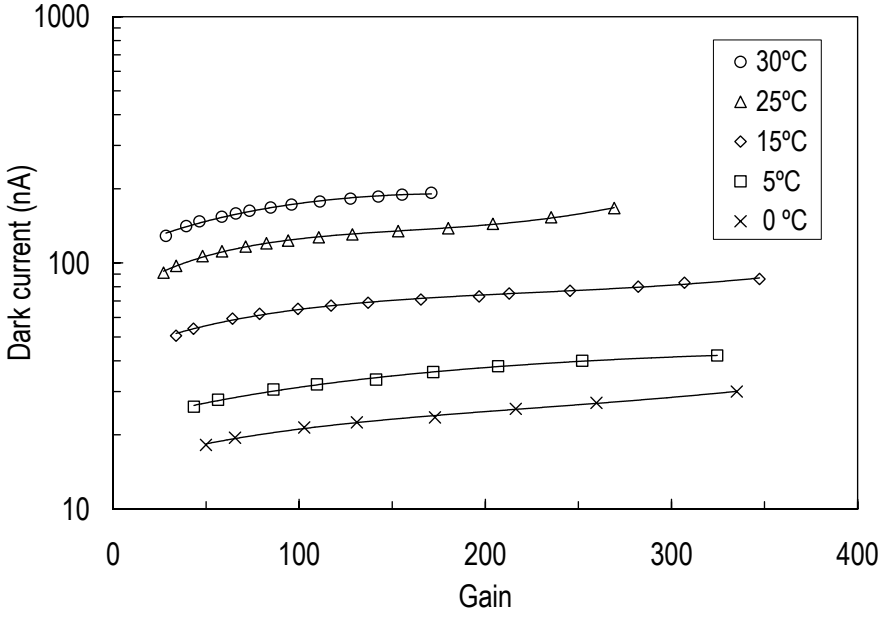

Figure 3.4 – Dark current as a function of the LAAPD gain for different temperatures.

For each temperature, the optimum gain, corresponding to the minimum energy resolution, was found to be around 130. According to the theoretical estimate, defined by Equation 1.31, some temperature dependence should occur:

$$G_{\text{opt}} = \left[\frac{2}{k_{ef}} \left(I_{DS} + 2 \frac{k_B T}{q} \frac{R_{eq} C_T^{\,2}}{\tau^2} \right) \Big/ \left(I_{DV} + \frac{4\,q}{e^2 \tau} \frac{E}{\varepsilon} \right) \right]^{1/3} \qquad \text{(Eq. 3.5)}$$

The optimum gain should increase with the superficial component (I_{DS}) of the dark current and decrease with the volumetric component (I_{DV}). However, both components increase with temperature. For 500 ns shaping time constants and for 0 ºC:

$$2\,k_B T\,R_s C_T^{\,2}/(q\tau^2) \cong 100 \text{ nA}$$

For temperatures in the range investigated, the previous factor undergoes a variation of only 12%, considering that the remaining parameters do not vary with temperature. Moreover, for 5.9 keV X-rays:

$$4\,qE\,/(e^2\tau\,\varepsilon) \cong 0.3 \text{ nA}.$$

The influence of dark current on the optimum gain described by Equation 3.5 is significant only for higher temperatures, where the dark current components are close to the previous factors. As temperature decreases, the influence is less significant, explaining the weak dependence of the optimum gain on temperature. The gain estimated by Equation 3.5 is about 100 if the dark current components are neglected. Due to the experimental errors in the energy resolution determination, a good agreement between the theoretical estimate and experimental results should be obtained.

The LAAPD behaviour as a function of the X-ray energy was studied using the fluorescence produced in several samples by ^{55}Fe and ^{109}Co radioactive sources. Good energy linearity was established in the 2-20 keV range, independently on temperature. However, the energy resolution tends to improve as the temperature decreases since the electronic noise contribution is reduced [Fernandes *et al.* 2004A]. The electronic noise effect on the energy resolution is higher for lower energy X-rays due to the greater proximity between the corresponding signals and the noise. As expected, the energy resolution decreases as the X-ray energy increases. However, it tends to stabilize for higher energies due to the greater distortion of the X-ray peak, resulting from a larger number of interactions in the multiplication region.

The cooling system based on the Peltier cell is not useful to investigate the LAAPD response for temperatures lower than -5 ºC due to the presence of very high leakage currents between the several electrodes, resulting from water condensation effects. In the next section, an alternative system is used, providing temperature stabilization for temperatures below 0 ºC. Thus, the LAAPD characteristics may be evaluated in a wider temperature range.

3.3. X-ray and visible-light detection with LAAPDs as a function of temperature (down to -40 ºC)

During the muonic hydrogen Lamb shift experiment, described in Chapter 4, a cooling system was assembled at the PSI in order to test the behaviour of avalanche photodiodes at low temperatures. The system, based on liquid nitrogen, was adequate to study the performance of LAAPDs as a function of temperature, providing LAAPD cooling down to about -40 ºC.

Figure 3.5 shows a schematic view of the cooling system based on liquid nitrogen. The detection system includes the LAAPD, a support structure for the photodiode irradiation and a thermocouple to measure the LAAPD operation temperature. The system was placed, together with the preamplifier, inside a box that provides thermal isolation from the exterior. The faces of the box are covered by gloomy plastic plates to protect the box volume against the ambient light. The cooling of the box volume is made through a continuous flow of cooled nitrogen gas. The gas enters the box through a plastic tube that connects the box to a liquid nitrogen reservoir and leaves through a tube placed on top of the box. Temperature stabilization is obtained through a heating resistor, with regulating power up to the maximum value of 200 W, which provides cooling down to about -40 ºC. The controller associated to the thermocouple indicates the LAAPD temperature with a precision of ± 0.5 ºC, not as good as for the LAAPD with integrated Peltier cell, where a ± 0.1 ºC precision was achieved.

The system presented in Figure 3.5 was used to study the LAAPD response to X-ray detection as a function of temperature, widening the temperature range used in the previous section to values below 0 ºC (down to about -40 ºC). The LAAPD response to the detection of visible-light pulses produced by a LED, with a peak emission at 635 nm, was also investigated.

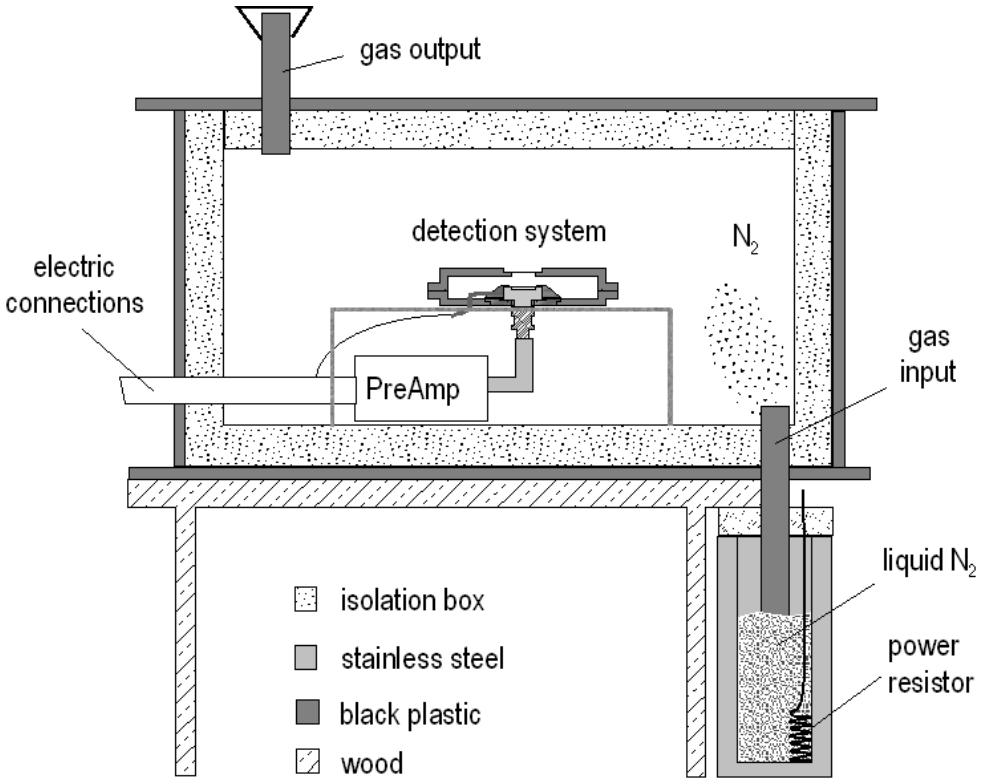

Figure 3.5 – Experimental system used for the LAAPD cooling through liquid nitrogen.

The LED was initially placed inside the box, together with the X-ray source, in order to irradiate the active area of the LAAPD. However, the amplitude of the light pulses emitted by the LED varies significantly with temperature. Afterwards, the LED was placed in the exterior in order to avoid great fluctuations on its temperature. The light emitted by the LED is guided to the detection system inside the box through a light guide, as shown in Figure 3.6.

Beyond a typical LAAPD, manufactured by API, a planar LAAPD from RMD was also tested. This type of photodiodes was used to substitute the API LAAPDs in the Lamb shift experiment since a significantly larger detection area is possible due to their compact shape. Both photodiodes were simultaneously irradiated by X-ray and visible-light sources (Figure 3.6). APD1 (from API) presents a circular area with 16 mm diameter, while APD2 (from RMD) presents a square shaped area of 14×14 mm^2.

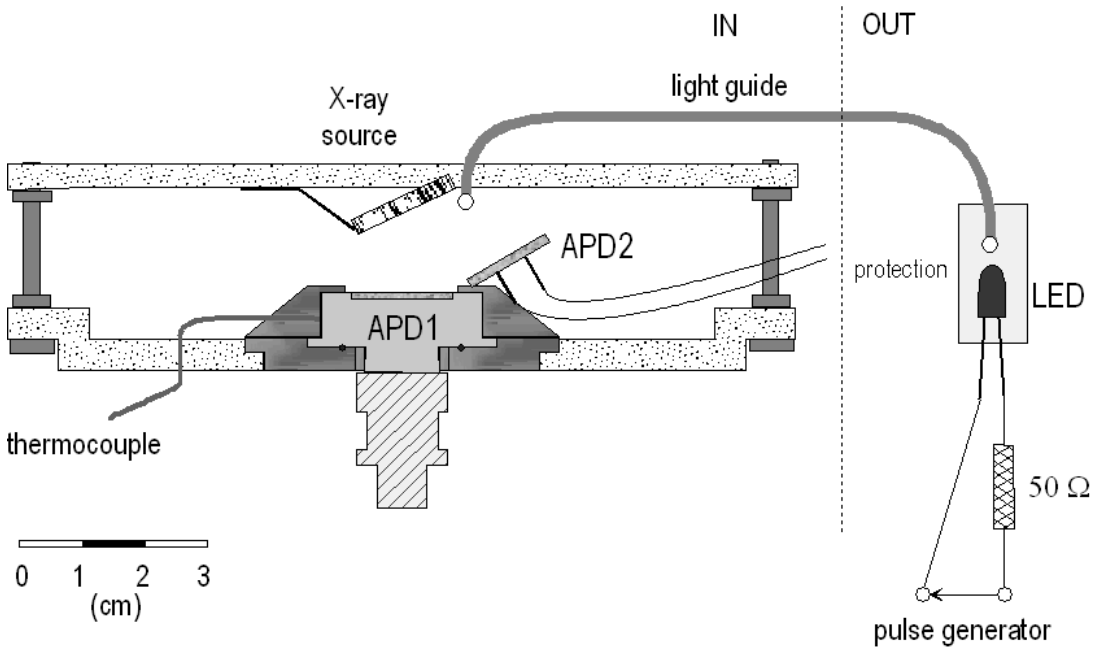

Figure 3.6 – Detail of the experimental system, showing the relative position of the investigated photodiodes (APD1 and APD2) and the radiation sources (X-ray source and LED).

The intensity of the visible-light pulses is determined by the LED current, which is defined by the resistance in series with the LED and the amplitude of the applied voltage pulse. The pulse generator used to polarize the LED (LED pulser *PSI LP103*) requires a 50 Ω output resistance and generates pulses with 6 to 500 ns width and amplitude up to 10 V. The width and amplitude of the pulses determine the amplitude of the signal produced in the LAAPD.

The performance characteristics of the LAAPD from API (APD1 in Figure 3.7) were evaluated for 5.9 keV X-rays and visible-light pulses, for different temperatures, being presented in the paper: "LAAPD low temperature performance in X-ray and visible-light detection", published in *IEEE Trans. Nucl. Sci.*, vol. 51 (2004), pages 1575-1580 [Fernandes *et al.* 2004C], attached at the end of this chapter (page 115). In addition to gain and energy resolution measurements, non-linearity effects and the several contributions to the energy resolution have been discussed, as well as the application of LAAPDs to X-ray spectrometry.

3.3.1. Gain measurements and non-linearity effects

The LAAPD gain was determined for 5.9 keV X-rays and visible-light pulses as a function of the bias voltage, for different temperatures. Since the signal-to-noise ratio is reduced for X-ray detection, the unitary gain was assessed by light pulses with 100 ns width. For visible light, the relative gain variation with temperature was found to be about -5% per ºC for the highest gains [Fernandes *et al.* 2004A,C], somewhat higher than the one obtained for X-rays but considerably higher than the value suggested by the manufacturer [API 1999].

Gain non-linearity was observed between X-rays and VUV light [Fernandes et al. 2002A] and between X-rays with different energies [Fernandes et al. 2001], as discussed in Chapter 2. The non-linearity measured for VUV light is more significant than the one reported for visible light [Moszynski et al. 2002A], showing that the non-linear behaviour cannot be attributed only to space charge effects as it happens for X-rays with different energies.

The non-linearity between the gains for X-rays and visible light was evaluated as a function of the light gain, for different temperatures, by means of simultaneous measurements of the amplitude of the signals produced by 5.9 keV X-rays from a ^{55}Fe source and light pulses emitted by the LED (Figure 3.6). It was shown that the ratio between the gains obtained for X-rays and visible light presents variations lower than 2% for gains up to 250, in the temperature range from -12 to 23 ºC, and increases with temperature [Fernandes *et al.* 2004C].

The average absorption length of visible-light photons in silicon is about 1 μm [Barnard *et al.* 1993] while for 5.4 keV X-rays it is 22 μm [Birks *et al.* 1981], approximately equal to the distance between the LAAPD surface and the multiplication region. Thus, practically all light photons leave their energy before that region, while a number of 5.4 keV X-rays are absorbed there, originating partial signal amplification. As the temperature increases, the avalanche zone also increases, worsening the previous effect and originating a higher number of pulses with lower amplitude. As a result, the ratio between X-ray and visible-light gains decreases.

Despite the variation with temperature, the deviation from linearity observed between X-rays and visible light is significantly lower than the one demonstrated for VUV-light pulses [Lopes *et al.* 2003]. As discussed in the previous chapter, those differences are related to the superficial absorption of VUV photons in the LAAPD.

The LAAPD non-linearity was also investigated for X-rays with different energies by determining the amplitude ratio between the signals produced by 14.4 and 6.4 keV X-rays emitted by a ^{57}Co source as a function of gain for different temperatures. The ratio decreases with gain, reaching a 3% variation for gains of about 300 [Fernandes *et al.* 2004C]. This result agrees with the one obtained for 16.6 and 5.9 keV X-rays (4% variation for a gain of 250) [Moszynski *et al.* 2002A] and for 22.1 and 5.9 keV X-rays (6% variation for the same gain) [Fernandes *et al.* 2001].

Considering that the relative amplitude for X-rays with different energies (E_1 and E_2) decreases linearly with gain, as the previous results indicate, the non-linearity (NL) of the gain obtained for X-rays with energy E_2 relatively to the gain (G) obtained for X-rays with energy E_1 (being $E_1 < E_2$) can be determined by:

$$NL \cong \frac{G}{114}\left(\frac{E_2}{E_1} - 1\right) \qquad \text{(Eq. 3.6)}$$

The previous equation leads to the estimate of the relative gain variation for X-rays with energies E_2 and E_1 (being E_1 about 6 keV) for LAAPDs manufactured by API.

The gain non-linearity for X-rays with different energies is practically independent on temperature, in opposite to the non-linearity between X-rays and visible light. The increase of the X-ray absorption length with the energy reflects in a significant efficiency reduction for energies above 6 keV since a higher number of X-rays cross the LAAPD depletion zone without being absorbed. For X-ray energies higher than 6 keV, the average absorption length is greater than the distance between the LAAPD surface and the multiplication region. Thus, the effect of temperature in the avalanche size does not vary significantly with the energy. In this case, the deviation from linearity results only from space charge effects, which obviously increases with energy.

3.3.2. Energy resolution analysis

The energy resolution of the LAAPD was determined as a function of the gain for 5.9 keV X-rays and visible light for different temperatures. For both types of radiation, the minimum energy resolution is achieved for gains in the 60-80 range for the temperature range investigated. The optimum gain practically does not depend on temperature and is in accordance with the theoretical estimate defined by Equation 3.5. In this equation, for 200 ns shaping constants and for $T = 293$ K:

$$2\, k_B T\, R_{eq} C_T^{\,2} / (q\tau^2) \cong 700 \text{ nA}$$

The previous factor does not vary significantly with the temperature. Additionally, for 5.9 keV X-rays:

$$4\, qE / (e^2 \tau\, \varepsilon) \cong 0.7 \text{ nA}$$

As the dark current components are negligible when compared to the previous factors, the optimum gain does not depend significantly on temperature.

According to the estimate of Equation 3.5, the optimum gain for visible-light pulses with 9.3 keV of energy deposited in the LAAPD is lower than the one for 5.9 keV X-rays by a factor $\sqrt[3]{9.3/5.9} \cong 1.16$. Due to the errors in energy resolution measurements, such a small difference could not be recognized.

The optimum gain of the present LAAPD is lower than the one of the LAAPD with Peltier cell. However, the optimum gain estimate defines a higher value for the present LAAPD due to the use of lower shaping time constants. Additionally, the experimental system associated to this photodiode was installed in an environment without electrostatic shielding, where the presence of parasite capacitances contributes significantly to the electronic noise, increasing its contribution to the energy resolution and affecting the optimum gain.

It was shown that the energy resolution for X-rays and visible light improves with the LAAPD cooling. However, its variation is less significant for temperatures lower than 0 ºC [Fernandes *at al.* 2004C]. To understand the energy resolution variation with temperature an analysis of the several contributions is necessary, mainly the dark current and the excess noise factor.

As discussed in Chapter 1, below the optimum gain the energy resolution decreases with the gain due to the increase of the signal-to-noise ratio. Above the optimum gain, the resolution slightly increases due to the raise with gain of the dark current and the excess noise factor. For X-rays, an additional contribution results from spatial non-uniformity. However, considering σ_U/G to be constant, the effect of the non-uniformity is not responsible for the energy resolution degradation with gain.

The dark current was registered for each voltage applied to the LAAPD and it was represented as a function of gain for different temperatures [Fernandes *at al.* 2004C]. For each temperature, the dark current components can be determined from a linear fit to the obtained curves:

$$I_D = I_{DS} + I_{DV}\ G \qquad \text{(Eq. 3.7)}$$

Figure 3.7 shows the dark current components (I_{DS} and I_{DV}) as functions of temperature. The variation of each component with temperature was determined from an exponential fit to the two series of points shown. The fit shows that both components have approximately equal dependences on temperature. For temperatures below -7 ºC, dark current measurements were not possible due to the minimum limit imposed by the power supply (1 nA). In the temperature range from -7 to 27 ºC, the dark current may be approximately described by (with the temperature T in K):

$$I_D = (9.5 + 0.026\ G)\ \exp\big(0.1\ (T - 273)\big)\ \text{[nA]} \qquad \text{(Eq. 3.8)}$$

The electronic noise contribution to the energy resolution (Equation 1.20) depends on dark current as well as on the excess noise factor, which also affects the intrinsic resolution of the LAAPD in light and X-ray detection, as determined by Equations 1.10

and 1.13. In order to estimate the energy resolution, based on the different contributions, the knowledge of the dependence of F on temperature is necessary.

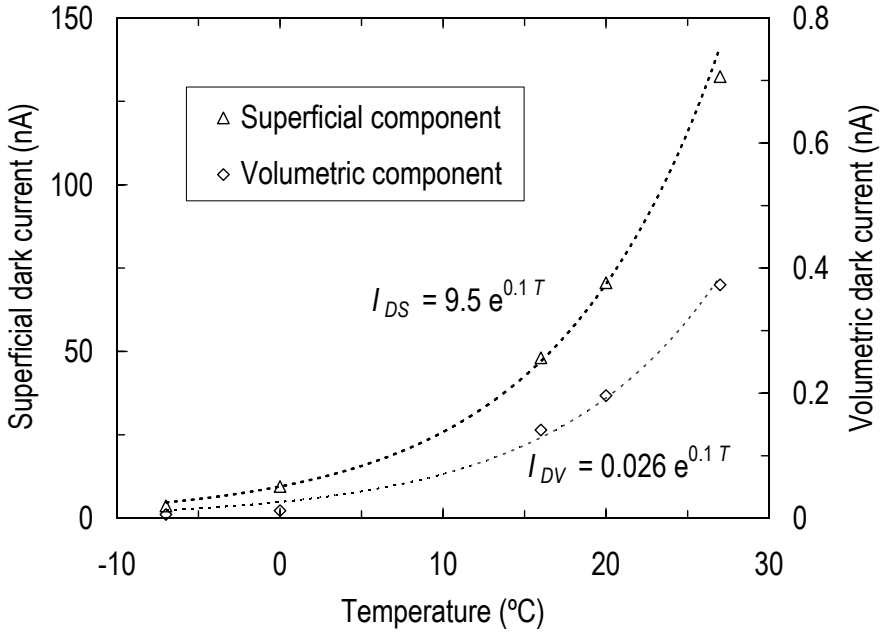

Figure 3.7 – Dark current components (I_{DS} and I_{DV}) as functions of temperature. The exponential fit provides the determination of the dependence of each component on temperature T (in ºC).

The excess noise factor was determined as a function of gain, for different temperatures, by measuring simultaneously the signals produced in the LAAPD by 5.4 keV X-rays from a ^{54}Mn source and visible-light pulses from the LED. The used method and the obtained results are presented in: "Excess noise factor in large area avalanche photodiodes for different temperatures", published in *Nucl. Instr. Meth. A*, vol. 531 (2004), pages 566-568 [Fernandes *et al.* 2004B]. The letter is attached at the end of the chapter (page 121). The results show that F practically does not vary with temperature and increases linearly with gain, according to:

$$F = (0.0021 \pm 0.0001)\,G + (1.715 \pm 0.011) \qquad \text{(Eq. 3.9)}$$

The obtained values are in accordance with the previous measurements carried out at room temperature [Moszynski *et al.* 2002A] and at liquid nitrogen temperature

[Moszynski *et al.* 2002B] for API photodiodes. The experimental values are lower than the theoretical estimate (Equation 1.26) and this difference is higher for lower gains.

The energy resolution dependence on temperature is not related to the excess noise factor, being the dark current its main limiting factor. The excess noise factor variation is reflected on the energy resolution degradation for high gains.

Electronic noise contribution

In the performed measurements, the noise contribution was determined as the full-width-at-half-maximum of the peak corresponding to the signal produced in the LAAPD by a pulse generator. The obtained values can be compared to the theoretical estimate for the electronic noise contribution, defined by Equation 1.20, taking into account the dark current components determined from Figure 3.7:

$$\Delta E_R^{\,2} = \left(2.36\,\frac{e\varepsilon}{qG}\right)^2 \left[\frac{k_B\,T\,R_{eq}}{2\tau}\,C_T^{\,2} + \frac{\tau\,q}{4}\,(9.5 + 0.026\,G^2\,F)\times 10^{-9}\,\exp\!\big(0.1\,(T-273)\big)\right]$$

Taking into account that the typical capacitance of API avalanche photodiodes with 16 mm diameter is 130 pF [API 1999] and that a *Canberra 2004* preamplifier was used, then $C_T \cong 130$ pF and $R_{eq} \cong 33\ \Omega$. In this manner, the previous equation can be used to estimate the noise contribution (in keV) as a function of gain for different temperatures, with F being defined by Equation 3.9.

Figure 3.8 shows the noise contribution, obtained from signals produced by the pulse generator, as a function of gain for different temperatures. The two hatched curves, also represented in the figure, correspond to theoretical estimates for temperatures of 0 and 23 ºC and for 200 ns shaping time constants. Due to the strong dependence of dark current on temperature, the electronic noise increases with temperature according to Figure 3.8, being the main factor responsible for the energy resolution variation with temperature.

Figure 3.8 shows that the noise behaviour as a function of gain depends on temperature. For higher temperatures, the electronic noise level initially decreases with gain, reaches a minimum value and increases slightly for higher gains. For 23 ºC, the increase takes place at gains above 200, being confirmed by the theoretical estimate for that temperature. For lower temperatures (0 ºC and below), the noise level decreases always with the gain, what is also confirmed by the theoretical estimate for 0 ºC.

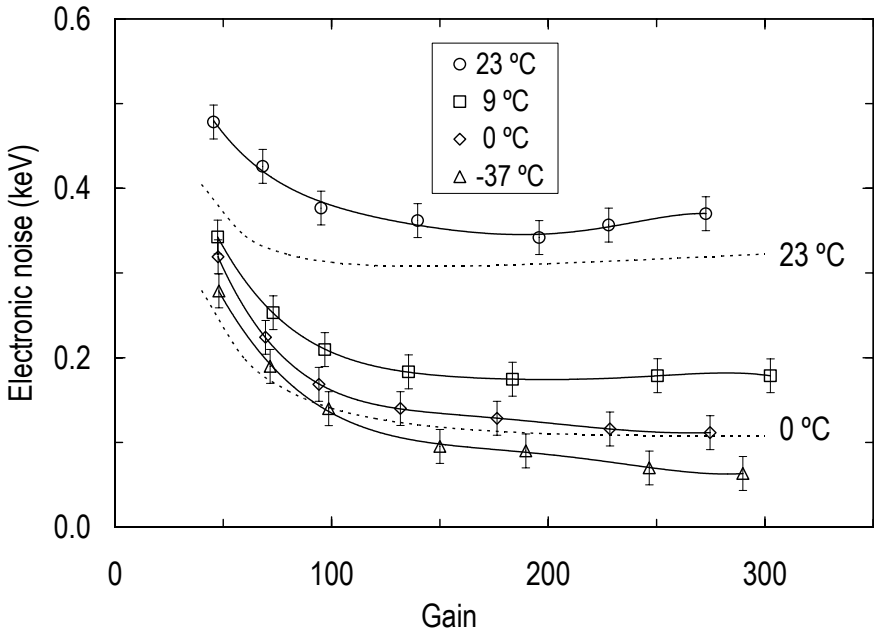

Figure 3.8 – Electronic noise contribution to the peak broadening of the signals produced in the LAAPD as a function of gain, for different temperatures. The hatched curves represent theoretical estimates (Equation 1.20) for temperatures of 0 and 23 ºC.

For each temperature, the difference between theoretical estimates and experimental values of the electronic noise is greater at lower gains, what may be related to the presence of parasite capacitances in the experimental system, as it was suggested before. This phenomenon is responsible for the increase of the noise associated to the preamplifier, which is more significant at reduced gains (Equation 1.20). For high gains, the noise is mainly determined by the dark current and the excess noise factor and that difference is smaller.

Intrinsic resolution

From excess noise factor measurements, described by Equation 3.9, the LAAPD intrinsic resolution may be determined. Additionally, from electronic noise estimates (Figure 3.8) the total energy resolution can be estimated and compared to the experimental values.

The intrinsic resolution was determined according to Equation 1.10 for 5.4 keV X-rays considering a 3% non-uniformity. Then, the total energy resolution has been estimated. Figure 3.9 presents the intrinsic resolution and the total energy resolution estimated for 5.4 keV X-rays as a function of gain for a temperature of 0 ºC. The measured energy resolution is also represented.

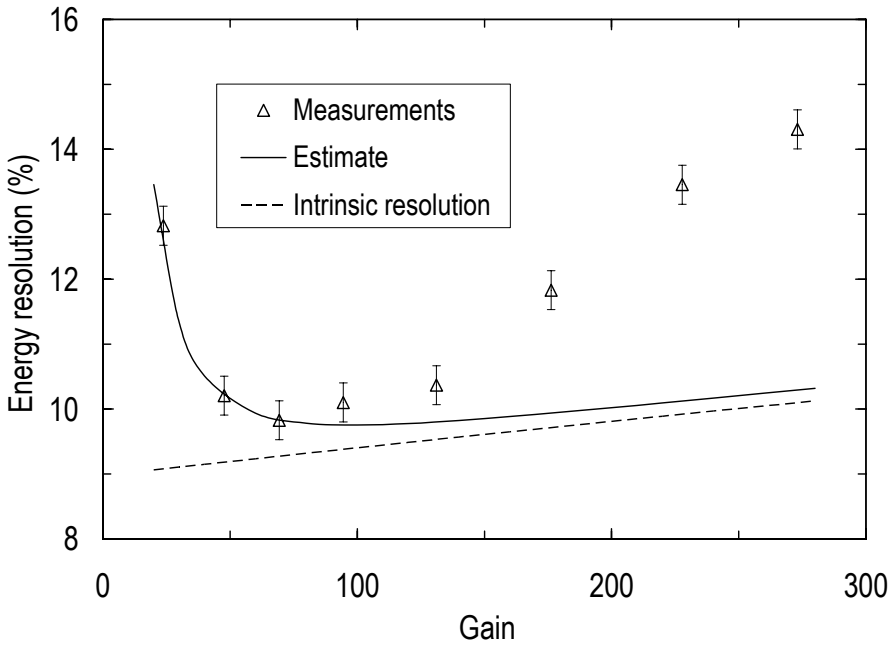

Figure 3.9 – Energy resolution (estimate and measurements) for 5.4 keV X-rays and intrinsic resolution as a function of gain, for a temperature of 0 ºC, assuming 3% non-uniformity.

The intrinsic resolution does not depend on temperature and increases with gain due to the excess noise factor, which limits the total energy resolution for high gains. Figure 3.9 shows that the energy resolution estimate for 3% non-uniformity is in agreement with the experimental values for gains below the optimum. For higher gains, the energy

resolution degradation is significant. As discussed previously, this behaviour is verified since lines K_α and K_β overlap in the same peak, originating a deficient fitting of the obtained amplitude distribution.

Although the energy resolution estimate agrees with measurements for lower gains, Figure 3.8 shows that at these gains the electronic noise estimate presents a greater deviation from the experimental values. The difference is nevertheless less significant for 0 ºC. This suggests that the LAAPD non-uniformity must be slightly lower than 3%, the value considered for the energy resolution estimate.

In addition, the advantages of the LAAPD cooling in its performance are evidenced in the energy spectra [Fernandes *et al.* 2004C] by the reduction of the electronic noise level and the improvement on the energy resolution as the temperature decreases. For temperatures below 0 ºC the energy resolution variation is nevertheless much lower. The effect of the temperature reduction is more significant for fluorescence X-rays with lower energies, closer to the noise level.

3.3.3. The planar LAAPD (from RMD)

The use of planar manufacture techniques, typical in semiconductor materials, lead to the development by RMD of avalanche photodiodes with different forms and larger areas at reduced costs. The edges of the silicon wafers used in the manufacture of APDs tend to have a high concentration of defects, which can cause electric discharges for lower electric fields. To correct this problem, the previous photodiodes (from API) presented bevelled edges, which required the use of special manufacture techniques, limiting the yield and increasing the cost of the APDs. Moreover, photodiodes obtained through that technique presented necessarily a circular shape. The technique developed by RMD eliminated the bevelled edge requirement, varying the doping profile in the several silicon layers. The width of the doped layers varies in order to originate a sloped profile as a replacement for the bevelled edge. This change provides a larger area for the electric field and locates the photodiode active area away from the defective edges.

Photodiodes manufactured through planar techniques, square shaped with a 14×14 mm^2 area, have been used as 1.9 keV X-ray detectors in the second phase of the muonic hydrogen Lamb shift experiment (Chapter 4). Besides the square shape, those photodiodes present relatively thin edges of inactive material, leading to the implementation of a configuration with larger detection area compared to the photodiodes previously used, with circular shape.

As stated in the previous section, the cooling system of Figure 3.5 was also used to investigate the performance of a planar LAAPD from RMD (APD2 in Figure 3.6) for X-ray and visible-light detection as a function of temperature. This photodiode presents relatively high dark current, hindering its use at room temperature, where the dark current can reach about 2 μA. Therefore, the LAAPD must be conveniently cooled in order to reduce sufficiently its dark current. The measurements for APD2 are detailed in [Ludhova *et al.* 2005]. The main results are summarized next.

Gain

APD2 unitary gain was determined using visible-light pulses from the LED, by measuring the amplitude of the corresponding signals produced in the LAAPD as a function of the bias voltage. Measurements were carried out at a temperature of 7 ºC because it was impossible to acquire complete measurements at room temperature, where the dark current is excessively high. The dark current was also measured for each applied voltage. The variation of the amplitude and dark current with the bias voltage is significantly higher for APD2 when compared to APD1.

The gain was measured as a function of the APD2 bias voltage for 5.9 keV X-rays and visible light, for different temperatures. As for APD1, for each applied voltage the relative gain variation with temperature is practically constant in the temperature range between -40 and 16 ºC. The gain drift with temperature increases with the LAAPD bias voltage, reaching -3.3% and -6.3% per ºC for 1530 and 1720 V, respectively. For visible light, variations of -2.8% and -5.6% per ºC were obtained for 1550 and 1660 V, respectively, similar to the results obtained with APD1.

Non-linearity

The non-linearity between the gains obtained in APD2 for X-rays and visible light was investigated for different temperatures by irradiating the LAAPD with 5.4 keV X-rays from a ^{54}Mn source and visible-light pulses from the LED. These pulses originate LAAPD signals with an amplitude equivalent to the one produced by 12 keV X-rays. The ratio between the X-ray and visible-light gains was determined as a function of the light gain. In the investigated temperature range, between -12 and 10 ºC, the non-linearity variation with temperature is not observed since there are large experimental errors resulting from the high noise level in the photodiode. A 15% reduction in the X-ray to visible light gain ratio was verified when the light gain was increased from 100 to about 700. The deviation from linearity (about 5% for a gain of 250) is considerably higher that the one obtained for APD1. However, as the photodiodes present different structures, high charge densities produced by X-ray interactions in the LAAPD for high gains originate different effects in the local electric field and heating in the avalanche zone, leading to different deviations from linearity.

The APD2 non-linearity was also investigated for X-rays with different energies (14.4 and 6.4 keV X-rays from a ^{57}Co source). The ratio between the amplitude of the two signals was determined as a function of gain, for different temperatures (1 and -20 ºC). A reduction of about 12% was obtained when the gain was increased from 50 to 500, independently on temperature. This variation is considerably higher relatively to the one of APD1, although being independent on temperature for both LAAPDs.

Energy resolution

The energy resolution of APD2 was determined as a function of gain for different temperatures for 5.9 keV X-rays and visible-light pulses. The energy resolution dependence on gain is similar to the one verified for APD1. However, its minimum value is obtained for considerably higher gains. This difference can be attributed to the dark current differences between the photodiodes, originating different noise levels,

considerably higher for APD2. The noise contribution to the energy resolution is greater in the low-gain region, affecting the optimum gain.

An optimum gain of about 200 was measured for 5.9 keV X-rays, while for visible light a value of about 400 was obtained, independent on temperature. The energy resolution degradation for high gains is less significant for visible light. For X-rays, the energy resolution raise above the optimum gain can be attributed to the overlap between K_α and K_β lines (5.9 and 6.4 keV) and to the inability to fit two Gaussians in the resulting distribution. This behaviour was also observed for APD1.

The energy resolution tends to improve with temperature reduction. For 5.9 keV X-rays, 23, 17 and 16% minimum values were obtained for temperatures of 10, -7 and -40 ºC, respectively. These values are considerably higher than the ones obtained for APD1. For both photodiodes, the energy resolution variation is less significant for temperatures below 0 ºC, although being more significant for APD2.

The main factors that contribute to the obtained energy resolution, namely the dark current and the excess noise factor, were also determined as a function of gain for different temperatures.

In the investigated temperature range, between -33 and 10 ºC, the dark current variation with the temperature T (in K) and the gain G can be described by:

$$I_D = (51 + 0.45\,G)\exp\big(0.11\,(T - 273)\big) \quad \text{[nA]} \qquad \text{(Eq. 3.10)}$$

For each temperature, the previous equation indicates dark current values considerably higher than for APD1, leading to worse energy resolution. On the other hand, the dark current relative variation with temperature is somewhat higher than for APD1. A reduction of about two orders of magnitude was observed when the temperature was decreases from 10 to -33 ºC. As a result, the improvement on the APD2 performance by cooling is more significant.

The excess noise factor was determined by simultaneous measurements of the signals produced by 5.4 keV X-rays, visible-light pulses and the signals from a pulse generator.

The results are similar to the ones obtained with APD1, despite the experimental errors being considerably larger for APD2. As expected, for gains between 50 and 700 the excess noise factor (F) increases linearly with gain (G), independent on temperature, according to:

$$F = 0.0014\,G + 1.95 \qquad \text{(Eq. 3.11)}$$

The results for APD2 demonstrate that the energy resolution dependence on temperature is not related to the excess noise factor, as verified for APD1. Thus, the electronic noise contribution is the main limiting factor of the energy resolution obtained at low temperatures.

Due to the strong variation of the dark current with temperature, the noise level is significantly reduced as the temperature decreases. The variation is however less significant below 0 ºC. Even though, APD2 variations are higher than the ones observed for APD1. As the dark current is higher for APD2, to obtain the same noise level as for APD1 considerably lower operation temperatures are required in order to decrease sufficiently the APD2 dark current.

As stated before, planar photodiodes of APD2 type, from RMD, have been chosen as substitutes for the photodiodes produced by API in the experiment described in the next chapter, where LAAPDs are used as 1.9 keV X-ray detectors. In the experiment, the operation temperature of RMD photodiodes should be lowered in comparison with API LAAPDs in order to reach the same performance for those X-rays.

Available online at www.sciencedirect.com
SCIENCE DIRECT®
Nuclear Instruments and Methods in Physics Research A 504 (2003) 331–334
NUCLEAR INSTRUMENTS & METHODS IN PHYSICS RESEARCH Section A
www.elsevier.com/locate/nima

VUV detection in large-area avalanche photodiodes as a function of temperature

J.A.M. Lopes[a], L.M.P. Fernandes[a], J.M.F. dos Santos[a,*], R.E. Morgado[b], C.A.N. Conde[a]

[a] *Departamento de Física, da Universidade de Coimbra, Coimbra 3004-516, Portugal*
[b] *Los Alamos National Laboratory, New Mexico, NM 87545, USA*

Abstract

The response of a Peltier-cooled large-area avalanche photodiode to VUV-light is investigated as a function of the operation temperature. The reduction of the temperature down to 5°C will improve both photodiode light-level detection limit and statistical fluctuations; further temperature reduction will not result in improved performance. Optimum operation characteristics are already achieved for gains around 100 and do not depend significantly on the operation temperature. The relative variation of the gain with temperature increases with the biasing voltage presenting values that are almost a factor of two higher than for visible light detection.

PACS: 07.60.Rd; 29.40.Mc; 85.60.Dw

Keywords: LAAPD; VUV; Photon-detection

1. Introduction

Avalanche photodiodes (APDs) have increasingly assumed important roles in instrumentation for medium- and high-energy physics. Particularly, they present alternatives to UV- and visible-photon detectors, as well as to X-ray detectors. They are compact, have low-power consumption and are simple operation devices. Operational characteristics as high quantum efficiency, relatively high internal gain and insensitiveness to strong magnetic fields, combined with relatively low response to ionising particles, make them competitive for using in the electromagnetic calorimeter of the CMS detector at the LHC [1,2]. Also, their application to PET devices is under investigation [3,4]. Recently, their application as the VUV photosensor in gas proportional scintillation counters (GPSC) has been investigated [5,6]. It was shown that VUV large area APDs (LAAPDs) can replace the photomultiplier tubes with advantages.

The dependence of photodiode gain on the temperature requires temperature stabilisation and/or compensation during measurements, which is a drawback for many applications. In particular, the knowledge of the gain variation with the temperature is important to allow for corrections

*Corresponding author. Tel.: +351-239-410667; fax: +351-239-829158.
E-mail address: jmf@gian.fis.uc.pt (J.M.F. dos Santos).

0168-9002/03/$ - see front matter
doi:10.1016/S0168-9002(03)00763-0

due to small drifts in the operation temperature. This variation has been studied for visible-light detection reaching values about 3%/°C for maximum gains [7]. However, it has been proved that some LAAPD characteristics are different for visible- and VUV-light detection, namely linearity effects [8] and the response under intense magnetic fields [9]. While visible photons interact deeper in the diode, VUV photons interact within the first few atomic layers: penetration depths in Si are about 5 nm and 1 μm for 172- and 520-nm photons [10], respectively.

In the present work we will use a Peltier-cooled LAAPD [7] as the VUV scintillation readout of a xenon-GPSC to study the photodiode response to VUV as a function of the temperature. The photodiode gain and overall statistical fluctuations will be studied for different diode temperatures.

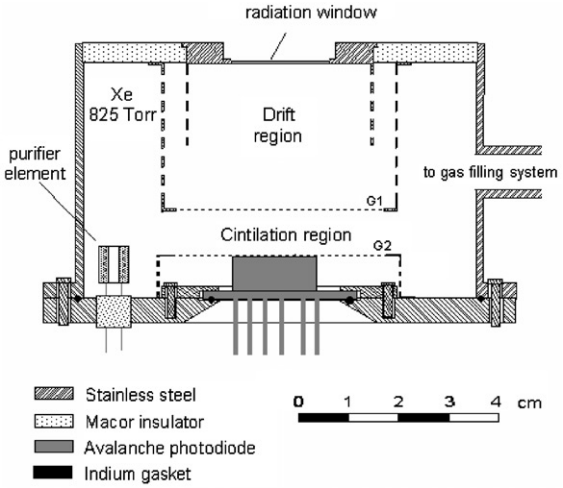

Fig. 1. Schematic of the GPSC with the Peltier-cooled LAAPD photosensor.

2. Description

The LAAPD is used as the VUV photosensor of a GPSC. Through the last decades GPSCs have been studied in detail and its use was mainly directed to X-ray spectrometry. However, the electroluminescence mechanism characteristic of the GPSC operation can be used for VUV production with known photon output (e.g. [5,6]).

The GPSC integrated with the LAAPD is depicted schematically in Fig. 1. It features a 3.1-cm deep absorption region, a 0.9-cm scintillation region, and is filled with pure xenon at 825 Torr ($\sim 1.09 \times 10^5$ Pa) continuously purified by a gettering device. G1 and G2 are highly transparent stainless-steel wire mesh grids used to establish the electric fields inside the detector. The LAAPD has a 16-mm active diameter and presents 105% quantum efficiency at 172 nm [7].

To produce a fixed amount of VUV photons incident on the LAAPD, 5.9-keV X-rays Mn K_α X-rays from a ^{55}Fe radioactive source, with the K_α-line absorbed by a chromium foil, were allowed to interact in the GPSC. The 5.9-keV X-rays interact in the drift region producing a cloud of $N_e = E_x/w = 269$ primary electrons, where $E_x = 5900$ eV and $w \sim 22$ eV/ion pair. The primary electron cloud drifts towards the scintillation region, under the influence of a weak electric field between the entrance window and grid G1, chosen to be below the xenon scintillation threshold. In the scintillation region, the electrons gain energy in the high electric field between grids G1 and G2 that is chosen to be above the scintillation threshold but below the electron impact ionisation threshold. The radiation window is biased at negative high voltage and electric fields of 0.8 and 6.2 V cm^{-1}Torr^{-1} were used in the drift and scintillation regions, respectively.

For the described conditions about 118 VUV photons were collected in the LAAPD for each primary electron traversing the scintillation region [5], resulting in a total of about 3.2×10^4 detected photons per X-ray interaction. The scintillation photons incident on the LAAPD produced photoelectrons that were amplified by the avalanche process. The signals were fed through a Canberra 2004 preamplifier and a HP5582A amplifier, with 2-μs shaping time constants, to a Nucleus PCA-II MCA. The 5.9-keV X-ray pulse-height distributions were fitted to a gaussian function superimposed on a linear background, from which the centroid and the full-width at half-maximum were determined.

3. Experimental results and discussion

In Fig. 2 we depict the LAAPD gain as a function of the biasing voltage for different LAAPD operation temperatures. The gain increases with decreasing temperature, with maximum achievable gains increasing from 300 to values above 700 as the temperature decreases from 25°C to −5°C. For each measurement, the diode temperature was stabilised within ±0.1°C.

From the data of Fig. 2 we obtained the LAAPD gain as a function of the temperature, for different biasing voltages, Fig. 3. For each voltage, the gain relative variation is almost constant through the measured temperature range, increasing from 2.7% to 5.6%/°C as the LAAPD bias increases from 1633 to 1826 V. For gains around 200 and for room temperature, the results show relative amplitude variations that are almost a factor of two higher than the ~3%/°C obtained for visible light [7].

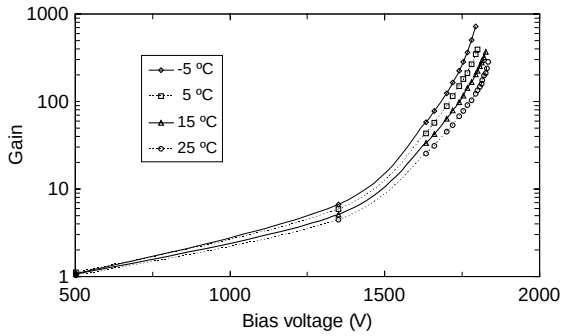

Fig. 2. LAAPD gain as a function of the biasing voltage for different operation temperatures.

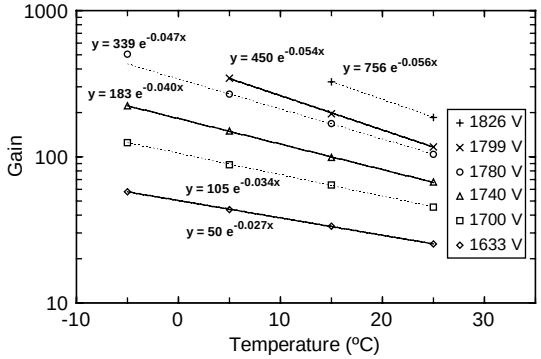

Fig. 3. LAAPD gain as a function of the operation temperature for different biasing voltages.

The electronic noise-tail limits the minimum number of detectable VUV-photons (MDP), defined as the number of photons corresponding to the amplitude-limit where the electronic-noise tail rises above the background level. This value is a measure of how effective the LAAPD gain is in separating a VUV-light signal from the noise. Fig. 4 depicts the MDP as a function of the gain for the different operation temperatures. The MDP stabilises for gains around 100 and improves with decreasing LAAPD temperature but, below 5°C, the observed improvement is not significant.

The statistical fluctuations associated with the light amplification process in GPSCs are negligible compared to those associated with the primary electron cloud formation and with the photon detection and signal amplification in the photosensor. The statistical fluctuations associated with the primary electron cloud formation in a gaseous detector are well known [11] and, thus, we can estimate the statistical fluctuations associated with the LAAPD VUV detection from the measured statistical fluctuations observed for the 5.9-keV X-rays in the GPSC. Fig. 5 presents the relative fluctuations estimated for the LAAPD detection of VUV photons as a function of the diode gain, for different diode temperatures. The correlation between Figs. 4 and 5 is noticeable: for each temperature, the minimum energy resolution is

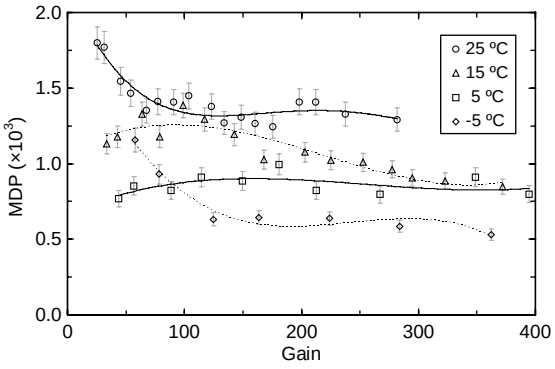

Fig. 4. Minimum number of detectable VUV photons (MDP) in the LAAPD as a function of the gain for different operation temperatures.

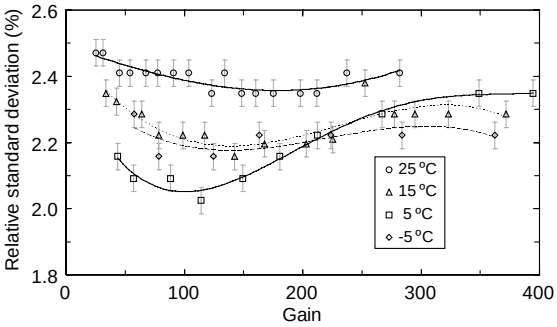

Fig. 5. Relative standard deviation for the fluctuations associated with the detection of 3.2×10^4 VUV-photons as a function of the LAAPD gain, for different operation temperatures.

achieved for the lowest gains where the MDP stabilises, and operation temperatures below 5°C will not result in a significant improvement of the statistical fluctuations.

4. Conclusions

The VUV photon detection with LAAPD improves with decreasing photodiode operation temperature. However, for temperatures below 5°C the improvement is not significant. Optimum operation characteristics are already achieved for gains around 100 and do not depend significantly on the operation temperature. The significant increase of the excess noise factor [12] (a factor that is related to the gain fluctuations in the multiplication process) for high gains becomes dominant, resulting in degraded performance of the photodiode.

The relative variation of gain with temperature increases with the biasing voltage, presenting values that increase from 2.7%/°C to 5.6%/°C when the voltage is increased from 1633 to 1826 V. These values are almost a factor of two higher than for visible light detection.

Acknowledgements

This work was performed in Unit 217/94, FCTUC. Support is acknowledged to project CERN/FIS/43785/01. LMP Fernandes acknowledges grant SFRH/BD/5426/2001 from Fundação para a Ciência e a Tecnologia, Portugal.

References

[1] A. Karar, Y. Musienko, J.Ch. Vanel, Nucl. Instr. and Meth. A 428 (1999) 413.
[2] K. Deiters, Y. Musienko, S. Nicol, et al., Nucl. Instr. and Meth. A 442 (2000) 193.
[3] A. Ruru Chen, A. Fremout, S. Tavernier, et al., Nucl. Instr. and Meth. A 433 (1999) 637.
[4] V.N. Solovov, V. Chepel, M.I. Lopes, et al., IEEE Trans. Nucl. Sci. NS-47 (2000) 1307.
[5] J.A.M. Lopes, J.M.F. Dos Santos, R.E. Morgado, C.A.N. Conde, IEEE Trans. Nucl. Sci. NS-48 (2001) 312.
[6] C.M.B. Monteiro, J.A.M. Lopes, P.C.P.S. Simões, et al., IEEE Trans. Nucl. Sci. NS-48 (2001) 1081.
[7] Advanced Photonix, Camarillo, CA, USA: Windowless large area APDs ($5 \times \phi$ deep-UV series), Application Notes.
[8] L.M.P. Fernandes, J.A.M. Lopes, C.M.B. Monteiro, et al., Nucl. Instr. and Meth. A 478 (2002) 395.
[9] L.M.P. Fernandes, A. Antognini, M. Boucher, et al., Nucl. Instr. and Meth. A 498 (2003) 362.
[10] T.W. Barnad, MM.I. Crockett, J.C. Ivaldi, et al., Anal. Chem. 65 (1993) 1231.
[11] J.M.F. dos Santos, J.A.M. Lopes, J.F.C.A. Veloso, et al., X-ray Spectrom. 30 (2000) 373.
[12] M. Moszynski, M. Szawlowski, M. Kapusta, M. Balcerzyk, D. Wolski, Nucl. Instr. and Meth. A 442 (2000) 230.

Available online at www.sciencedirect.com
SCIENCE DIRECT®
Nuclear Instruments and Methods in Physics Research B 213 (2004) 267–271
NIM B
Beam Interactions with Materials & Atoms
www.elsevier.com/locate/nimb

X-ray spectrometry with Peltier-cooled large area avalanche photodiodes

L.M.P. Fernandes, J.A.M. Lopes, J.M.F. dos Santos *, C.A.N. Conde

Departamento de Física da Universidade de Coimbra, 3004-516 Coimbra, Portugal

Abstract

Performance characteristics of the response of a Peltier-cooled large-area avalanche photodiode are investigated. Detector gain, energy linearity, energy resolution and minimum detectable energy are studied at different operation temperatures. Detector energy resolution and lowest detectable X-ray energy present a strong improvement as the operation temperature is reduced from 25 to 15 °C and slower improvements are achieved for temperatures below 10 °C.

PACS: 07.85.Fv; 29.40.Wk; 85.60.Dw
Keywords: Avalanche photodiode; X-ray spectrometry; Peltier-cooling

1. Introduction

Large-area avalanche photodiodes (LAAPD) are compact, simple to operate monolithic devices made of silicon p–n junctions. When a reverse high voltage is applied to the LAAPD the internal electric field increases with the depth, presenting a maximum around the p–n junction. The electric field can reach values high enough to allow electron multiplication by impact ionisation [1–3]. An incident photon produces electron hole pairs and the resulting electrons are accelerated towards the n^+-contact, undergoing avalanche multiplication due to the high electric field around the junction.

LAAPDs have been used mainly as optical photosensors coupled to scintillators for X- and γ-ray detection in applications such as the electromagnetic calorimeter of the CMS detector in the LHC at CERN [4], nuclear physics [5] and PET instrumentation for medicine [6]. The application of LAAPDs to direct X-ray detection has also been investigated [7]. Since LAAPDs useful thickness for X-ray detection is only a few tens of micrometers, their detection efficiency decreases rapidly for X-ray energies above 5 keV, being about 45%, 25%, 8% and 4% for 8, 10, 15 and 20 keV, respectively.

The performance of LAAPDs for energy-dispersive X-ray fluorescence analysis was studied [8]. Energy resolutions similar to those of proportional counters were obtained and the minimum detectable X-ray energy (MDE) was in the 1–2 keV range. The LAAPD dark current affects the

* Corresponding author. Tel.: +351-239-410667; fax: +351-239-829158.
E-mail address: jmf@gian.fis.uc.pt (J.M.F. dos Santos).

0168-583X/$ - see front matter © 2003 Elsevier B.V. All rights reserved.
doi:10.1016/S0168-583X(03)01607-0

achieved detector energy resolution and limits the MDE. However, the LAAPD gain and dark current depend significantly on the temperature, a drawback for many practical applications. This dependence requires temperature control and stabilisation during measurements. Temperature stabilisation can be achieved by Peltier-cooling. LAAPDs with built-in Peltier-cooled devices are commercially available. On the other hand, the operation of LAAPDs at reduced temperatures may result in improved performance and lower X-ray energy detection limit: the LAAPD dark current can be reduced by about one order of magnitude when its temperature is reduced from room temperature to 0 °C.

In this work we investigate the performance of a Peltier-cooled LAAPD for X-ray detection as a function of the temperature. The photodiode gain, energy resolution and MDE will be studied for different photodiode temperatures.

2. Operational characteristics

The Peltier-cooled LAAPD [9], with 16-mm diameter active area, was operated in a light-tight box to shield it from ambient light. The LAAPD signals were fed through a low-noise charge preamplifier (Canberra 2004, with a sensitivity of 45 mV/MeV) to a spectroscopy amplifier (Tennelec TC 243, with gains of 32–256 and 500 ns shaping time) and were pulse–height analysed by a 1024-channel multi-channel analyser (Nucleus PCA II).

For pulse amplitude and energy resolution measurements, the X-ray pulse–height distributions were fitted to a Gaussian function superimposed on a linear background, from which the centroid and the full-width at half-maximum were determined. The electronic noise tail at low energies limits the MDE, which we define as the energy limit where the electronic-noise tail raises above the background level.

The operational characteristics of the LAAPD at different temperatures were evaluated with 5.9-keV X-rays, using count rates of the order of 10^3 c/s. For X-ray spectrometry applications, fluorescence X-rays were induced in single and multi-element samples by ^{55}Fe and ^{109}Cd collimated sources, as shown in Fig. 1.

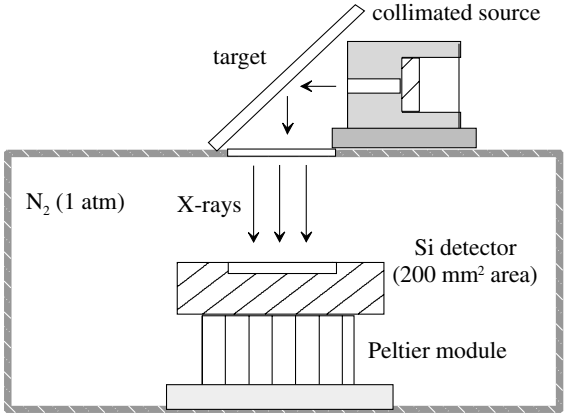

Fig. 1. Experimental setup for X-ray spectrometry applications.

The LAAPD gain was calibrated with 170 nm UV light, chosen for being fully absorbed in the LAAPD before the multiplication region. The operating temperature was stabilised within ±0.1 °C.

In Fig. 2 we depict the LAAPD gain as a function of the operation temperature for different biasing voltages. For each voltage, the gain relative variation is almost constant through the measured temperature range, increasing from 2.4% to 4.5% per °C, as the LAAPD biasing increases from 1633 to 1807 V. This ratio is somewhat higher than that measured for visible light, which is only about 3% for the highest gains [10].

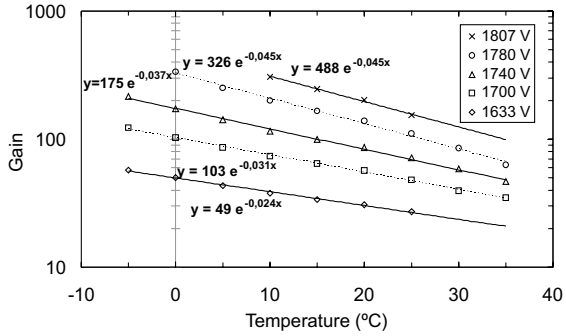

Fig. 2. LAAPD gain as a function of operating temperature for different bias voltages.

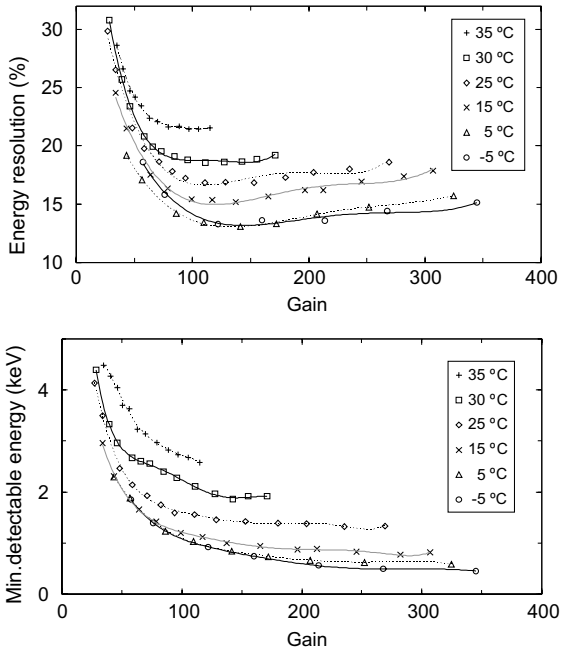

Fig. 3. LAAPD energy resolution and minimum detectable energy as a function of gain for different operating temperatures.

In Fig. 3 we present the detector energy resolution and the MDE as a function of the gain for different temperatures. The data clearly show the advantages of operating the photodiode at low temperatures. Best detector energy resolutions are achieved at gains of about 130, almost independent from the operation temperature, while the minimum detectable energy stabilises for gains above 200.

Table 1 presents the LAAPD optimum operational characteristics for 5.9-keV X-rays as well as the best MDE achieved, for the different studied temperatures. For temperatures below 5 °C both energy resolution and MDE do not improve significantly. At 5 °C, the MDE is about a factor of 2 and 3 less than that achieved at 20 and 25 °C, respectively.

Fig. 3 reflects the effect of the dark current on the LAAPD performance. Higher dark current will result in worse device performance for both detector energy resolution and MDE. Detector energy resolution degradation with increasing detector biasing, for gains above ~130, cannot be related to the dark current only, since MDE stabilises. In fact, for gains above ~130 the contribution of the excess noise factor [10,11] becomes dominant. This factor is related to the gain fluctuations in the multiplication region and increases significantly for high gains [7].

The optimum operation gain depends on the individual LAAPD, and for each one a compromise between the gain and the device's dark current has to be established [8]. We note that, for low energy X-rays, this compromise is achieved for increasing gains since the noise contribution to the detector energy resolution becomes more significant as the X-ray energy approaches the MDE. For these cases, a higher gain will result in a lower MDE with a lower contribution of the noise to the energy resolution.

3. X-ray spectrometry applications

The energy linearity and energy resolution of the LAAPD were determined in the 2–20 keV X-ray

Table 1
LAAPD optimum operational characteristics for 5.9-keV X-rays and best MDE achieved for temperatures in the −5 to 35 °C range

Temperature (°C)	Voltage (V)	Gain	En. Res. (%)	MDE (keV)	Best MDE (keV)
−5	1700	122	13.3	0.9	0.5
0	1720	131	13.1	0.9	0.5
5	1740	141	13.1	0.8	0.6
10	1747	126	14.6	1.0	0.7
15	1760	127	15.2	1.1	0.8
20	1770	124	15.7	1.2	1.0
25	1794	130	16.8	1.5	1.3
30	1820	128	18.5	2.0	1.9
35	1847	115	21.5	2.6	2.6

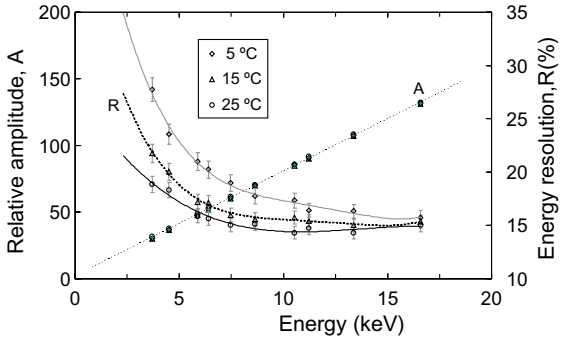

Fig. 4. Detector amplitude and energy resolution as a function of X-ray energy for different operation temperatures.

energy range using the fluorescence radiation induced in single-element samples. The centroid and relative full-width at half-maximum values of the pulse–height distributions are plotted in Fig. 4 as a function of the X-ray energy for different temperatures. At each temperature the LAAPD was operated with a biasing voltage corresponding to the gain of 130.

While the detector energy linearity presents the same slope for all temperatures, the energy resolution improves with decreasing temperature. This is due to the decrease with temperature of the electronic noise which is more significant for lower energy values.

Fig. 5 depicts typical pulse–height distributions obtained for sulphur and biotite samples for different operation temperatures, excited with ^{55}Fe and ^{109}Cd X-ray sources. The spectra are similar to those obtained with a conventional PC.

Table 2 presents the LAAPD optimum operational characteristics for 2.3-keV X-rays for each temperature. As discussed, best energy resolutions for 2.3-keV X-rays are achieved for higher gains than for 5.9-keV X-rays and best results are reached for lower operation temperatures. The MDE is about a factor of 2 higher than achieved for the conditions at which 5.9-keV X-ray peaks were obtained due to the much lower count rate reached for the sulphur peak, 4 c/s.

4. Conclusions

Detector energy resolution and lowest detectable X-ray energy present a strong improvement as

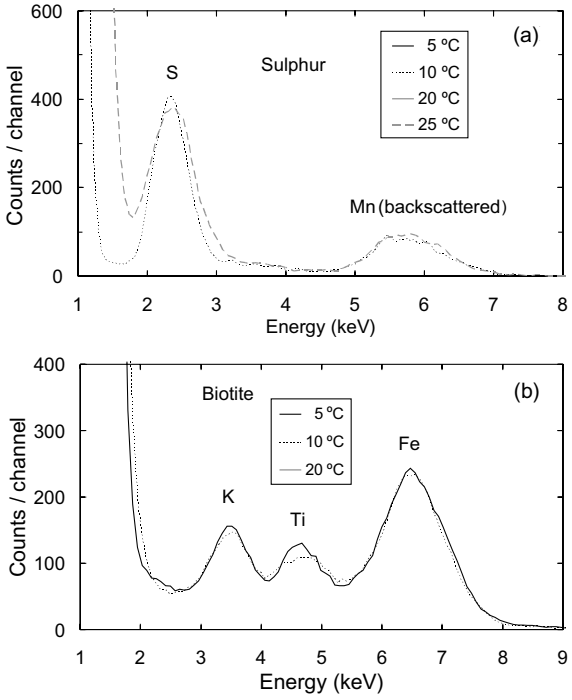

Fig. 5. Pulse–height distributions obtained with the Peltier-cooled LAAPD for sulphur (a) and biotite (b) fluorescence X-rays and for different operation temperatures.

Table 2
LAAPD optimum operational characteristics for 2.3-keV X-rays achieved for temperatures in the −5 to 25 °C range

Temperature (°C)	Voltage (V)	Gain	En. Res. (%)	MDE (keV)
−5	1766	345	22.4	1.1
0	1780	335	22.8	1.2
5	1793	325	23.3	1.1
10	1807	307	23.8	1.3
15	1815	282	24.1	1.3
20	1820	247	27.4	1.4
25	1838	235	29.9	1.7

the operation temperature is reduced from 25 to 10 °C and much slower improvements for temperatures below 10 °C. While for 5.9-keV X-rays the performance does not improve significantly for temperatures below 5–10 °C, for lower energies lower operation temperatures may further improve the detector performance. Additionally, while for 5.9-keV X-rays optimum gains, around 130, are

only slightly dependent on the operation temperature, for low energy X-rays optimum performance is obtained for increasing gains, reaching values above 300 for operation temperatures below 10 °C and for 2.3-keV X-rays.

References

[1] A.Q.R. Baron, S.L. Ruby, Nucl. Instr. and Meth. A 343 (1994) 517.
[2] E.M. Gullikson, E. Gramsch, M. Szawlowski, Appl. Opt. 34 (1995) 4662.
[3] J.P. Pansart, Nucl. Instr. and Meth. A 387 (1997) 186.
[4] K. Deiters, Y. Musienko, S. Nicol, et al., Nucl. Instr. and Meth. A 442 (2000) 193.
[5] R. Farrel, F. Olschner, K. Shah, M.R. Squillante, Nucl. Instr. and Meth. A 387 (1997) 194.
[6] A. Ruru Chen, A. Fremout, S. Tavernier, et al., Nucl. Instr. and Meth. A 433 (1999) 637.
[7] M. Moszynski, M. Szawlowski, M. Kapusta, et al., Nucl. Instr. and Meth. A 442 (2000) 230.
[8] L.M.P. Fernandes, J.A.M. Lopes, J.M.F. dos Santos, C.A.N. Conde, X-ray Spectrom. 30 (2001) 164.
[9] Advanced Photonix Inc., 1240 Avenida Acaso, Camarillo, CA 93012, USA.
[10] Advanced Photonix Inc., Windowless large area APDs (5×0 deep-UV series), Application Notes.
[11] J.A.M. Lopes, J.M.F. dos Santos, C.A.N. Conde, IEEE Trans. Nucl. Sci. 48 (2001) 312.

LAAPD Low Temperature Performance in X-Ray and Visible-Light Detection

L. M. P. Fernandes, J. A. M. Lopes, J. M. F. dos Santos, P. E. Knowles, L. Ludhova, F. Mulhauser, F. Kottmann, R. Pohl, and D. Taqqu

***Abstract*—The performance of a large area avalanche photodiode (LAAPD) has been investigated for X-ray and visible-light detection as a function of temperature. Energy resolution improves significantly with decreasing temperature down to 0 °C and, below that value, at a much slower rate, achieving 9.6% for 5.9 keV X-rays at 0 °C and for a gain of 60. The gain drift with temperature increases with the reverse bias voltage and is almost constant for temperatures above −15 °C, reaching rates higher than −5% per degrees Celsius, for a bias voltage of 1770 V. Similar results were obtained for X-ray and visible-light detection. LAAPD nonlinearity between X-ray and light gains is less than 2%, even for gains around 300, and decreases with temperature, being less than 0.5% at 0 °C, for gains up to 200. For X-rays, the minimum detectable energy is about 0.7 keV at operation temperatures around 16 °C, for gains above 100, decreasing to about 0.3 keV at temperatures less than 0 °C, for gains above 200.**

I. Introduction

LARGE-AREA AVALANCHE PHOTODIODES (LAAPD) are compact, simple to operate, monolithic devices, made of silicon p-n junctions. When a reverse high voltage is applied to the LAAPD, the internal electric field increases with depth presenting a maximum around the p-n junction and reaching values high enough to allow electron multiplication by impact ionization [1]–[3]. An incident photon produces electron-hole pairs and the resulting electrons are accelerated toward the n^+ contact, undergoing avalanche multiplication due to the high electric field around the junction. Gains of several hundred can be achieved in this process.

The growing interest in applications of LAAPDs triggered the development of industrial production of such devices, and the study and characterization of the different commercially available APDs is being carried out (e.g., Hamamatsu [4]–[6], EG&G [6]–[8], API [4], [9], [10], and RMD [11], [12]).

LAAPDs have been used mainly as optical photosensors coupled to scintillators for X- and γ-ray detection, in applications such as the electromagnetic calorimeter of the CMS detector in the LHC at CERN [3], [5], [6], nuclear physics [10], [11], PET instrumentation for medicine [8], [13], [14], and in X-ray spectrometry with gas proportional scintillation counters [15], [16], delivering a performance similar or even better than PMTs. High quantum-efficiency, low power-consumption, ruggedness, compactness, and insensitivity to intense magnetic fields [17] are the main advantages of LAAPDs over conventional PMTs, while the lower gain, higher noise, reduced sensitive area, and susceptibility to radiation damage present the main limitations.

The application of LAAPDs to direct X-ray detection has also been investigated [1]–[4], [9], [18]–[22]. Low-energy X-ray detection techniques with APDs were mainly developed to measure charge carrier properties of the device, using X-rays as a reference for light measurements [3], [6], [9], [10], [22], [23]. Since the LAAPD thickness that is useful for X-rays is only a few tens of micrometers, their detection efficiency decreases rapidly for X-ray energies above 5 keV, being about 45, 25, 8, and 4% for 8, 10, 15, and 20 keV, respectively.

The LAAPD dark current affects the achieved detector energy resolution and limits the minimum detectable energy. As dark current is strongly reduced with decreasing temperature, the operation of LAAPDs at reduced temperatures may result in improved performance [5], [18], [19], [24]–[27]. However, a systematic and detailed study of the different characteristics for different operation temperatures has not been carried out. A detailed study of LAAPD characteristics at 100 K temperature is reported in [24], [25]. In [26], [27] the gain, energy resolution, and minimum detectable energy in X-ray and VUV detection was investigated for temperatures down to −5 °C, for an LAAPD with a built-in Peltier cooling-element [28]. Below −5 °C, it was not possible to operate the LAAPD correctly, due to leak currents between the different electrodes.

In this work, we investigate the performance of a standard LAAPD [28] for X-ray and visible-light detection as a function of the temperature. Photodiode dark-current, gain, gain drift with temperature, energy resolution, minimum detectable energy, and nonlinearity effects are measured and compared for both radiation types for different temperatures in the −40 to 27 °C range.

II. Experimental Setup

The LAAPD used in these experiments is a "Deep UV 500 Windowless series" from Advanced Photonix Inc. (API) [28] with a 16 mm diameter active area and was operated in a light-tight box to shield it from ambient light. The box also provides

Manuscript received May 28, 2004; revised July 21, 2004. This work was supported in part under Project POCTI/FNU/41720/01, in part by the Fundação para a Ciência e Tecnologia (FCT), and in part by the Fundação Luso-Americana para o Desenvolvimento (FLAD).

L. M. P. Fernandes and J. M. F. dos Santos are with the Physics Department, University of Coimbra, P-3004-516 Coimbra, Portugal (e-mail: pancho@gian.fis.uc.pt).

J. A. M. Lopes is with the Instituto Superior de Engenharia de Coimbra, P-3030 Coimbra, Portugal.

P. E. Knowles, L. Ludhova, and F. Mulhauser are with the Department of Physics, University of Fribourg, CH-1700 Fribourg, Switzerland.

F. Kottmann is with ETHZ, CH-8093 Zürich, Switzerland.

R. Pohl is with Max-Planck-Institut für Quantenoptik, DE-85748 Garching, Germany.

D. Taqqu is with Paul Scherrer Institute, Villigen CH-5232, Switzerland.

Digital Object Identifier 10.1109/TNS.2004.832976

thermal insulation and temperature is controlled through a continuous flow of cooled gaseous nitrogen. The temperature stabilization was achieved within ± -0.5 °C.

The X-ray detection was studied for energies up to 15 keV, using ^{54}Mn, ^{55}Fe and ^{57}Co radioactive sources. The response for the light signal was measured with pulses from a LED with peak emission at 635 nm. The LED was connected to a 50 Ω resistance and supplied by a "LED-pulser" providing pulses of 6 to 500 ns width and amplitude up to 10 V. A light guide was used to carry the light pulses to the LAAPD window.

The LAAPD signals were fed through a low-noise charge preamplifier (Canberra 2004, with a sensitivity of 45 mV/MeV) to a linear amplifier (HP 5582A, with gain of 16 to 128 and 200 ns integration and differentiation time constants) and were pulse-height analyzed by a 1024 channel analyzer (Nucleus PCA II).

For pulse-amplitude and energy resolution measurements, each X-ray pulse-height distribution was fitted to a Gaussian function superimposed on a linear background, from which the centroid and the full-width-at-half-maximum were determined. The electronic noise-tail in the low-energy end limits the minimum detectable energy (MDE), defined as the energy-limit where the noise-tail raises above the background level.

III. Experimental Results and Discussion

A. Gain Measurements

Absolute gain measurements were obtained by determining the LAAPD unitary gain. Gain was assessed measuring the amplitude of 100 ns long visible-light LED pulses as a function of the bias voltage. Results are presented in Fig. 1. The gain dependence with reverse bias voltage is exponential for low gains, before the contribution of the holes to the avalanche process becomes significant. However, for voltages approaching 0 V, the electric field is not high enough to prevent recombination and only a fraction of the charge is collected. Since below 500 V, the LAAPD has unitary gain [29], and above 300 V, the effect of recombination is negligible, the unitary gain was calculated averaging the experimental data within that range (Fig. 1). An associated error of ±4% was obtained using this crude method, higher than that can be obtained with DC methods [4], [25]. Additionally, the variation of the APD capacity with bias voltage affects the measured gain within about 1% for the present method.

In Fig. 2, we present the detector gain as a function of the temperature for different reverse bias voltages, for 5.9 keV X-rays [Fig. 2(a)] and visible light [Fig. 2(b)]. As expected, the results obtained for X-rays and visible light are very similar, since a good proportionality is observed between the X-ray and visible-light peaks, as will be discussed in the next section.

For each bias voltage, the relative gain variation is almost constant above −15 °C, increasing from −2.1% to −5.4% per degrees Celsius, as the LAAPD biasing increases from 1500 to 1770 V. These results are in good agreement with our previous measurements for X-rays [26] and VUV light [27].

For gains above 100 and for room temperature, the results show relative amplitude variations that are almost a factor of two higher than what was previously indicated for visible light,

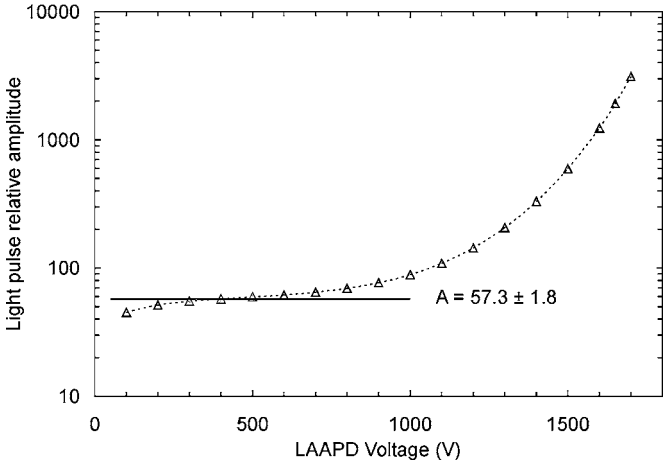

Fig. 1. LAAPD relative pulse amplitude as a function of the reverse bias voltage for visible-light pulses. The horizontal line presents the amplitude A corresponding to the unitary gain.

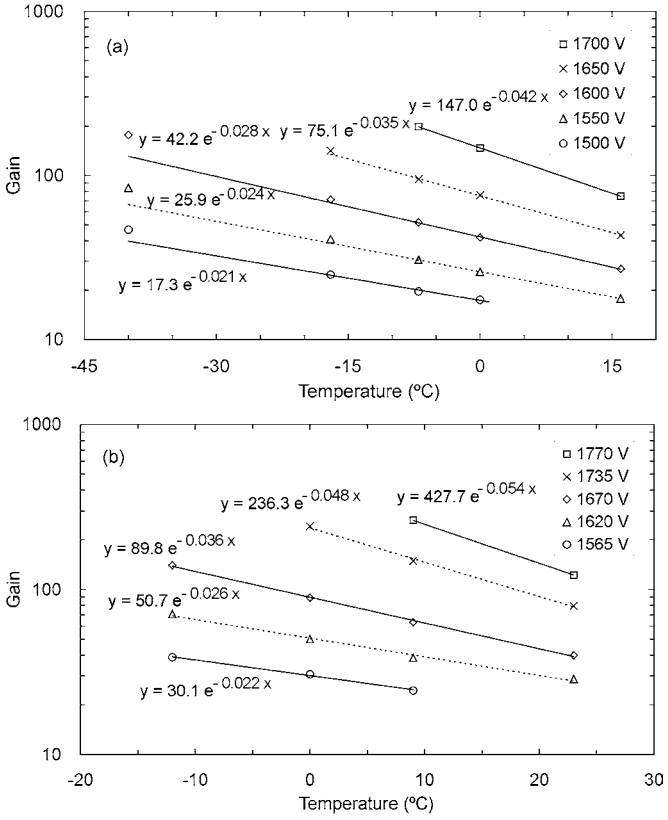

Fig. 2. LAAPD gain as a function of temperature for different reverse bias voltages (a) for 5.9 keV X-rays and (b) visible light.

about −3% per degrees Celsius for the highest gains [29]. Compared to other APD types, these results show relative gain variations with temperature lower than those obtained for EG&G APDs [6] and similar to those obtained for Hamamatsu [5], −3.5% and −2.3% per degrees Celsius, respectively, for gains around 50.

B. Nonlinearity Effects

The nonproportionality between APD gains for X-rays and visible light is well known, as well as between X-rays with dif-

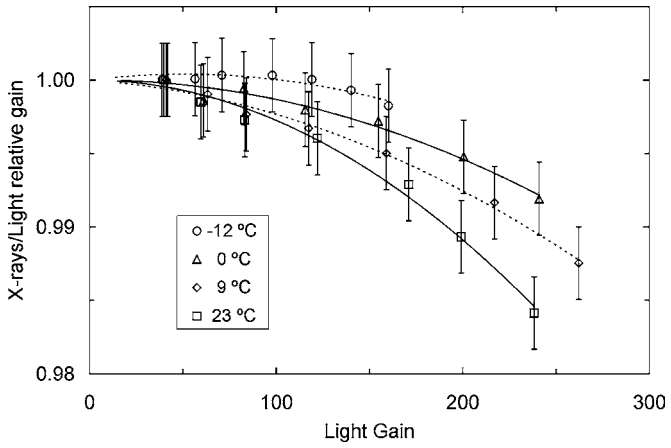

Fig. 3. Ratio of LAAPD gains for 5.4 keV X-rays and visible-light pulses as a function of the light gain, for different temperatures.

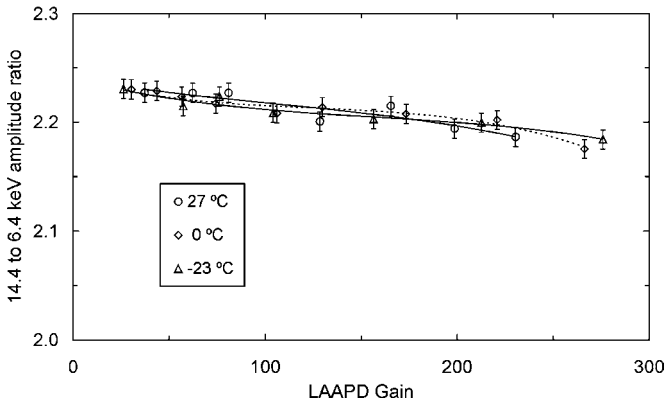

Fig. 4. Ratio of the pulse amplitudes for 14.4 and 6.4 keV X-rays, from a ^{57}Co source, as a function of the LAAPD gain, for different operation temperatures.

ferent energies [3], [6], [9], [10], [22], [23]. This is due to space charge effects caused by high signal current densities produced by X-rays, mainly at high gains, resulting in a decrease of the local electric field and local heating in the avalanche region.

The number of electron-hole pairs produced in the APD by the scintillation light is often determined by comparison of the relative pulse amplitude with that of the pulses produced by the direct absorption of X-rays. This comparison is only valid if strict linearity between the initial number of electron-hole pairs and the resulting pulse amplitude is observed, which is compromised by this nonlinear response.

The nonlinear response may be significant mainly at high gains, reaching values as high as a few tens of percent [6], [9]. This effect is less significant for the LAAPD from API when compared to others, exhibiting a relative gain variation of about 4% for 5.9 keV X-rays, for a gain of 300 [6], [9]. For VUV scintillation, the observed nonlinearity was about 4.5 and 10% for 128 nm light, for respective gains of 100 and 200, and about 3.5% and 6%, respectively, for 172 nm light [30].

To study that effect as function of temperature, the LAAPD was simultaneously irradiated with X-rays from a ^{54}Mn radioactive source and visible light from the LED; their gain dependence with the bias voltage was studied for different operation temperatures. The LED intensity was chosen to produce a pulse with an amplitude equivalent to 9.3 keV X-rays. Fig. 3 presents the amplitude ratio between 5.4 keV X-ray signals and visible-light pulses as function of the light gain.

For the present photodiode, a variation of less than 2% was obtained for gains of about 250. Moreover, Fig. 3 shows that nonlinear response is reduced with decreasing temperature, presenting variations that are less than 1.0 and 0.5% at 23 and 0 °C, respectively, for gains up to 200. The observed dependence of the linearity with temperature may be related to the increase of the avalanche region depth with temperature. This effect is important when using X-rays as a reference in light measurements.

The detector nonlinear response for X-rays with different energies was also investigated. Fig. 4 depicts the amplitude ratio for the 14.4 and 6.4 keV X-rays emitted from a ^{57}Co source as function of the gain, for different operation temperatures. Relative amplitude variations decrease with increasing gain and can be as high as 1% and 3% for gains of about 170 and 250, respectively. These results are consistent with those obtained in [20] for 5.9 and 22.1 keV X-rays, and in [22], for 5.9 and 16.6 keV X-rays (6% and 4%, respectively, for gains of 250). Opposite to the nonlinear effect in the LAAPD response between X-rays and light detection, no dependence was found with the temperature.

Apart from this effect, a good energy linearity response is observed for X-ray energies up to 20 keV at the optimum gain [26].

C. Energy Resolution Measurements

In Fig. 5, we present the detector energy resolution as function of the gain for different temperatures, for Mn K_α line X-rays [Fig. 5(a)] and visible-light pulses [Fig. 5(b)]. The measurements were made for full illumination of the LAAPD active area with both X-rays and visible light. The data show the advantages of operating the LAAPD at low temperatures.

In the case of X-rays [Fig. 5(a)], the lowest energy resolutions are obtained for gains in the 50 to 70 range, almost independent on the operation temperature. The energy resolution improves from 11% to 9.6 and 9.2% as the temperature decreases from 24 °C to 0 and −40 °C. The measured significant degradation of the energy resolution for high gains is mainly due to the incorrect fitting to two different Gaussian functions for the Mn K_α and K_β lines, which are superimposed. In fact, when only the Mn K_α line was used, filtering the K_β line with a chromium film, only a small degradation of the energy resolution was observed at high gains [20], [26], a behavior also observed for the energy resolution obtained for the visible-light peak [Fig. 5(b)].

The energy resolution decreases rapidly with the onset of gain and, for high gains, it begins to increase as the dark current and the excess noise factor increase. For X-rays, an additional contribution to the resolution degradation results from the spatial nonuniformity of the LAAPD. Nonuniform material resistivity of the LAAPD results in gain fluctuations due to localized electric field variations and the LAAPD response depends on the X-ray incident point on the LAAPD surface. An increase in the bias voltage and thus in the gain results in larger local differences of the electric field, leading to larger differences in the avalanche multiplication gain, degrading the energy resolution.

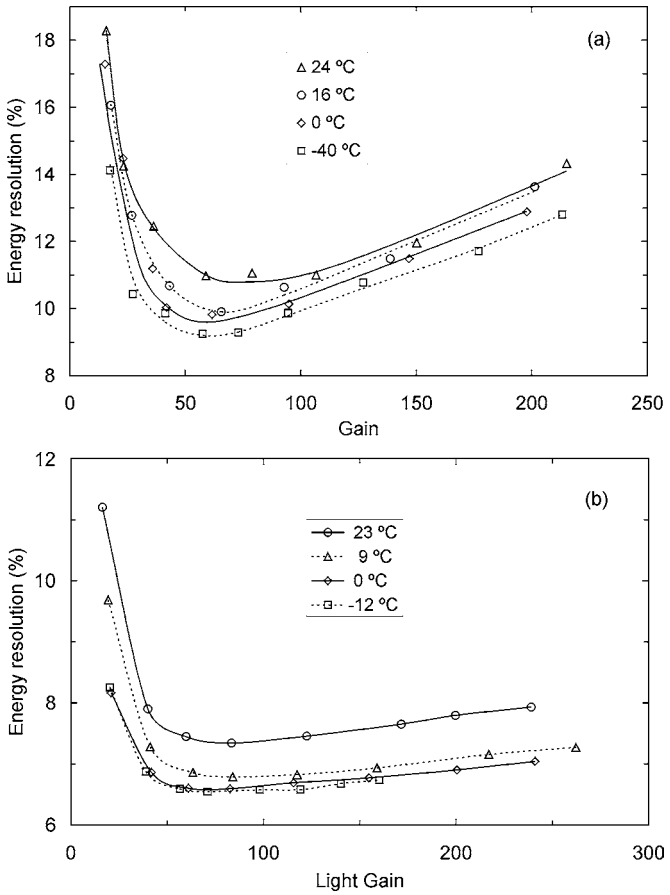

Fig. 5. Measured LAAPD energy resolution as a function of gain for different temperatures, for (a) Mn K_α X-rays and for (b) visible light.

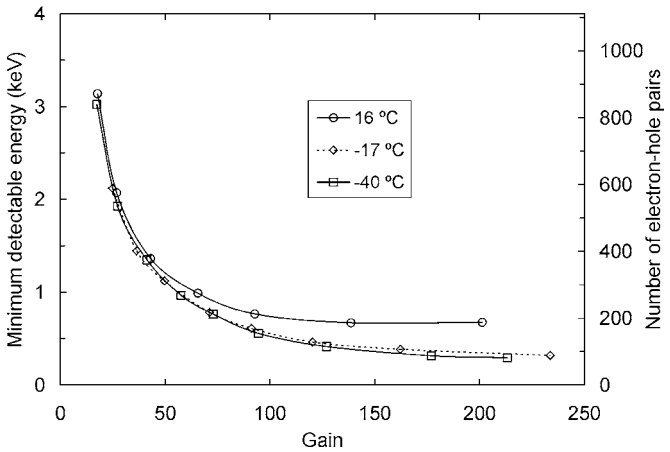

Fig. 6. Minimum detectable energy as a function of gain for different temperatures.

D. Minimum Detectable Energy

In Fig. 6, the minimum detectable energy (MDE), defined as the energy-limit where the electronic-noise-tail rises above the background level on the pulse-height distribution, is depicted as a function of the gain for different operation temperatures. The MDE presents a fast initial decrease with the gain and tends to stabilize for high gains. It shows that the LAAPD is useful for X-ray detection down to about 0.7 keV, or even down to 0.3 keV, if the diode is cooled down to negative temperatures. Taking into account the value of 3.6 eV for the mean energy required to produce an electron-hole pair in silicon, the MDE values correspond to a minimum number of primary electron/hole pairs of about 200 and 80, respectively, to produce a signal above the noise.

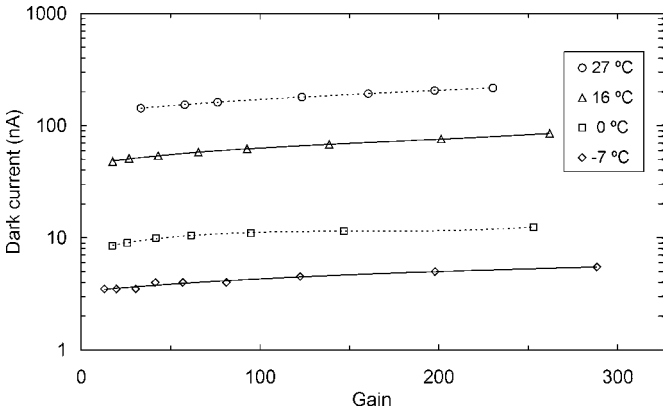

Fig. 7. LAAPD dark current as a function of gain for different temperatures.

Although the MDE depends on the LAAPD irradiation conditions, such as the counting rate and the presence of high energy X-rays, these measurements can be taken as a rough estimation. The MDE measurements were obtained for full irradiation of the LAAPD active area with ^{55}Fe X-rays, at count rates of about 10^2c/s.

The LAAPD dark current sets a limit to the electronic noise tail and, thus, to the lowest detectable energy and affects the detector energy resolution. In Fig. 7, we present the measured dark current as function of gain, for different operation temperatures. For a given gain, the dark current is reduced by more than one order of magnitude as the APD operation temperature is reduced from 24 to 0 °C, which is in accordance to the manufacturer specifications [29]. However, this significant improvement is not reflected in the obtained energy resolution and MDE. This indicates that both parameters are not limited by the dark current at low temperatures. On the other hand, LAAPD nonuniformity might be one limiting factor for the energy resolution at low operation temperatures.

E. X-Ray Spectrometry Applications

Typical pulse-height distributions are depicted in Fig. 8 for direct irradiation of the full active area of the LAAPD with a ^{57}Co source [Fig. 8(a)] and for the X-ray fluorescence of a gypsum ($CaSO_4$) sample excited with a ^{55}Fe radioactive source [Fig. 8(b)]. The pulse-height distributions are presented for different operation temperatures and for a gain of about 70. The benefits from reducing the LAAPD temperature are evidenced by the improved energy resolution and lower electronic noise level. On the other hand, the temperature reduction shows no effect on the background level.

Energy resolutions of 28, 12.8, 9.8, and 8.5% were obtained for 2.3, 4.5, 6.4, and 14.4 keV X-rays, respectively, at operation temperatures of 0 °C.

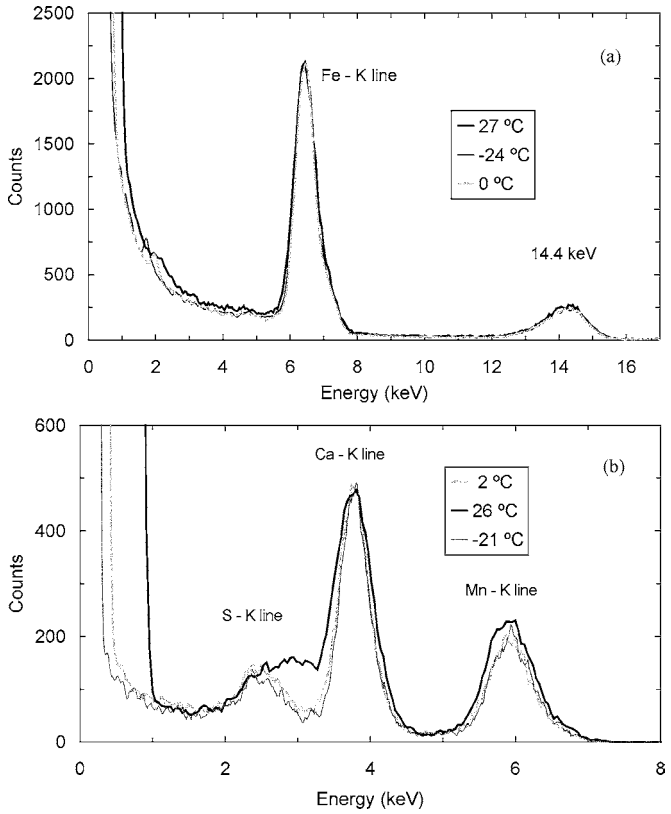

Fig. 8. (a) X-rays from a ^{57}Co source and (b) the X-ray fluorescence of a $CaSO_4$ sample irradiated with a ^{55}Fe source, at different temperatures.

IV. Conclusion

The operational characteristics of a "Deep UV 500 Windowless series" LAAPD from API was investigated for different operation temperatures.

The performance improves with decreasing temperature. However, below 0 °C, the improvement is not significant. Energy resolution is better than that observed in proportional counters, improving significantly with decreasing temperature down to 0 °C and, below that value, at a much slower rate. Energy resolutions of about 11, 9.6, and 9.2% were obtained for 5.9 keV X-rays at 24, 0, and −40 °C, respectively, operating the LAAPD with gains around 70. For X-rays, the minimum detectable energy is around 0.7 keV for temperatures around 16 °C, decreasing to about 0.3 keV for temperatures below 0 °C.

The gain drift with temperature increases with the reverse bias voltage from −2.1% to −5.4% per degrees Celsius, as the LAAPD biasing increases from 1500 to 1770 V and, for each voltage, is almost constant for temperatures above −15 °C. The gain drift with temperature is similar for X-rays and visible light, and is somewhat higher than previously known for visible light.

The LAAPD nonlinear response between X-ray and light is less than 2%, even for gains around 250, and decreases with temperature, being less than 1.0 and 0.5% at 23 and 0 °C, respectively, for gains up to 200. The LAAPD nonlinear response between X-rays with different energies was found to be temperature independent and is less than 1% for gains around 100, but can be as high as few percent for high gains, depending on the X-ray energy.

Acknowledgment

The authors would like to thank the Atomic and Nuclear Instrumentation Group of the Instrumentation Centre (Unit 217/94) of the Physics Department, University of Coimbra, Portugal, where this work was carried out.

References

[1] A. Q. R. Baron and S. L. Ruby, "Time resolved detection of X-rays using large area avalanche photodiodes," *Nucl. Instrum. Methods A*, vol. 343, pp. 517–526, 1994.

[2] E. M. Gullikson, E. Gramsch, and M. Szawlowski, "Large-area avalanche photodiodes for the detection of soft X-rays," *Appl. Opt.*, vol. 34, pp. 4662–4668, 1995.

[3] J. P. Pansart, "Avalanche photodiodes for particle detection," *Nucl. Instrum. Methods A*, vol. 387, pp. 186–193, 1997.

[4] M. Moszynski, M. Kapusta, M. Balcerzyk, M. Szawlowsky, D. Wolski, I. Wegrzecka, and M. Wegrzecki, "Comparative study of avalanche photodiodes with different structures in scintillation detection," *IEEE Trans. Nucl. Sci.*, vol. 48, pp. 1205–1210, Aug. 2001.

[5] K. Deiters, Y. Musienko, S. Nicol, B. Patel, D. Renker, S. Reucroft, R. Rusack, T. Sakhelashvili, J. Swain, and P. Vikas, "Properties of the most recent avalanche photodiodes for the CMS electromagnetic calorimeter," *Nucl. Instrum. Methods A*, vol. 442, pp. 193–197, 2000.

[6] A. Karar, Y. Musienko, and J. C. Vanel, "Characterization of avalanche photodiodes for calorimetry applications," *Nucl. Instrum. Methods A*, vol. 428, pp. 413–431, 1999.

[7] R. J. McIntyre, P. P. Webb, and H. Dautet, "A short-wavelength selective reach-through avalanche photodiode," *IEEE Trans. Nucl. Sci.*, vol. 43, pp. 1341–1346, Aug. 1996.

[8] R. Lecomte, C. Pepin, D. Rouleau, H. Dautet, R. J. McIntyre, D. McSwen, and P. Webb, "Radiation detection measurements with a new "buried junction" silicon avalanche photodiode," *Nucl. Instrum. Methods A*, vol. 423, pp. 92–102, 1999.

[9] M. Moszynski, M. Szawlowsky, M. Kapusta, and M. Balcerzyk, "Large area avalanche photodiodes in scintillation and X-rays detection," *Nucl. Instrum. Methods A*, vol. 485, pp. 504–521, 2002.

[10] ——, "Avalanche photodiodes in scintillation detection," *Nucl. Instrum. Methods A*, vol. 497, pp. 226–233, 2003.

[11] R. Farrel, F. Olschner, K. Shah, and M. R. Squillante, "Advances in semiconductor photodetectors for scintillation," *Nucl. Instrum. Methods A*, vol. 387, pp. 194–198, 1997.

[12] R. Farrel, K. Shah, K. Vanderpuye, R. Graziaso, R. Myers, and G. Entine, "APD arrays and large-area APDs via a new planar process," *Nucl. Instrum. Methods A*, vol. 442, pp. 171–178, 2000.

[13] B. Pichler, G. Böning, E. Lorenz, R. Mirzoyan, W. Pimpl, M. Schwaiger, and S. I. Ziegler, "Studies with a prototype high resolution PET scanner based on LSO-APD modules," *IEEE Trans Nucl. Sci.*, vol. 45, pp. 1298–1302, Aug. 1998.

[14] A. Ruru Chen, A. Fremout, S. Tavernier, P. Bruyndonckx, D. Clément, J.-F. Loude, and C. Morel, "Readout of scintillator light with avalanche photodiodes for positron emission tomography," *Nucl. Instrum. Methods A*, vol. 433, pp. 637–645, 1999.

[15] J. A. M. Lopes, J. M. F. Dos Santos, R. E. Morgado, and C. A. N. Conde, "A xenon gas proportional scintillation counter with a UV-sensitive, large-area avalanche photodiode," *IEEE Trans. Nucl. Sci.*, vol. 48, pp. 312–319, Feb. 2001.

[16] C. M. B. Monteiro, J. A. M. Lopes, P. C. P. S. Simões, J. M. F. dos Santos, and C. A. N. Conde, "An argon gas proportional scintillation counter with UV avalanche photodiode scintillation readout," *IEEE Trans. Nucl. Sci.*, vol. 48, pp. 1081–1086, June 2001.

[17] L. M. P. Fernandes, A. Antognini, M. Boucher, C. A. N. Conde, O. Huot, P. Knowles, F. Kottmann, L. Ludhova, F. Mulhauser, R. Pohl, J. M. F. dos Santos, L. A. Schaller, D. Taqqu, and J. F. C. A. Veloso, "Behavior of large-area avalanche photodiodes under intense magnetic fields for VUV, visible and X-ray photon detection," *Nucl. Instrum. Methods A*, vol. 498, pp. 362–368, 2003.

[18] R. Farrel, K. Vanderpuye, G. Entine, and M. R. Squillante, "High resolution low energy avalanche photodiode X-ray detectors," *IEEE Trans. Nucl. Sci.*, vol. 38, pp. 144–147, Feb. 1991.

[19] A. Ochi, Y. Nishi, and T. Tanimori, "Study of a large area avalanche photodiode as a fast photon and soft X-ray detector," *Nucl. Instrum. Methods A*, vol. 378, pp. 267–274, Feb. 1996.

[20] L. M. P. Fernandes, J. A. M. Lopes, J. M. F. dos Santos, and C. A. N. Conde, "Application of a large area avalanche photodiode in energy dispersive X-ray fluorescence analysis," *X-ray Spectrom.*, vol. 30, pp. 164–169, 2001.

[21] L. M. P. Fernandes, A. Antognini, M. Boucher, C. A. N. Conde, O. Huot, P. E. Knowles, F. Kottmann, L. Ludhova, F. Mulhauser, R. Pohl, J. M. F. dos Santos, L. A. Schaller, D. Taqqu, and J. F. C. A. Veloso, "Application of large-area avalanche photodiodes to X-ray spectrometry of muonic atoms," *Spectrochim. Acta B*, vol. 58, pp. 2255–2260, 2003.

[22] M. Moszynski, M. Kapusta, M. Szawlowsky, and D. Wolski, "Large area avalanche photodiodes in X-rays and scintillation detection," *Nucl. Instrum. Methods A*, vol. 442, pp. 230–237, 2000.

[23] C. P. Allier, H. Valk, V. R. Bom, R. W. Hollander, and C. W. E. van Eijk, "Comparative study of silicon detectors," *IEEE Trans. Nucl. Sci.*, vol. 45, pp. 576–580, Apr. 1998.

[24] V. Solovov, F. Neves, V. Chepel, M. I. Lopes, R. Ferreira Marques, and A. J. P. L. Policarpo, "Low temperature performance of a large area avalanche photodiode," *IEEE Trans. Nucl. Sci.*, vol. 47, pp. 1307–1310, June 2000.

[25] M. Moszynski, W. Czarnacki, M. Szawlowsky, B. L. Zhou, M. Kapusta, D. Wolski, and P. Schotanus, "Performance of large area avalanche photodiodes at liquid nitrogen temperature," *IEEE Trans. Nucl. Sci.*, vol. 49, pp. 971–976, June 2002.

[26] L. M. P. Fernandes, J. A. M. Lopes, J. M. F. dos Santos, and C. A. N. Conde, "X-ray spectrometry with Peltier-cooled large area avalanche photodiodes," *Nucl. Instrum. Methods B*, vol. 213, pp. 267–271, 2004.

[27] J. A. M. Lopes, L. M. P. Fernandes, J. M. F. dos Santos, R. E. Morgado, and C. A. N. Conde, "VUV detection in large area avalanche photodiodes as a function of temperature," *Nucl. Instrum. Methods A*, vol. 504, pp. 331–334, 2003.

[28] Advanced Photonix, Inc., Camarillo, CA.

[29] Advanced Photonix, Inc., Camarillo, CA.

[30] L. M. P. Fernandes, J. A. M. Lopes, C. M. B. Monteiro, J. M. F. dos Santos, and R. E. Morgado, "Non-linear behavior of large-area avalanche photodiodes," *Nucl. Instrum. Methods A*, vol. 478, pp. 395–399, 2002.

Available online at www.sciencedirect.com
SCIENCE DIRECT®
ELSEVIER
Nuclear Instruments and Methods in Physics Research A 531 (2004) 566–568
NUCLEAR INSTRUMENTS & METHODS IN PHYSICS RESEARCH Section A
www.elsevier.com/locate/nima

Excess noise factor in large area avalanche photodiodes for different temperatures

L.M.P. Fernandes[a], J.A.M. Lopes[a,b,*], J.M.F. dos Santos[a]

[a] *Departamento de Física, Universidade de Coimbra, P-3004-516 Coimbra, Portugal*
[b] *Instituto Superior de Engenharia de Coimbra, Rua Pedro Nunes, Quinta da Nora, Apartado 4065, P-3030-199 Coimbra, Portugal*

Received 20 January 2004; received in revised form 3 May 2004; accepted 10 May 2004

Available online 15 June 2004

Abstract

The excess noise factor (ENF) of a large area avalanche photodiode was measured as a function of gain for different temperatures, in the −40 to 27°C range. Results show that ENF does not depend significantly with temperature attaining values of about 1.8 and 2.3 for gains of 50 and 300, respectively.

PACS: 29.40.Wk; 85.60.Dw; 85.60.Jb

Keywords: Large area avalanche photodiodes; Excess noise factor; Energy resolution

Large-area avalanche photodiodes (LAAPD) are compact, simple to operate, monolithic devices made of silicon p–n junctions. When a reverse high voltage is applied to the LAAPD, the internal electric field increases with depth presenting a maximum around the p–n junction and reaching values high enough to allow electron multiplication by impact ionization [1,2]. An incident photon produces electron–hole pairs and the resulting electrons are accelerated towards the n^+ contact, undergoing avalanche multiplication due to the high electric field around the junction. Typical gains of several hundred can be achieved in this process.

The application of LAAPDs to direct X-ray detection has been investigated [1–4], mainly to measure charge carrier properties of the device, using X-rays as a reference for visible light measurements [2,3,5,6].

The LAAPD dark current affects the achieved detector energy resolution and limits the minimum detectable energy. As dark current is strongly reduced with decreasing temperature, the operation of LAAPDs at reduced temperatures results in improved performance [7–9].

The performance of a standard LAAPD for X-ray and visible-light detection was investigated as a function of the temperature. Dark current, the achieved gain, energy resolution, and minimum detectable energy in X-ray detection were measured for different temperatures [8,11]. Measuring at the same time both X-ray and visible-light pulse

*Corresponding author. Tel.: +351-239-790300; fax: +351-239-790201.
E-mail address: zematias@isec.pt (J.A.M. Lopes).

0168-9002/$ - see front matter © 2004 Elsevier B.V. All rights reserved.
doi:10.1016/j.nima.2004.05.085

signals, the excess noise factor (ENF) can be determined [3].

The energy resolution obtained with LAAPDs is mainly limited by three factors: the statistical contribution associated with the number of primary electron–hole pairs and the avalanche process; gain non-uniformity across the diode detection area; noise of the diode-preamplifier system. The variance associated to the statistical factor can be expressed in terms of the number of primary electrons as:

$$\sigma_{\mathrm{st}}^2 = \sigma_n^2 + N\sigma_A^2/M^2 \quad (1)$$

where N is the number of primary electrons and σ_n^2 the correspondent variance, M is the LAAPD gain and σ_A^2 the variance of the gain. In this equation, the first term describes the statistical fluctuation of the primary electrons and the second one the fluctuations of the avalanche gain in the LAAPD. Defining the excess noise factor as

$$F = 1 + \sigma_A^2/M^2 \quad (2)$$

Eq. (1) can be rewritten as

$$\sigma_{\mathrm{st}}^2 = \sigma_n^2 + N\,(F-1). \quad (3)$$

In particular, for light pulse detection, the variance of primary electrons is described by Poisson statistics

$$\sigma_n^2 = N. \quad (4)$$

This way, the statistical limitation of the energy resolution is given by

$$\sigma_{\mathrm{st}}^2 = NF. \quad (5)$$

Since all the diode area is illuminated, local gains are averaged out and the non-uniformity contribution to the peak broadening can be excluded. Assuming a Gaussian shape of the detected peak, the energy resolution ΔE of the peak due to the light pulse can be described by the following equation, expressed in keV:

$$\Delta E^2 = (2.355)^2 FE\varepsilon + \Delta_n^2. \quad (6)$$

In Eq. (6), F is the ENF, E the energy of the light peak in keV, ε the energy per electron-hole pair creation (3.6 eV for silicon) and Δ_n the noise contribution (FWHM) of the diode-preamplifier system, in keV. Since X-rays are used as an energy reference for the light signal, E is normalized to the energy of the X-ray signal. Δ_n is determined with a pulse generator. The ENF is then obtained measuring at the same time the signals due to X-rays (for example, 5.4 keV from a ^{54}Mn source), the light pulse and the test pulse. The present method was previously used for the ENF determination at room and LN2 temperatures [3,12]. Fig. 1 presents a typical obtained spectrum, showing all necessary parameters.

The used LAAPD is a "Deep UV 500 Windowless series" from Advanced Photonix Inc. [10] with a 16-mm-diameter active area. It was operated in a light-tight box to shield it from ambient light. The box also provides thermal insulation and temperature is controlled through continuous flow of cooled gaseous nitrogen. Temperature stabilization was achieved within $\pm 0.5^{\circ}$C.

The X-ray signal was obtained from a ^{54}Mn source giving 5.4 keV X-rays. The light signal was provided by a light emitting diode (LED) with peak emission at 635 nm.The LED was connected to a 50 Ω resistance and supplied by a "LED-pulser" producing pulses of 6–500 ns width and up to 10 V amplitude. A light guide was used to carry the light pulses to the LAAPD.

The LAAPD signals were fed through a low-noise charge preamplifier (Canberra 2004, with a sensitivity of 45 mV/MeV) to a linear amplifier (HP 5582A, with gain of 16–128 and 200 ns integration and differentiation time constants) and were pulse-height analyzed by a 1024-channel multi-channel analyzer (Nucleus PCA II).

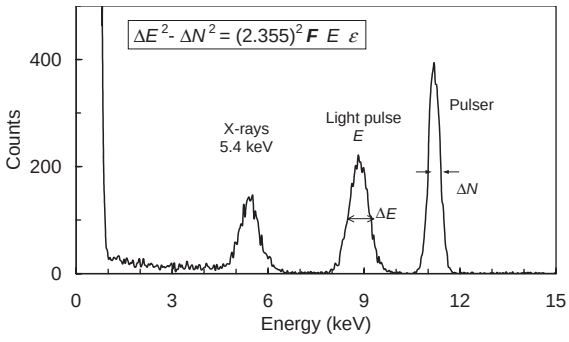

Fig. 1. Typical energy spectrum for the ENF determination. Three different peaks are shown: the X-ray peak produced by 5.4 keV X-rays from a ^{54}Mn radioactive source, the light peak produced by a LED pulse and the peak from a pulse generator.

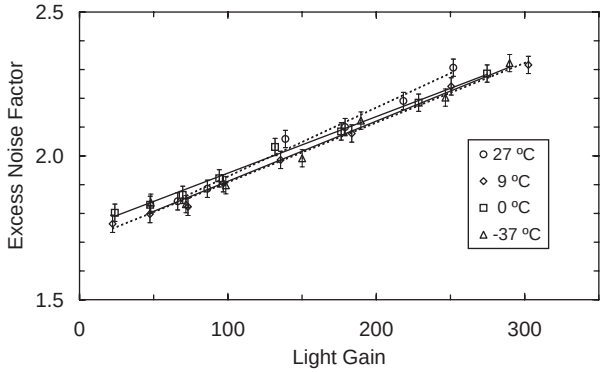

Fig. 2. Excess noise factor as function of gain for different temperatures.

To measure all quantities at the same time, for different temperatures, the LAAPD was simultaneously irradiated with X-rays and visible-light. The LED intensity was chosen to produce a pulse with an amplitude equivalent to about 9 keV X-rays. The test pulser was fed through the preamplifier test input. Fig. 2 presents the ENF, calculated according to Fig. 1, as function of the LAAPD gain for different temperatures.

As shown in Fig. 2, ENF increases almost linearly with gain and does not have significant variations with temperature. The present results are in good agreement with previous measurements, performed at room temperature [3] and LN2 temperature [12].

In previous works, energy resolution dependence on temperature was observed and could be related to variation of both ENF and dark current-derived noise level. It is now clear that this dependence is not related with the ENF. Thus, decreasing temperature will significantly improve the signal-to-noise ratio, leading to lower-energy resolution.

Acknowledgements

This work was carried out under Project POCTI/FNU/41720/01 of the Atomic and Nuclear Instrumentation Group of the Physics Department, University of Coimbra.

References

[1] E.M. Gullikson, E. Gramsch, M. Szawlowski, Appl. Opt. 34 (1995) 4662.
[2] J.P. Pansart, Nucl. Instr. and Meth. A 387 (1997) 186.
[3] M. Moszynski, M. Szawlowski, M. Kapusta, M. Balcerzyk, D. Wolski, IEEE Trans. Nucl. Sci.-NS 47 (2000) 1297.
[4] L.M.P. Fernandes, J.A.M. Lopes, J.M.F. dos Santos, C.A.N. Conde, X-ray Spectrom. 30 (2001) 164.
[5] M. Moszynski, M. Kapusta, M. Szawlowski, D. Wolski, I. Wegrzecka, M. Wegrzecki, IEEE Trans. Nucl. Sci.-NS 48 (2001) 1205.
[6] C.P. Allier, H. Valk, V.R. Bom, R.W. Hollander, C.W.E. van Eijk, IEEE Trans. Nucl. Sci.-NS 45 (1998) 576.
[7] V. Solovov, et al., IEEE Trans. Nucl. Sci.-NS 47 (2000) 1307.
[8] L.M.P. Fernandes, J.A.M. Lopes, J.M.F. dos Santos, C.A.N. Conde, Nucl. Instr. and Meth. B 213 (2004) 267.
[9] J.A.M. Lopes, L.M.P. Fernandes, J.M.F. dos Santos, R.E. Morgado, C.A.N. Conde, Nucl. Instr. and Meth. A 504 (2003) 331.
[10] Advanced Photonix Inc., 1240Av.Acaso, Camarillo, CA 93012, USA.
[11] L.M.P. Fernandes, J.A.M. Lopes, J.M.F. dos Santos, et al., LAAPD low temperature performance in X-ray and visible-light detection, IEEE Trans. Nucl. Sci., to be published in August 2004, (Vol. 51, issue 4).
[12] M. Moszynski, M. Czarnacki, M. Szawlowski, B.L. Zhou, M. Kapusta, D. Wolski, P. Schotanous, IEEE Trans. Nucl. Sci.-NS 49 (2002) 971.

Chapter 4

Application of LAAPDs to the muonic hydrogen Lamb shift experiment

An experiment called "Laser spectroscopy of the muonic hydrogen" [Taqqu *et al.* 1999] has been carried out at the *Paul Scherrer Institute* (PSI), Villigen, Switzerland. The experiment involves the contribution of several institutions, including the *Atomic and Nuclear Instrumentation Group* (GIAN) of the Physics Department of the University of Coimbra. The purpose of the experiment is to measure the energy difference between the 2S and 2P levels of the first excited state (Lamb shift) in the muonic hydrogen atom. For the expected conditions, the Lamb shift can be measured with a precision of 40 ppm, leading to the determination of the mean square value of the proton charge radius with a relative precision of 0.1%, about 20 times more precise than presently known.

In order to perform the experiment, a compact detector able to detect 1.9 keV X-rays operating under a 5 T magnetic field is necessary. The GIAN has been responsible for the development of such a detector. Some prototypes of gas proportional scintillation counters have been developed and tested. However, the LAAPD as direct X-ray detector has been chosen due to its excellent performance under the influence of intense magnetic fields, among others factors.

In this chapter, the details of the experiment to determine the Lamb shift in muonic hydrogen are described, with particular emphasis on the optimization of the LAAPD performance and operating conditions. The response of LAAPDs under intense magnetic fields is evaluated in comparison to other X-ray detectors. To evaluate the LAAPD performance in the detection of X-rays emitted by muonic atoms under the intense radiation environment of the experiment, tests with a muon beam interacting in

different gas targets have been carried out. The positive result of these tests has determined the LAAPD as the X-ray detector to be used in the experiment. The details of this experimental assay are presented and the results of two different phases of the experiment are discussed.

4.1. Introduction

Before presenting the results of LAAPD tests performed in order to validate the LAAPD application to the experiment, theoretical considerations on the Lamb shift are given, the principle of the experiment is described and the experimental system requirements are discussed.

4.1.1. Lamb shift

According to the solution of the Schrödinger equation for the hydrogen atom, the energy levels of the electron depend only on the main quantum number n [Beiser 1995]:

$$E_n = -\frac{M q^4}{8 \varepsilon_0{}^2 h^2} \frac{1}{n^2} = \frac{-13.6 \text{ eV}}{n^2}, \quad n = 1, 2, 3, ... \qquad \text{(Eq. 4.1)}$$

being M the atom reduced mass, q the electron electric charge, ε_0 the vacuum electric permittivity and h the Planck constant.

In 1947, Willis Lamb has discovered that the $2s_{1/2}$ and $2p_{1/2}$ states have a small energy difference, the Lamb shift, as Figure 4.1 represents. The $2p_{1/2}$ state presents a slightly lower energy than the $2s_{1/2}$ state. The basis of this process is the "exchange force model" of the electromagnetic force. According to this model, charges interact by exchange of photons [Rohlf 1994]. This leads to the formulation of quantum electrodynamics (QED), which is the theory where electromagnetic fields as well as particles are quantized. The electron can suffer a self-interaction by emission or absorption of a

virtual photon. The continuous exchange of such photons by electrons smears out the electron position over a range of about 0.1 fm and originates a slight weakening of the force on the electron when it is very close to the nucleus. This effect slightly reduces the absolute value of the binding energy of the 2S state relative to the 2P state since electrons in the 2S state are closer to the nucleus.

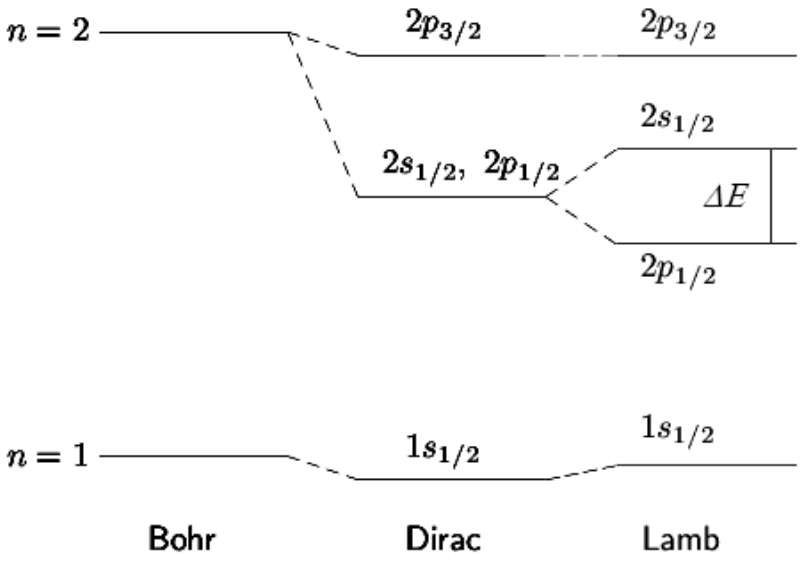

Figure 4.1 – Energy levels in the hydrogen atom according to Bohr, Dirac and Lamb. The Lamb shift (ΔE) is the energy difference between the $2p_{1/2}$ and $2s_{1/2}$ states.

The Lamb shift in the hydrogen atom is difficult to measure by inducing transitions in the visible or ultraviolet regions of the electromagnetic spectrum. The measurement is nevertheless possible inducing the 2S-2P transition directly in the microwave region, as made by Willis Lamb in his measurements, where an energy deviation of 4.372×10^{-6} eV was obtained [Lamb 1952, Triebwasser 1953].

The Lamb shift constitutes the most precise measurement of the effect of quantum electrodynamics in bound systems. When it was experimentally determined, the Lamb shift provided a great precision verification of the predictions of the quantum theory of electrodynamics. Up to now, it was possible to make measurements only with the electronic hydrogen. However, due to an increasing experimental effort during last years in PSI, those measurements can now be extended to the muonic hydrogen.

The muonic hydrogen (μp) is a bound system of a proton and a negative muon. Its lifetime is finite and essentially determined by the muon decay ($\tau = 2.2\times10^{-6}$ s). Since the muon mass is about 207 times larger than the electron one and the energy of each level is proportional to the reduced mass of the system (Equation 4.1), muonic hydrogen levels are about 186 times more energetic than the ones of electronic hydrogen. The energy of the ground state in muonic hydrogen is 2.53 keV, against 13.6 eV in electronic hydrogen, and the transitions to that state are in the low-energy X-ray region.

For each energy level, the radius of the electron orbit around the proton is inversely proportional to the system reduced mass, being 186 times smaller in muonic hydrogen. The overlap between the wave function of the muon and the nucleus in muonic hydrogen is stronger relative to the wave function of the electron and the nucleus in normal hydrogen by a factor $(m_\mu / m_e)^3 \cong 10^7$, where m_μ and m_e are the muon and the electron masses [Pachucki 1996]. Thus, the effective potential experienced by the muon is much more sensitive to the charge distribution and to the proton magnetic momentum when compared to the electron.

The effect of the proton finite size contributes with 2% for the Lamb shift in muonic hydrogen. A precise Lamb shift measurement will provide the knowledge of the mean square value of the proton radius with better accuracy. The knowledge of this value is very important for the tests of quantum electrodynamics in bound systems, where the theoretical predictions are strongly limited by the lack of precision on the nucleus structure. The uncertainty of the proton radius dominates largely the theoretical uncertainties in the predictions of the Lamb shift in the hydrogen atom. A 0.1% precision in the proton radius measurement would cause a 10^{-7} precision level in the electronic hydrogen Lamb shift, one order of magnitude better than the present limit.

The determination of the Lamb shift in muonic hydrogen will improve the precision in the proton radius by a factor of about 20 times in comparison to the currently known value. Previous proton radius measurements had been obtained by optical spectroscopy [Schwob *et al.* 1999] and electron scattering [Simon *et al.* 1980, Rosenfelder 2000]. The scattering experiments are however difficult to perform and to analyze, leading to

inconsistent results [Pohl *et al.* 2001A]. One of the values obtained by electron scattering was 0.862 ± 0.012 fm [Simon *et al.* 1980]. Recently, values obtained from electron scattering experiments have been revised [Sick 2003] and new corrections have been introduced. From the new analysis, the value 0.895 ± 0.018 fm for the proton radius was suggested, significantly higher than the previous one and with worse precision.

Several contributions to the Lamb shift in muonic hydrogen have been investigated and theoretically calculated. In 1996, Pachucki determined the contribution of the several effects of quantum electrodynamics to the energy levels of muonic hydrogen and obtained the following value for the Lamb shift (E_L) [Pachucki 1996]:

$$E_L = (205.932 \pm 0.010)\ \text{meV} - 5.197\ (\text{meV fm}^{-2})\ r_p^{\,2} \qquad \text{(Eq. 4.2)}$$

where $r_p^{\,2}$ is the mean square value of the proton radius. The uncertainty of E_L is widely dominated by the imprecision on the proton charge radius. Using the r_p value obtained by Simon, the Pachucki E_L value is 202.070 ± 0.108 meV.

In 1999, Pachucki made a complete revision of all contributions to the proton structure [Pachucki 1999]. All terms have been recalculated with better precision, defining a new estimate:

$$E_L = (206.085 \pm 0.003)\ \text{meV} - 5.2256\ (\text{meV fm}^{-2})\ r_p^{\,2} + 0.0363\ (\text{meV fm}^{-3})\ r_p^{\,3} \qquad \text{(Eq. 4.3)}$$

The new result for the Lamb shift, 202.225 ± 0.108 meV, differs from the previous one by a value higher than the error estimated before. This was attributed to an error in the addition of the previous contributions [Pachucki 1996] and to the inclusion of new terms in the later calculation: the uncertainty in the first term of Equation 4.2 was improved by the introduction of new contributions of the vacuum polarization and by the proton polarizability correction. Neglecting the terms dependent on the proton radius, the theoretical value for the Lamb shift is limited by the uncertainty on the proton polarizability shift.

In summary, recent calculations set an error of 20 ppm in the theoretical value of the muonic hydrogen Lamb shift if the terms dependent on the proton radius are omitted. With precise theoretical predictions, the experimental measurement of the Lamb shift will lead to a more precise value for the proton charge radius.

4.1.2. Principle of the experiment

The principle of the experiment consists on stopping a beam of negative muons in a hydrogen gas volume, producing μp atoms highly excited. The majority of these atoms decay promptly to the ground state, but a small fraction remains in the 2S metastable state. A laser pulse, tuned to approximately 6 μm (the wavelength corresponding to the energy difference between 2P and 2S states), is sent to an optical cavity delimiting the gas target in order to sweep the whole volume and to induce the 2S-2P transition in atoms found in the 2S metastable state. The μp atoms in the 2P state decay to the ground state, emitting 1.9 keV X-rays (Figure 4.2), delayed relative to the instant of the muon entrance in the target.

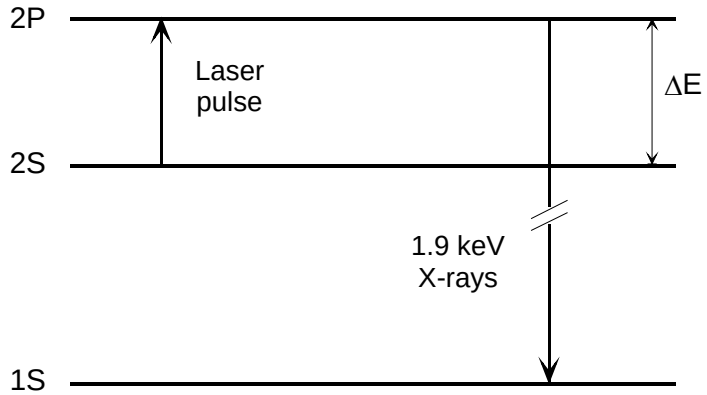

Figure 4.2 – Energy levels in the muonic hydrogen atom and transitions associated with the experiment for determination of the Lamb shift (ΔE).

The Lamb shift is determined from a resonance curve by measuring the number of 1.9 keV X-rays detected in time coincidence with the laser pulse as a function of the laser

wavelength [Kottmann *et al.* 2001]. The number of X-rays is determined from the corresponding time spectrum (Figure 4.3).

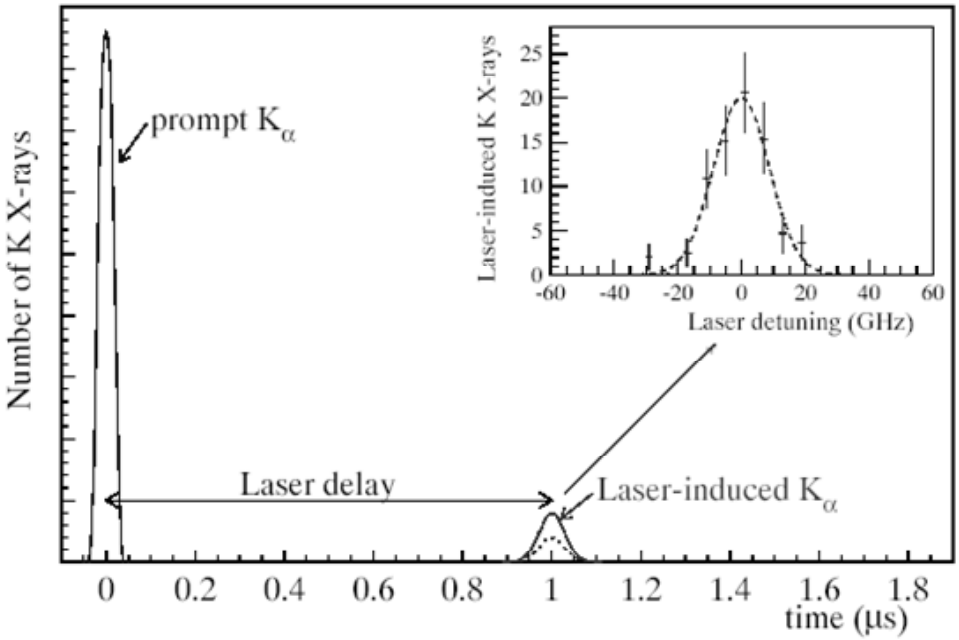

Figure 4.3 – Idealized time spectrum for 1.9 keV X-rays, from which the laser resonance curve is obtained, leading to the determination of the Lamb shift in muonic hydrogen [Pohl 2001].

An essential feature of the experiment is the availability of μp atoms in the metastable 2S state. Thus, the knowledge of the population and lifetime of this state is necessary. The existence of μp atoms in the 2S state was suggested by analysing the kinetic energy distribution of μp atoms [Kottmann *et al.* 1999]. The average kinetic energy of these atoms decreases significantly as the gas density is reduced. Earlier studies, based on K-line yield measurements for X-rays produced when a muon beam is stopped in a low pressure hydrogen volume, showed that about 4% of the muons reach the 2S state, depending on the gas pressure [Anderhub *et al.* 1984]. However, the μp atoms can be excited to the 2P state by collisions within the gas. For kinetic energies below the threshold for 2S-2P transitions (0.31 eV) this process is energetically forbidden and μp (2S) atoms have long lifetimes, about 1 μs at 1 mbar pressures [Pohl *et al.* 2000].

Theoretical considerations show that, for μp atoms produced with energies up to a few eV, the cross section for quenching (de-excitation) and the one for slowing down are of

the same order of magnitude [Jensen *et al.* 2000]. Thus, atoms created with kinetic energies higher than 0.31 eV have an appreciable probability to slow down without being de-excited, increasing the final number of long-lived μp (2S) atoms. Therefore, the fraction of μp (2S) atoms depends on the kinetic energy distribution.

The kinetic energy distribution of μp (1S) atoms was determined through the time of flight technique. Taking into account that 4% of muons (at 16 mbar) reach the 2S state, for each muon interacting in the hydrogen volume about 1% of μp atoms are produced in the 2S state [Pohl *et al.* 2000].

The metastability of μp (2S) atoms was investigated at low pressures [Pohl *et al.* 2001B]. Measuring directly the signal produced by μp atoms, a high-energy component (about 900 eV) in the kinetic energy distribution has been attributed to μp (2S) atoms. The observed high-energy component results from the decay of those atoms to the ground state through a non-radiative process. It is a collisional process involving the formation of a resonant molecule and its subsequent self-dissociation [Wallenius *et al.* 2001]. The time distribution of the 900 eV atoms found out a population for the 2S state of about 1% and a disappearance rate of 5×10^5 s^{-1} p_H, where p_H is the hydrogen pressure (in mbar) [Pohl *et al.* 2001B]. The previous study was performed for different pressures, from 4 to 64 mbar. An optimum pressure of 1-2 mbar was found for the laser experiment since the 2S state lifetime has to be of the same order as the time interval between the muon interaction in the gas and the laser pulse trigger (about 1 μs).

4.1.3. Requirements of the experimental system

The Lamb shift experiment requires an apparatus for the muon beam production, a system to detect and stop low energy muons, a hydrogen target at low pressure (about 1 mbar), a 6 μm laser beam, an optical cavity to concentrate the laser in the whole hydrogen volume and a detector for 1.9 keV X-rays with the associated electronics.

The muon beam

The experiment requires a beam of low energy negative muons. A new line was recently built at the PSI (πE5 area) in order to stop a sufficiently high number of muons in a small hydrogen volume under a few mbar pressures. The line is schematically presented in Figure 4.4 and includes an apparatus to collect the high-energy pions and to produce low-energy muons (cyclotron trap), a muon extraction channel (MEC) for transport and selection of muons and a superconducting (PSC) solenoid with two transmission detectors to define the instant of the muon entrance in the gas, which sets the time-zero.

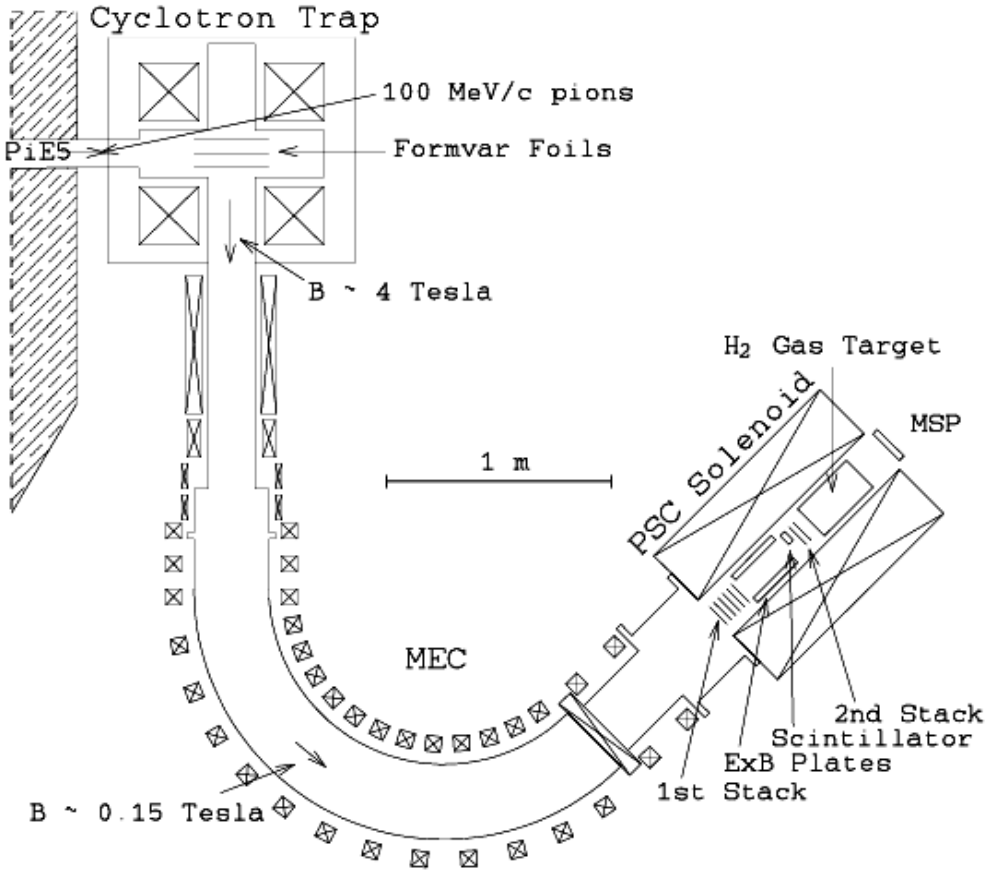

Figure 4.4 – Schematic view of the πE5 area in PSI showing the muon beam line, which includes the apparatus for extraction of pions (cyclotron trap), the muon extraction channel (MEC) and the superconducting solenoid [Kottmann *et al.* 2001].

Negative pions are driven out from the πE5 beam line with a momentum of 100 MeV/c. The muons resulting from pion decay are created with MeV kinetic energies, being then slowed down by a thin plastic foil (Formvar) and remaining with keV energies. An axial electric field ejects the muons to the cyclotron trap exit, a region with a 4 T magnetic field [DeCecco *et al.* 1997].

Muons, typically with 20 keV energy (and 2 MeV/c momentum), are carried through a curved toroidal magnet (the MEC) operating at 0.15 T, leaving a region with high neutron background (near the pion beam exit) towards the solenoid, where the laser resonance experiment is carried out. The MEC acts simultaneously as a filter since particles with momentum above 4 MeV/c are not carried through the curvature and electrons with keV energies are vertically separated from muons due to the toroidal field. This makes it possible to remove high electron flows produced when charged particles (spiralling in the magnetic field of the trap) cross the extraction foils for many times. About 90% of useful muons (with about 20 keV) are carried from the cyclotron trap to the solenoid. The vertical deviation of each particle, relative to the magnetic field lines, is proportional to its momentum. This way, muon trajectories are deviated by about 2 cm. Since the electron deviation is negligible, muons can be separated from the intense flow of electrons [Kottmann *et al.* 2001].

The superconducting solenoid produces a 5 T magnetic field. Figure 4.5 shows a schematic view of the experimental system installed inside the solenoid, illustrating the trajectories of the muons and secondary electrons emitted by the muon passage, as well as the detectors required to set the laser pulse trigger.

When the muon beam enters the solenoid, it crosses a stack of ultra-thin carbon foils (S_1) with 5 μg/cm^2 thickness and a voltage difference of 1.8 kV applied between the foils to compensate the muon energy loss [Mühlbauer *et al.* 1999]. The stack of carbon foils acts as a transmission detector since the secondary electrons emitted by the muon passage through the foils are accelerated towards a plastic scintillator (connected to the photomultiplier PM_1), where they are detected originating a first muon signal. Between the stack of carbon foils and the scintillator, a drift field $\vec{E} \times \vec{B}$ induces a transversal shift of charged particles. The shift is greater for muons than for electrons, providing a

muon passage underneath the scintillator, towards the hydrogen target. After passing underneath the scintillator, muons reach a second stack of carbon foils (S_2), placed in front of the target. The secondary electrons emitted are accelerated to a few keV, being detected by another scintillator (connected to the photomultiplier PM_2) and originating a second muon signal. The time of flight information obtained from both muon signals leads to an optimized detection of muons interacting within the target. The muon time of flight between stacks S_1 and S_2 is typically 150 ns. The laser trigger is originated by the simultaneous detection of a muon with the correct time of flight in both detectors. A third scintillator (D_3), placed behind the target in order to detect muons that do not stop in the gas, is used in anticoincidence with the other scintillators for setting the laser trigger. The laser light enters the target through a window in one of the mirrors (M_1 and M_2) composing the optical cavity.

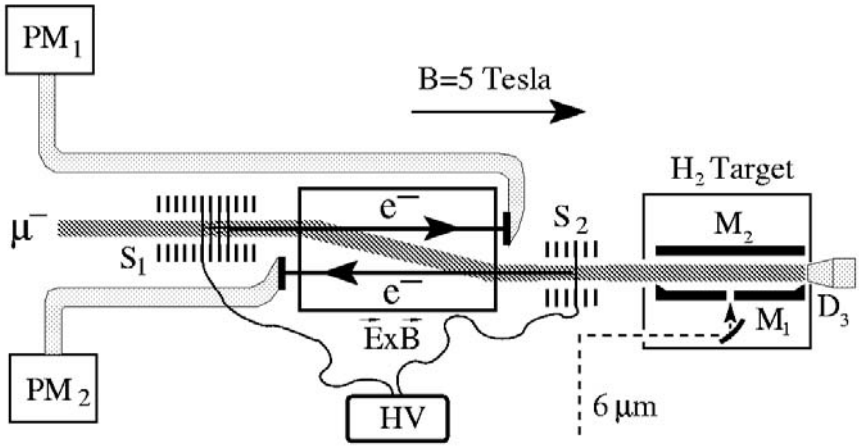

Figure 4.5 – Schematic view of the experimental system installed inside the PSC solenoid, showing the trajectories of the muons and secondary electrons, as well as the detectors required to set the laser trigger.

Laser system and optical cavity

A laser pulse of energy E, injected in an optical cavity with length L and width d, originates an energy density $\varepsilon = E\,\eta\,N/(L\,d)$, where η is the laser injection efficiency and N is the number of passes in the cavity [Taqqu *et al.* 1999].

For the experiment, a good probability for the 2S-2P transition in muonic hydrogen requires a laser pulse of about 0.2 mJ. This energy was obtained for 6 μm through stimulated Raman dispersion in hydrogen [Rabinowitz *et al.* 1986]. The pumping scheme was based on a Nd:YAG (Neodymium-doped $Y_3Al_5O_{12}$) laser, which cannot be used in this experiment because it does not provide a laser pulse randomly triggered, with a maximum delay time of about 1 μs and 50 Hz repetition rate. The laser to be used in the experiment is a high power XeCl excimer that provides ultraviolet-light pulses with 308 nm wavelength, 28 ns width and 500 mJ energy for the maximum frequency of 50 Hz. The laser system is composed by three stages: the excimer, the combination of a dye laser and a titanium-sapphire (Ti:Sa) laser, and a Raman cell (Figure 4.6).

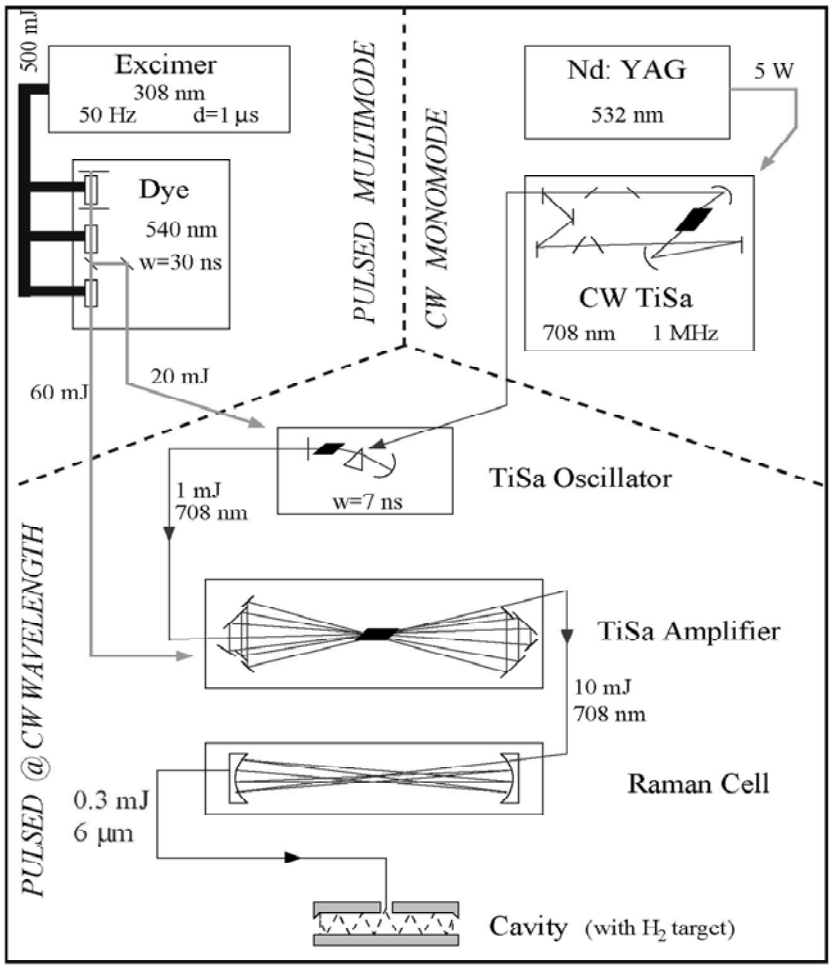

Figure 4.6 – Schematic of the laser system components, showing how the light wavelength is converted into the desired 6.02 μm [Antognini *et al.* 2004].

The laser is triggered when a muon is detected in time coincidence in both transmission detectors, connected to photomultipliers PM_1 and PM_2, and in anti-coincidence with scintillator D_3, as described before. Due to the short muon lifetime the laser pulse must arrive in the target in about 1 μs. The delay originated by the excimer relative to the pulse trigger is of the same order.

In the second stage, the pulse wavelength conversion from 308 into 708 nm is made in two steps. The 308 nm pulses arrive at a dye cell, where they are efficiently converted into 540 nm green light. This light is optimum to pump the Ti:Sa laser system, composed by a Ti:Sa oscillator and the corresponding amplifier. This system requires 20 mJ pump energy for the oscillator and 60 mJ for the amplifier. The oscillator has a short length (7 cm), assuring short pulses (about 7 ns) with 1 mJ energy and a delay shorter than 50 ns. The amplifier provides a multiplication factor of 10. The beam quality of the oscillator-amplifier system and the wavelength tuning of the 708 nm pulse, as well as the 6 μm final pulse, is controlled by a continuous wave (CW) Ti:Sa laser [Antognini *et al.* 2004].

In the third stage, the 708 nm light is converted into 6.02 μm by the Raman shift [Rabinowitz *et al.* 1986] in a hydrogen cell working under high pressure (15 bar). It is a stainless steel tube with 2 m length, where the frequency of the 708 nm photons is converted by three subsequent Stokes shifts to the infrared spectral region, exciting the hydrogen molecules from the $\upsilon = 0$ to the $\upsilon = 1$ vibrational state. To increase the conversion efficiency, the laser pulses cross the tube 33 times, a process controlled by two silver coated mirrors placed inside the tube. The final pulse wavelength is calibrated by scanning over a water absorption line, λ = 6.01391736 μm, known with a precision of 0.04 ppm.

The infrared laser beam, with 7 ns width and an energy of about 0.3 mJ, is focused through a series of mirrors towards the gas target inside the solenoid, being injected in the optical cavity surrounding the target in order to efficiently illuminate the whole volume. To prevent partial absorption of the beam by water vapour, the laser beam line was filled with dry nitrogen.

The optical cavity is made up by two highly reflecting mirrors, placed sideways relative to the target. Since the light sweeps the target for successive times, the mirrors have curvatures to prevent light loss. One of the mirrors contains a small hole (with 0.6 mm diameter) where the laser beam enters and, after many reflections, part of the beam leaves the cavity. The retro-reflected light is guided to an infrared detector which analyses the light that flows in the cavity. The light intensity inside the cavity decreases exponentially, with a time constant of about 145 ns, leading to an average number of 1700 reflections of the laser pulses inside the cavity [Kottmann *et. al.* 2003]. Under these conditions, a laser beam with 0.13 mJ energy at the cavity entrance is sufficient to saturate the 2S-2P transition.

The 1.9 keV X-ray detector

The X-ray detector to be used in the experiment has to fulfil some requirements. First, it has to support intense magnetic fields since the target where muons interact is placed inside a solenoid operating at 5 T.

Since only a few laser-induced events per hour are expected, the detector has to achieve an energy resolution of about 20% and a time resolution better than 50 ns for 1.9 keV X-rays in order to provide a good separation between signal and background.

After the prompt emission of the 1.9 keV X-ray, electrons resulting from muon decay (with MeV energies) generate signals with high amplitudes when they hit an APD. The "delayed-coincidence" between an electron signal and the X-ray pulse will substantially reduce the background. A pulse risetime shorter than 500 ns makes it possible to determine a double-pulse sequence of an X-ray followed by an electron, measured in the same APD, which occurs with a relatively high probability.

The solid angle for X-ray detection has to be as large as possible in order to maximize the event rate. Several prototypes of gaseous detectors were also tested, mainly xenon gas proportional scintillation counters providing large detection areas [Veloso *et al.* 2002]. However, large area avalanche photodiodes used for direct X-ray detection

present advantages when compared to those detectors. First, they are practically insensitive to intense magnetic fields, as will be shown in the next subchapter. Additionally, they have short pulse risetimes (about 25 ns for API photodiodes) and an excellent time resolution (lower than 30 ns) for 1.9 keV X-rays. The energy resolution fulfils the requirements of the laser experiment.

The great limitation of LAAPDs is their small detection area. However, as they are compact and can be installed in vacuum, without window, the sensitive area can be placed closer to the volume where muonic hydrogen is produced, practically compensating the solid angle loss and the absorption by the window and its support structures in gas detectors. Using a series of photodiodes in the target, the effective detection area becomes significant, compensating the reduced area of each APD.

4.2. Behaviour of LAAPDs under intense magnetic fields

Under the work program of other thesis [Veloso 2000, Lopes 2002], some prototypes of GPSC had been assembled and tested under intense magnetic fields in order to verify their viability to be used in the experiment. For technical reasons, the voltage in the scintillation region of these prototypes was applied at the entrance radiation window. Since muons stop in the hydrogen volume near the detector entrance, such high negative voltage is enough to hinder muons from entering the gas target and often originates gas discharges, making it impossible to use the prototypes in the final experiment.

In order to circumvent the disadvantages of GPSCs for the experiment, the use of LAAPDs was considered. The behaviour of LAAPDs under intense magnetic fields was investigated and the results are presented in comparison to the results obtained with GPSC prototypes, showing the characteristics of the LAAPD as direct X-ray detector that lead its application to the experiment. Beyond the energy response, the LAAPD time response was also studied.

The effect of the magnetic field on the operation of avalanche photodiodes was already mentioned in the literature but detailed experimental were not found. Moreover, the majority of the studies was carried out for visible-light detection, disregarding the detection of ultraviolet light and X-rays. In this way, we considered appropriate to extend the LAAPD tests under intense magnetic fields to visible-light and VUV-light detection. The study of the LAAPD performance for VUV-light detection was of particular importance for the experiment since its use as VUV photosensor in a GPSC constituted an alternative for the experiment.

4.2.1. Gas detectors as alternatives for X-ray detection

Different GPSC prototypes were tested in magnetic fields. The detectors were built without drift region in order to provide a faster time response. The volume of each detector was filled with xenon and the scintillation light produced within the gas was detected by different photosensors, as Figure 4.7 shows. A microstrip plate coated by a CsI film was used as VUV-light photosensor in prototypes A and B, being positioned directly in the xenon volume for the prototype A and in a separate chamber with a P-10 mixture for the prototype B. The P-10 mixture provides considerably higher gains [Veloso *et al.* 2001]. In the prototype C, a LAAPD was used as photosensor.

The effect of the magnetic field on the electron cloud produced in the GPSC can be shown in Figure 4.8, where the relative orientations of the electric field in the detector and the magnetic field inside the solenoid are shown. The deviation of the drift direction of electrons, defined by the Lorentz angle α_L, depends on the ratio between the magnetic and electric forces applied to the electrons and on the drift velocity. Under the working conditions of the detectors, α_L is small, about 4º for a 5 T magnetic field [Lopes 2002].

For photosensors based on microstrip plates the avalanche process in the gas depends on the magnetic field [Veloso *et al.* 2002]. For avalanche photodiodes, studies previously carried out did not suggest any variation with the magnetic field [Pansart 1997]. However, no studies with ultraviolet light were performed up to now and the fact that

VUV photons interact in the first atomic layers of the photodiode may introduce some dependence of the LAAPD response on the magnetic field intensity.

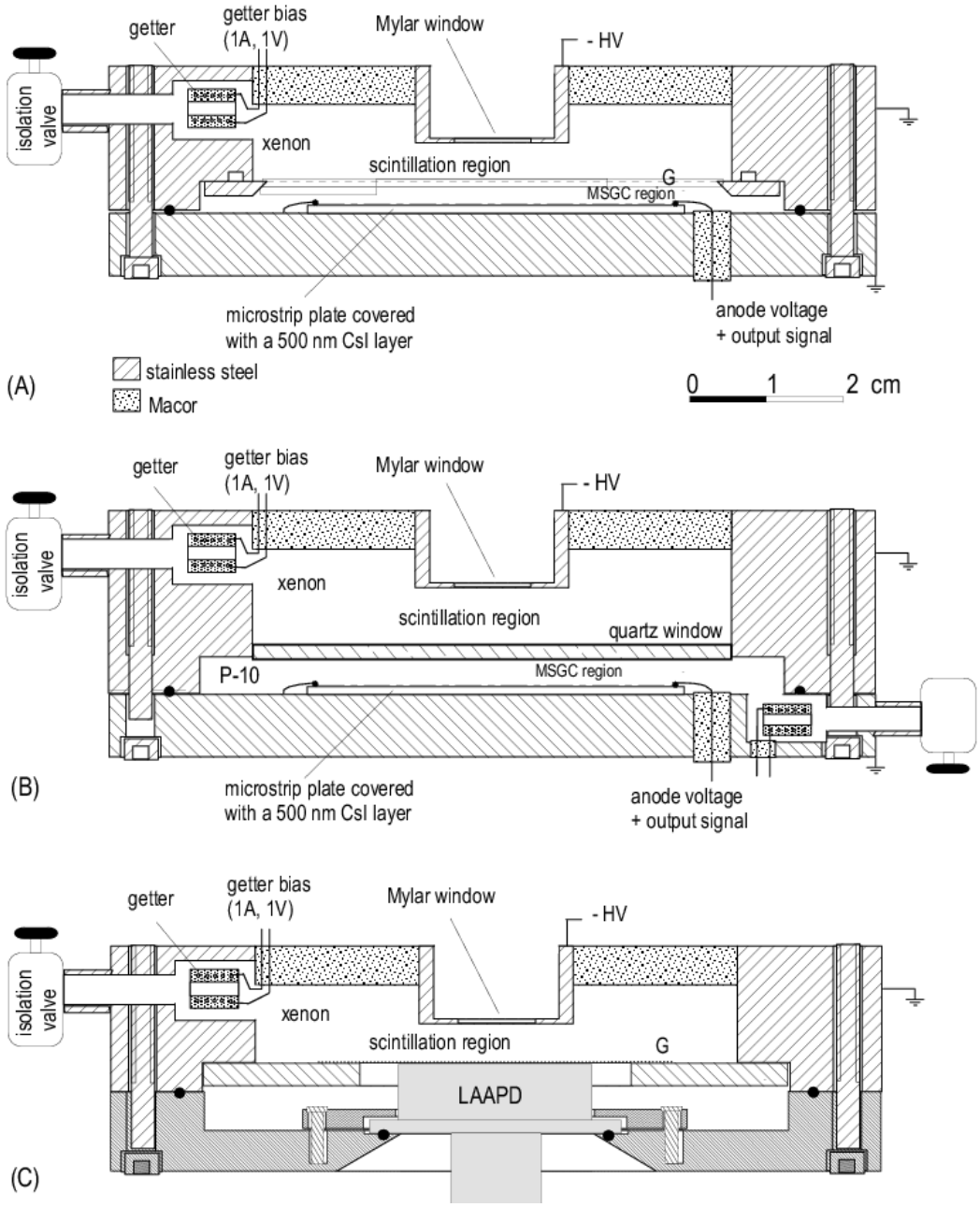

Figure 4.7 – GPSC prototypes tested under intense magnetic fields as alternatives for detection of 1.9 keV X-rays. Different photosensors had been used: a microstrip plate coated to a CsI film operating in the xenon volume (A), the same photosensor operating in a separate chamber with a P-10 mixture (B), and a LAAPD (C). The thickness of the scintillation region for prototypes A, B and C is 0.85, 0.6 and 1.1 cm, respectively [Veloso *et al.* 2002].

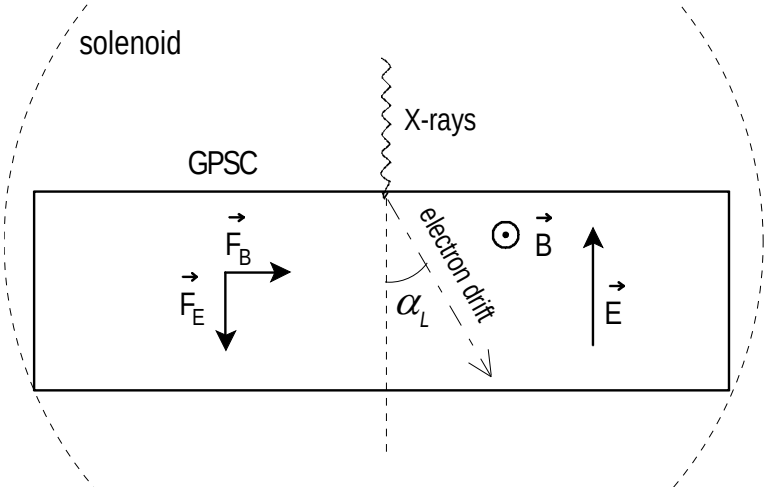

Figure 4.8 – Schematic view of the relative orientation of the electric field in the GPSC and the magnetic field in the solenoid during the test of the GPSC prototypes [Lopes 2002].

The tests of GPSC prototypes in magnetic fields were carried out in the interior of a superconducting solenoid composed by a cylindrical cavity with 20 cm diameter and 1 m length. The maximum intensity of the magnetic field inside the solenoid is 5 T. The field is practically uniform (10 ppm) throughout an axial distance of 30 cm from the centre of the solenoid.

For each detector, a sulphur sample irradiated by a ^{55}Fe radioactive source was placed above the GPSC window and the characteristic X-rays emitted were detected. The amplitude and energy resolution of the resulting signals were determined as a function of the magnetic field [Veloso *et al.* 2002].

For a 5 T magnetic field, the amplitude of the pulses produced by 2.3 keV X-rays was reduced by 25% for the prototype A, while for the prototype B it was reduced by less than 2%. Although the Lorentz angle effect is very small in both cases, the trajectory of the photoelectrons is changed in the microstrip chamber, leading to dispersion of some electrons to the photocathode, which are not collected. The photoelectron backscattering is much higher for xenon than for the P-10 mixture [Veloso *et al.* 2002], explaining the discrepancy between the results obtained for prototypes A and B.

For prototype C, backscattering effects are not present [Lopes 2002] but a reduction of 11% was measured in the pulse amplitude. However, as the LAAPD area is much

smaller than the microstrip plate one, prototype C is much more sensitive to solid angle variations. The amplitude variation in this detector can be attributed to the transversal shift of the electron clouds (Lorentz angle), which originates an inferior collection of scintillation photons by the LAAPD and subsequently signals with smaller amplitudes. In addition, since VUV photons are absorbed superficially in the LAAPD, the dependence of the LAAPD response on the magnetic field intensity must be considered.

The magnetic field effect is also perceptible in the energy resolution obtained for 2.3 keV X-rays, which increases from 27 to 31% for prototype A and from 18 to 26% for prototype C, as the magnetic field increases from 0 to 5 T. For prototype B, the obtained energy resolution (about 27%) practically did not vary.

The time response of the several prototypes was also investigated. The pulse risetime was determined at the preamplifier output. Average values of 1.1, 0.5 and 1.2 μs were measured for prototypes A, B and C, respectively. As the time response of the used photosensors is much shorter than the drift time of the electron cloud produced in the gas, the pulse risetime is practically equal to the drift time. The variation of the pulse risetime with the applied magnetic field is not significant [Veloso *et al.* 2002].

The time resolution of the detectors was determined using 5.4 keV X-rays and 835 keV γ-rays emitted in time coincidence by a ^{54}Mn source. Each GPSC prototype was used to detect X-rays, while γ-rays were detected by a NaI(Tl) scintillator with known time resolution. A time resolution above 200 ns was obtained for prototype A, while for prototypes B and C values of 25 and 30 ns were registered, respectively [Veloso *et al.* 2002]. No measurements were obtained in the presence of magnetic field due to the impossibility to put the system inside the solenoid. However, as the time resolution depends mainly on the drift time of the electrons in the gas and on the time response of the photosensors, a dependence on the magnetic field is not expected.

Due to its lower sensitivity to magnetic fields up to 5 T, the prototype B is the one more suitable to be used in the muonic hydrogen Lamb shift experiment. However, LAAPDs present important advantages for direct X-ray detection, as it will be recognized next.

4.2.2. Energy response of LAAPDs

The response of avalanche photodiodes was studied as a function of the magnetic field for detection of X-rays, visible light and VUV light. The experimental system used in each case and the obtained results are described in the paper: "Behaviour of large-area avalanche photodiodes under intense magnetic fields for VUV, visible and X-ray photon detection", published in *Nucl. Instr. Meth. A*, vol. 498 (2003), pages 362-368 [Fernandes *et al.* 2003A], attached at the end of this chapter (page 169). It was proved that LAAPDs can operate under magnetic fields up to 5 T without significant degradation of their performance for X-ray and visible-light detection, while for VUV-light detection a significant degradation was observed in the pulse amplitude and energy resolution. An amplitude reduction of 24% was measured for 5 T.

In addition to the presented results, the LAAPD response was studied for lower energy X-rays, closer to the 1.9 keV X-rays proposed to detect in the muonic hydrogen Lamb shift experiment. A sulphur sample was irradiated by a ^{55}Fe source, emitting characteristic X-rays whose main fluorescence line (K_α) corresponds to 2.3 keV. The study was performed as a function of the magnetic field by positioning the system inside the solenoid with the photodiode axe perpendicular to the magnetic field direction. The amplitude and energy resolution of the signals produced by the sulphur characteristic X-rays were determined.

Figure 4.9 shows the relative amplitude and the energy resolution of the 2.3 keV X-ray signal as a function of the magnetic field. No significant degradation of the amplitude and energy resolution for 2.3 keV X-rays was observed, as it was verified for 5.4 keV X-rays [Fernandes *et al.* 2003A]. When the magnetic field increases from 0 to 5 T, the amplitude variation is lower than 3%, approximately equal to the experimental errors, and an absolute energy resolution variation of 2% was observed. As energy resolution improves significantly for lower temperatures [Fernandes *et al.* 2004A], the use of LAAPDs in the experiment requires the reduction of their operation temperature.

The previous results show that LAAPDs can operate under magnetic fields up to 5 T without significant performance degradation for low energy X-rays.

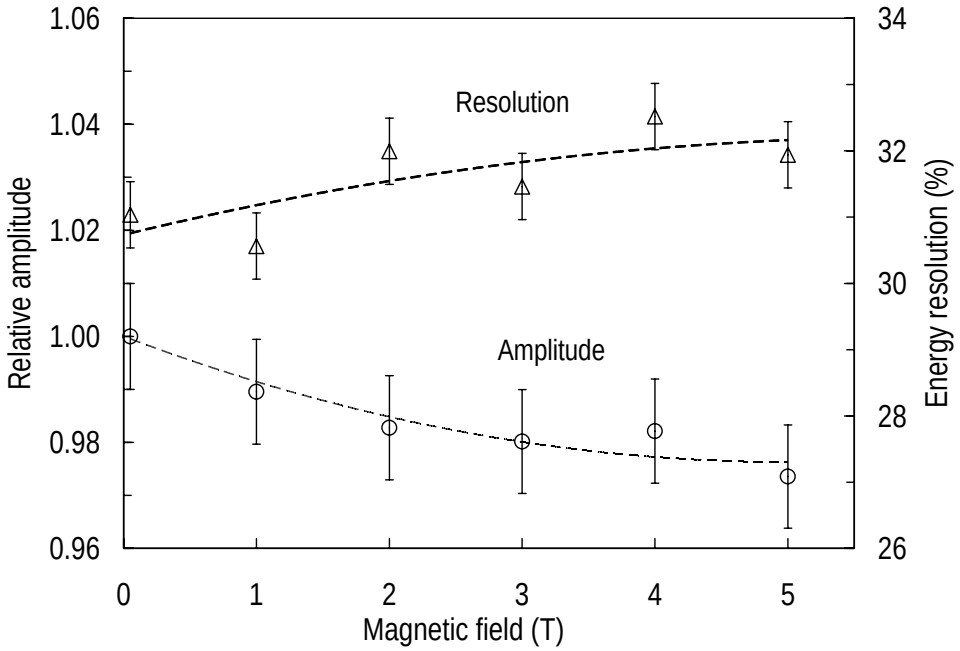

Figure 4.9 – Relative amplitude and energy resolution of the pulses produced in the LAAPD by 2.3 keV characteristic X-rays from a sulphur sample irradiated by a ^{55}Fe source as functions of the magnetic field inside the solenoid.

4.2.3. Time response of LAAPDs

The time response is very important in the choice of the detector for 1.9 keV X-rays to be used in the experiment. Parallel to the amplitude measurements of LAAPD signals, the pulse risetime obtained at the preamplifier output was determined as a function of the magnetic field. The time variation of the pulses at the preamplifier output is presented in Figure 4.10 for magnetic fields of 0 and 5 T. As shown, the shape of the pulses does not depend significantly on the magnetic field.

The distributions presented in Figure 4.10 lead to the determination of the pulse risetime, defined as the time interval corresponding to a relative pulse amplitude variation between 10 and 90%. Figure 4.11 shows the risetime of the pulses produced in two different photodiodes as a function of the magnetic field. The pulses result from 5.9 and 5.4 keV X-rays absorbed in the LAAPDs, for different relative orientations of the electric and magnetic fields (perpendicular and parallel, respectively).

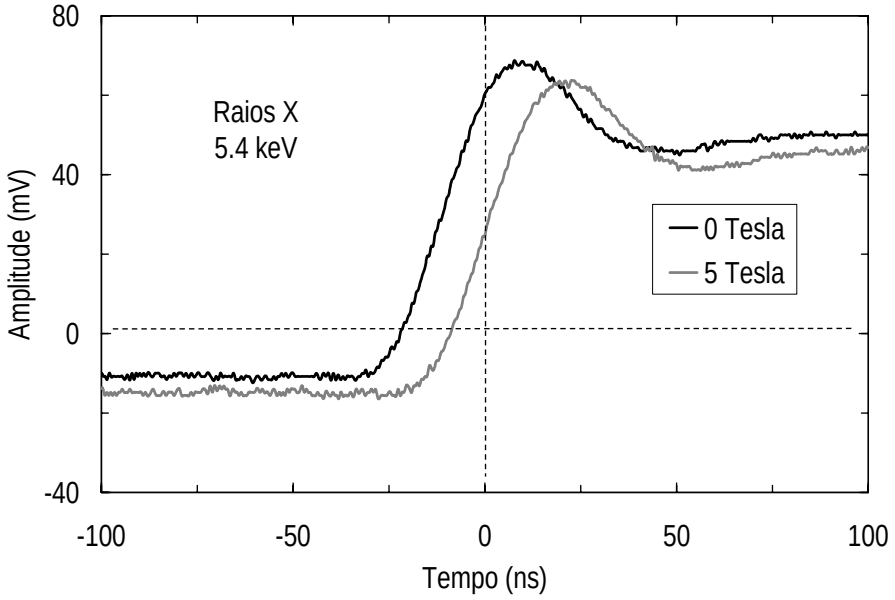

Figure 4.10 – Shape of the pulses obtained at the preamplifier output, resulting from 5.4 keV X-rays absorbed in the LAAPD, for magnetic field intensities of 0 and 5 T.

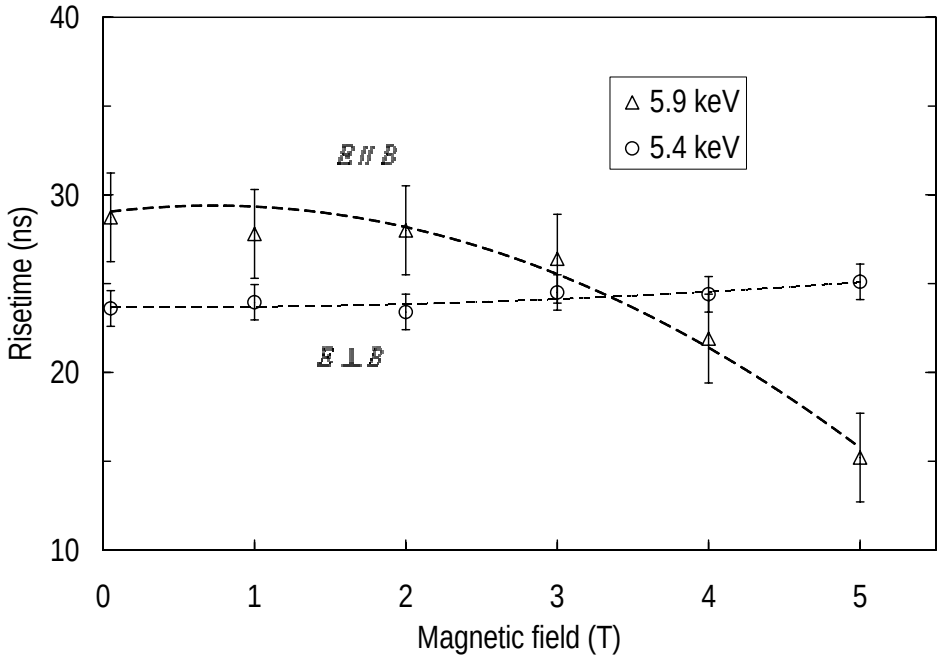

Figure 4.11 – Risetime of the pulses obtained at the preamplifier output, resulting from 5.4 and 5.9 keV X-rays absorbed in two different photodiodes, as a function of the magnetic field.

For the most unfavourable situation, where the magnetic field is perpendicular to the electric field, the risetime of 5.4 keV X-ray pulses practically does not vary with the magnetic field, being about 25 ns. For the case where the electric and the magnetic fields have the same direction, the risetime of 5.9 keV X-ray pulses undergoes a significant variation, from 30 to 15 ns as the magnetic field increases from 0 to 5 T. Since the electronic noise affected differently both photodiodes, being much higher in the second case, the influence of the magnetic field on the risetime is not clear.

The risetime was also determined for pulses produced in the LAAPD by 2.3 keV X-rays obtained by fluorescence of a sulphur sample irradiated by a ^{55}Fe source. Values between 20 and 32 ns were measured for magnetic fields between 0 and 5 T.

In comparison to GPSCs, which present risetimes of about 1 μs, the response of avalanche photodiodes is considerably faster, providing pulses with risetimes in the range 20-30 ns, an important advantage when the detection of events in time coincidence is necessary.

The LAAPD time resolution was determined from the coincidence between 5.4 keV X-rays and 835 keV γ-rays emitted by a ^{54}Mn source. X-rays are detected by the LAAPD and γ-rays by a NaI(Tl) scintillator. The relative orientation of the detectors and the radioactive sources is represented in Figure 4.12. The time-zero is defined by the instant where a γ-ray is detected in the scintillator. The time stops when an X-ray is detected by the LAAPD. Selecting the events detected in time coincidence in both detectors, a time spectrum is obtained, from which the time resolution is determined.

Figure 4.13 shows a typical time spectrum of the coincidences between the signals produced by 835 keV γ-rays and 5.4 keV X-rays, obtained for 1 and 1.8 kV voltages applied to the NaI(Tl) detector and to the LAAPD, respectively. The number of coincidences between the pulses obtained in both detectors was registered in intervals of 2 ns. The full-width-at-half-maximum of the peak in the represented distribution defines the time resolution of the system composed by the two detectors, being 10 ns in this case. The measurements were repeated and values between 10 and 12 ns were obtained. The time resolution of the system is equal to the quadratic addition of the time

resolutions of each detector. Since NaI(Tl) detectors present a time resolution of 3-5 ns, the LAAPD time resolution is about 10 ns. Compared to other investigated detectors, the LAAPD presents the best time response, being the preferred detector for 1.9 keV X-rays emitted by muonic hydrogen atoms in the Lamb shift experiment.

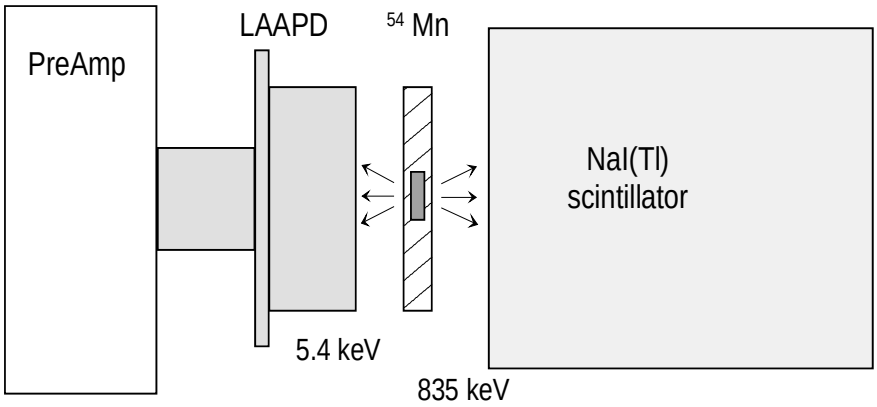

Figure 4.12 – Experimental system used to measure the time resolution of the LAAPD. The ^{54}Mn radioactive source emits 5.4 keV X-rays and 835 keV γ-rays in time coincidence, detected respectively by the LAAPD and a NaI(Tl) scintillator.

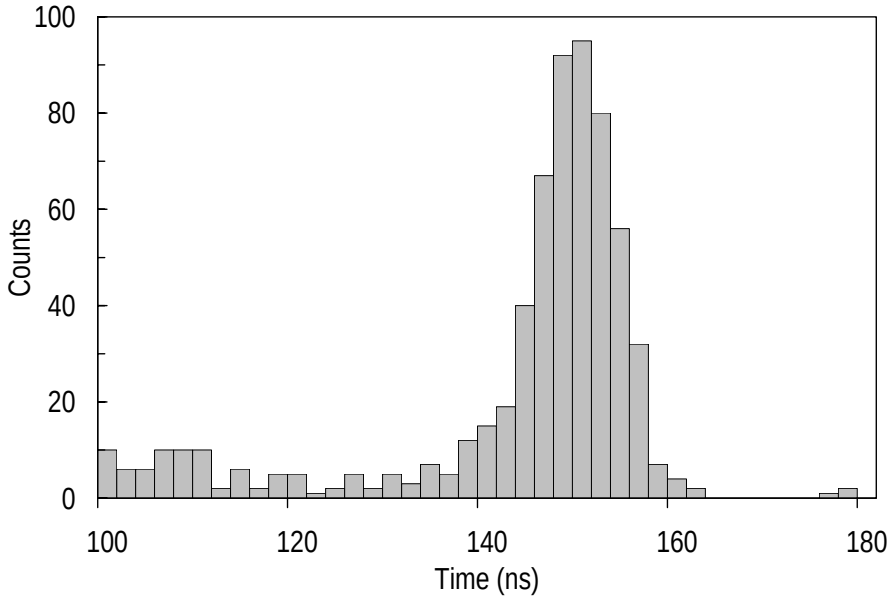

Figure 4.13 – Time spectrum of the coincidences between the signals produced in the NaI(Tl) detector and the LAAPD by 5.4 keV X-rays and 835 keV γ-rays, respectively.

4.3. Test of LAAPDs in the intense radiation environment of muon experiments

LAAPDs have been tested in the presence of the muon beam. The tests were carried out in the μE4 area of PSI and the main objective was to verify the capability of LAAPDs for detection of X-rays emitted by muonic atoms, particularly the muonic hydrogen K_α line (1.9 keV X-rays), in the intense radiation environment of these experiments.

The determination of the Lamb shift in muonic hydrogen requires a very low energy muon beam. However, the line of the μE4 area produces an intense muon beam with momentum in the range 30-100 MeV/c.

The environment of intense radiation and low counting rate, typical for muon experiments, makes it difficult to identify the peaks in the energy spectra resulting from X-ray absorptions in the photodiode, due to the presence of a background caused by electrons passing through the photodiode. The time discrimination of X-ray signals relative to the signal produced by the muon entrance is used as a technique of background reduction. Furthermore, the coincidence between the X-ray signal and the signals produced by the electrons resulting from muon decay leads to the improvement of the X-ray discrimination against the background. The effect of the discrimination techniques on the electron background reduction was investigated for different gases in the target. The simultaneous analysis of time and energy spectra is very important for selecting the events of interest.

The LAAPD tests with the muon beam are described in the paper: "Application of large-area avalanche photodiodes to X-ray spectrometry of muonic atoms", published in *Spectrochimica Acta B*, vol. 58 (2003), pages 2255-2260 [Fernandes *et al.* 2003B], attached at the end of this chapter (page 177). In the paper, the experimental system, including the gas target and the surrounding detectors, is described and the main results of the LAAPD time and energy response to muonic X-rays are discussed.

4.3.1. Optimization of the muon momentum

Low energy muons interact in a gas target under a pressure of 1 atm. Different gases have been used in the target: helium, hydrogen and a mixture of hydrogen and methane. The target is surrounded by several detectors, required to detect the muons that enter the target, the X-rays produced there and the electrons resulting from muon decay. Several plastic scintillators have been used as muon and electron detectors. Besides two photodiodes used for X-ray detection, two high-purity germanium (HPGe) detectors have been used as X-ray and γ-ray detectors for monitoring purposes, specifically to register the number of muons that stop in the gas (by the small HPGe detector) and in the walls (by the large HPGe detector). This way, the momentum of the muon beam can be optimized in order to maximize the number of stops in the gas and to minimize the number of stops in the walls of the chamber.

The HPGe detectors have been calibrated using radioactive sources emitting radiation with energies within the sensitivity range of each detector. The small HPGe detector was calibrated with 5.9 and 6.5 keV X-rays emitted by a ^{55}Fe source. The large HPGe detector was calibrated with a ^{60}Co source, emitting 1.17 and 1.33 MeV γ-rays. The calibration of the LAAPDs was performed using 5.4 and 5.9 keV X-rays emitted by the ^{54}Mn and ^{55}Fe sources, respectively.

When muons are stopped in a gas volume, muonic atoms are produced in excited states, which decay to the ground state emitting X-rays. Moreover, muons stopping in the walls create γ-rays and electrons contributing to the background. More electrons are produced as a result of the muon decay. Basically, a free muon decays exponentially with a lifetime of 2.197 μs in the laboratory frame.

The capture of negative muons by the nuclei of gas atoms originates a change on the muon decay process. In addition to the gas, muons stopping in the walls are captured by heavier atoms (gold, aluminium). The muon lifetime depends on the material where it is captured, being shorter for atoms with higher atomic number. For example, the muon lifetime in gold is only 75 ns [Suzuki *et al.* 1987]. Since the target was covered by a thin

gold layer, muons that reach the walls are promptly captured and practically no electrons are emitted.

The time spectrum of LAAPD pulses must illustrate the exponential behaviour characteristic for muon decay. Since the most part of the obtained pulses result from electrons, the time spectrum depends on the ratio between the number of muon stops in the gas and in the walls. For gas mixtures, the time spectrum depends also on the competition between the different atoms of the mixture for the muon capture and on muon transfer.

Several techniques have been used in order to suppress the background produced by γ-rays and electrons resulting from muon stops in the walls and from the muon decay process [Fernandes *et al.* 2003B]. One condition for electron background reduction is associated with the detection of electrons by the scintillators. Only pulses happening in the time-interval between 0.2 and 5.2 μs, relative to the instant of the muon entrance in the target, have been considered. The minimum limit (0.2 μs) was chosen because electrons resulting from muon capture by gold atoms have a very low probability (about 12%) of being emitted after 0.2 μs (about 3 muon lifetimes in gold). The background associated with pulses resulting from muon capture by other materials, as aluminium, is not efficiently suppressed since the muon lifetime is longer in these materials.

An important condition for electron background reduction consists on requiring delayed coincidence between the signal produced by the muon entrance and the signal produced by the electrons resulting from muon decay, registered by any pair of scintillators. A reduction of the electron background can be obtained by selecting only prompt events. Events are considered prompt if they occur in the time interval between -30 and 30 ns relative to the muon entrance, which sets the time-zero, and delayed if they take place more than 30 ns after the muon entrance.

The momentum of the muons has to be optimized in order to maximize the number of muons stopping in the gas. An optimum value of 31 MeV/c has been obtained for a helium target through a simulation program, used as the starting point. To determine the

real optimum momentum, a scanning in the vicinity of 31 MeV/c is necessary, determining the fraction of muons stopping in the gas for each chosen momentum.

The momentum can be easily optimized using a gas mixture in the target. In a mixture of H_2 and CH_4, besides muonic hydrogen and muonic carbon (μp, μC) atoms produced by direct muon capture, also muon transfer from a μp atom to a carbon atom may occur:

$$\mu p + C \rightarrow \mu C + p \qquad \text{(Eq. 4.4)}$$

The production of μC atoms is mostly originated by muon transfer [Schellenberg 1993] and the resulting pulses are delayed. By looking at the energy distributions for X-rays emitted by μC atoms, the muon momentum can be optimized in order to maximize the number of delayed pulses relative to the number of muons that enter the target. A scanning in the vicinities of 31 MeV/c was made in multiples of 0.5 MeV/c and the energy spectra obtained with the large HPGe detector were registered for delayed events in coincidence with electrons resulting from muon decay, detected by plastic scintillators. Figure 4.14 shows the energy distributions obtained for a mixture of H_2 and CH_4 (4%) for different momentum values (in the 31-32 MeV/c range).

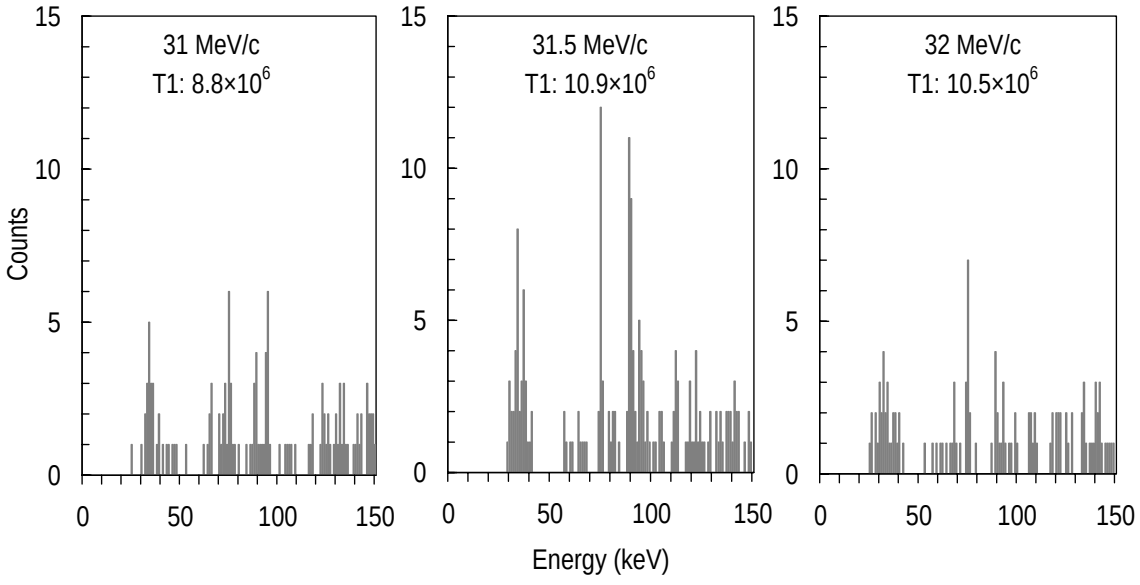

Figure 4.14 – Energy spectra of the events registered in the large HPGe detector for a mixture of H_2 and CH_4 (4%), for three values of the muon momentum. Only delayed events in coincidence with electrons resulting from muon decay were selected.

Figure 4.14 shows the K_α and K_β lines of muonic carbon atoms (with energies around 75 and 90 keV). The other lines correspond to heavier muonic atoms produced by muon transfer to atoms of the chamber walls. The number of delayed pulses produced in the HPGe detector by X-rays emitted by μC atoms, normalized to the number of muons that enter the target (registered by the scintillator T1), is higher for 31.5 MeV/c. As a result, this is the momentum that maximizes the fraction of muons stopping in the gas.

Figure 4.15 shows the number of pulses registered in the large HPGe detector, delayed and in coincidence with electrons resulting from muon decay, with energies between 20 and 150 keV, as a function of the muon beam momentum. The number of events is normalized to the total number of muons that entered the target. The figure shows that the optimum momentum is about 31.5 MeV/c.

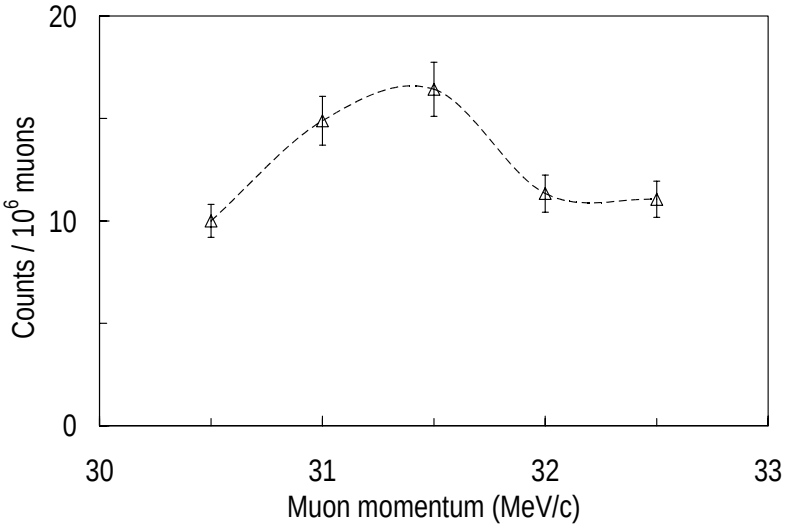

Figure 4.15 – Number of pulses with energies between 20 and 150 keV, obtained in the large HPGe detector, delayed and in coincidence with electrons resulting from muon decay, as a function of the muon beam momentum.

4.3.2. Time response

Different gases were used in the target: pure gases (hydrogen and helium) and a mixture of hydrogen and methane. The same muon beam momentum of 31.5 MeV/c was used.

A comparison between the muon lifetimes for each gas can be made by analysing the obtained time spectra. Several time distributions were considered, using different discrimination techniques of the events.

Pure gases

Helium was used as the first gas target. Figure 4.16 shows different time spectra of the pulses obtained in photodiodes L1 and L2. The distribution of all detected events (total) is considerably different in the two LAAPDs due to the use of different noise discrimination levels. The ratio between the number of prompt and delayed events is lower for L2, what is attributed to a higher noise discrimination level, leading to a partial loss of events of interest. Figure 4.16 also shows the distribution of events with energies between 1.5 and 9 keV, which is very similar for both LAAPDs. Since the noise level is about 1 keV, the use of that energy range eliminates the events associated with noise. However, a large amount of pulses in this energy range corresponds to electrons resulting from muon decay. The exponential behaviour seen in the distribution of events with energies between 1.5 and 9 keV determines a lifetime of 1.25 μs for both photodiodes (the time constant is τ = 1.81 μs). This value corresponds to events resulting from muon stops in the gas and walls. The distribution of events with energies between 1.5 and 9 keV in coincidence with electrons resulting from muon decay is also presented. As expected, in this distribution practically all events are prompt and the background characteristic for muon decay is not observed.

The time spectra of LAAPD pulses have been registered for a hydrogen gas target. The distribution of the events with energies between 1.5 and 9 keV is similar for both photodiodes, defining 1.27 and 1.29 μs lifetimes for L1 and L2, respectively. These values are similar to the ones obtained with helium.

The majority of events with energies between 1.5 and 9 keV corresponds to electrons that deposit part of their energy in the photodiodes. A large amount of electrons are produced by muons stopping in the walls and not in the gas, making it difficult to compare the muon lifetimes for the two gases (helium and hydrogen). However, the

proximity between the lifetimes obtained in the two cases anticipates a small difference between the muon lifetimes in the two gases.

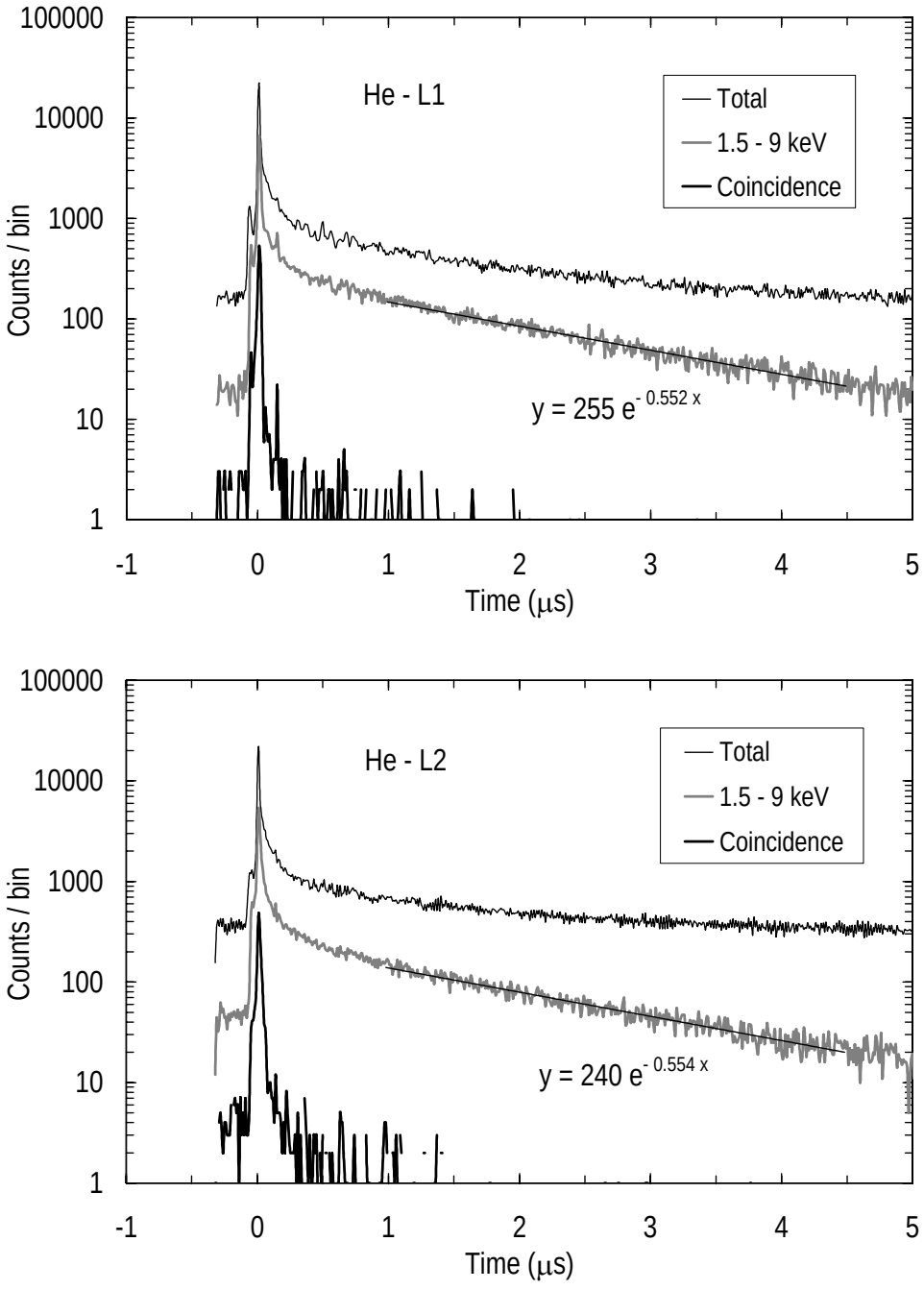

Figure 4.16 – Time spectra of the pulses obtained in photodiodes L1 and L2 for a helium target. Different distributions are represented: all detected events, events with energies between 1.5 and 9 keV, and events in coincidence with electrons resulting from muon decay (bin = 10 ns).

Gas mixtures (H_2 and CH_4)

A mixture of H_2 and CH_4 has also been used in the target. As stated before, a μC atom can be produced by direct muon capture or by muon transfer from a μp atom to a carbon atom. Thus, the time spectrum depends on the competition between hydrogen and carbon atoms for capture of muons and on the muon transfer.

The μC atoms obtained by direct muon capture are created in excited levels with high main quantum number (n), about 14, de-exciting within 1 ns. For states with high n, the de-excitation occurs mainly by Auger effect. The transitions between levels with a difference of secondary quantum numbers $\Delta l = -1$ are preferred, what tends to populate the orbits with $l = n-1$. For states with lower n the transitions with $\Delta l = -1$ dominate and characteristic X-rays are emitted. Events resulting from direct muon capture are prompt.

Muon transfer may also take place. If a neutral μp atom approaches a carbon atom, the muon may be captured originating a μC atom. The lifetime of the μp atoms in the ground state (1S) is then determined by three processes:

1) muon decay: $\mu \rightarrow e + \nu_\mu + \overline{\nu}_e$
2) creation of a pμp molecule: $p + \mu p \rightarrow p\mu p$
3) muon capture by a carbon atom: $C + \mu p \rightarrow (\mu C)^* + p$

The probability of the two last processes depends strongly on the concentrations of carbon and hydrogen in the mixture. Consequently, the lifetime of μp (1S) atoms should vary with those concentrations. The μC atoms obtained by muon transfer can be created in states with lower n relative to the ones originated by direct capture ($n \sim 14$). The transfer process to carbon atoms occurs at a rate of $0.95(5)\times10^{11}$/s [Schellenberg 1993], originating delayed events. The time spectrum of the corresponding X-rays has an exponential shape.

The time spectrum of the X-rays emitted in mixtures of H_2 and CH_4 results from the overlap of the peak corresponding to prompt events originated by direct capture and the exponential shape resulting from muon transfer.

Figure 4.17 shows time distributions of events with energies between 1.5 and 9 keV produced in the photodiode L1 for two mixtures of H_2 and CH_4. The distributions include X-ray pulses and electron background. Muon lifetimes of 1.23 and 1.27 μs were obtained for CH_4 concentrations of 4 and 16%, respectively. These values are of the same order as the values obtained for the previous gases (helium and hydrogen) since the majority of events corresponds to electron pulses.

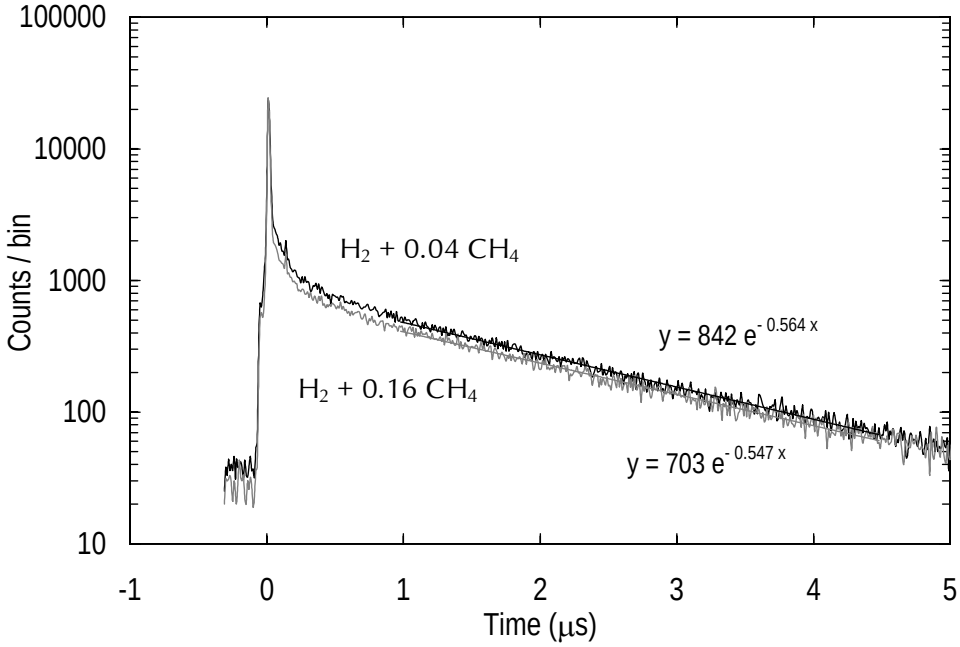

Figure 4.17 – Time spectra of events with energies between 1.5 and 9 keV, obtained in the photodiode L1, for two mixtures of H_2 and CH_4 with CH_4 concentrations of 4 and 16%.

The time distribution of pulses with energies between 1.5 and 9 keV in coincidence with electrons resulting from muon decay was measured for the two mixtures, as shown in Figure 4.18. For times above 250 ns, the number of events registered is higher for the mixture with 4% of CH_4. For a higher CH_4 concentration in the mixture the muon transfer process is more frequent and as a result the lifetime of μp (1S) atoms is shorter. Thus, the events of interest occur predominantly at shorter times and the ratio between the number of delayed and prompt events is lower.

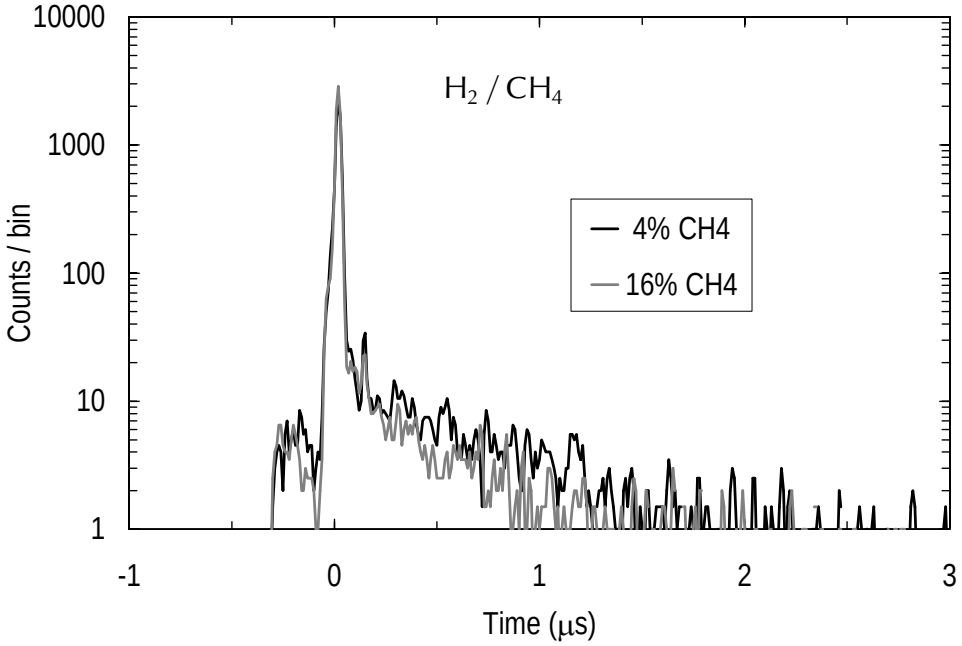

Figure 4.18 – Time spectra of pulses with energies between 1.5 and 9 keV, in coincidence with electrons resulting from muon decay, for mixtures of H_2 and CH_4 (4 and 16%).

4.3.3. Energy response

In the analysis of the energy response of LAAPDs, the use of the small HPGe detector is important since it provides a comparison to the LAAPD for X-ray detection. Both detect low energy X-rays but, while the HPGe detects X-rays with energies above 3 keV, the LAAPD is more efficient for low energy X-rays. To compare the performance of both detectors, a signal-to-noise ratio sufficiently large is necessary. Helium has been chosen as the first gas in the target since X-rays from the K-line of muonic helium atoms present energies high enough (8-10 keV) to be distinguished from the noise.

A comparison between LAAPDs and the HPGe detector can be made using the signal produced by 8.2 keV X-rays (K_α line). The counting rate expected in each case depends on the solid angle for each detector and on the respective efficiency. For 8.2 keV X-rays, the LAAPD efficiency is about 30%, being 100% for the HPGe detector. However, the solid angle is considerably bigger for the LAAPD due to its larger active area and higher proximity to the centre of the target. According to the experimental

system geometry, the fraction of solid angle is about 2.5% for the LAAPD and 0.06% for the HPGe detector. Consequently, the fraction of 8.2 keV X-rays that reaches the detectors is about 10 times higher for the LAAPD. This confirms the peaks obtained in the LAAPD by comparison to the HPGe detector.

Table 4.1 presents the main transitions in the different muonic atoms (μp, μHe, μC) obtained and the energy of the corresponding X-rays emitted.

Table 4.1 – Main transitions in different muonic atoms (μp, μHe, μC) and energy of the corresponding X-rays emitted.

Muonic hydrogen (μp)		Muonic helium (μHe)		Muonic carbon (μC)	
Line	Energy (keV)	Line	Energy (keV)	Line	Energy (keV)
K_α	1.9	L_α	1.52	N_α	2.26
K_β	2.25	L_β	2.05	N_β	3.48
K_γ	2.37	L_γ	2.29	N_γ	4.22
		L_δ	2.43	N_δ	4.70
		K_α	8.23	M_α	4.88
		K_β	9.74	M_β	7.14
		K_γ	10.28	M_γ	8.36
		K_δ	10.48		

Helium and hydrogen

The identification of X-ray peaks in the energy spectra is not possible if all events are considered, without any discrimination, due to the high electron background. This background can be reduced by considering only prompt events. Furthermore, the selection of events in coincidence with the electrons resulting from muon decay results in a more effective background reduction, as observed in the energy distributions of the

events produced in the LAAPDs by muon interactions in helium and hydrogen targets [Fernandes *et al.* 2003B]. For helium, the X-ray peaks corresponding to the K and L lines of μHe atoms are not distinguished from the background and the electronic noise in the total distribution, the L-line is reasonably discriminated considering only prompt events, while the selection of events in coincidence with the electrons provides the identification of the K_α and K_β peaks. For hydrogen, the background reduction is also significant in the distributions of prompt events and the events in coincidence with electrons resulting from muon decay (Figure 4 in the paper, page 180).

The discrimination efficiency for events of interest is significant using the coincidence with the electrons resulting from muon decay, what leads to a substantial background reduction. In these conditions, the counting rate is nevertheless reduced to about 25%.

Only distributions of pulses obtained in the photodiode L1 were presented [Fernandes *et al.* 2003B]. The noise discrimination level is higher for L2, causing a partial loss of low energy X-ray pulses. For this reason, X-ray peaks corresponding to the L-line of μHe atoms are different in the two LAAPDs. The same happens to the K-line of μp atoms, which is very different in the two LAAPDs.

For helium, the L-lines (L_α and L_β) in the distribution of events in electron coincidence were fitted to two Gaussians. The proximity between the L_α line (1.5 keV) and the noise level provides a deficient discrimination of that line, while the energy resolution obtained for the L_β line (2 keV) was 30%.

For hydrogen, the fit of two Gaussians in the region corresponding to the K-line of μp atoms determines an energy resolution of 33% for 1.9 keV X-rays. The obtained energy resolution is higher than the one required for the muonic hydrogen Lamb shift experiment. The resolution may be improved by cooling the photodiodes down to temperatures below 0 ºC [Fernandes *et al.* 2004A,C]. The cooling originates a reduction of the noise level due to the significant reduction of the dark current, leading to a better separation between the signal and the noise. In this way, the noise discrimination level can be reduced, avoiding loss of events of interest.

Mixtures of H_2 and CH_4

The energy spectra obtained for mixtures of H_2 and CH_4 were also registered for CH_4 concentrations of 4 and 16% [Fernandes *et al.* 2003B]. In the resulting distributions, the effect of time discrimination of the events is relevant, although the identification of some peaks is not obvious since the energies of the involved X-rays (emitted by μp and μC atoms) are very close (Table 4.1).

For the distribution of prompt events and events with electron coincidence, the number of X-rays emitted by μC atoms increases with the CH_4 concentration, while the K-line yield for μp atoms decreases slightly. Since the prompt events result from direct muon capture by hydrogen and carbon atoms, the results are in accordance with the relative concentration of those atoms in the mixture.

As stated before, μC atoms produced by muon transfer produce delayed events and the ratio between the number of delayed and prompt events is lower for a higher CH_4 concentration in the mixture, as observed by analysing the time spectra. The number of X-rays emitted by delayed μC atoms can be determined from time discrimination. In Figure 4.19 the energy distribution of delayed events in coincidence with electrons resulting from muon decay is presented for CH_4 concentrations of 4 and 16%. As observed, the number of X-rays from the M and N lines of muonic carbon is higher for a 4% fraction of CH_4, what is in accordance with the results of the time analysis. Therefore, the simultaneous analysis of time and energy spectra leads to the discrimination of events resulting from muon stops in the target in order to select the events of interest.

The energy distribution of the electrons that reach the LAAPDs extends by the whole region of interest of low energy X-rays emitted by muonic atoms. It was demonstrated that the background reduction techniques, based on time discrimination, are very efficient. In particular, the selection of events in delayed coincidence with electrons resulting from muon decay provides a substantial background reduction. However, the technique leads to significant reduction of the acquisition rate, a drawback for low counting rate experiments, such as the muonic hydrogen Lamb shift experiment.

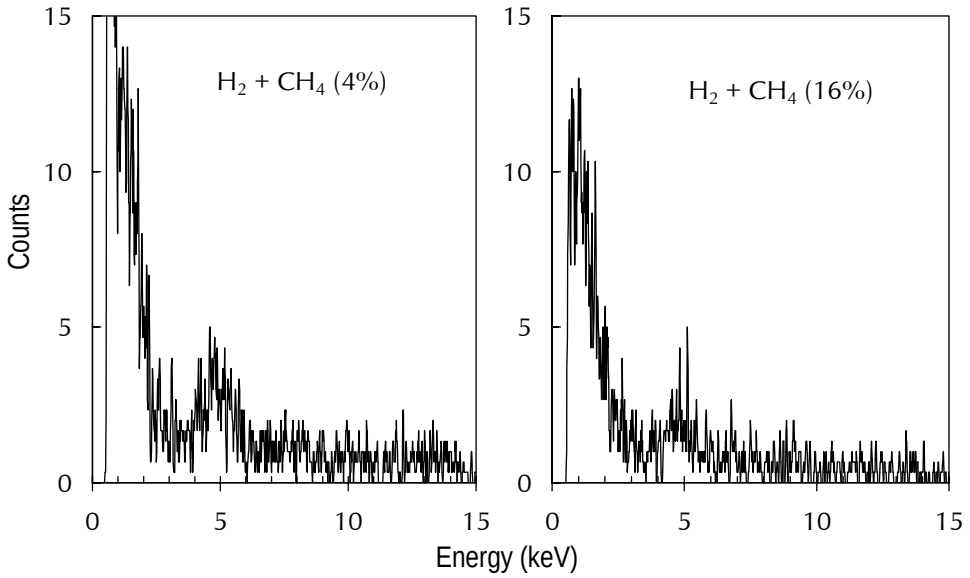

Figure 4.19 – Energy spectra of delayed pulses in coincidence with electrons resulting from muon decay, obtained in the photodiode L1, for H_2 and CH_4 mixtures with CH_4 concentrations of 4 and 16%.

4.4. Implementation of the experiment

Two phases of the muonic hydrogen Lamb shift experiment have already been carried out, using different types of avalanche photodiodes as X-ray detectors. The several parts of the complex experimental system have been kept working during each phase. Figure 4.20 shows a photograph of the experimental system used. The working principle of each part of the system has been described in section 4.1.

4.4.1. Phase I (2002)

The first phase of the experiment was carried out in 2002. The target was filled with hydrogen under a pressure of 1.4 mbar, the optimum value for the laser resonance experiment. The lifetime of μp (2S) atoms is about 850 ns for 1.4 mbar [Kottmann *et al.*

2003]. Therefore the laser has to be triggered approximately 1 μs after the muon entrance in the target. The muon beam line (Figure 4.20) has been optimized and about 120 muons per second have been obtained in time of flight coincidence of the two transmission detectors based on stacks of carbon foils.

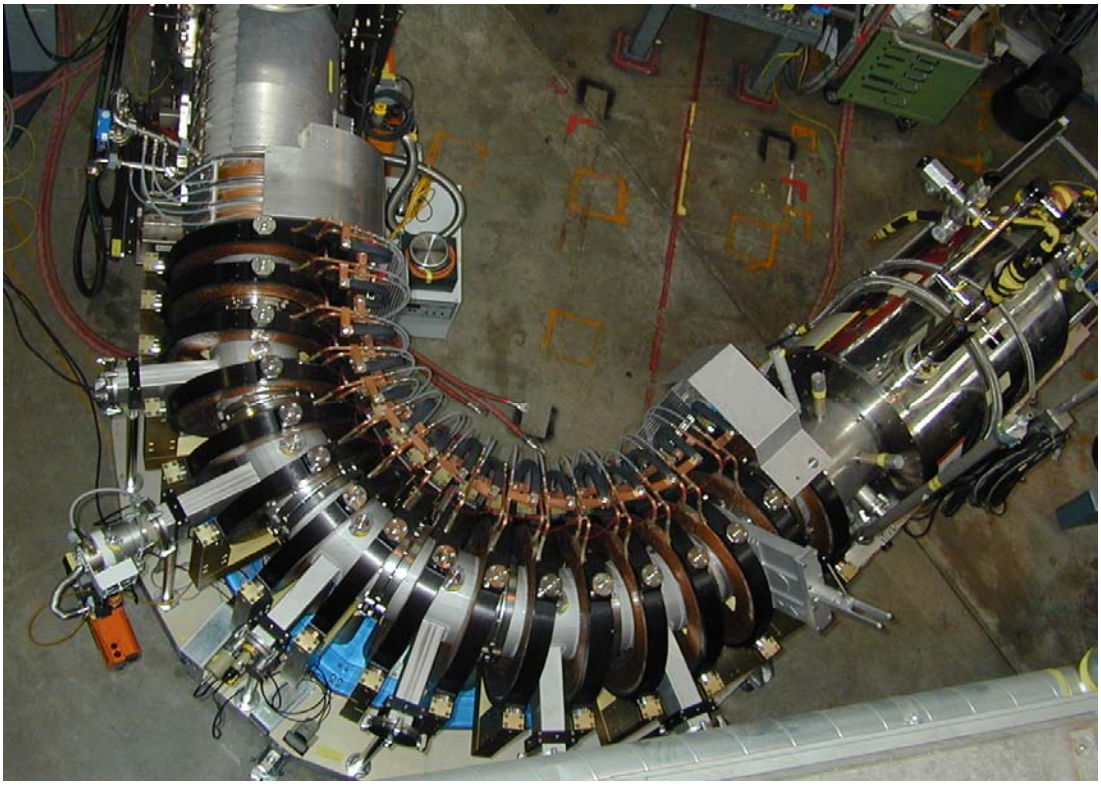

Figure 4.20 – Photograph of the experimental system placed in the πE5 area of PSI, showing the muon beam line and the solenoid where the detection system has been installed.

The gas target presents several windows: 30 nm thick Formvar foils for the muon entrance, polypropylene foils with 1.5 μm thickness and 18 mm diameter for the X-ray detectors, and a CaF_2 window for the laser beam entrance. Figure 4.21 shows a photograph of the structure holding the target, showing a series of photodiodes and the mirrors of the optical cavity. Two series of 6 photodiodes were placed on top and bottom of the target, at a vertical distance of only 8 mm relative to the centre of the muon beam, while the mirrors of the optical cavity for the laser were placed sideways. The mirrors, with 19 cm length and 1.2 cm height, have very high reflectivity (99.97% for $\lambda = 6$ μm). LAAPDs from API, with 16 mm diameter, were used as X-ray detectors.

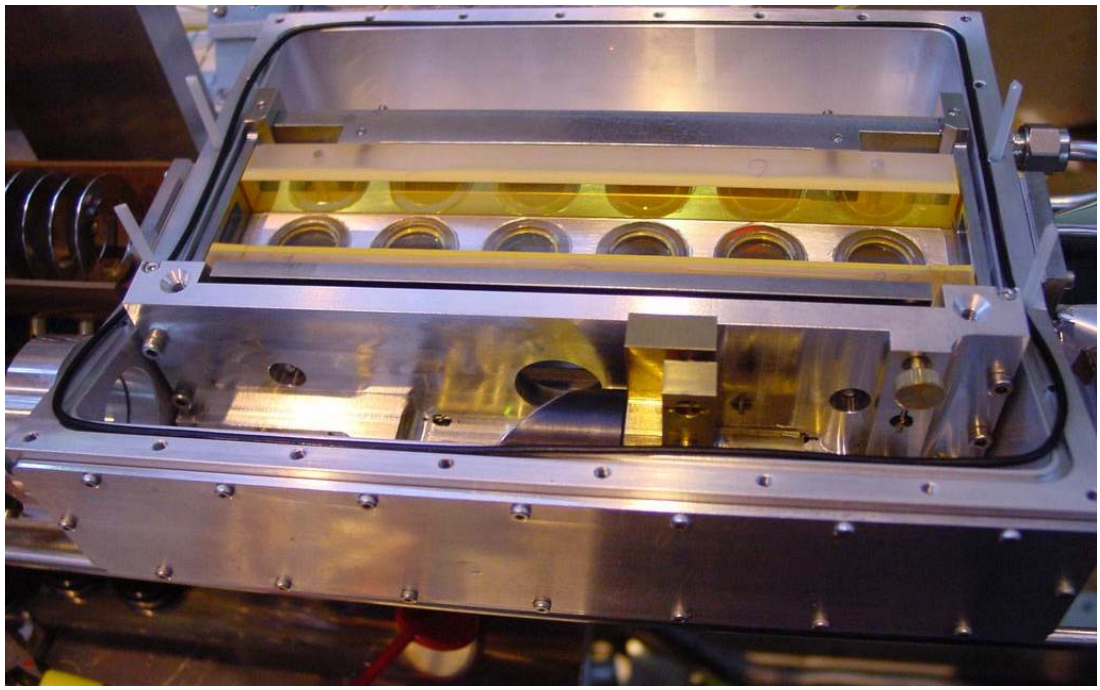

Figure 4.21 – Photograph of the structure holding the target, showing a series of photodiodes underneath the target and the mirrors of the optical cavity sideways.

Several plastic scintillators were placed around the target in order to detect the electrons resulting from muon decay. Figure 4.22 shows a photograph of a section view of the solenoid where the detection system was installed, showing the target (in the centre), the preamplifiers for LAAPDs (on top and bottom of the target), the cooling system for LAAPDs and the plastic scintillators.

The 12 LAAPDs have been cooled down to -10 ºC in order to improve the energy resolution for 1.9 keV X-rays and the signal-to-noise ratio [Fernandes *et al.* 2004A]. Figure 4.23 presents the sum of the energy spectra obtained for all LAAPDs. Three different distributions are represented. The distribution of all detected pulses ("total") presents a high background due to the electrons resulting from muon decay. The distribution of prompt events, which take place in the time interval from -0.2 to 0.4 μs relative to the muon entrance, leads to a reduction of the electron background. However, the background is practically eliminated considering only events in delayed coincidence with electrons resulting from muon decay (detected by the plastic scintillators). In the

distribution of events with electron coincidence, practically only the K-lines of muonic hydrogen X-rays are visible.

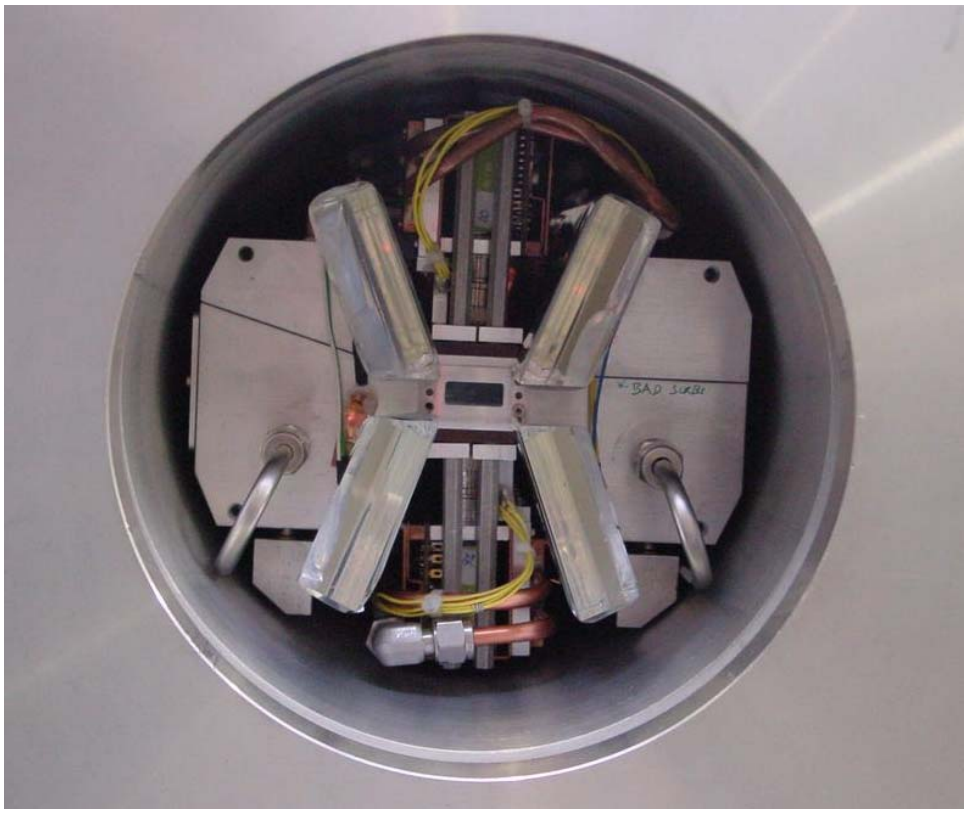

Figure 4.22 – Photograph of the detection system installed inside the solenoid, showing the target, the preamplifiers for LAAPDs and the plastic scintillators.

The discrimination techniques described have been used before (section 4.3). The acquisition efficiency for the electron coincidence discrimination is now considerably higher since the solid angle subtended by the scintillators is larger.

The energy resolution obtained for 1.9 keV X-rays, averaged for all 12 LAAPDs, was 25%. The time spectrum of events with energies between 1.5 and 2.8 keV is shown in Figure 4.24. Two different distributions are presented: all pulses with energies in the range 1.5-2.8 keV ("total") and the pulses in coincidence with electrons resulting from muon decay.

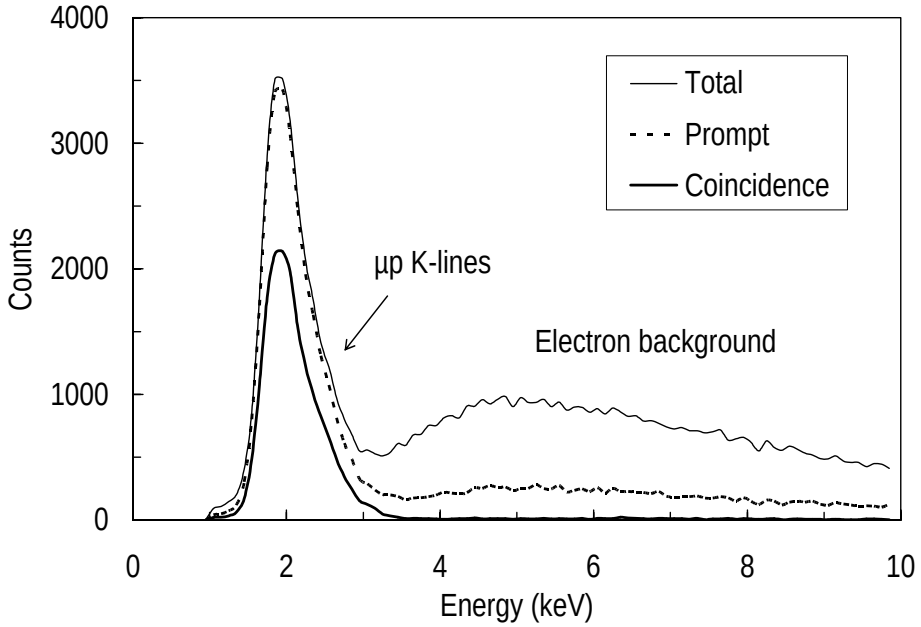

Figure 4.23 – Energy distributions of the pulses obtained in 12 LAAPDs used in the experiment. Different distributions are represented: all detected events (total), prompt events and events in delayed coincidence with the electrons resulting from muon decay.

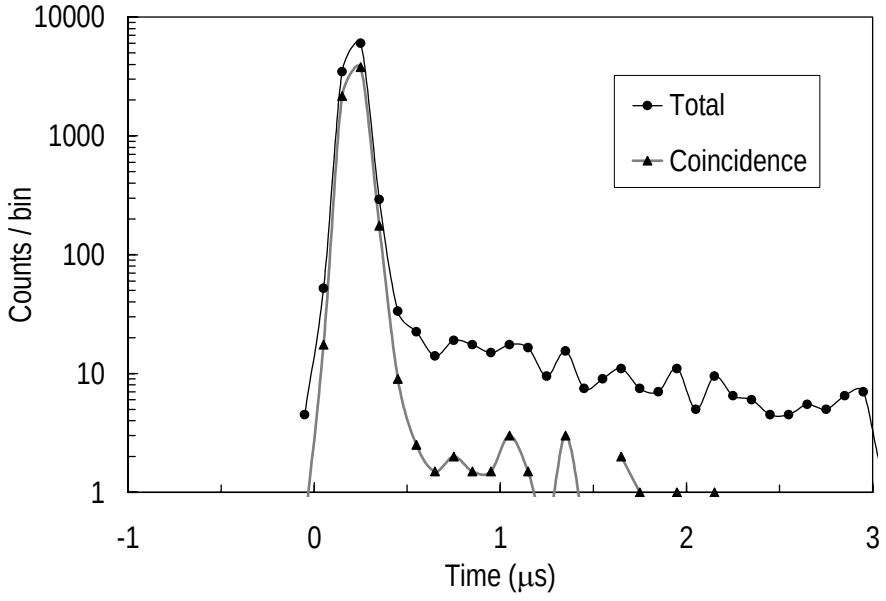

Figure 4.24 – Time spectra of the pulses obtained in all 12 LAAPDs, with energies between 1.5 and 2.8 keV. The distribution of the events in coincidence with electrons resulting from muon decay is also presented (bin = 100 ns).

Towards the end of the data acquisition time, the laser worked correctly with pulses of 0.3 mJ energy and a delay time of about 1.4 μs relative to the muon entrance in the target. In the time distribution of events with electron coincidence (Figure 4.24), there are only 1-2 events per hour (associated with the background) in the interval 1.3-1.5 μs, the time interval where the laser-induced signals will take place. Since the counting rate expected for the events in coincidence with the laser is 3-4 per hour and the time available for the acquisition is short, the laser resonance curve was not obtained.

4.4.2. Phase II (2003)

A second phase of the experiment was carried out in 2003. The essential parts of the experimental system (muon beam, X-ray detectors and laser system) have been improved relative to the 2002 assay. About 300 muons per second, with kinetic energies between 3 and 6 keV, were detected in time of flight coincidence by both transmission detectors and in anti-coincidence with the D_3 scintillator (Figure 4.5).

The target where the muons interact is 20 cm long and was filled with hydrogen under a pressure of 0.6 mbar. The muons that cross the target without interacting are efficiently detected by a LYSO (Lutetium Yttrium Orthosilicate) scintillator connected to a gold layer. The lifetime of μp (2S) atoms is 1.3 ± 0.2 μs for 0.6 mbar [Pohl *et al.* 2001B]. The gas pressure and the resulting 2S-lifetime are reasonably adjusted to the 1.4 μs delay of the laser pulse. The basic difference in the laser system, in comparison to the 2002 assay, was the use of two excimers in the first stage of the laser system.

For the LAAPDs used in 2002 the ratio between the sensitive area and the physical area required for each LAAPD is relatively small, limiting the solid angle useful for the detection of 1.9 keV X-rays. The development of a planar process on the manufacture of photodiodes (by RMD) provided the production of squared photodiodes delimited by a thin edge of inactive material [Farrell *et al.* 2000]. In this way, the arrangement of a detector with a significantly larger area has been possible. The LAAPDs now used, manufactured by RMD, present squared areas of 14×14 mm^2. The X-ray detector is arranged in two series of 10 LAAPDs placed on top and bottom of the target. Figure

4.25 shows the central part of a series of photodiodes. The detector thus formed provides an average solid angle of 30% throughout the whole volume for muon stops.

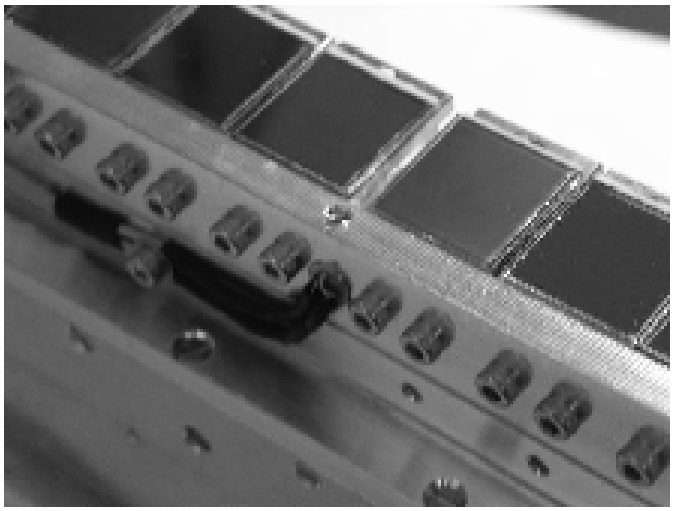

Figure 4.25 – Photograph of the central part of a series of photodiodes composing the X-ray detector. The preamplifiers are positioned behind the surface of each LAAPD.

LAAPDs manufactured by RMD present dark currents relatively high at room temperature (2 μA), hindering their use as low energy X-ray detectors. These LAAPDs were therefore mounted in aluminium plates with a stabilized temperature of -30 ºC. Thus, the dark current is reduced to about 30 nA and its contribution to the energy resolution is small. The performance of the LAAPDs from RMD was described in Chapter 3 as a function of temperature by comparison with the LAAPDs from API.

The detection system has been used inside the solenoid for three weeks, operating under a 5 T magnetic field without problems, and about 2×10^7 laser pulses have been triggered. The laser has been operated at 15 different wavelengths, corresponding to a range of $\pm 3\sigma$ on the uncertainty of the proton radius. The counting rate expected for the events in laser resonance is about 2 per hour, while the background rate is lower than 1 per hour. A careful analysis of the results is still going on, including 10^6 K-line transitions in muonic hydrogen. So far, a valid resonance curve was not obtained. With non conclusive results, a new phase of the experiment is foreseen for 2006 or 2007.

Available online at www.sciencedirect.com
SCIENCE DIRECT®
Nuclear Instruments and Methods in Physics Research A 498 (2003) 362–368
NUCLEAR INSTRUMENTS & METHODS IN PHYSICS RESEARCH Section A
www.elsevier.com/locate/nima

Behaviour of large-area avalanche photodiodes under intense magnetic fields for VUV- visible- and X-ray photon detection

L.M.P. Fernandes[a], A. Antognini[b], M. Boucher[c], C.A.N. Conde[a], O. Huot[c], P. Knowles[c], F. Kottmann[d], L. Ludhova[c], F. Mulhauser[c], R. Pohl[b,e], L.A. Schaller[c], J.M.F. dos Santos[a,*], D. Taqqu[e], J.F.C.A. Veloso[a]

[a] *Departamento de Física da Universidade de Coimbra, 3004-516 Coimbra, Portugal*
[b] *MaX-Planck-Institut für Quantenoptik, DE-85748 Garching, Germany*
[c] *Departement de Physique de l'Université, CH-1700 Fribourg, Switzerland*
[d] *Institut für Teilchenphysik, ETHZ, CH-8093 Zürich, Switzerland*
[e] *Paul Scherrer Institut, CH-5232 Villigen-PSI, Switzerland*

Received 19 April 2002; received in revised form 29 October 2002; accepted 18 November 2002

Abstract

The behaviour of large-area avalanche photodiodes for X-rays, visible and vacuum-ultra-violet (VUV) light detection in magnetic fields up to 5 T is described. For X-rays and visible light detection, the photodiode pulse amplitude and energy resolution were unaffected from 0 to 5 T, demonstrating the insensitivity of this type of detector to strong magnetic fields. For VUV light detection, however, the photodiode relative pulse amplitude decreases with increasing magnetic field intensity reaching a reduction of about 24% at 5 T, and the energy resolution degrades noticeably with increasing magnetic field.

PACS: 07.85.F; 29.40.M; 85.60.D

Keywords: Photon detectors; X-ray detection; Avalanche photodiodes; Magnetic field

1. Introduction

Recent advances on the development of large-area avalanche photodiodes (LAAPDs) with higher gains and improved spatial uniformity have prompted intensive studies of their characteristics for scintillation detection. LAAPDs have been mostly used as optical photodetectors coupled to inorganic scintillators for X- and γ-ray detection, substituting for photomultiplier tubes. Applications include instrumentation for nuclear physics [1, 2], high–energy physics [3, 4] and medicine [5, 6]. Additionally, these devices are fairly good X-ray spectrometers [7, 8] presenting energy resolutions similar to those of proportional counters [8].

More recently, windowless LAAPDs with sensitivity extended to the vacuum-ultra-violet (VUV) region became commercially available and their

*Corresponding author. Tel.: + +351-239410667; fax: +351-239829158..
E-mail address: jmf@gian.fis.uc.pt (J.M.F. dos Santos).

0168-9002/03/$ - see front matter
doi:10.1016/S0168-9002(02)02081-8

application as VUV photonsensors for the scintillation light from noble gases and liquids in positron-emission tomography, X- and γ-ray spectroscopy is under investigation [9–11].

The use of LAAPDs in an experiment to measure the Lamb-shift of the 2S–2P atomic states in muonic hydrogen (μp) is being considered [12]. The experiment, to be carried out at the Paul Scherrer Institute (PSI), Switzerland, in collaboration with nine institutions, consists in obtaining long-lived μp atoms in the 2S-metastable state by stopping a low energy μ^- beam in a small volume of low-pressure hydrogen in a 5 T magnetic field. A pulsed beam from a tuneable laser induces the 2S–2P transition in μp and the 1.9-keV X-ray photons resulting from the 2P–1S de-excitation will be detected. Measuring the coincidences between the laser pulse and the 1.9-keV X-rays as a function of the laser wavelength, the Lamb shift can be determined. Low counting rates are expected and the 1.9-keV X-ray background will be reduced by gating its coincidence with the signal resulting from the high-energy electron produced by the subsequent muon decay. The X-ray detector should be compact and insensitive to a 5 T magnetic field.

The LAAPD can be used in two detector configurations: as the VUV photosensor of a xenon gas proportional scintillation counter (GPSC) [13] or as a direct X-ray detector [8]. The superior signal-to-noise ratio, large-area capability and energy resolution of a GPSC are advantages. However, the compactness and windowless design, the simple operation and the use of much lower biasing high-voltage, for the LAAPD operation as a direct X-ray detector configuration, present important advantages in this application. In both cases, the LAAPD needs to be operated under intense magnetic fields, up to 5 T.

The very small effect of magnetic field on the operation of the avalanche photodiodes has often been referred to in the literature [3, 4, 14]. However, detailed experimental results on this issue are scarce. Also, the experimental results available from manufacturers have not been published, to the best of our knowledge. Additionally, most of the studies with LAAPDs were carried out for visible light leaving aside the VUV and X-ray range. It has been proved that some LAAPD characteristics are different for visible- and VUV-light detection [15, 16].

In this work we present an experimental study on the behaviour of LAAPDs under magnetic fields up to 5 T for X-ray, VUV- and visible-light detection. LAAPDs were used to detect directly 5.4-keV X-rays, to read the scintillation light of a xenon GPSC and the scintillation light of a CsI (Tl) scintillation crystal. Detectors mean pulse amplitudes and energy resolutions were monitored as a function of the magnetic field. The experiment was performed in a cryogenic superconducting solenoid at PSI [17].

2. Experimental set-up

Avalanche photodiodes are compact, monolithic devices made of a silicon p–n junction where the internal electric field can reach values high enough to allow electron multiplication by impact ionisation [14, 18, 19]. When a high voltage is applied to the photodiode only a small region of the p-layer in the front part of the diode remains undepleted—the drift region (Fig. 1). The electric field in this region is low but in the depleted region increases with the depth, presenting a maximum around the p–n junction. An incident photon, absorbed in the drift region or in the p-depleted layer, produces electron–hole pairs and the resulting electrons are accelerated towards the n+-contact, undergoing avalanche multiplication due to the high electric field around the junction. Charge gains of a few 100 are typical, depending exponentially on the applied voltage.

The different detector configurations used in this work are presented in Fig. 2. In all cases, LAAPDs 16-mm in diameter,[1] biased with 1800 V, were used. For each run, ambient temperature inside the superconducting bore remained at about 20°C within ±1°C and amplitude corrections of 5.4% per °C were carried out [16]. The thickness of the LAAPD drift region is about 10 μm, while the charge-multiplication region begins at a depth of

[1] Advanced Photonix, Inc., 1240 Avenida Acaso, Camarillo, CA 93012, USA.

about 20 μm in the depleted region and has a thickness of about 20 μm [14].

For direct detection of X-rays with LAAPD an X-ray beam from a ^{54}Mn radioactive source was used (Fig. 2a). The X-ray interacts directly in the Si and the resulting primary electrons are amplified by the intense electric field around the junction producing a pulse with amplitude that is, in average, proportional to the X-ray energy.

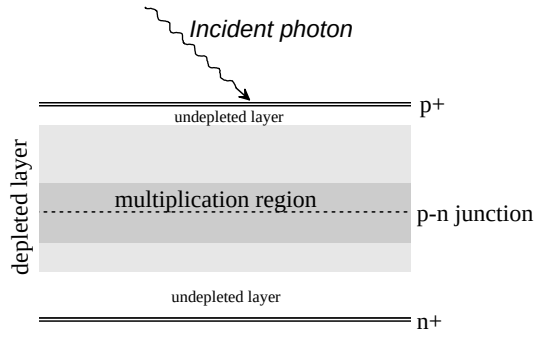

Fig. 1. Schematic diagram of a typical avalanche photodiode section.

For visible-light detection, 835-keV γ-rays emitted from the ^{54}Mn radioactive source were allowed to interact in a $1 \times 1 \times 1$-cm^3 CsI (Tl) scintillation crystal, placed above the LAAPD used to readout the scintillation (wavelength around 520 nm) produced by each γ–ray interaction (Fig. 2b). The pulse amplitude at the LAAPD output is proportional to the amount of detected scintillation and, thus, in average to the γ-ray energy.

For VUV-light detection the LAAPD was placed inside the gas envelope of a driftless GPSC [13], which has a 1.1-cm thick scintillation region filled with xenon at 1140 mbar (Fig. 2c). The gas volume is sealed and uses a small getter for gas purification (SAES St 172). The 12.5-μm-thick, 10-mm-diameter aluminised Mylar window is maintained at −6 kV. A Macor ceramic insulates the window holder from the detector body. The LAAPD was positioned just below the anode grid (80-μm-diameter stainless steel wire with 900-μm spacing). The anode grid, the photosensor body, and the detector body were maintained at ground

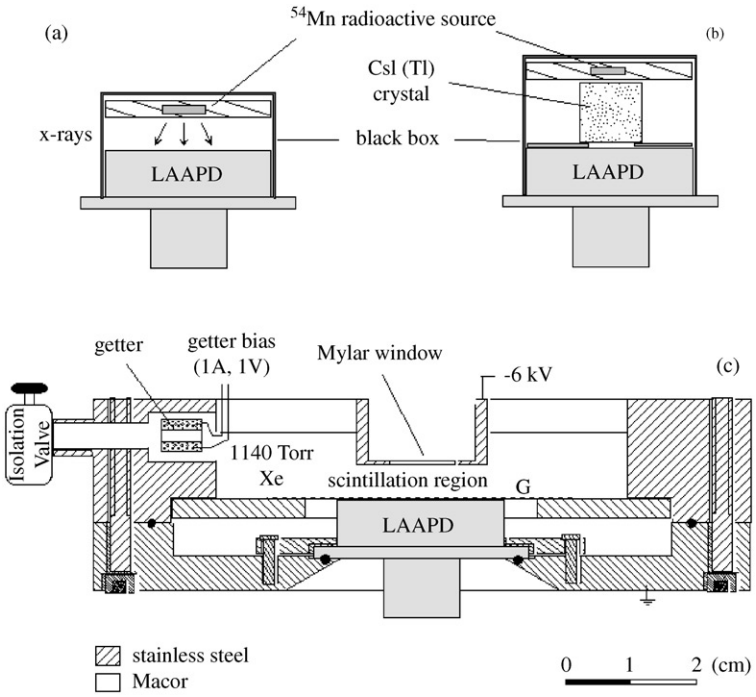

Fig. 2. Different detector set-ups for LAAPD-detection of X-rays (a), visible-light (b) and VUV-light (c).

potential. The Macor, the radiation window and holder and the detector body were vacuum-sealed using a low-vapour pressure epoxy, while the photosensor body was vacuum-sealed to the detector body by compressing an indium gasket. A 2-mm collimated X-ray beam from a ^{55}Fe radioactive source was allowed to interact in the xenon. The electric field inside the detector is sufficiently high for the primary electrons resulting from each X-ray interactions to excite but not ionise the gas atoms along their path towards the anode grid. In the de-excitation processes VUV scintillation photons (wavelength around 172 nm) are emitted and the average amount of scintillation light detected by the LAAPD is proportional to the X-ray energy.

The detectors were installed in a black box to shield from the ambient light. The LAAPD signals were fed through a low-noise charge preamplifier (Canberra 2004, with a sensitivity of 45 mV/MeV) to a spectroscopy amplifier and were pulse-height analysed by a multi-channel analyser. Shaping time-constants of 0.2, 1 and 2 μs were used in the main amplifier for X-ray, visible and VUV detection, respectively: 0.2 μs is optimum for X-ray pulses in the LAAPD; 1 μs corresponds to the time characteristic of the CsI(Tl) scintillation; 2 μs corresponds to the electron drift time in the xenon gas. For pulse-amplitude and energy resolution measurements the pulse-height distributions are fitted to a Gaussian function superimposed on a linear background, from which the centroid and the full-width at half-maximum (FWHM) are determined.

Each detector system was placed in a 1-m-long and 20-cm-bore-diameter superconducting solenoid capable of achieving magnetic fields up to 5 T, uniform (10^{-4}) over an axial distance of 30 cm from the centre. The amount of scintillation light collected in the LAAPD was kept constant during the experiment for both visible and VUV cases. Detector pulse amplitude and energy resolution were monitored as a function of the magnetic field, varying the magnetic field intensity inside the solenoid in 1 T steps up to 5 T. The detector orientation inside the solenoid was chosen such that the LAAPD axis was perpendicular to the magnetic field direction, the most unfavourable orientation, Fig. 3.

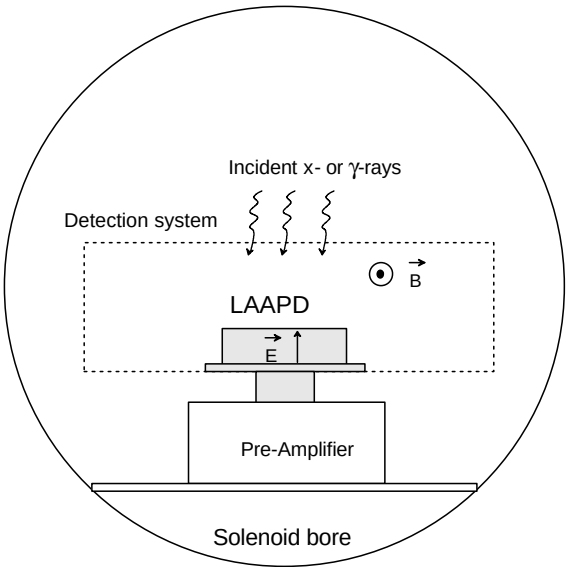

Fig. 3. Schematic of the detector/LAAPD orientation relative to the electric and magnetic fields in the experimental set-up.

3. Experimental results and discussion

In Fig. 4 we present pulse-height distributions obtained for each case, and for magnetic fields of 0 and 5 T. For the X-ray detection cases (Figs. 4a and 4c), spectral features include the Cr or the Mn K-lines, the respective escape peaks and the tail due to the electronic noise in the low-energy limit. For the γ-ray detection (Fig. 4b) the pulse-height distribution depicts the peak corresponding to the full-energy absorption, the Compton continuum and the electronic noise tail. As shown in Fig. 4, there is no significant degradation of the obtained pulse-height distributions with the magnetic field intensity for the cases of X-rays and visible light detection with the LAAPD. On the other hand, for the VUV-scintillation detection, pulse amplitude reduction above 20% can be observed. In all cases, the electronic noise tail in the low-energy limit did not change with the magnetic field.

Figs. 5a and b present the detector relative pulse amplitude and energy resolution, respectively, as a function of the magnetic field intensity for the three different cases. For X-ray and visible-light detection with the LAAPD, amplitude variations are less than 1.5%, being within the experimental

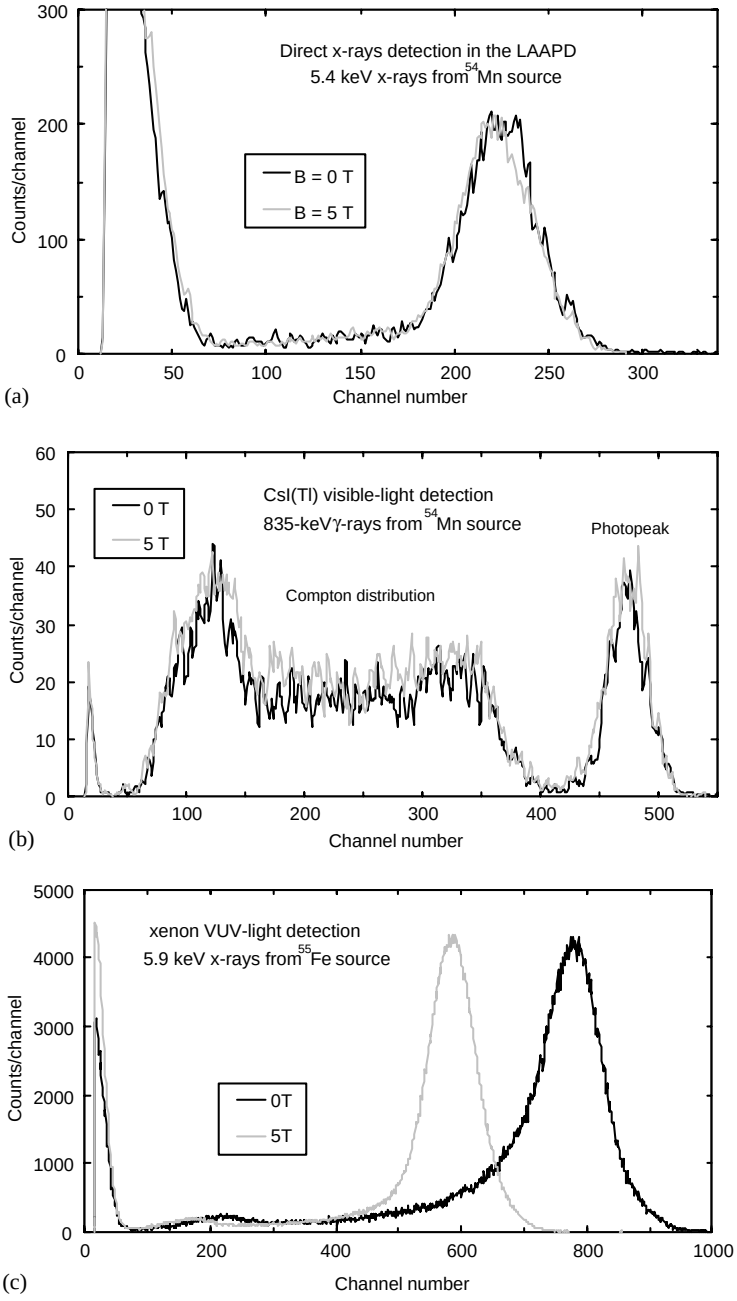

Fig. 4. Pulse-height distributions obtained with the different detector set-ups. (a) direct Cr $K_{\alpha,\beta}$ X-ray detection in the LAAPD, (b) 835-keV γ-rays interacting in a CsI(Tl) crystal and (c) Mn $K_{\alpha,\beta}$ X-rays interacting in a Xe-GPSC, using the LAAPD for the visible- and VUV-scintillation detection, respectively.

error. Also, no significant variations of the energy resolution are observed for these two cases. For the VUV-light detection with the LAAPD significant variations are noticeable: the relative pulse amplitude decreases gradually with increasing magnetic field intensity reaching a reduction of

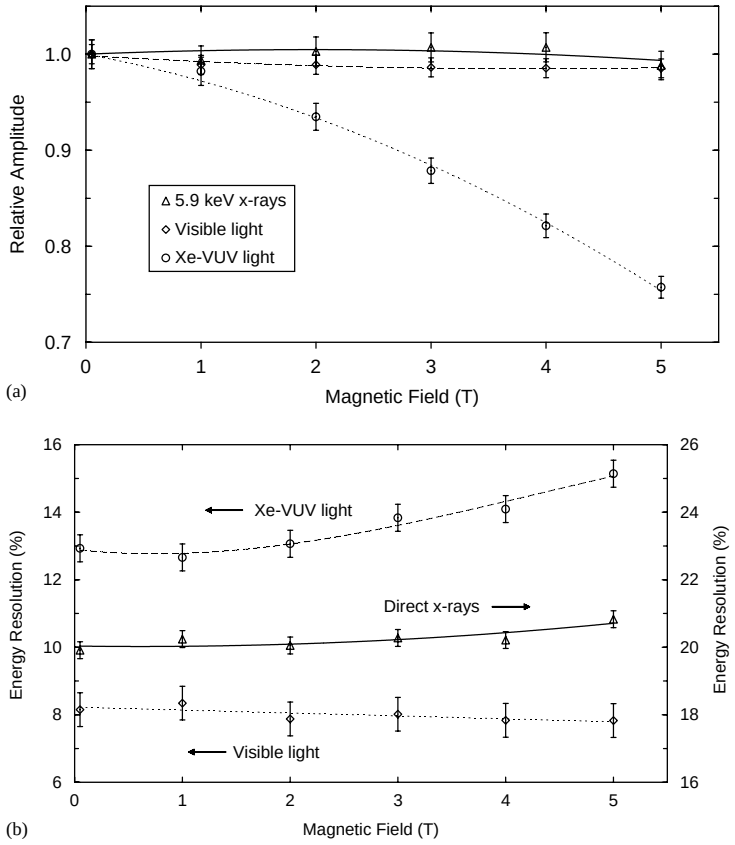

Fig. 5. Relative pulse amplitude (a) and energy resolution (b) for the different detector systems as a function of the magnetic field intensity: direct 5.4-keV X-ray interactions in the LAAPD; visible-light interactions in the LAAPD, resulting from 835 γ-ray interactions in CsI(Tl) and VUV-light interactions in the LAAPD, resulting from 5.9–keV X-ray interactions in a xenon-GPSC.

24% at 5 T, while the detector energy resolution degrades from 12.9% to 15.1% as the magnetic field increases from 0 to 5 T.

The effect of the magnetic field on the GPSC scintillation is negligible [20,21]: since the X-ray beam is well collimated and aligned with the axis, possible variations in the solid angle subtended by the LAAPD relative to the region where the scintillation takes place, due to Lorentz angle effect [20], are negligible. Thus, the noticeable influence of the magnetic field has its origin in the VUV-light detection in the LAAPD. Although the dependence of the avalanche photodiode amplitude and the respective statistical fluctuations on the magnetic field is not significant for X-ray and visible-light detection, it becomes important for VUV-detection. Since VUV photons interact within the first atomic layers, the effect of the magnetic field on the photoelectrons and subsequent secondary electrons diffusion may be responsible for increased charge carrier losses to the front electrode with increasing magnetic field. Penetration depths in Si are about 5 nm and 1 μm for 172- and 520-nm photons [22], respectively, and 22 μm for 5.4-keV X-rays [23].

Presently, the LAAPD manufacturing technology is well established and quite good reproducibility is obtained. Thus, it is expected that the observed behaviour for individual LAAPDs are representative for any of these devices [24,25]. The response to VUV could be improved if the electric field intensity in the drift region would be

increased. However, this cannot yet be achieved due to the increase of discharge probability at the surface [25].

4. Conclusions

We have shown that large-area avalanche photodiodes can operate in strong magnetic fields up to 5 T with negligible performance degradation when used for X-ray or visible-light detection. However, for VUV-light detection a noticeable degradation in the avalanche photodiode pulse-amplitude and in the respective statistical fluctuations is observed. The relative pulse amplitude decreases with increasing magnetic field intensity, reaching a reduction of 24% at 5 T.

Acknowledgements

Support is acknowledged to Fundação para a Ciência e a Tecnologia (FCT) through Projects POCTI/FIS/13140/98 and CERN/FIS/43785/01, and to Swiss National Science Foundation. J.F.C.A. Veloso acknowledges support grant from FCT.

References

[1] E. Lorentz, S. Natkaniec, D. Renker, B. Schwartz, Nucl. Instr. and Meth. A 344 (1994) 64.
[2] R. Farrel, F. Olschner, K. Shah, M.R. Squillante, Nucl. Instr. and Meth. A 387 (1997) 194.
[3] A. Karar, Y. Musienko, J.C. Vanal, Nucl. Instr. and Meth. A 428 (1999) 413.
[4] K. Deiters, Y. Musienko, S. Nicol, B. Patel, D. Renker, S. Reucroft, R. Rusack, T. Sakhelashvili, J. Swain, P. Vikas, Nucl. Instr. and Meth. A 442 (2000) 193.
[5] B. Pichler, G. Böning, E. Lorenz, R. Mirzoyan, W. Pimpl, M. Schwaiger, S.I. Ziegler, IEEE Trans. Nucl. Sci. NS-45 (1998) 1298.
[6] A. Ruru Chen, A. Fremout, S. Tavernier, P. Bruyndonckx, D. Clément, J.-F. Loude, C. Morel, Nucl. Instr. and Meth. A 433 (1999) 637.
[7] A. Ochi, Y. Nishi, T. Tanimori, Nucl. Instr. and Meth. A 378 (1996) 267.
[8] L.M.P. Fernandes, J.A.M. Lopes, J.M.F. dos Santos, C.A.N. Conde, X-ray Spectrom. 30 (2001) 164.
[9] J.A.M. Lopes, J.M.F. dos Santos, R.E. Morgado, C.A.N. Conde, IEEE Trans. Nucl. Sci. NS-48 (2001) 312.
[10] C.M.B. Monteiro, J.A.M. Lopes, J.M.F. dos Santos, C.A.N. Conde, IEEE Trans Nucl. Sci. NS-48 (2001) 1081.
[11] V.N. Solovov, A. Hitachi, V. Chepel, M.I. Lopes, R. Ferreira Marques, A.J.P.L. Policarpo, Nucl. Instr. Meth. A 488 (2002) 572.
[12] F. Kottmann, et al. (24 authors), Hyp. Interact. 138 (2001) 55.
[13] J.F.C.A. Veloso, J.A.M. Lopes, C.A.N. Conde, L.M.P. Fernandes, E.D.C. Freitas, O. Huot, P. Knowles, F. Kottmann, F. Mulhauser, J.M.F. dos Santos, D. Taqqu, IEEE Trans. Nucl. Sci. 49 (2002) 899.
[14] A.Q.R. Baron, S.L. Ruby, Nucl. Instr. Meth. A 343 (1994) 517.
[15] L.M.P. Fernandes, J.A.M. Lopes, C.M.B. Monteiro, J.M.F. dos Santos, R.E. Morgado, Nucl. Instr. Meth. A 478 (2002) 395.
[16] J.A.M. Lopes, L.M.P. Fernandes, J.M.F. dos Santos, R.E. Morgado, C.A.N. Conde, VUV detection in large-area avalanche photodiodes as a function of temperature, presented to 3rd Beaune Conference on New Developments in Photondetection, Beaune, France, June 17–21, 2002, Nucl. Instr. and Meth. A. submitted for publication.
[17] D. Taqqu, Nucl. Instr. Meth. A 247 (1986) 288.
[18] E.M. Gullikson, E. Gramsch, M. Szawlowski, Appl. Opt. 34 (1995) 4662.
[19] J.P. Pansart, Nucl. Instr. and Meth. A 387 (1997) 186.
[20] J.F.C.A. Veloso, J.M.F. dos Santos, C.A.N. Conde, F. Mulhauser, P. Knowles, C. Donche-Gay, O. Huot, D. Taqqu, F. Kottmann, Nucl. Instr. and Meth. A 460 (2001) 297.
[21] J.F.C.A. Veloso, C.A.N. Conde, O. Huot, P. Knowles, F. Kottmann, F. Mulhauser, J.M.F. dos Santos, D. Taqqu, Nucl. Instr. Meth. A 489 (2002) 266.
[22] T.W. Barnard, M.I. Crockett, J.C. Ivaldi, P.L. Lundberg, D.A. Yates, P.A. Levine, D.J. Sauer, Anal. Chem. 65 (1993) 1231–1239.
[23] L.S. Birks, J. Criss, Mass photoelectric absorptions coefficients, In: J. W. Robinson (Ed.), Handbook of Spectroscopy, Vol. III, CRC Press, Boca Raton, FL, USA, 1981.
[24] J.A.M. Lopes, Gas proportional scintillation counters: new applications and technologies in integrated photosensors, Ph.D. Thesis, Physics Department, University of Coimbra, Portugal, 2002.
[25] M. Szawlowsky, Advanced Photonix Inc., private communication.

Available online at www.sciencedirect.com
SCIENCE DIRECT®
Spectrochimica Acta Part B 58 (2003) 2255–2260
SPECTROCHIMICA ACTA PART B
www.elsevier.com/locate/sab

Application of large-area avalanche photodiodes to X-ray spectrometry of muonic atoms☆

L.M.P. Fernandes[a], A. Antognini[b], M. Boucher[c], C.A.N. Conde[a], O. Huot[c], P.E. Knowles[c], F. Kottmann[d], L. Ludhova[c], F. Mulhauser[c,*], R. Pohl[b,e], J.M.F. dos Santos[a], L.A. Schaller[c], D. Taqqu[e], J.F.C.A. Veloso[a]

[a]*Departamento de Física da Universidade de Coimbra, 3004-516 Coimbra, Portugal*
[b]*Max-Planck-Institut für Quantenoptik, DE-85748 Garching, Germany*
[c]*Département de Physique de l'Université, CH-1700 Fribourg, Switzerland*
[d]*Institut für Teilchenphysik, ETHZ, CH-8093 Zurich, Switzerland*
[e]*Paul Scherrer Institut, CH-5232 Villigen-PSI, Switzerland*

Received 10 November 2002; accepted 16 May 2003

Abstract

Large-area avalanche photodiodes have been investigated as 1.9-keV X-ray detectors for the muonic hydrogen Lamb-shift experiment. We report experimental tests carried out for evaluation of the avalanche photodiode capabilities for X-ray detection in the intense radiation and low counting rate environment of experiments with muonic atoms. Several muonic atoms were used and it was shown that the electronic background of muonic atom X-ray spectra can be reduced simply by timing the X-ray signal against the gate signal produced by the muon entrance. Furthermore, the background can be eliminated using coincidences between the X-ray signal and the signal resulting from the electron due to the muon decay. This coincidence discrimination results, however, in a reduction of the X-ray detection efficiency.

Keywords: Lamb shift; Muonic atoms X-ray spectrometry; Avalanche photodiodes

1. Introduction

An experiment to measure the energy difference between atomic states 2S−2P (Lamb shift) in muonic hydrogen (μp) is undergoing at the Paul Scherrer Institute (PSI) [1,2]. The experiment consists of obtaining long-lived μp atoms in the 2S metastable state by stopping low energy negative muons (μ^-) in a small volume of low-pressure hydrogen in a 5 T magnetic field. A pulsed beam from a tunable laser ($\sim$6 μm wavelength) induces the 2S−2P transition in μp. Muonic atoms in the 2P state decay immediately to the ground state and 1.9-keV X-rays are emitted (Fig. 1). Since the atomic energy levels of muonic hydrogen are a factor of 186 more energetic than

☆ This paper was presented at the 9th Symposium on Total Reflection X-Ray Fluorescence Analysis and Related Methods, held in Madeira, Portugal, September 2002, and is published in the Special Issue of *Spectrochimica Acta Part B*, dedicated to that conference.

*Corresponding author. Tel.: +41-26-3009060; fax: +41-26-3009747.
E-mail address: francoise.mulhauser@unifr.ch (F. Mulhauser).

0584-8547/03/$ - see front matter © 2003 Elsevier B.V. All rights reserved.
doi:10.1016/S0584-8547(03)00214-3

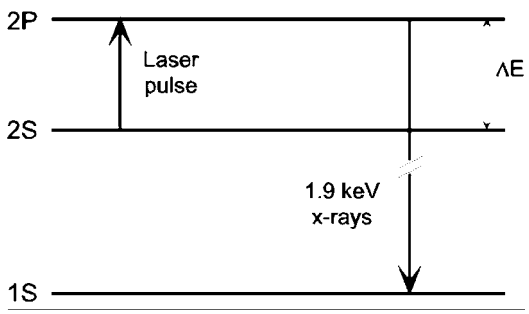

Fig. 1. Muonic hydrogen atomic levels, showing the transitions taking place in the Lamb-shift (ΔE) experiment.

those of normal hydrogen, according to the ratio of reduced masses, the transitions in μp lie in the soft X-ray region.

The 2S–2P energy difference (ΔE) can be determined by measuring, as function of the laser wavelength, the number of coincidences between the laser pulse and the delayed 1.9-keV photon. The contribution of the RMS proton charge radius to the Lamb shift in μp amounts to 2%. Measuring the Lamb shift to a precision of 30 ppm will allow us to deduce the RMS proton charge radius with 0.1% accuracy, 20 times more precise than presently known [3,4].

The X-ray detector should be compact and insensitive to a 5 T magnetic field. To achieve the attended accuracy, we need an energy resolution of approximately 20% for 1.9-keV X-rays. To differentiate between prompt X-rays resulting from the 2P–1S transition of muonic cascade in hydrogen and laser-induced delayed events, a time resolution better than 100 ns is also necessary. Large-area avalanche photodiodes (LAAPDs) are compact, monolithic devices suitable for soft X-ray spectrometry [5] and can operate in magnetic fields up to 5 T with negligible performance degradation [6,7]. They also match the other experimental requirements: they present good time resolution and the energy resolution can be reduced to the desired values because its performance in X-ray detection can be improved by decreasing the operating temperature [8]. Therefore, LAAPDs of 16 mm diameter [9] will be used during the first run, in September/October 2002. Because low counting rates are expected, the LAAPD limited area (200 mm^2) is a drawback. However, a series of 12 LAAPDs will be used in the final experiment.

We report experimental tests carried out for evaluation of the capabilities of LAAPDs in the detection of muonic atom (μp, μHe, μC) X-rays in the intense radiation environment of the experiment. The main aim was to verify the ability of detecting the 1.9-keV X-rays, corresponding to the 2P–1S transition of μp, and to study the possibilities of reducing the huge X-ray spectra background present on such muonic atom experiments.

2. Experimental setup

The realization of the μp Lamb-shift experiment requires a very low energy muon beam line. However, the reported tests were obtained from a different muon beam line, the μE4 area at PSI. This beam line was designed to produce muons in the 30–100 MeV/c momentum range. To optimally stop the muons in our gas volume, we selected a beam momentum of 31.5 MeV/c. Before entering the gas chamber, incoming muons were detected in a 1-mm-thick scintillator.

Fig. 2 shows a schematic muon view of the target and detectors. The gas chamber ($100\times115\times50$ mm^3) is made of 15-mm-thick aluminum covered with 5–7 μm gold. Four 10-μm-thick and 30-mm-diameter aluminized Mylar windows were installed to allow muons to enter the chamber and low energy X-rays to reach the two LAAPDs and the G1 germanium detector. Since LAAPDs are light sensitive, we chose aluminized Mylar in order to prevent the light to enter the chamber. The thickness was chosen such as to hold the slight overpressure in the chamber and to minimize the X-ray absorption. Apart from the LAAPDs, we used two germanium detectors to measure X-rays for monitoring purposes. G1 is a small volume (0.17 cm^3) high purity germanium detector, suitable for X-ray detection in the 3–25 keV energy range and was essentially used to monitor if the muons were mainly stopping in the gas volume. G2 is a larger volume (75 cm^3) high purity germanium detector, suitable for 70–1500 keV energy range detection and was used to monitor the number of muons that interact in the

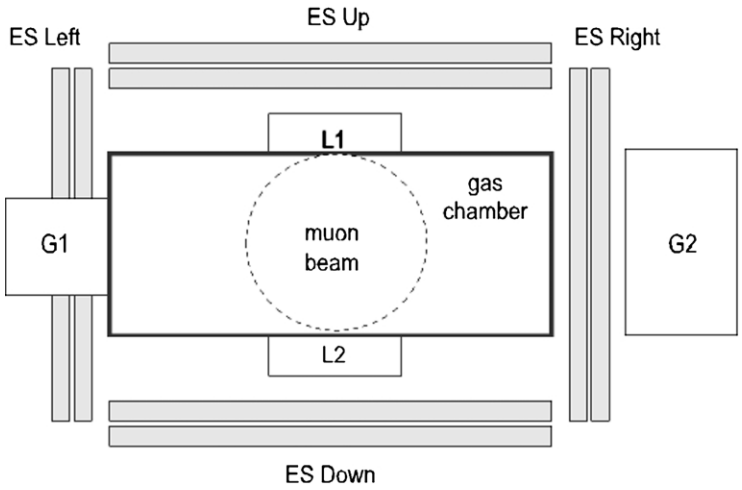

Fig. 2. Schematic muon view of the experimental system, showing the target and surrounding detectors.

chamber walls. This way, the muon beam momentum was optimized to maximize the muon stops in the gas and minimize the muon stops in the walls. No window was necessary in front of the G2 detector; however, the target wall thickness was reduced from 15 to 3 mm.

Surrounding the target and the detectors, four pairs of scintillators (ES Left, ES Right, ES Up, ES Down) were installed to detect muon decay electrons. The scintillators have a planar shape and cover almost all space around the chamber, maximizing the solid angle for electron detection. Each scintillator (eight in total) has its own phototube. Using coincidence signals between two scintillator plates allows us to discriminate between heavy charged particles and electrons. Only the last ones can leave traces in both scintillator plates.

Different gases, such as hydrogen, helium and a mixture of hydrogen and methane, were used in our experiments. In all cases, a continuous gas flow was used.

LAAPDs, 16 mm in diameter, biased with 1800 V, were used to detect the muonic X-rays produced in the gas. X-rays interact directly in the Si and the resulting primary electrons are amplified by the intense electric field around the junction, producing a pulse with amplitude that is, in average, proportional to the X-ray energy.

The LAAPD signals were fed through the *Rutherford Appleton Laboratory* (*RAL*) low-noise preamplifier [10], model *108-A*, to a spectroscopy amplifier and were pulse-height analyzed by a multi-channel analyzer. The *RAL 108-A* preamplifier is a charge-sensitive thick ceramic board specially designed to amplify negative input signals and to give positive output signals. Short shaping time constants of 100 ns were used in the main amplifier to achieve an optimum energy resolution.

Only events taking place in coincidence with the signal given by the scintillator that monitors the muon entering the gas chamber (which set the time-zero) were recorded. For each LAAPD event, energy and time were recorded. Offline analysis permits any combination of energy and time from the different detector types to produce spectra.

3. Results and discussion

When muons are stopped in a gas volume, muonic atoms are produced in an excited state. Those atoms decay to the ground state and the subsequent X-rays can be detected. Muon collisions with the chamber walls produce γ rays and electrons, contributing to the background. Additional delayed electrons are produced in consequence of the muon decay process. The muon

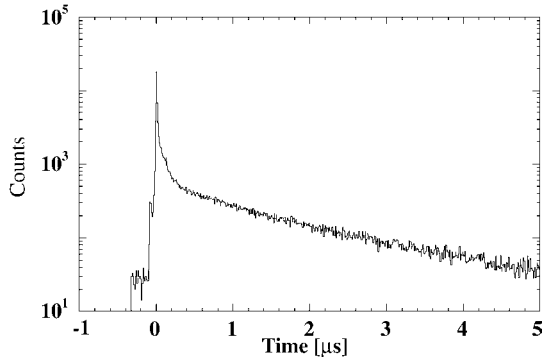

Fig. 3. Time spectrum for muonic hydrogen X-rays showing the exponential behavior of the muon decay process.

lifetime depends on the gas inside the chamber. The time spectra of LAAPD events show the exponential behavior characteristic of the muon decay, as shown in Fig. 3 for muonic hydrogen. An exponential fit would give the muon lifetime in the different elements of the target, namely, the gas and the walls. The muon lifetime in hydrogen is 2.2 μs [11].

Since X-rays are produced just after the muon capture in a pure gas, we distinguish between prompt and delayed events, corresponding to events that take place at times shorter and longer than 30 ns, respectively, in the attempt to reduce the X-ray background. The value 30 ns was chosen looking at energy and time spectra. Selecting only events in the useful energy range (between 1.5 and 2.5 keV in muonic hydrogen) and checking the corresponding time, almost all events lie within ±30 ns. Fig. 4 presents different pulse-height distributions obtained with LAAPDs, for hydrogen and helium gases. The total distribution includes all events (X-rays and electrons) without any discrimination, while the prompt one includes only prompt events (time between ±30 ns relative to muon entrance). The resulting energy spectra from prompt events present a considerable background reduction, showing that the time discrimination is a powerful tool for effective X-ray background reduction. The background can be almost totally eliminated if a coincidence between the X-rays in the LAAPD and the corresponding electrons resulting from the muon decay, detected by scintillators within a 200–5200 ns time range, are further considered, as seen in the e-coincidence pulse-height distribution of Fig. 4. K_α and K_β μHe X-rays can be efficiently discriminated from the electron background only when using coincidence with the muon decay electrons. However, the X-ray counting rate drops by a factor of approximately 5 due to the discrimination parameters and the solid angle for the electron detection.

Fig. 5 depicts the total, prompt and electron-coincidence X-ray pulse-height distributions for the $H_2+4\%CH_4$ and $H_2+16\%CH_4$ mixtures, obtained using the same discrimination timing parameters as in Fig. 4. For these mixtures, muons are captured either by hydrogen or carbon atoms.

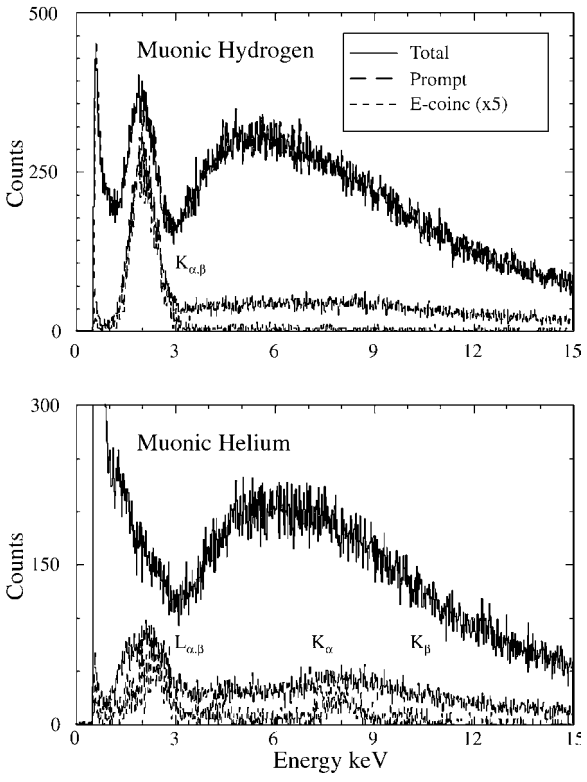

Fig. 4. Pulse-height distributions obtained with LAAPDs in two different pure gases. For hydrogen, the 1.89 keV K_α and 2.25 keV K_β μp X-rays are shown. For helium, the 8.23 keV K_α and 9.74 keV K_β μHe X-rays are visible, as well as the 1.52 keV L_α and 2.05 keV L_β μHe X-rays. The big 'bump' above 3 keV is due to electrons depositing energy in the LAAPD.

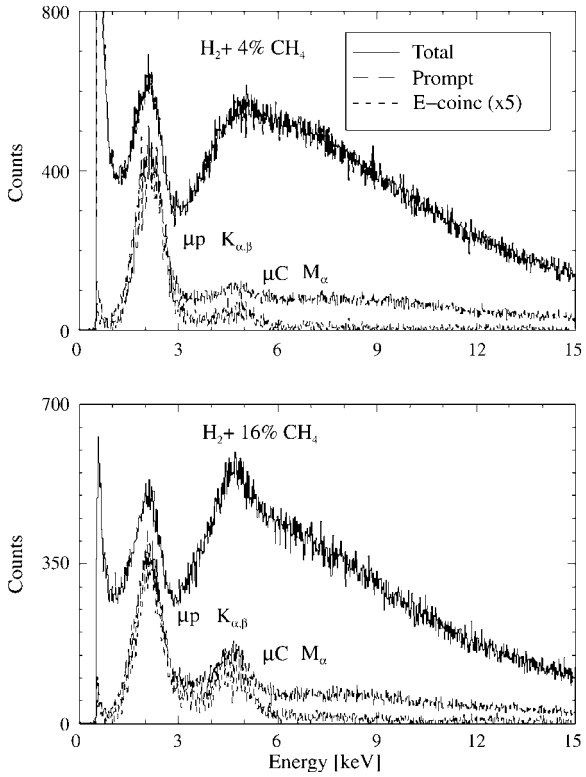

Fig. 5. Pulse-height distributions obtained for $H_2+4\%CH_4$ and $H_2+16\%CH_4$ mixtures. In both cases, K_α and K_β μp X-rays were detected, as well as the 4.88 keV M_α μC X-rays. As seen, μC peak intensities are directly dependent on the relative concentration of carbon in the mixture.

When hydrogen atoms capture muons, muon transfer to carbon takes place, with a reduced transfer rate of $0.95(5)\times10^{11}$/s (relative to liquid hydrogen density) [12], producing delayed muonic carbon (μC) atoms. Again, the e-coincidence spectra in Fig. 5 show the capability to identify the unique signature of muonic atom X-rays that allow to effectively eliminate the background.

4. Conclusions

LAAPDs are alternative detectors for muonic atom X-ray spectrometry. Its compactness, insensitivity to intense magnetic fields and ionizing particles and radiation hardness are advantages to its use in the demanding environment of such experiments. However, its limited detection efficiency for X-rays with energies above 10 keV may be a drawback in that case. Effective background reduction of the X-ray spectrum is achieved by discriminating the events taking place few tens of nanosecond after the muon entrance in the chamber. Additionally, the background can be effectively eliminated by further discriminating LAAPD events establishing its coincidence with the respective muon decay electrons.

Acknowledgments

Support is acknowledged to Fundação para a Ciência e a Tecnologia (FCT) through Project POCTI/FNU/41720/01 and to Swiss National Science Foundation. J.F.C.A. Veloso acknowledges support grant from FCT.

References

[1] D. Taqqu, F. Biraben, C.A.N. Conde, T.W. Haensch, F.J. Hartmann, P. Hauser, P. Indelicato, P. Knowles, F. Kottmann, F. Mulhauser, C. Petitjean, R. Pohl, R. Rabinowitz, R. Rosenfelder, J.M.F. Santos, W. Schott, L.M. Simons, J.F.C.A. Velosa, Laser spectroscopy of the Lamb Shift in muonic hydrogen, Hyp. Interact. 119 (1999) 311–315.

[2] F. Kottmann, W. Amir, F. Biraben, C.A.N. Conde, S. Dhawan, C. Donche-Gay, T.W. Haensch, F.J. Hartmann, V.W. Hughes, O. Huot, P. Indelicato, L. Julien, P. Knowles, S. Kazamias, Y.-W. Liu, F. Mulhauser, F. Nez, R. Pohl, P. Rabinowitz, J.M.F. dos Santos, L.A. Schaller, H. Schneuwly, W. Schott, D. Taqqu, J.F.C.A. Velosa, The muonic hydrogen Lamb Shift experiment at PSI, Hyp. Interact. 138 (2001) 55–60.

[3] P.J. Mohr, B.N. Taylor, Rev. Mod. Phys. 72 (2000) 351.

[4] S.G. Karshenboim, Can. J. Phys. 77 (1999) 241.

[5] L.M.P. Fernandes, J.A.M. Lopes, J.M.F. dos Santos, C.A.N. Conde, X-Ray Spectrom. 30 (2001) 164.

[6] M. Boucher, O. Huot, P.E. Knowles, L. Ludhova, F. Mulhauser, L.A. Schaller, C.A.N. Conde, J.M.F. dos Santos, L.M.P. Fernandes, J.F.C.A. Velosa, F. Kottmann, A. Antognini, R. Pohl, D. Taqqu, Large-area APDs for low energy X-ray detection in intense magnetic fields, Nucl. Instr. Meth. A. 505 (2003) 136–139.

[7] L.M.P. Fernandes, A. Antognini, M. Boucher, O. Huot, P.E. Knowles, F. Kottmann, L. Ludhova, F. Mulhauser, R. Pohl, J.M.F. dos Santos, D. Taqqu, J.F.C.A. Velosa, Behaviour of large-area avalanche photodiodes under intense magnetic field for VUV- visible and X-ray photon detection, Nucl. Instr. Meth. A. 498 (2003) 362–368.

[8] L.M.P. Fernandes, J.A.M. Lopes, J.M.F. dos Santos C.A.N. Conde, 2003. X-ray spectrometry with Peltier-cooled large-area avalanche photodiodes, Nucl. Instr. Meth. B, in press.
[9] Advanced Photonix Inc., 1240 Avenida Acaso, Camarillo, CA 93012, USA.
[10] CLRC Rutherford Appleton Laboratory, Chilton, Didcot, Oxfordshire, OX11, 0QX, England.
[11] T. Suzuki, D.F. Measday, J.P. Koalsvig, Phys. Rev. C 35 (1987) 2212.
[12] L. Schellenberg, A. Adamczak, R. Jacot-Guillarmod, F. Mulhauser, C. Piller, L.A. Schaller, H. Schneuwly, Y.-A. Thalmann, S. Tresch, A. Werthmueller, Muon transfer to light atoms, Hyp. Interact. 101/102 (1996) 215–220.

Conclusions

The studies performed throughout this thesis show that large area avalanche photodiodes can be used as X-ray detectors in the low and medium energy range (up to about 25 keV for API photodiodes), being compact and robust detectors with simple operation and low consumption. These characteristics make the LAAPDs particularly useful in X-ray spectrometry applications, such as the laser spectroscopy of muonic hydrogen, described in Chapter 4, where LAAPDs are used as 1.9 keV X-ray detectors operating under a 5 T magnetic field.

The operational characteristics of several avalanche photodiodes manufactured by API, used as X-ray detectors, have been investigated at room temperature. The energy resolution depends significantly on each individual photodiode since the dark current varies significantly among different LAAPDs. The minimum energy resolution obtained for 5.9 keV X-rays varies between 10 and 18% for the four investigated photodiodes. Similarly, the electronic noise associated with each LAAPD, which determines the minimum detection limit, depends on the dark current. The minimum detectable energy is lower than 1 keV for LAAPDs with inferior dark current. The choice of LAAPDs with lower dark current make them useful in applications of low and medium energy X-ray spectrometry, where an energy resolution better than the one of typical proportional counters can be obtained, but still not as good as the one obtained with gas proportional scintillation counters.

The energy linearity of LAAPDs was demonstrated between 1.7 and 25 keV for the optimum gain (about 50), corresponding to the minimum energy resolution. There is however a small effect of non-linearity due to the spatial charge distribution of the electron cloud produced by the local absorption of X-rays, which weakens the localized electric field, decreasing the LAAPD gain. This effect increases with energy and gain due to higher concentration of produced charges. For gains below 100, the ratio between the amplitude of the signals produced by 22.1 and 5.9 keV X-rays changes by less than

1%, originating a LAAPD response practically linear for gains close to the optimum gain for the related energy range.

The non-uniformity of the silicon resistivity originates fluctuations of the LAAPD gain, depending on the interaction point of each X-ray in the crystal. The effect of spatial non-uniformity on the gain has been investigated for different photodiodes. Relative standard deviations of 2-3% have been obtained, typical for API avalanche photodiodes. The requirement of good uniformity prevents a significant degradation of the energy resolution in X-ray detection when the full area of the LAAPD is used.

The compact structure of the LAAPD and the possibility to detect X-rays with better energy resolution constitute advantages comparatively to proportional counters. The absence of a window in the LAAPD is important for the detection of low energy X-rays. An additional advantage of the LAAPD results from its high counting rate capability, making it possible to detect counting rates up to about 10^4/s without significant degradation of the amplitude and energy resolution. On the other hand, its limited area and sensitivity to light and temperature are drawbacks.

The detection of X-rays in a LAAPD originates peaks in the energy spectra with a tail towards lower energies due to X-ray interactions in different regions of the photodiode. Digital discrimination techniques, based on pulse risetime, have been used in order to reduce the background. It was demonstrated that the risetime discrimination leads to the elimination of pulses with smaller amplitude which undergo partial amplification in the LAAPD, improving the energy resolution and the peak-to-background ratio. In addition, the discrimination provides a better separation between signals of interest and the noise since the noise pulses present longer risetimes. Nevertheless, a compromise between the acquisition efficiency of the X-ray pulses and the noise discrimination threshold is necessary. A lower discrimination level causes more dead time, the fraction of time required to analyze noise pulses online.

The strong dependence of the LAAPD gain on temperature makes it necessary to control the temperature during the measurements. The LAAPD temperature is stabilized using Peltier elements, which provide temperature control with a precision of ± 0.1 ºC.

A LAAPD with integrated Peltier cell has been used in order to investigate the LAAPD response as a function of temperature. This system provides efficient LAAPD cooling down to -5 ºC. For lower temperatures, the electronic noise increases abruptly, hindering a good operation of the LAAPD. The study of the characteristics of LAAPDs has been extended to a wider temperature range using a cooling system based on liquid nitrogen, which provides a LAAPD cooling down to about -40 ºC. The results obtained for both cases are in agreement. The relative variation of the gain for 5.9 keV X-rays with temperature has found to be about -5% per ºC for the highest gains. This value is considerably higher than the one specified by the manufacturer for visible light (relative variation of -3% per ºC).

The significant reduction of the dark current improves the LAAPD performance at low temperatures. For the LAAPD with an integrated Peltier cell, energy resolutions of 21.5 and 13.1% (for 5.9 keV X-rays) have been obtained for temperatures of 35 and 5 ºC, while the minimum detectable energy was 2.6 and 0.8 keV, respectively. For the LAAPD cooled by liquid nitrogen, minimum energy resolutions of 11, 9.6 and 9.2% have been obtained for temperatures of 24, 0 and -40 ºC. The dark current has been measured as a function of gain for different temperatures. A linear dependence on gain and an exponential one on temperature have been confirmed. The dependence on the temperature is responsible for the improvement of the LAAPD performance for low temperatures. However, the variations are not significant below 0 ºC. The excess noise factor has been also determined, being independent on temperature and varying linearly with the gain. The results demonstrate that the dependence of the energy resolution on temperature cannot be attributed to the excess noise factor, being mainly determined by the dark current, which affects the electronic noise.

An important application of API LAAPDs is their use as photosensors of ultraviolet light with wavelength down to 120 nm. In this way, avalanche photodiodes have been used as VUV photosensors in gas proportional scintillation counters and their response has been investigated as a function of temperature. The relative gain variation with temperature for VUV light is slightly higher than the one demonstrated for X-rays. As a result of the dark current variation, the minimum detection limit varies with the

temperature. For VUV radiation produced by xenon scintillation (~ 173 nm), the minimum number of detectable VUV photons in the LAAPD is 1.3×10^3 and 0.5×10^3 for temperatures of 25 and -5 ºC, respectively. Moreover, the energy resolution associated with the detection of 3.2×10^4 VUV photons also improves at lower temperatures, presenting values of 5.4 and 4.8% for 25 and 5 ºC, respectively.

The characterization of the LAAPD in light detection, namely the determination of the number of detected photons or the number of produced charge carriers, is made by comparison with the pulses resulting from X-ray interactions in the LAAPD. Studies of the LAAPD non-linearity in X-ray detection, comparatively to VUV-light detection, have been carried out in this work for the first time. The results show variations higher than the ones stated in the literature for visible light. The gain ratio between 5.9 keV X-rays and VUV light decreases with the gain, presenting a variation of about 10% for a gain of 200 for the argon scintillation (~128 nm), and about 6% for the same gain for the xenon scintillation (~173 nm). The gain ratio between 5.9 keV X-rays and visible light has also been investigated, presenting significantly lower variations (1 and 0.5% for temperatures of 23 and 0 ºC, for a gain of 200). For the optimum gain, the non-linearity reaches about 3 and 2% for scintillation light of argon and xenon, respectively, and less than 0.5% for visible light.

The previous results show that the non-linearity does not depend only on space charge effects associated with high current densities observed for high gains due to local absorption of X-rays, but depends also on the type of light considered. The study also shows that the ratio between the gains obtained for VUV and visible light increases with the gain, what can be attributed to a superior efficiency (relative to the gain) in the collection of charge carriers produced by radiation absorbed closer to the LAAPD surface, such as VUV photons.

As VUV-light photons are absorbed superficially, the LAAPD response varies significantly with the magnetic field due to partial loss of primary electrons to the dead layer at the photodiode entrance. The response in X-ray and visible-light detection has demonstrated a small sensitivity to the magnetic field due to the deeper absorption of the corresponding photons.

The muonic hydrogen Lamb shift experiment requires the use of a 1.9 keV X-ray detector capable to operate under a 5 T magnetic field with energy and time responses adequate to the objectives of the experiment. LAAPDs have been chosen as the X-ray detectors to be used in the experiment due to several factors:

- They are compact, easy to operate and its response practically does not vary with the application of magnetic fields up to 5 T.
- An energy resolution of about 20% can be obtained if the LAAPDs are appropriately selected, with low dark current, and if they are conveniently cooled, leading to an additional decrease of the dark current.
- They present a fast time response, with risetimes of 20-30 ns and a time resolution of about 10 ns for 1.9 keV X-rays (for API photodiodes).

The small detection area of LAAPDs, considered as a disadvantage in comparison with gas detectors, is partially compensated by the use of a series of several LAAPDs. This is possible since LAAPDs do not need an additional window and, because they are more compact, they may be placed closer to the region where muons interact.

The LAAPD response has found to be adequate to the intense radiation environment of the experiment, making it possible to identify efficiently the desired events by the discrimination of X-rays produced in the LAAPD in coincidence with muon interactions in the target and the subsequent detection of the electrons resulting from muon decay, and by the selection of X-rays with the desired energy.

In the two phases of the experiment, carried out in 2002 and 2003, LAAPDs from API and RMD have been used, operating at temperatures of -10 and -30 ºC, respectively. Due to their squared shape, photodiodes from RMD provide larger useful detection areas. However, their dark current is considerably higher and a better cooling is necessary in order to reach the desired performance. For both phases of the experiment, the 2S-2P resonance line was not yet found due to the low counting rate for the events in resonance with the laser. A new phase of the experiment is expected for 2006 or 2007.

As future perspectives of large area avalanche photodiodes, their application as position detectors is pointed out. Moreover, since the LAAPD quantum efficiency is precisely known, the use of LAAPDs as a reference for other detectors may be important, providing electroluminescence measurements.

References

Allier C.P., H. Valk, Huizenga J., Bom V.R., Hollander R.W., van Eijk C.W.E., "Comparative study of silicon detectors", *IEEE Trans. Nucl. Sci.* 45 (**1998**) 576-580.

Anderhub H., von Arb H.P., Böcklin J., Dittus F., Ferreira Marques R., Hoper H., Kottmann F., Taqqu D., Unternährer J., "Measurement of the K-line intensity ratios in muonic hydrogen between 0.25 and 150 torr gas pressures", *Phys. Lett. B* 143 (**1984**) 65-68.

Antognini A., Amaro F.D., Biraben F., Cardoso J.M.R., Conde C.A.N., Dax A., Dhawan S., Fernandes L.M.P., Hänsch T.W., Hughes V.W., Huot O., Indelicato P., Julien L., Knowles P.E., Kottmann F., Liu Y.W., Ludhova L., Monteiro C.M.B., Mulhauser F., Nez F., Perry B.N., Pohl R., Rabinowitz P., dos Santos J.M.F., Schaller L.A., Schwob C., Taqqu D., Veloso J.F.C.A., "Powerful fast triggerable 6 μm laser for the muonic hydrogen Lamb shift experiment", submitted for publication to *Optics Communication* (**2004**).

API (Advanced Photonix Inc.) Application Note: "Noise characteristics of Advanced Photonix avalanche photodiodes" (**1991**).

API (Advanced Photonix Inc.) Application Notes: "Windowless large area APDs" (**1999**).

Barnard T.W., Crockett M.I., Ivaldi J.C., Lundberg P.L., Yates D.A., Levine P.A., Sauer D.J., "Solid-state detector for ICP-OES", *Anal. Chem.* 65 (**1993**) 1231-1239.

Baron A.Q.R., Ruby S.L., "Time resolved detection of X-rays using large area avalanche photodiodes", *Nucl. Instr. Meth. A* 343 (**1994**) 517-526.

Beiser A., "Concepts of Modern Physics", Fifth Edition, *McGraw-Hill* International Editions (**1995**).

Birks L.S., Criss J., "Mass photoelectric absorption coefficients", *J.W. Robinson* Edition, Handbook of Spectroscopy, Vol. III, *CRC Press*, Boca Raton, FL, USA (**1981**).

Canfield L.R., Vest R.E., Korde R., Schmidtke H., Desor R., "Absolute silicon photodiodes for 160 nm to 254 nm photons", *Metrologia* 35 (**1998**) 329-334.

Chen A. Ruru, Fremout A., Tavernier S., Bruyndonckx P., Clément D., Loude J.F., Morel C., "Readout of scintillator light with avalanche photodiodes for positron emission tomography", *Nucl. Instr. Meth. A* 433 (**1999**) 637-647.

Conde C.A.N., "Gas proportional scintillation counters for X-ray spectrometry", *Advances in X-ray Spectrometry: Trends in New X-ray Devices*, John Wiley & Sons, London (**2003**).

DeCecco P., Hauser P., Horváth D., Kottmann F., Simons L.M., Taqqu D., "A new method to produce a negative muon beam of keV energies", *Nucl. Instr. Meth. A* 394 (**1997**) 287-294.

Farrell R., Vanderpuye K., Entine G., Squillante M.R., "High resolution, low energy avalanche photodiode X-ray detectors", *IEEE Trans. Nucl. Sci.* 38 (**1991**) 144-147.

Farrell R., Olschner F., Shah K., Squillante M.R., "Advances in semiconductor photodetectors for scintillation", *Nucl. Instr. Meth. A* 387 (**1997**) 194-198.

Farrell R., Shah K., Vanderpuye K., Grazioso R., Myers R., Entine G., "APD arrays and large-area APD's via a new planar process", *Nucl. Instr. Meth. A* 442 (**2000**) 171-178.

Fernandes L.M.P., Lopes J.A.M., dos Santos J.M.F., Conde C.A.N., "Application of large area avalanche photodiodes to energy dispersive X-ray fluorescence analysis", *X-Ray Spectrometry* 30 (**2001**), 164-169.

Fernandes L.M.P., Lopes J.A.M., Monteiro C.M.B., dos Santos J.M.F., Morgado R.E., "Non-linear behaviour of large-area avalanche photodiodes", *Nucl. Instr. Meth. A* 478 (**2002**) 395-399. (**A**)

Fernandes L.M.P., Simões P.C.P.S., dos Santos J.M.F., Morgado R.E., "Digital risetime discrimination of large-area avalanche photodiode signals in X-ray detection", *IEEE Trans. Nucl. Sci.* 49 (**2002**) 1699-1703. (**B**)

Fernandes L.M.P., Antognini A., Boucher M., Conde C.A.N., Huot O., Knowles P.E., Kottmann F., Ludhova L., Mulhauser F., Pohl R., Schaller L.A., dos Santos J.M.F., Taqqu D., Veloso J.F.C.A., "Behaviour of large-area avalanche photodiodes under intense magnetic fields for VUV, visible and X-ray photon detection", *Nucl. Instr. Meth. A* 498 (**2003**) 362-368. (**A**)

Fernandes L.M.P., Antognini A., Boucher M., Conde C.A.N., Huot O., Knowles P.E., Kottmann F., Ludhova L., Mulhauser F., Pohl R., dos Santos J.M.F., Schaller L.A., Taqqu D., Veloso J.F.C.A., "Application of large-area avalanche photodiodes to X-ray spectrometry of muonic atoms", *Spectrochimica Acta B* 58 (**2003**) 2255-2260. (**B**)

Fernandes L.M.P., Lopes J.A.M., dos Santos J.M.F., Conde C.A.N., "X-ray spectrometry with Peltier-cooled large area avalanche photodiodes", *Nucl. Instr. Meth. B* 213 (**2004**) 267-271. (**A**)

Fernandes L.M.P., Lopes J.A.M., dos Santos J.M.F.," Excess noise factor in large area avalanche photodiodes for different temperatures", *Nucl. Instr. Meth. A* 531 (**2004**) 566-568. (**B**)

Fernandes L.M.P., Lopes J.A.M., dos Santos J.M.F., Knowles P.E., Ludhova L., Mulhauser F., Kottmann F., Pohl R., Taqqu D., "LAAPD low temperature performance in X-ray and visible-light detection", *IEEE Trans. Nucl. Sci.* 51 (**2004**) 1575-1580. (**C**)

Gullikson E.M., Gramsch E., Szawlowski M., "Large-area avalanche photodiodes for the detection of soft X-rays", *Appl. Optics* 34 (**1995**) 4662.

Jensen T.S., Markushin V.E., "Collisional quenching of the 2S state of muonic hydrogen", Report PSI-PR-99-32, nucl-th/0001009 (**2000**).

Karar A., Musienko Y., Vanel J.C., "Characterization of avalanche photodiodes for calorimetry applications", *Nucl. Instr. Meth. A* 428 (**1999**) 413-431.

Knoll G.F., "Radiation Detection and Measurements", Third Edition, *John Wiley & Sons*, New York, USA (**2000**).

Koren B., Szawlowski M., "Large-area avalanche photodiodes challenge PMTs", Advances and applications in Optoelectronics, *Laser Focus World* (November **1998**).

Kottmann F., Daniel H., Hartmann F.J., Hauser P., Maierl C., Markushin V.E., Mühlbauer M., Petitjean C., Pohl R., Schott W., Taqqu D., "Kinetic energies of exotic H atoms at formation and cascade", *Hyperfine Interact.* 119 (**1999**) 3-10.

Kottmann F., Amir W., Biraben F., Conde C.A.N., Dhawan S., Hänsch T.W., Hartmann F.J., Hughes V.W., Huot O., Indelicato P., Julien L., Knowles P., Kazamias S., Liu Y.W.,

Mulhauser F., Nez F., Pohl R., Rabinowitz P., dos Santos J.M.F., Schaller L.A., Schneuwly H., Schott W., Taqqu D., Veloso J.F.C.A., "The muonic hydrogen Lamb shift experiment at PSI", *Hyperfine Interact.* 138 (**2001**) 55-60.

Kottmann F., Antognini A., Biraben F., Boucher M., Conde C.A.N., Dax A., Dhawan S., Fernandes L.M.P., Hänsch T.W., Hartmann F.J., Hughes V.W., Huot O., Indelicato P., Julien L., Knowles P., Liu Y.W., Lopes J.A.M., Ludhova L., Monteiro C.M.B., Mulhauser F., Nez F., Pohl R., Rabinowitz P., dos Santos J.M.F., Schaller L., Shy J.T., Taqqu D., Veloso J.F.C.A., "The muonic hydrogen Lamb shift experiment at PSI", *Proceedings of the International Workshop on Exotic Atoms* (EXA2002), Austrian Academy of Sciences Press, Vienna (**2003**) 159-166.

Lamb W.E., Retherford R.C., "Fine structure of the hydrogen atom. IV", *Phys. Rev.* 86 (**1952**), 1014-1022.

Liu W., Boshier M.G., Dhawan S., van Dyck O., Egan P., Fei X., Perdekamp M.G., Hughes V.W., Janousch M., Jungmann K., Kawall D., Mariam F.G., Pillai C., Prigl R., zu Putlitz G., Reinhard I., Schwarz W., Thompson P.A., Woodle K.A., "High precision measurements of the ground state hyperfine structure interval of muonium and of the muon magnetic moment", *Phys. Rev. Lett.* 82 (**1999**) 711-714.

Lopes J.A.M., dos Santos J.M.F., Morgado R.E., Conde C.A.N., "Silicon photodiodes as the VUV photosensor in gas proportional scintillation counters", *IEEE Trans. Nucl. Sci.* 47 (**2000**) 928-932. (**A**)

Lopes J.A.M., dos Santos J.M.F., Conde C.A.N., "A large area avalanche photodiode as the VUV photosensor for gas proportional scintillation counters", *Nucl. Instr. Meth. A* 454 (**2000**) 421-425. (**B**)

Lopes J.A.M., dos Santos J.M.F., Morgado R.E., Conde C.A.N., "A xenon gas proportional scintillation counter with a UV-sensitive large-area avalanche photodiode", *IEEE Trans. Nucl. Sci.* 48 (**2001**) 312-319.

Lopes J.A.M., "Contadores gasosos de cintilação proporcional: novas aplicações e tecnologias de fotossensores integrados", Thesis for the degree of Doctor of Philosophy in Physics, speciality of Technological Physics, submitted to the Faculty of Sciences and Technology in the University of Coimbra (**2002**).

Lopes J.A.M., Fernandes L.M.P., dos Santos J.M.F., Morgado R.E., Conde C.A.N., "VUV detection in large-area avalanche photodiodes as a function of temperature", *Nucl. Instr. Meth. A* 504 (**2003**) 331-334.

Ludhova L., Amaro F.D., Antognini A., Biraben F., Cardoso J.M.R., Conde C.A.N., Covita D.S., Dax A., Dhawan S., Fernandes L.M.P., Hänsch T.W., Hughes V.W., Huot O., Indelicato P., Julien L., Knowles P.E., Kottmann F., Lopes J.A.M., Liu Y.W., Monteiro C.M.B., Mulhauser F., Nez F., Pohl R., Rabinowitz P., dos Santos J.M.F., Schaller L.A., Taqqu D., Veloso J.F.C.A, "Planar LAAPDs: temperature dependence, performance, and application in low-energy X-ray spectroscopy", *Nucl. Instr. Meth. A* 540 (**2005**) 169-179.

McIntyre R.J., "Multiplication noise in uniform avalanche diodes", *IEEE Trans. Electron Devices* 13 (**1966**) 164-168.

McIntyre R.J., "The distribution of gains in uniformly multiplying avalanche photodiodes: theory", *IEEE Trans. Electron Devices* 19 (**1972**) 703-713.

Monteiro C.M.B., Lopes J.A.M., Simões P.C.P.S., dos Santos J.M.F., Conde C.A.N., "An argon gas proportional scintillation counter with UV avalanche photodiode scintillation readout", *IEEE Trans. Nucl. Sci.* 48 (**2001**) 1081-1086.

Moszynski M., Kapusta M., Balcerzyk M., Szawlowski M., Wolski D., Wegrzecka I., Wegrzecki M., "Comparative study of avalanche photodiodes with different structures in scintillation detection", *IEEE Trans. Nucl. Sci.* 48 (**2001**) 1205-1210.

Moszynski M., Szawlowski M., Kapusta M., Balcerzyk M., "Large area avalanche photodiodes in scintillation and X-rays detection", *Nucl. Instr. Meth. A* 485 (**2002**) 504-521. (**A**)

Moszynski M., Czarnacki M., Szawlowski M., Zhou B.L., Kapusta M., Wolski D., Schotanous P., "Performance of large area avalanche photodiodes at liquid nitrogen temperature", IEEE Trans. Nucl. Sci. 49 (**2002**) 971-976. (**B**)

Mühlbauer M., Daniel H., Hartmann F.J., Hauser P., Kottmann F., Petitjean C., Schott W., Taqqu D., Wojciechowski P., "Frictional cooling: experimental results", *Hyperfine Interact.* 119 (**1999**) 305-310.

Nicholson P.W., "Nuclear Electronics", Wiley-Interscience Publication, *John Wiley & Sons*, London (**1974**).

Ochi A., Nishi Y., Tanimori T., "Study of a large area avalanche photodiode as a fast photon and a soft X-ray detector", *Nucl. Instr. Meth. A* 378 (**1996**) 267-274.

Pachucki K., "Theory of the Lamb shift in muonic hydrogen", *Phys. Rev. A* 53 (**1996**) 2092-2100.

Pachucki K., "Proton structure effects in muonic hydrogen", *Phys. Rev. A* 60 (**1999**) 3593-3598.

Pansart J.P., "Avalanche photodiodes for particle detection", *Nucl. Instr. Meth. A* 387 (**1997**) 186-193.

Perotti F., Fiorini C., "Observed energy dependence of Fano factor in silicon at hard X-ray energies", *Nucl. Instr. Meth. A* 423 (**1999**) 356-363.

Pohl R., Biraben F., Conde C.A.N., Donche-Gay C., Hänsch T.W., Hartmann F.J., Hauser P., Hughes V.W., Huot O., Indelicato P., Knowles P., Kottmann F., Liu Y.W., Mulhauser F., Nez F., Petitjean C., Rabinowitz P., dos Santos J.M.F., Schaller L.A., Schneuwly H., Schott W., Simons L.M., Taqqu D., Trehin F., Veloso J.F.C.A., "Experiment to measure the Lamb shift in muonic hydrogen", *Hyperfine Interact.* 127 (**2000**) 161-166.

Pohl R., "Measurement of the kinetic energies of μp(1S) and the lifetime of μp(2S)", private communication (**2001**).

Pohl R., Biraben F., Conde C.A.N., Donche-Gay C., Hänsch T.W., Hartmann F.J., Hauser P., Hughes V.W., Huot O., Indelicato P., Knowles P., Kottmann F., Liu Y.W., Markushin V.E., Mulhauser F., Nez F., Petitjean C., Rabinowitz P., dos Santos J.M.F., Schaller L.A., Schneuwly H., Schott W., Taqqu D., Veloso J.F.C.A., "Towards a measurement of the Lamb shift in muonic hydrogen", *Springer LNP* 570 (**2001**) 454-466. (**A**)

Pohl R., Daniel H., Hartmann F.J., Hauser P., Liu Y.W., Kottmann F., Maierl C., Markushin V.E., Mühlbauer M., Petitjean C., Schott W., Taqqu D., "Observation of the molecular quenching of μp(2S) atoms", *Hyperfine Interact.* 138 (**2001**) 35-40. (**B**)

Rabinowitz P., Perry B.N., Levinos N., "A continuously tunable sequential Stokes Raman laser", *IEEE J. Quant. Elec.* 22 (**1986**) 797-802.

Rohlf J.W., "Modern physics from alpha to Z-zero" (Sec. 8-9), Wiley (**1994**).

Rosenfelder R., “Coulomb corrections to elastic electron–proton scattering and the proton charge radius”, *Phys. Lett. B* 479 (**2000**) 381-386.

Santos J.M.F., “Contadores gasosos de cintilação proporcional para análise por fluorescência de raios X”, Thesis for the degree of Doctor of Philosophy in Physics, speciality of Applied Physics, submitted to the Faculty of Sciences and Technology in the University of Coimbra (**1994**).

Schellenberg L., “Recent experiments on muon transfer in gas mixtures”, *Hyperfine Interact.* 82 (**1993**) 513-517.

Schwob C., Jozefowski L., de Beauvoir B. Hilico, L., Nez F., Julien L., Biraben F., Acef O., Clairon A., “Optical frequency measurement of the 2S-12D transitions in hydrogen and deuterium: Rydberg constant and Lamb shift determinations”, *Phys. Rev. Lett.* 82 (**1999**) 4960-4963.

Sick I., “On the rms-radius of the proton”, *Phys. Lett. B* 576 (**2003**) 62-67.

Simon G.G., Schmidt C., Borkowski F., Walther V.H., “Absolute electron-proton cross sections at low momentum transfer measured with a high pressure gas target system”, *Nucl. Phys. A* 333 (**1980**) 381-391.

Suzuki T., Measday D.F., Roalsvig J.P., “Total nuclear capture rates for negative muons”, *Phys. Rev. C* 35 (**1987**) 2212-2224.

Taqqu D., Biraben F., Conde C.A.N., Hänsch T.W., Hartmann F.J., Hauser P., Indelicato P., Knowles P., Kottmann F., Mulhauser F., Petitjean C., Pohl R., Rabinowitz P., Rosenfelder R., J.M.F. dos Santos, W. Schott, L.M. Simons, J.F.C.A. Veloso, “Laser spectroscopy of the Lamb shift in muonic hydrogen”, *Hyperfine Interact.* 119 (**1999**) 311-315.

Triebwasser S., Dayhoff E.S., Lamb W.E., “Fine structure of the hydrogen atom. V”, *Phys. Rev.* 89 (**1953**), 98-106.

Veloso J.F.C.A., "Detectores gasosos de radiação baseados em Microestruturas ", Thesis for the degree of Doctor of Philosophy in Physics, speciality of Technological Physics, submitted to the Faculty of Sciences and Technology in the University of Coimbra (**2000**).

Veloso J.F.C.A., dos Santos J.M.F., Conde C.A.N., "Gas proportional scintillation counters with a CsI-covered MSP UV photosensor for high-resolution X-ray spectrometry", *Nucl. Instr. Meth. A* 457 (**2001**) 253-261.

Veloso J.F.C.A., Lopes J.A.M., Conde C.A.N., Fernandes L.M.P., Freitas E.D.C., Huot O., Knowles P.E., Kottmann F., Mulhauser F., dos Santos J.M.F., Taqqu D., "Gas proportional scintillation counters for the Lamb-shift experiment", *IEEE Trans. Nucl. Sci.* 49 (**2002**) 899-906.

Wallenius J., Jonsell S., Kino Y., Froelich P., "Muonic atom deexcitation via formation of metastable molecular states", *Hyperfine Interact*. 138 (**2001**) 285.

Webb P.P., McIntyre R.J., "Large area reach-through avalanche diodes for X-ray spectroscopy", *IEEE Trans. Nucl. Sci.* 23 (**1976**) 138-144.

Zhou B., Szawlowski M., "An explanation on the APD spectral quantum efficiency in the deep UV range", Advanced Photonix, Inc. Interoffice Memo (**1999**).